

**OPTIMAL LANDSLIDE SUSCEPTIBILITY AND RISK
ANALYSES AT KHAO PHANOM BENCHA,
KRABI PROVINCE, THAILAND**

Thidapath Anucharn



**A Thesis Submitted in Partial Fulfillment of the Requirements for the
Degree of Doctor of Philosophy in Geoinformatics
Suranaree University of Technology**

Academic Year 2015

การวิเคราะห์ความอ่อนไหวและความเสี่ยงดินถล่มที่เหมาะสม
บริเวณเขาพนมเบญจา จังหวัดกระบี่ ประเทศไทย



วิทยานิพนธ์นี้เป็นส่วนหนึ่งของการศึกษาตามหลักสูตรปริญญาวิทยาศาสตรดุษฎีบัณฑิต

สาขาวิชาภูมิสารสนเทศ
มหาวิทยาลัยเทคโนโลยีสุรนารี
ปีการศึกษา 2558

**OPTIMAL LANDSLIDE SUSCEPTIBILITY AND RISK
ANALYSES AT KHAO PHANOM BENCHA,
KRABI PROVINCE, THAILAND**

Suranaree University of Technology has approved this thesis submitted in partial fulfillment of the requirements for the Degree of Doctor of Philosophy.

Thesis Examining Committee

(Assoc. Prof. Dr. Suwit Ongsomwang)

Chairperson

(Assoc. Prof. Dr. Songkot Dasananda)

Member (Thesis Advisor)

(Asst. Prof. Dr. Sunya Sarapirome)

Member

(Assoc. Prof. Dr. Suttisak Soralump)

Member

(Assoc. Prof. Dr. Charlie Navanugraha)

Member

(Prof. Dr. Sukit Limpijumnong)

Vice Rector for Academic Affairs

and Innovation

(Prof. Dr. Santi Maensiri)

Dean of Institute of Science

ชิตาภัทร อนุชาญ : การวิเคราะห์ความอ่อนไหวและความเสี่ยงดินถล่มที่เหมาะสม
บริเวณเขาพนมเบญจา จังหวัดกระบี่ ประเทศไทย (OPTIMAL LANDSLIDE
SUSCEPTIBILITY AND ANALYSES AT KHAO PHANOM BENCHA, KRABI
PROVINCE, THAILAND) อาจารย์ที่ปรึกษา : ผู้ช่วยศาสตราจารย์ ดร.ทรงกต ทศานนท์,
344 หน้า.

วิทยานิพนธ์ฉบับนี้มีวัตถุประสงค์หลักสามประการคือ (1) เพื่อกำหนดวิธีที่เหมาะสมที่สุด
สำหรับการจัดทำแผนที่ความอ่อนไหวต่อการเกิดดินถล่มเหนือพื้นที่ศึกษาที่ต้องการ คือ พื้นที่ลุ่มน้ำ
เขาพนมเบญจาในเขตจังหวัดกระบี่ จากรายการของตัวเลือกที่ได้รับการเสนอ (2) เพื่อพัฒนาแผนที่
ความเสี่ยงต่อการเกิดดินถล่มและความเสี่ยงต่อการเกิดความเสียหายที่เกี่ยวข้องกับเหตุการณ์ดังกล่าว
สำหรับพื้นที่โดยการประยุกต์วิธีที่เหมาะสมที่สุดซึ่งพบก่อนหน้านี้ (3) เพื่อประเมินความเสี่ยงต่อการ
เกิดดินถล่มแบบ โคลนหลากรุนแรงสำหรับพื้นที่โดยการประยุกต์แบบจำลอง Flow-R ที่ต้องการ
ทั้งนี้ เพื่อให้บรรลุวัตถุประสงค์แรก ได้มีการประเมินและเปรียบเทียบความถูกต้องของผลงาน ที่ได้
จากวิธีสร้างแผนที่ความอ่อนไหวที่มีชื่อเสียงจำนวนเจ็ดวิธี คือ วิธี conventional weighted linear
combination (WLC) วิธี analytical hierarchy process (AHP) วิธี frequency ratio (FR) วิธี integrated
FR-fuzzy วิธี multiple logistic regression (MLR) วิธี artificial neural network (ANN) และ วิธี
integrated ANN-fuzzy โดยในทุกกรณีจะใช้ปัจจัยเกื้อหนุนสำคัญต่อการเกิดดินถล่มในเขต โชน
ร่อนจำนวน 10 ประเภท เป็นข้อมูลนำเข้าเพื่อสร้างแผนที่ความอ่อนไหวที่ต้องการ ได้แก่ ความสูง
ความลาดชัน ทิศด้านลาด ความโค้งพื้นผิว ดัชนีความชื้นเชิงภูมิประเทศ ระยะห่างจากทางน้ำ
ลักษณะทางธรณีวิทยา ระยะห่างจากแนวรอยเลื่อนของแผ่นดิน ลักษณะเนื้อดิน และลักษณะของ
การใช้ประโยชน์ที่ดินและตัวสิ่งปกคลุมดิน (LULC) ทั้งนี้ การประเมินความถูกต้องดำเนินการโดย
ใช้วิธีการที่ต่างกันจำนวน 2 วิธี คือวิธี Area-Under-Curve (AUC) และวิธี Receiver Operating
Characteristic (ROC) curve analysis

จากการศึกษาพบว่าหากพิจารณาเรื่องของความถูกต้องเฉลี่ยของแผนที่ผลผลิตจากแต่ละวิธี
วิธีซึ่งประสบความสำเร็จมากที่สุด 4 ลำดับแรก คือ วิธี FR (93.98%) วิธี MLR (92.98%) วิธี FR-
Fuzzy (92.84%) วิธี ANN-Fuzzy (92.47%) และในขณะที่วิธีซึ่งประสบความสำเร็จน้อยที่สุดคือ
AHP (83.37%) อย่างไรก็ตาม ถึงแม้ทั้งสี่วิธีซึ่งประสบความสำเร็จมากที่สุด จะมีค่าความถูกต้องของ
แผนที่ผลลัพธ์ที่ใกล้เคียงกันมาก แต่ท้ายที่สุดวิธี FR ได้รับการพิจารณาว่าเป็นวิธีที่เหมาะสมที่สุด
สำหรับการศึกษาขั้นต่อไป เนื่องมาจากการมีโครงสร้างการทำงานที่เรียบง่ายที่สุด รวมถึงการมีหลัก
ของการทำงานที่เข้าใจได้ง่ายที่สุดด้วย ทั้งนี้ ได้มีการตรวจสอบผลของการเพิ่มข้อมูลน้ำฝนสองแบบ

(ค่าเฉลี่ยรายปีระยะยาวและค่าสะสมระยะสั้น 3 วัน) ต่อการสร้างแผนที่ความเสี่ยงด้วย ซึ่งพบว่ามันส่งผลกระทบต่อระดับความถูกต้องในระดับต่ำ (มีการผันแปรของค่าความถูกต้องเฉลี่ย < 0.5%)

จากนั้นได้มีการสร้างแผนที่ความเสี่ยงต่อการเกิดดินถล่มของพื้นที่ขึ้น โดยการบูรณาการแผนที่ความอ่อนไหวที่สร้างมาจากวิธี FR ก่อนนั้น เข้ากับแผนที่โอกาสของการเกิดฝนเหนือพื้นที่ศึกษาสองกรณี คือปริมาณฝน 100 มม./วัน และ 300 มม./3 วัน ซึ่งเป็นค่าวิกฤติของการเริ่มต้นเกิดดินถล่มที่กำหนด ซึ่งผลที่ได้รับจากแผนที่ดังกล่าวที่ผ่านการจำแนกระดับแล้วจากทั้งสองวิธี บ่งชี้ว่ามีพื้นที่เพียงส่วนน้อยเท่านั้น (< 10%) ซึ่งมีความเสี่ยงดังกล่าวในระดับสูงถึงสูงมาก ขณะที่พื้นที่ประมาณ 80% ตั้งอยู่ในเขตซึ่งที่มีความเสี่ยงในระดับต่ำมากถึงต่ำ ซึ่งแผนที่ความเสี่ยงต่อภัยดินถล่มดังกล่าวได้รับการบูรณาการกับแผนที่ความเปราะบางต่อความเสียหายของพื้นที่ เพื่อสร้างเป็นแผนที่เสี่ยงต่อการเกิดความเสียหายขององค์ประกอบห้าประเภท คือ อาคารที่พักอาศัย ยางพารา พืชสวน พืชไร่ และนาข้าว ผลจากแผนที่ความเสี่ยงต่อความเสียหายที่ได้รับของทั้งสองกรณี แสดงให้เห็นว่ามีพื้นที่เพียงประมาณ 0.005% ซึ่งตั้งอยู่ในเขตที่มีค่าความเสี่ยงสูงถึงสูงมาก ขณะที่พื้นที่เกือบ 100% ตั้งอยู่ในเขตที่มีความเสี่ยงต่ำมากถึงต่ำ นอกจากนี้ ได้มีการสร้างแผนที่เสี่ยงภัยจากโคลนไหลกรุนแรงขึ้นมาด้วยโดยใช้แบบจำลองเชิงประจักษ์ Flow-R เพื่อกำหนดเขตเสี่ยงต่อภัยดังกล่าวสูงของพื้นที่ซึ่งพบว่าแผนที่ซึ่งได้รับจากแบบจำลองดังกล่าว มีความสอดคล้องกับหลักฐานของเหตุการณ์ที่พบบนภาพดาวเทียมความละเอียดสูงซึ่งใช้อ้างอิงเป็นอย่างดี

THIDAPATH ANUCHARN : OPTIMAL LANDSLIDE SUSCEPTIBILITY
AND RISK ANALYSES AT KHAO PHANOM BENCHA,
KRABI PROVINCE, THAILAND. THESIS ADVISOR : ASST. PROF.
SONGKOT DASANANDA, Ph.D. 344 PP.

LANDSLIDE INVENTORY / LANDSLIDE SUSCEPTIBILITY / LANDSLIDE
HAZARD / LANDSLIDE RISK / RUNOUT / KHAO PHANOM BENCHA

There are three principal objectives for this thesis work: (1) to identify optimal method for the formulation of landslide susceptibility map of the preferred study area, Khao Phanom Bencha in Krabi Province, from list of proposed candidates, (2) to develop the associated landslide hazard and risk maps for the study area through application of the optimal approach found earlier, (3) to assess landslide-induced runout hazard for the area through application of the preferred Flow-R runout model. To achieve the first objective, seven prominent methods were evaluated and compared for accuracy of the eventual output. These are, the conventional weighted linear combination (WLC), analytical hierarchy process (AHP), frequency ratio (FR), integrated FR-fuzzy, multiple logistic regression (MLR), artificial neural network (ANN), and integrated ANN-fuzzy models. In all cases, ten important contributing factors to landslide occurrence in the tropical region were utilized as input data for the generation of the susceptibility maps, i.e., elevation, slope gradient, slope aspect, slope curvature, topographic wetness index, distance from drainage, lithology, distance from lineament, soil texture and land use/land cover (LULC). The accuracy assessment were done using two different methods; the Area-Under-Curve (AUC) and the Receiver Operating Characteristic (ROC) curve analysis.

It was found that, in terms of average accuracy of the yielded maps, the four most successful methods are FR (93.98%), MLR (92.98%), FR-Fuzzy (92.84%), ANN-Fuzzy (92.47%) and while the least productive one is AHP (83.37%). Through, these top four methods are highly comparable in terms of achieved accuracy, however, FR was finally considered to be an optimal candidate regarding to its simplest and most comprehensible concept. Effects of rainfall incorporation in the construction of the preferred susceptibility map in two cases (long-term annual average and short-term 3-days accumulated) were also examined with relatively low impact evidenced (<0.5% change in average accuracy).

Landslide hazard maps were then derived based on integration of the obtained FR-based susceptibility map and rainfall probability of occurrence maps in two cases; 100 mm/day and 300 mm/3-days (assumed critical conditions for landslide initiation in the area). The classified maps of both cases indicated that only small proportion of land (< 10%) located in the high to very high hazard zone while about 80% situated in the very low to low hazard one. The landslide risk maps for five groups of the element at risk (i.e. building, para rubber, horticulture, field crop, paddy field) were then made through the integration of the produced hazard and vulnerability maps. Results in both cases indicated that just about 0.005% of the total area stayed in the high to very high risk zone while nearly 100% had very low to low risk level. In addition, the associated runout hazard map was also produced through the empirical Flow-R model to identify area at high risk from landslide-induced runout. The output map seemed to agree well with evidences seen on the reference high-resolution satellite imagery.

School of Remote Sensing

Student's Signature _____

Academic Year 2015

Advisor's Signature _____

ACKNOWLEDGEMENTS

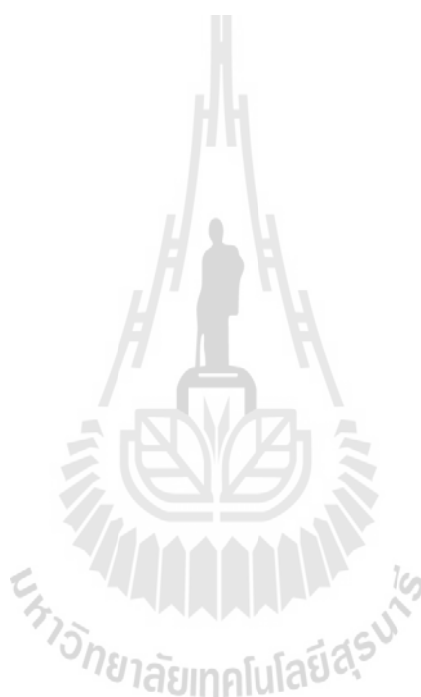
Foremost, I would like to express my sincere gratitude to my advisor, Asst. Prof. Dr. Songkot Dasananda, for his continuous support of my Ph.D. study and research with patience and enthusiasm to make this thesis completed. Apart from this, I gratefully thank all members of my thesis defense committee: Assoc. Prof. Dr. Suwit Ongsomwang (chairman), Asst. Prof. Dr. Sunya Sarapirome, Assoc. Prof. Dr. Suttisak Soralump, and Assoc. Prof. Dr. Charlie Navanugraha, for their helps and insightful comments on my thesis work.

Sincere thanks are also due to several state agencies for providing needed data in my work, i.e., Geo-Informatics and Space Technology Development Agency (GISTDA), Office of Agricultural Economics, Land Development Department, Department of Mineral Resources, Royal Irrigation Department, Royal Thai Survey Department, and the Thai Meteorological Department. Granted opportunity and scholarship from Hatyai University to support my doctoral study at SUT are also highly appreciated. In addition, contribution of the eight experts through the questionnaire responses are also gracefully acknowledged.

Similarly, I owe a debt of gratitude to many people for the willful help and warm encouragement throughout, especially, Dr. Niti Iamchuen, Dr. Satith Sangpradid, Dr. Rawee Rattanakom, Dr. Siriwan Ruamkaew, Mr. Prasert Nimman, Mr. Jangsak Onkaew, and Mr. Pornchai Salao. My heartfelt thanks also go to all friends in the School of Remote Sensing, SUT, for the productive and long-lasting friendship.

Finally, I would like to express my utmost thanks and gratefulness to my parent and family for their financial and spiritual supports on my Ph.D. education as well as for the affection and great care given to me all along.

Thidapath Anucharn



CONTENTS

	Page
ABSTRACT IN THAI.....	I
ABSTRACT IN ENGLISH	III
ACKNOWLEDGEMENTS.....	V
CONTENTS.....	VII
LIST OF TABLES	XII
LIST OF FIGURES	XVII
LIST OF ABBREVIATIONS.....	XXV
CHAPTER	
I INTRODUCTION.....	1
1.1 Problem background and significance of the study	1
1.2 Research objectives	8
1.3 Scope and limitations of the study	8
1.4 Study area.....	9
1.4.1 Location.....	9
1.4.2 Climate	9
1.4.3 Land use patterns	10
1.4.4 Landslide incidence	10
1.5 Benefits of the study.....	10

CONTENTS (Continued)

	Page
II BASIC CONCEPTS AND LITERATURE REVIEWS.....	12
2.1 Definition of landslide.....	12
2.2 Type of landslides	14
2.3 Landslide initiation mechanism	18
2.4 Principal causative factors.....	21
2.5 Concept of landslide risk analysis.....	31
2.5.1 Preparation of landslide inventory maps	36
2.5.2 Preparation of landslide susceptibility maps	39
2.5.3 Preparation of landslide hazard maps.....	44
2.5.4 Preparation of landslide risk maps	49
2.6 Relevant landslide susceptibility mapping methods	51
2.6.1 Conventional weighted linear combination (WLC).....	52
2.6.2 Analytic hierarchy process (AHP)	54
2.6.3 Frequency ratio (FR)	63
2.6.4 Logistic regression (LR).....	66
2.6.5 Artificial neural network (ANN).....	69
2.6.6 Fuzzy logic approach	72
2.7 Accuracy assessment of yielded susceptibility maps.....	78
2.7.1 The Area-Under-Curve (AUC) method	78
2.7.2 Receiver operating characteristic (ROC) curves	80

CONTENTS (Continued)

	Page
2.8 Concept of the landslide-induced runout	83
2.8.1 Algorithms for the spreading assessment.....	86
2.8.2 Runout distance assessment	88
2.9 Roles of GIS and remote sensing in landslide risk analysis.....	91
2.9.1 Applications of GIS technology	92
2.9.2 Applications of remote sensing technology	94
2.9.3 Landslide activity in Thailand.....	97
III RESEARCH METHODOLOGY.....	103
3.1 Data preparation	103
3.2 Construction of a landslide inventory map	122
3.3 Construction and verification of the landslide susceptibility maps	133
3.4 Construction of the hazard, vulnerability, and risk map	144
3.5 Construction of the runout map.....	149
IV RESULTS AND DISCUSSION.....	152
4.1 Establishment of landslide susceptibility maps	152
4.1.1 Application of the weighted linear combination (WLC) method..	153
4.1.2 Application of the analytical hierarchy process (AHP) method....	158
4.1.3 Application of the frequency ratio (FR) method	165
4.1.4 Application of the integrated FR and fuzzy logic (FR-Fuzzy method)	176

CONTENTS (Continued)

	Page
4.1.5 Application of multiple logistic regression (MLR) method	167
4.1.6 Application of artificial neural network (ANN) method	179
4.1.7 Application of the integrate ANN and fuzzy logic (ANN-Fuzzy model)	188
4.2 Comparison and Verification of the yielded susceptibility maps	196
4.2.1 Map comparison and discussion	196
4.2.2 Map validation and optimal method identification discussion	206
4.2.3 Factor sensitivity analysis	210
4.3 Effects of rainfall integration on the susceptibility analysis	213
4.4 Establishment of landslide hazard and risk maps	216
4.4.1 Construction and evaluation of the landslide hazard maps.....	216
4.4.2 Construction and evaluation of the landslide risk map.....	220
4.5 Runout hazard analysis	225
V CONCLUSION AND RECOMMENDATION	240
5.1 Landslide susceptibility maps formulation and evaluation.....	240
5.1.1 Factor priority analysis	241
5.1.2 Susceptibility map comparison and evaluation	243
5.1.3 Map accuracy assessment and optimal method identification	244
5.2 Landslide hazard and risk maps formulation and evaluation.....	245
5.3 Runout hazard zonation.....	247
5.4 Reccomendations	254

CONTENTS (Continued)

	Page
REFERENCES	256
APPENDICES	287
APPENDIX A DEFINITIONS FOR TYPICAL TERMS USED IN LANDSLIDE ZONING	288
APPENDIX B QUESTIONNAIRE AND LIST OF EXPERTS	291
APPENDIX C CONVENTIONAL WEIGHTED LINEAR COMBINATION METHOD: WLC'S FACTOR WEIGHTS AND WLC'S CLASS WEIGHTS	309
APPENDIX D THE PAIR-WISE COMPARISON METHOD: AHP'S FACTOR WEIGHTS	314
CURRICULUM VITAE.....	344



LIST OF TABLES

Table	Page
1.1 List of some past prominent landslide incidences in Thailand (data acquired from Soralump, 2007 and DMR, 2012).....	4
2.1 Major types of landslides according to Varnes (1978) (USGS, 2004).....	18
2.2 Typical landslide zoning mapping scales and the applications (AGS, 2007a)	36
2.3 Classification of well-known landslide susceptibility determination methods (Aleotti and Chowdhury, 1999, Guzzetti et al., 1999, and Kanungo et al., 2009)	42
2.4 Examples of factor weights and class weights (or rating) for input thematic layers and their attributes for the WLC method as reported in Kanungo et al. (2006)	54
2.5 Scale of preference between pair of factors in pairwise comparison process of the AHP method (Saaty and Vargas, 2001)	56
2.6 Random index (RI) given by Saaty (1980) as a function of matrix size (n). ...	60
2.7 Example of the pair-wise comparison matrix, or preference matrix, reported in Thanh and De Smedt (2012) along with the corresponding normalized eigenvector (representing factor, or attribute, weights of the analysis).....	62
2.8 Information of essential variables used in the consistency analysis reported in Thanh and De Smedt (2012)	62

LIST OF TABLES (Continued)

Table	Page
2.9 Frequency ratio (FR) index given in Vijith and Madhu (2008)	65
2.10 Example landslide susceptibility analysis using FR and logistic regression by Lee and Pradhan (2007) in Selangor, Malaysia	69
2.11a Examples of the FR-based fuzzy membership values for the respective attributes of a specific contributing factor presented in Lee (2007)	76
2.11b Examples of the FR-based fuzzy membership values for the respective attributes of a specific contributing factor presented in Bui et al. (2012)	77
2.12 Report of accuracy scales for used fuzzy logic operators in Lee (2007)	78
2.13 Contingency table for ROC curve analysis method	81
2.14 Symbol description of ROC curves on landslide prediction issue	82
2.15 Implemented weightings of the persistence function in the assessment of the flow spreading	88
3.1 List of necessary data and their respective sources	105
3.2 Lithological description of Krabi Province (DMR)	119
3.3 Proportion of land for each type of the input factor	121
3.4 Statistics of rainfall at the nearby rainfall station (data for 1951-2012)	140
3.5a List of rainfall stations in Krabi Province and their annual mean of rainfall .	140
3.5b Statistics of monthly mean rainfall of Krabi Province at the listed stations ..	141
3.6 Statistics of rainfall during 2011 landslide event (data for 27th-29th March)	141

LIST OF TABLES (Continued)

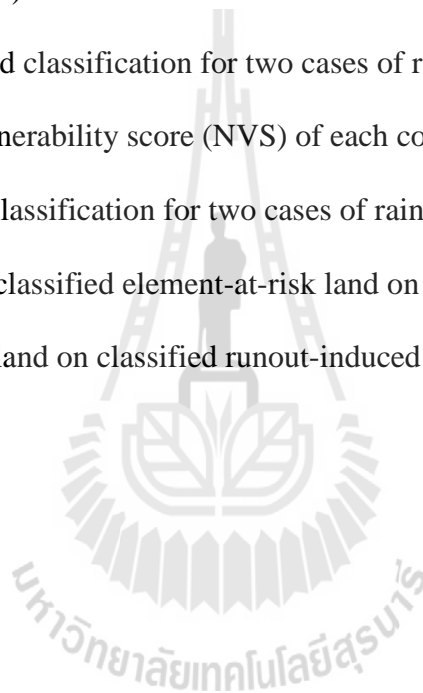
Table	Page
3.7a Statistics of annual rainfall probability at measuring stations in Krabi Province.....	145
3.7b Statistics of return period for maximum rainfall at measuring stations in Krabi Province	146
4.1 Expert-based factor and class (attribute) weights for the WLC method.....	154
4.2 Landslide susceptibility classification of land based on the WLC method....	156
4.3 Factor weights from pair-wise comparison matrix yielded from 8 experts ...	159
4.4 Class weights from pair-wise comparison matrix based on expert opinions .	160
4.5 Factor and class (attribute) weights of all input factors from the AHP method.....	162
4.6 Landslide susceptibility classification of land based on the AHP method	163
4.7 Frequency ratio (FR) and associated membership value (MV) in fuzzy logic	166
4.8 Landslide susceptibility classification of land based on the FR method.....	167
4.9 Achieved map accuracies of the considered fuzzy operators (FR-Fuzzy)	170
4.10 Landslide susceptibility classification of land (FR-Fuzzy method: $\lambda = 0.90$)	175
4.11 Coefficients of each input parameter in the MLR and ANN methods.....	175
4.12 Landslide susceptibility classification of land based on the MLR method....	177
4.13a Input-hidden-output connection weights (ANN method)	182

LIST OF TABLES (Continued)

Table	Page
4.13b Connection weight products (WP) for each input layer and their associated absolute weight (AW) (ANN method).....	184
4.13c Normalized weight (NW) data for each input attribute layer based on the known absolute weight (AW) (ANN method).	186
4.14 Landslide susceptibility classification of land based on the ANN method) ..	188
4.15 Membership values at attribute level in the ANN-Fuzzy method.....	189
4.16 Achieved map accuracies of the considered fuzzy operators (ANN-Fuzzy) .	191
4.17 Landslide susceptibility classification for the ANN-Fuzzy method ($\lambda = 0.90$).....	191
4.18 Landslide susceptibility classification of land for all examined methods.....	203
4.19 Correlation level (r) of the NSS data among all examined methods.....	204
4.20 Accuracy outcome in case of the sensitivity analysis for each used factor....	211
4.21 Accuracy outcome in case of the factor-preferred map formulation	211
4.22 FR values for the listed rainfall attributes in both cases	214
4.23a FR-based landslide susceptibility classification with the long-term annual mean rainfall data during 1951-2012 over the area integrated.....	214
4.23b FR-based landslide susceptibility classification with event-based rainfall data during 27th-29th March 2011 over the area integrated	214

LIST OF TABLES (Continued)

Table		Page
4.24	Comparison of area allocation on three FR-based susceptibility maps under consideration (original, with rainfall data integrated-long-term case, event-based case).....	215
4.25	Landslide hazard classification for two cases of rainfall critical thresholds..	220
4.26	Normalized vulnerability score (NVS) of each considered element at risk...	221
4.27	Landslide risk classification for two cases of rainfall critical thresholds	224
4.28	Distribution of classified element-at-risk land on the derived risk map	224
4.29	Distribution of land on classified runout-induced hazard map	226



LIST OF FIGURES

Figure	Page
1.1 Massive landslide activity at Nam Ko Yai village in Phetchabun Province due to the prolonged heavy rainfall in August 2001 (Yumuang, 2006).....	4
1.2 Photographs of landslide evidences seen within the study area.....	5
1.3 Photos of landslide runout over flat downstream zone in the study area.....	6
1.4 Location map of the study area (Khao Phanom Bencha Watershed).....	11
2.1 Principal components of (a) general landslide and (b) typical debris flow (Witt, 2005; NCGS, 2012)	13
2.2 Major types of landslide according to Varnes (1978) (AGS, 2007)	17
2.3 Diagrams showing geometry of the assumed infinite-slope stability model (SINMAP) and parameters seen in Eq. 2.2 (Deb and Kadi, 2009)	20
2.4 Landslide mechanisms due to road construction (van Westen, 2013)	24
2.5 Visual representation of plan curvature and profile curvature	29
2.6 Three fundamental types of (a) profile and (b) plan, or contour, curvature which are convex, concave and flat (or uniform) used in (+/- signs are as ArcGIS10).....	29
2.7 General conceptual framework for landslide risk analysis and management (Dai et al., 2002)	34
2.8 Main aspects of risk analysis process (van Westen et al., 2006)	34
2.9 Example of the landslide inventory map.....	38

LIST OF FIGURES (Continued)

Figure	Page
2.10 Typical found relationship of the magnitude-frequency relation observed in landslide inventories. Magnitude often displays in terms of landslide size (e.g. km ²) while frequency (non-cumulative) usually reports based on number of events per year	47
2.11 Relationship of daily rainfall at failure and antecedent rainfall in Korea (Kim, Hong, and Kim, 1992)	49
2.12 Conceptual relationship between hazard, elements at risk, vulnerability and risk (Alexander, 2002).....	50
2.13 Flow diagram for the landslide susceptibility assessment procedure using the conventional weighted linear combination method (Kanungo et al., 2006).....	53
2.14 A hierarchical structure of the analytic hierarchy process method (AHP) (Cortes, Serna, and Martinez, 2012).....	55
2.15 Typical ANN architecture for landslide classification (Yilmaz, 2009)	71
2.16 Typical ANN work flowchart for landslide susceptibility classification comprising of two steps; training and classifying (Kanungo et al., 2006).....	72
2.17 Example of the fuzzy set and its complement with the membership values of 0 to 100% (for “cool” and “not cool” conditions) (Fano, 2011)	74

LIST OF FIGURES (Continued)

Figure	Page
2.18 Graph showing an example of the combination of three fuzzy factors ($\mu_A = 0.8$, $\mu_B = 0.6$, $\mu_C = 0.4$) by fuzzy-gamma operation	77
2.19 Examples of the cumulative frequency diagram in AUC method showing landslide susceptibility index rank (x-axis) in relation to the cumulative percent of landslide occurrence (y-axis) (Intarawichian and Dasananda, 2011).....	80
2.20 Example of contingency tables for different values (cut off) of membership probability of a landslide susceptibility discriminant model (SafeLand - FP7, 2011).	83
2.21 Conceptual diagram of Flow-R.....	85
2.22 Illustration of the spreading of susceptibility value to the neighboring cells...	86
2.23 Illustration of the travel angle and the velocity limitation of the simplified friction-limited model (SFLM)	91
2.24 Examples of the geographic input data (vector/raster types) for the GIS operation (Schuurman 2004; NOAA, 2013).....	92
2.25 Satellite image of the 2011 landslide traces in Krabi Province, southern Thailand from the NASA-Advanced Land Imager (ALI) sensor aboard EO-1 satellite.....	95
2.26 Classified landslide susceptibility maps prepared by the DMR and GERD using equal-interval classification technique	100

LIST OF FIGURES (Continued)

Figure	Page
2.27 TRMM map of accumulated rainfall data over southern Thailand during period of 23th-30th March 2011	101
3.1 Conclusive work flowchart	104
3.2a Elevation map of the study area based on DEM data from topographic map of 1:50,000 scale	106
3.2b Slope gradient map of the study area based on DEM data from topographic map of 1:50,000 scale	107
3.2c Slope aspect map of the study area based on DEM data from topographic map of 1:50,000 scale	108
3.2d Slope curvature map of the study area based on Slope from topographic map of 1:50,000 scale	109
3.2e Topographic wetness index (TWI) map of the study area based on the slope and water accumulation data from the topographic map of 1:50,000 scale	110
3.2f Distance-from-drainage map of the study area based on DEM data from the topographic map of 1:50,000 scale	111
3.2g Distance from lineament map of the study area (at 1:250,000 scale)	112
3.2h Lithology map of the study area at 1:250,000 scale.....	113
3.2i Soil texture map of the study area modified from LDD soil data (soil series, plasticity, and depth) at 1:100,000 scale	114

LIST OF FIGURES (Continued)

Figure	Page
3.2j LULC map of the study area in 2009 modified from the original LDD data at 1:25,000 scale	115
3.2k Soil texture pyramid chart	118
3.3 Work flowchart of the landslide inventory mapping process	122
3.4 Examples of the high-resolution satellite images from four different sources; (a) THEOS satellite, (b) EO-1 satellite, (c) Google Earth website, (d) Bing Map website, showing landslide traces over the study area (from the incidence in late March 2011).....	124
3.5 Different characteristics between fresh and old landslide scars as shown on the THEOS satellite imagery	125
3.6 Examples of the derived landslide inventory map of the area	126
3.7 Location map of the 700 identified landslide incidences in the study area...	130
3.8 Examples of photos taken during the field survey of the study area in which evidences of landslide occurrences over the mountain's terrain are clearly visible	131
3.9 Work flowchart for the construction and verification of the susceptibility maps to find the optimal method for further application in subsequent work	132
3.10 Location map of the applied rainfall stations for (a) during 27th-29th March 2011 and (b) long-term average for the period 1951-2012 in this work	142

LIST OF FIGURES (Continued)

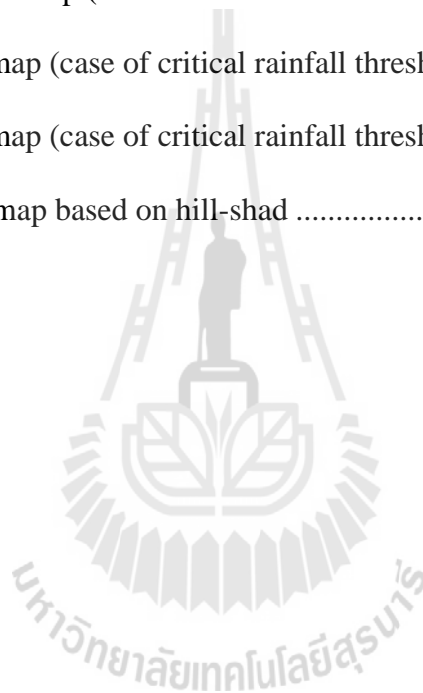
Figure	Page
3.11 Representative rainfall maps of the area for (a) during 27th-29th March 2011 and (b) long-term average for the period 1951-2012.....	143
3.12 Annual rainfall probability maps of the area for (a) 100 mm/day and (b) 300 mm/3-days	147
3.13 Element at risk maps for (a) building and (b) LULC.....	148
3.14 Flowchart of the runout analysis work.....	150
3.15 Example of the main user interface of the Flow-R model	151
4.1 Classified landslide susceptibility map yielded from the WLC method.....	157
4.2 Classified landslide susceptibility map yielded from the AHP method.....	164
4.3 Classified landslide susceptibility map yielded from the FR method.....	168
4.4 Classified landslide susceptibility map yielded from the FR-Fuzzy method.	171
4.5 Classified landslide susceptibility map yielded from the MLR method	178
4.6 Classified landslide susceptibility map yielded from the ANN method	187
4.7 Classified landslide susceptibility map from the ANN-Fuzzy method.....	192
4.8 Classified landslide susceptibility map based on all examined methods	197
4.9 NSS histograms of all derived susceptibility maps presented in Figure 4.8..	199
4.10 Proportion of land on classified susceptibility maps for all used methods. ...	204
4.11 Comparative illustration of accuracies achieved by all examined methods...	206
4.12 Graphic illustrations of the accuracy quantification by all three considered cases: (a) AUC-success rate, (b) AUC-predictive rate, and (c) ROC	207

LIST OF FIGURES (Continued)

Figure	Page
4.13 FR-based output maps form different combination of input factors	212
4.14 FR-based classified landslide susceptibility maps in two cases of rainfall data integration (long-term annual mean and event-based data)	215
4.15 Comparison of accuracies achieved from the three FR-based susceptibility maps (original, with rainfall data integrated-long-term case, event-based case).....	216
4.16a Landslide hazard map (case of critical rainfall threshold 100 mm/day)	218
4.16b Landslide hazard map (case of critical rainfall threshold 300 mm/3-days) ...	219
4.17 Normalized vulnerability score map of all examined element at risks	221
4.18a Landslide risk map (case of critical rainfall threshold 100 mm/day).....	222
4.18b Landslide risk map (case of critical rainfall threshold 300 mm/3-days).....	223
4.19 Runout hazard map based on hill-shad showing qualitative information on the runout spreading probabilities by the Flow-R model.....	228
4.20a A closer look over some specific parts on the yielded runout hazard map of the area (subdistrict-level).....	229
4.20b A case of Nakhao subdistrict.....	230
4.20c A case of Nakhao subdistrict	232
4.20d A case of Thapprik and Klonghin subdistrict.....	234
4.20e A case of Khophanom subdistrict	237
4.20f A case of Krabinoi subdistrict.....	239

LIST OF FIGURES (Continued)

Figure	Page
5.1 Landslide susceptibility map from the FR method	248
5.2 Landslide hazard map (case of critical rainfall threshold 100 mm/day).	249
5.3 Landslide hazard map (case of critical rainfall threshold 300 mm/3-days) ...	250
5.4 Landslide risk map (case of critical rainfall threshold 100 mm/day).....	251
5.5 Landslide risk map (case of critical rainfall threshold 300 mm/3-days).....	252
5.6 Runout hazard map based on hill-shad	253



LIST OF ABBREVIATIONS

AHP	=	Analytical Hierarchy Process
ANN	=	Artificial Neural Network
ARP	=	Annual Rainfall Probability
AUC	=	Area Under Curve
AW	=	Absolute Weight
CI	=	Consistency Index
CR	=	Consistency Ratio
CW	=	Class Weight
DDPR	=	Department of Disaster Prevention and Mitigation
DEM	=	Digital Elevation Model
DMR	=	Department of Mineral Resources
DWR	=	Department of Water Resources
FR	=	Frequency Ratio
FS	=	Factor of Safety
FW	=	Factor Weight
GERD	=	Geotechnical Engineering Research and Development Center
GIS	=	Geographic Information System
GISTDA	=	Geo-Informatics and Space Technology Development Agency
HI	=	Hazard Index
HH	=	High Hazard

LIST OF ABBREVIATIONS (Continued)

HR	=	High Risk
HS	=	High Susceptibility
LDD	=	Land Development Department
LHZ	=	Landslide Hazard Zoning
LR	=	Low Risk
LRZ	=	Landslide Risk Zoning
LS	=	Low Susceptibility
LH	=	Low Hazard
LSI	=	Landslide Susceptibility Index
LSS	=	Landslide Susceptibility Score
LSZ	=	Landslide Susceptibility Zoning
LULC	=	Land use and Land Cover
MH	=	Moderate Hazard
MLR	=	Multiple Logistic regression
MOAC	=	Ministry of Agriculture and Cooperatives
MR	=	Moderate Risk
MS	=	Moderate Susceptibility
NCW	=	Net Contributing Weight
NDVI	=	Normalized Differential Vegetation Index
NESDB	=	Office of the National Economic and Social Development Board
NSI	=	Normalized Susceptibility Index

LIST OF ABBREVIATIONS (Continued)

NSS	=	Normalized Susceptibility Score
NVS	=	Normalized Vulnerability Score
NW	=	Normalized Weight
RI	=	Random Index
RID	=	Royal Irrigation Department
RkI	=	Risk Index
RS	=	Runout Susceptibility
ROC	=	Receiver Operating Characteristic
RTSD	=	Royal Thai Survey Department
SAW	=	Simple Additive Weighting
SPI	=	Stream Power Index
TMD	=	Thai Meteorological Department
TRMM	=	Tropical Rainfall Measuring Mission
TWI	=	Topographic Wetness Index
VHH	=	Very High Hazard
VHR	=	Very High Risk
VHS	=	Very High Susceptibility
VLS	=	Very Low Susceptibility
VLH	=	Very Low Hazard
WLC	=	Weighted Linear Combination
VLR	=	Very Low Risk

LIST OF ABBREVIATIONS (Continued)

WoE = Weight of Evidence



CHAPTER I

INTRODUCTION

1.1 Problem background and significance of the study

Landslide is a well-known natural phenomenon involving a mass movement of soil (in forms of earth or debris) or rock downward along the slope under gravitational influence (Varnes, 1984; Cruden, 1991). At present, it has been regarded as being one of the most destructive hazards which causes substantial loss of life and great damage to property and natural environment worldwide (Dilley, Chen and Deichmann, 2005; Petley, 2012). Therefore, prior knowledge of the areas prone to substantial landslide is highly essential to most countries, especially those situated in tropical region, to help preparing proper strategies for effective prevention or mitigation of potential landslide occurrences or their associated risk. Conventionally, a detailed map illustrating spatial distribution of these landslide-prone areas is called a landslide susceptibility map.

Attention on the identification of landslide prone areas (or susceptibility analysis) and the assessment of its potential impacts on human and environment (risk analysis) has been risen dramatically in recent decades due to mounting public concern on these issues. And, as validity of a derived landslide susceptibility map depends principally on the used methods and their input data, comparative study to evaluate efficiency of several recommended methods in the preparation of landslide susceptibility maps for an area of interest was reported more often in recent years, such

as, in Yilmaz (2009); Choi, Oh, Lee, Lee, and Lee (2012); Xu, Xu, Dai, and Saraf (2012); and Park, Choi, Kim, and Kim (2013). Main objectives of these studies are to identify capability and of the evaluated methods in generating a satisfied landslide susceptibility map for the preferred area from which most effective procedure can then be identified for further use in the subsequent hazard and risk analysis afterwards.

In Thailand, landslide has also become constant threat to large number of people residing in mountainous region, especially those located in the northern and southern parts. Prominent landslide events normally occur during monsoon months of May to early October for most parts of the country due to high influence of the heavy rainfall over a susceptible area. However, an exception was evidenced for major landslides on eastern side of southern Thailand which usually took place during local rainy months of October to January. For examples, in August 2001, strong flashflood and disastrous landslide (in the form of debris flow) struck a remote village in Phetchabun Province at night which led to at least 136 deaths and more than 5 million US dollars in damage of property (Figure 1.1) (Yumuang, 2006). In May 2006, similar incidences occurred in Uttaradit, Phrae and Sukhothai Province resulted in 87 deaths and damages of more than 10 million US dollars (Asian Disaster Preparedness Center, 2006). List of some past notable landslide incidences is summarized in Table 1.1.

Through, imminent impact of landslide phenomenon to people and environment situating within the landslide-prone area is well acknowledged in Thailand at present, however, publications of research work on this issue are still relatively infrequent and mostly attributed to the preparation of landslide susceptibility maps by a single chosen method in which a validation process of the derived map was often ignored. However,

development of the associated landslide risk map was rarely found (e.g. in Tanavud, Yongchalermpchai, Bennui and Navanugraha, 2000; Soralump and Kulsuwan, 2006).

Therefore, to broaden traditional scope of the research on landslide susceptibility mapping and landslide risk analysis in Thailand, this thesis shall conduct comparative efficiency assessment for several widely-acknowledged methods in the formulation of landslide susceptibility maps for a concerned area from which the optimum algorithm shall be identified by the attained accuracy of their output maps along with associated benefits from their applications. This preferred methodology shall be then applied to build the landslide susceptibility maps for the entire area which are used as a basis for generating the associated landslide hazard and risk maps afterwards.

The area of interest in this study is the Khao Phanom Bencha Watershed in Krabi Province which experienced several devastated landslide incidences in recent decades (Figures 1.2 and 1.3). As mentioned earlier, this area was selected as case study based on previous reports of the expansive landslide activity found therein due to its rather rough mountainous landscape and fairly high amount of annual rainfall (DMR, 2011). Rapid changes in land use of the area due to continuous conversion of the forest lands into several kinds of economic agricultural plantations (e.g. para rubber and oil palm) and communities into the known landslide-prone locations have also become a cause for high public concern in recent years. This is because forest clearance for expansive plantations of the shallow-rooted crops, orchards, or trees, might enable more frequent appearances of massive landslide incidence with greater losses of human lives or high amount of the gross damages to the important infrastructures and natural environment (Tanavud et al., 2000; Soralump, 2010a).



Figure 1.1 Massive landslide runout at Nam Ko Yai village in Phetchabun Province due to the prolonged heavy rainfall in August 2001 (Yumuang, 2006).

Table 1.1 List of some past prominent landslide incidences in Thailand (data acquired from Soralump, 2007 and DMR, 2012).

Date	Place	Losses
November 22, 1988	Phipun/LanSaka District, Nakhon Si Thammarat	242 deaths; 1,612 houses destroyed
September 11, 2000	Lomsak/Muang District, Petchaboon	10 deaths
May 4, 2001	Wang Chin District, Phrae	43 deaths; 18 houses destroyed
August 11, 2001	Lomsak District, Petchaboon	136 deaths, 188 houses destroyed
October 18, 2004	Mueang District, Krabi	3 deaths; 25 houses destroyed
May 22, 2006	Tha Pla/Lablae/Mueang District, Uttaradit	75 deaths; 483 houses destroyed
November 6, 2009	Si Sakhon District, Narathiwat	10 deaths; 3 houses destroyed
March 30, 2011	Khao Phanom District, Krabi	10 deaths; many houses destroyed
August 3, 2011	Sop Moei District, Mae Hong Son	9 deaths; many houses destroyed
September 9, 2011	Nam Pat District, Uttaradit	6 deaths; > 50 houses destroyed



Source: DMR, <http://www.krobkruakao.com>, <http://www.oknation.net>

Figure 1.2 Photographs of landslide evidences seen within the study area.



Source: DMR, <http://www.oknation.net>

Figure 1.3 Photos of landslide runout over flat downstream zone in the study area.

In this research, seven different methods are primarily chosen for conducting the landslide susceptibility assessment and susceptibility map formation for the study area based on their widely-acknowledged merit and apparently distinct working concepts. These are the conventional weighted linear combination (WLC), analytical hierarchy process (AHP), frequency ratio (FR), integrated FR-fuzzy, multiple logistic regression (MLR), artificial neural network (ANN), and integrated ANN-fuzzy models. Among these, the first two methods (WLC and AHP) are of the qualitative type, conceptually, while the rest are of quantitative type. Here, concept of fuzzy logic is to be integrated to the FR and ANN models to evaluate its capability to improve mapping accuracy of these referred methods. In risk analysis part, the associated hazard maps (developed from susceptibility map of the identified optimal method) and corresponding landslide risk maps are prepared from which main interest of the analysis is on apparent impact of mapped landslide incidences to economic activities (crop plantation) and buildings or infrastructure within the area, in particular.

It is hoped that results gained from this study can provide better understanding on efficiency of the evaluated methods for landslide susceptibility mapping of the studied area. The preferred optimal candidate can then be implemented to formulate credible susceptibility maps along with the associated hazard and risk maps that can be used to support formulation of fruitful strategic planning on the prevention and mitigation of landslide occurrence and risk in the area by responsible agencies and local authorities. Knowledge on relationship of land use pattern and landslide activity within the area is also essential for issuing proper land use control in the near future.

1.2 Research objectives

Principal objectives of the thesis are as follows:

1.2.1 To identify optimal method for the formulation of landslide susceptibility map for the study area from a list of proposed candidates,

1.2.2 To develop the associated landslide hazard and risk maps for the study area through application of the optimal approach found earlier,

1.2.3 To assess landslide-induced runout hazard for the area through application of the preferred Flow-R runout model.

1.3 Scope and limitations of the study

Scope and limitations of this study can be summarized as follows:

1.3.1 Susceptibility, hazard, and risk maps are prepared for the landslide activity in general, not for a particular type of the landslide phenomenon existing in the area. In addition, all observed landslide traces were included in the analysis regardless of their original dates of formation (old or new scars).

1.3.2 The location-based nature of landslide occurrence, difficulty in identifying proper causative factors for mapped landslide activities, and lack of known data about past landslide occurrences over the area.

1.3.3 Lack of measured rainfall data due to limited amount of rain-measurement stations existing within the study area and its vicinity might lead to the less realistic of the interpolated rainfall maps. Similarly, lack of fine detailed land characteristics within the defined slope complex areas might also make this study less fruitful.

1.3.4 Differences in original scale of the input data maps might make the analysis less credible and appropriate rescaling might be required as appropriate.

1.4 Study area

1.4.1 Location

The preferred area is the Khao Phanom Bencha Watershed, Krabi Province, on the Andaman Coast of southern Thailand covering area of about 987.53 km². This is the mountainous region with highest elevation of 1,400 meter above mean sea level. The watershed territory is surrounding the central mountain network that aligns along the north-south direction, approximately, comprising parts of five nearby districts and several sub-districts, i.e., (1) Plai Phraya District (Plai Phraya, Khao Khen and Khiri Wong Sub-district), (2) Ao Luk District (Na Nuea, Khlong Hin, Ao Luk Nuea, Khao Yai, Khlong Ya and Ban Klang Sub-district), (3) Khao Phanom District (Khao Phanom, Khao Din and Na Khao Sub-district), (4) Mueang District (Krabi Noi, Khao Khram, Khao Thong, Thap Prik, Sai Thai Sub-district), (5) Mueang municipality, and (6) Nuea Khlong District (Nuea Khlong and Huai Yung Sub-district) (Figure 1.4).

1.4.2 Climate

Due to strong influence of tropical monsoons on both sides (i.e., northeast monsoon on the Gulf-of-Thailand side and southwest monsoon on the Andaman side), only two dominant seasons exist in this area; dry season (from January to April) and wet season (from May to December). Temperatures range is between 17-37°C.

1.4.3 Land use patterns

Land use (LU) in 2009 was dominated by just two LU categories: economic agricultural plantations (para rubber and oil palm, in particular) and dense forest area whose land proportions are as follows; oil palms (44.36%), para rubber (25.94%), and dense evergreen forest (23.83%) (Figure 3.2j)

1.4.4 Landslide incidence

Main focus is on the case of tragic landslide incidence taken place in Khao Phanom Bencha Watershed due to unusual heavy rainfall during 27-31th March 2011 which led to several deaths and expansive damage to the properties and infrastructures within the area (Figure 1.3).

1.5 Benefits of the study

1.5.1 Knowledge on the comparative efficiency of all incorporated methods and the optimal candidate for producing landslide susceptibility map of the study area.

1.5.2 Credential landslide susceptibility, hazard and risk maps of the area that can provide better understanding on landslide activity along with its potential impact over the area to aid effective warning, prevention and mitigating of future landslide hazard.

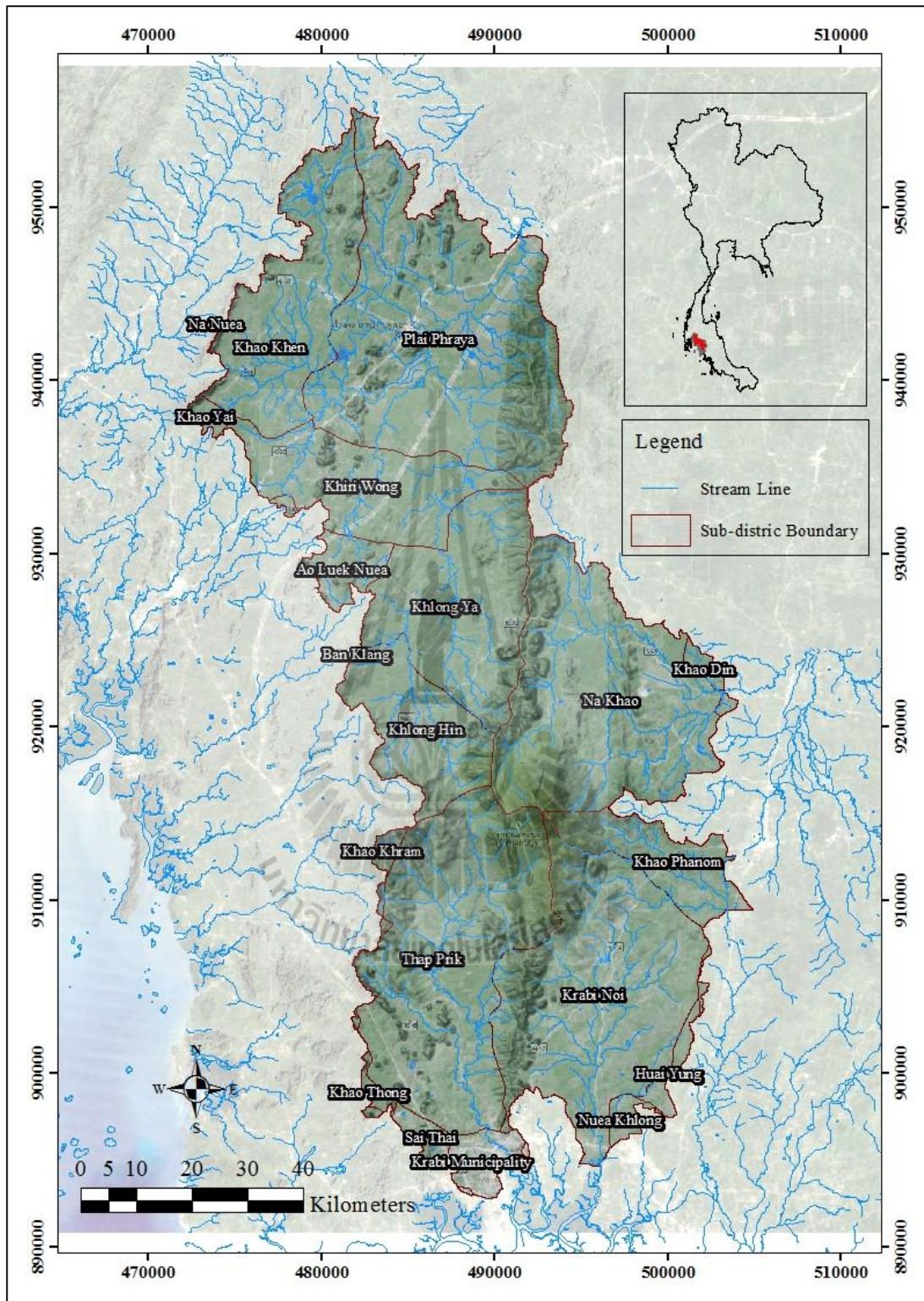


Figure 1.4 Location map of the study area (Khao Phanom Bencha Watershed).

CHAPTER II

BASIC CONCEPTS AND LITERATURE REVIEW

Basic concepts and relevant literatures are here reviewed in this chapter including (1) definition of landslide, (2) type of landslides, (3) landslide initiation mechanism, (4) principal causative factors, (5) concept of landslide risk analysis, (6) relevant landslide susceptibility mapping methods, (7) validation of the model application results, (8) the runout concepts, and (9) roles of GIS and remote sensing in landslide risk analysis.

2.1 Definition of landslide

Landslide is conventionally defined as a mass movement of soil (in forms of earth or debris) or rock downward along surface slope under gravitational influence (Varnes, 1984; Cruden, 1991). At present, it has become vital hazard in most mountainous and hilly areas around the world especially those in the tropics and earthquake-influenced zones, as well as areas along the considerably steep river bank or coastline. Landslide impacts depend fundamentally on their size and speed (or momentum), elements at risk within their paths and vulnerability condition of those elements. Every year, landslide incidences have generated large number of deaths and injuries to the at-risk people and substantial damages to the infrastructures (e.g. road,

railway, pipeline) and properties (e.g. building, agricultural land) (European Soil Portal, 2013).

Landslide phenomenon is conceptually a direct product of slope instability due to the gravitation as when the gravitational stresses exceed the strength of rock or soil that holds the surface soil layer together, slope failure shall often occur as a consequence. Most landslides are initiated by some triggering factors that shall increase stress and weaken strength of slope materials which include: (1) heavy rainfall, rapid snowmelt, or irrigation that load slopes with water, (2) shaking by earthquake, (3) natural erosion or human activities that increase slope angles or undercut the toes of surface slopes, e.g. road construction, (4) removal of the vegetation cover on land surface by, e.g. wildfire, logging, agriculture, or overgrazing, and (5) loading of slopes with huge piles of rock, ore, or mining waste (Idaho Geological Survey, 2013). Among these factors, the most predominant ones around the world are two natural processes; heavy rainfall and strong earthquake (Corominas and Moya, 2008).

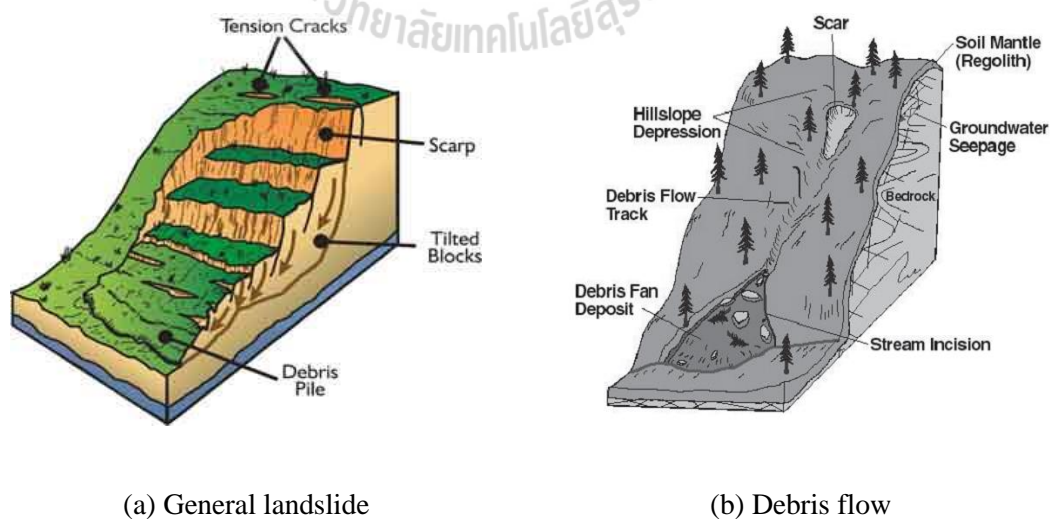


Figure 2.1 Principal components of (a) general landslide and (b) typical debris flow (Witt, 2005; NCGS, 2012).

Figure 2.1(a) illustrates principal components of the general landslide structure which include tension cracks that appear when land is gradually pulling apart from the hillside. With time, the ground surface on one side of these cracks may slide downhill forming a scarp and if the ground moves far enough, it shall leave an apparent mark called a scar. Typically, a fresh scar often has lighter color without vegetation cover if compared to the surrounding slopes. Landslide volume can vary greatly from less than a cubic kilometer (km^3) for the small and medium-size landslides to more than tens of cubic kilometers for the gigantic ones while speed might vary from a few centimeters per year for the slow-moving slides to several tens of kilometers per hour for the fast and destructive ones (Highland and Bobrowsky, 2008; European Soil Portal, 2013). Typically, the most destructive landslide incidences are often in form of the debris or mud flows as seen in Figure 2.1(b). These flows usually have rather rapid movement with combination volume of loose soil, rock, organic matter, air, and water mixed in the intense surface-water flow due to heavy precipitation or snow-melt.

2.2 Types of landslides

Landslides can be broadly classified into two fundamental categories: shallow type and deep-seated type. Shallow landslides normally involve sudden fail of top soil layer and upper regolith zone while deep-seated ones additionally include bedrock at higher depth and gradually develop over a relatively longer time period. Most natural shallow landslides are triggered by prolonged heavy rainfall that critically increase soil water pressure or accelerated ground due to earthquakes at tectonic fault nearby. Most deep-seated landslides tend to fail incrementally, rather than in the catastrophic manner of the shallow landslide. Their major causes are accumulated rainfall over a long period

(e.g. weeks to years) and also massive ground acceleration experienced during large magnitude earthquakes. The latter is commonly found in the seismically active regions around the world (NMFS, 2012).

Standard classification scheme of the existing landslide types has been developed based principally on work of Varnes (1978). In this system, landslides are categorized based on basis of their predominant composed material type (i.e., rock, debris, earth, or mud) in the first term and their movement type (i.e., fall, topple, avalanche, slide, flow, or spread) in the second term. Thus, the landslides can be identified using these terms that refer respectively to their major material and movement mode, e.g. rock fall, debris flow, earth slide, and so forth. In general, the material in landslide mass is either rock or soil (or both); the latter is described as “earth” if mainly composed of the sand-sized or finer particles (with $\geq 80\%$ of the particles are < 2 mm) and “debris” if composed of coarser fragments (with 20% to 80% of known particles are > 2 mm and the remainder are < 2 mm). Figure 2.2 and Table 2.1 provide information on dominant landslide types according to Varnes (1978) mentioned earlier (USGS, 2004; AGS, 2007b).

From Figure 2.2, slides consist of blocks of material moving on well-defined shear planes and there is a distinct zone of weakness that separates slide material from more stable underlying material. These are divided into the rotational slides that move along concave surface and translational slides that often move parallel to the referred ground surface. Falls are the sudden release of rocks or soils dropping freely through the air with little contact with other surfaces until impact. Topples are similar to falls except that initial movement involves forward rotation of the associated mass. Lateral spreads occur when liquefaction in underlying materials causes surface rocks or soils

to move down gentle slopes. Flows move entirely by shearing within the transported mass and act like viscous fluids. They consist of five kinds:

(1) Debris flow-a fast moving landslide in form of liquefied material of mixed and unconsolidated water and debris [as illustrated in Figure 2.1(b)].

(2) Debris avalanche-a variety of very rapid to extremely rapid debris flow.

(3) Earth flow-movement of slope material that liquefies and runs out forming a bowl or depression at the head and have a characteristic of “hourglass” shape.

(4) Mudflow-an earth flow consisting of the material wet enough to flow rapidly and contains at least 50% sand, silt, and clay-sized particles. In some cases, mudflows and debris flows are commonly referred to as “mudslides”.

(5) Creep-a slow, steady downward movement of slope-forming soil or rock.

The movement is called complex landslide if it involves combination of two or more types of the integrated movement. Debris flow and mudflow are among the most dangerous landslide-related incidences to life and property of the affected community, especially those in the tropical countries, due to the high speeds and sheer destructive force of their flow (USGS, 2004; AGS, 2007b).

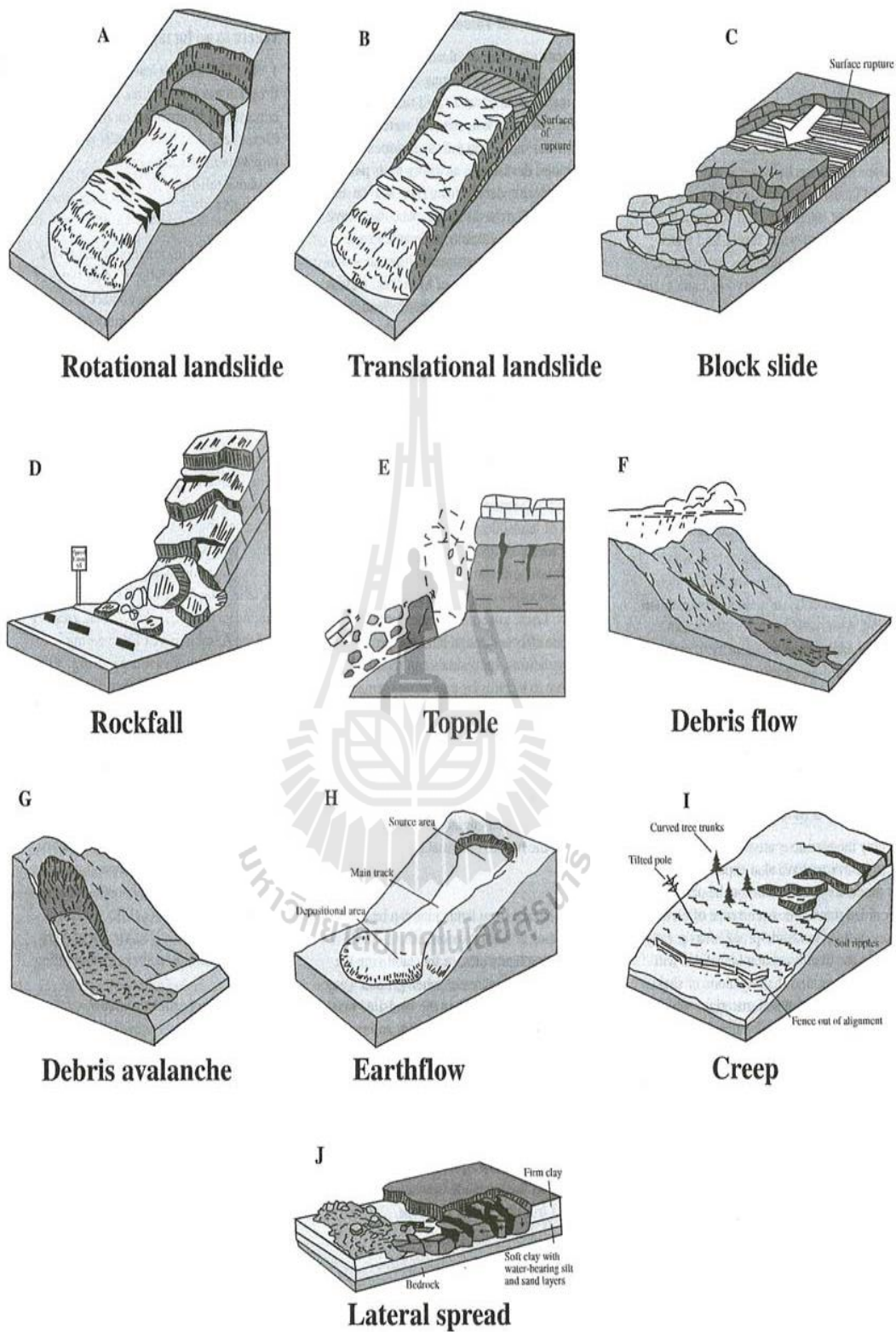


Figure 2.2 Major types of landslide according to Varnes (1978) (AGS, 2007b).

Table 2.1 Major types of landslides according to Varnes (1978) (USGS, 2004).

Type of Movement	Type of Material		
	Bedrock	Engineering Soils	
		Predominantly coarse	Predominantly fine
FALLS	Rock fall	Debris fall	Earth fall
TOPPLES	Rock topple	Debris topple	Earth topple
SLIDES ROTATIONAL TRANSLATIONAL	Rock slide	Debris slide	Earth slide
LATERAL SPREADS	Rock spread	Debris spread	Earth spread
FLOWS	Rock flow (deep creep)	Debris flow (soil creep)	Earth flow
COMPLEX	Combination of two or more principal types of movement		

2.3 Landslide initiation mechanism

As stated earlier, landslide incidence is a direct product of the slope instability due to gravitation. Theoretically, this phenomenon shall occur when the driving force (from gravity) overcomes the resisting force within the slope (from strength, or cohesion, of vegetation roots/slope materials and surface friction) which results in slope failure and landslide initiation. To quantify stability level of a particular slope, a widely-used index called the “factor of safety” (FS), or “safety factor” (SF), was introduced to support engineering purpose based on the following definition:

$$FS = \frac{\text{Resisting force (shear strength)}}{\text{Driving force (shear stress)}} = \frac{\text{cohesion (soil/root)} + \text{friction}}{\text{gravity force on tangent direction}} \quad (2.1)$$

In principle, areas with $FS > 1$ are considered safe for landslide activity as the slope is in a stable state while those with $FS < 1$ are believed to be prone to landslide

initiation as the slope is now considered as unstable (De Blasio, 2011). Normally, the FS values of 1.2-1.5 might be needed to support safe engineering construction on a natural slope (Hong Kong Geotechnical Engineering Office, 2000).

To determine slope instability level in terms of the FS parameter, the infinite-slope stability analysis is normally applied. In this situation, the studied landslides are assumed to be infinitely long, with depth of the failure surfaces is small compared to their length and width, and are destabilized by expansive areas of positive pore-water pressure (Gorsevski, Gessler, Boll, Elliot and Foltz, 2006; Godt et al., 2008). Several models were developed based on this assumption from which the widely-used one is called “SINMAP” (Stability INdex MAPping). SINMAP used infinite-slope stability model to balance destabilizing components of the gravitation against stabilizing parts of friction and cohesion on a failure plane parallel to ground surface. The safety factor (SF) is defined by ratio of the stabilizing forces (shear strength) to destabilizing forces (shear stress) on a failure plane parallel to the surface (Deb and Kadi, 2009):

$$SF = \frac{C_r + C_s + \cos^2 \theta [\rho_s g (D - D_w) + (\rho_s g - \rho_w g) D_w] \tan \phi}{D \rho_s g \sin \theta \cos \theta}, \quad (2.2)$$

where C_r is root cohesion (N/m^2), C_s is soil cohesion (N/m^2), θ is slope angle ($^\circ$), ρ_s is wet soil density (kg/m^3), ρ_w is density of water (kg/m^3), g is gravitational acceleration (9.81 m/s^2), D is vertical soil depth (m), D_w is vertical height of the water table within soil layer (m), and ϕ is the internal friction angle of the soil ($^\circ$). θ is arc tangent of the slope S , expressed as a decimal drop per unit horizontal distance.

Figure 2.3 illustrates geometry assumed in Eq. (2.2). Relationship of soil thickness, $h(m)$, and soil depth D is $h = D\cos\theta$, which produces dimensionless form of the infinite-slope stability model:

$$SF = \frac{C + \cos\theta[1 - wr]\tan\phi}{\sin\theta}, \quad (2.3)$$

where $w = D_w/D = h_w/h$ is the relative wetness, $C = (C_r + C_s)/(h\rho_s g)$ is the combined cohesion (root/soil) made dimensionless relative to the perpendicular soil thickness, and $r = \rho_w/\rho_s$ is the water-to-soil density ratio.

The yielded SF values are typically classified into 3 classes of the slope stability status as follows: ($SF < 1$) \equiv unstable slope conditions, ($SF = 1$) \equiv slope is at the critical point of failure, and ($SF > 1$) \equiv stable slope conditions.

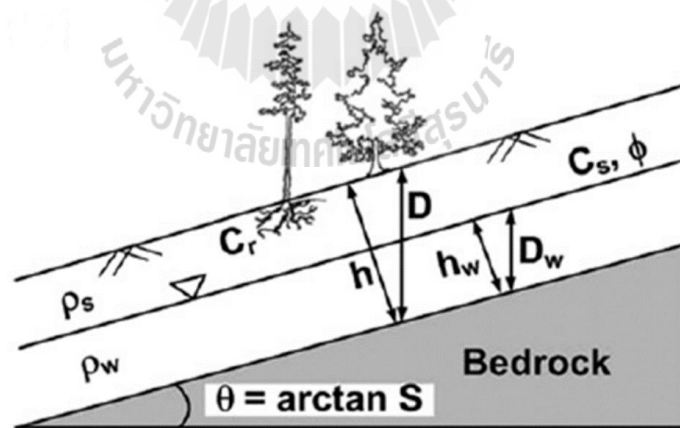


Figure 2.3 Diagrams showing geometry of the assumed infinite-slope stability model (SINMAP) and parameters seen in Eq. (2.2) (Deb and Kadi, 2009).

2.4 Principal causative factors

As stated earlier, formulation of landslide susceptibility map is often accomplished based on prior knowledge of past landslide activities over an area and their association to environmental characteristics of the evaluated area. As a result, recognition of actual contributing factors that control the occurrence of a landslide over a specific location is of primary importance. In general, prominent factors that determine the probability of landslide occurrence might be grouped into two categories:

(1) The contributing variables, or the environmental factors, which make slope susceptible to failure without actually initiating it. These are factors that control slope stability and landslide potential such as geology, slope gradient and aspect, elevation, soil geotechnical properties, vegetation cover, and drainage pattern.

(2) The triggering variables which shift slope condition from a marginally stable to an unstable state and thereby initiating slope failure over a susceptible area. The most important ones are prolonged heavy rainfall and strong earthquake.

As landslide initiation is complex mechanism involving interaction among several influencing factors to yield critical slope instability and landslide of a certain type as an outcome, therefore, knowledge on the landslide mechanism along with its contributing factors are essential for the effective preparation of a susceptibility map. In general, selection of proper factors for the landslide susceptibility assessment depends on types of the concerned landslide and availability of the existing data and resources. The most prominent input factors for this stated task are as follows (Van Westen, Castellanos and Kuriakose 2008; Kanungo, Arora, Sarkar and Gupta, 2009):

(1) Slope gradient. Naturally, steeper slopes tend to be more susceptible to slope failure due to their higher gravity-induced shear stress in the colluviums or residual soil

[as described in Eq. (2.1)]. However, at high slope angles, the terrain usually comprises of stable weathered rock unit which make them less prone to the landslide occurrence. As a consequence, landslide frequency [as defined in terms of the frequency ratio: FR described in Eq. (2.14)] is often found to gradually increase with the slope gradient until a maximum value is achieved followed by a notably decrease at higher- slope category (e.g. in Dai and Lee, 2002; Vijith and Madhu, 2008; Yilmaz, 2009; Regmi, Giardino and Vitek, 2010; Kannan, Saranathan and Anabalagan, 2012),

(2) Slope aspect. An aspect is conventionally defined as a compass direction that a geographic slope faces, usually measured in degrees from north. Or, in other words, the direction of maximum slope of a surface. In general, aspect defines exposure level of an area to the sunlight, local wind and wind-driven rainfall, which are important for activities like vegetation growth, weathering process and soil erosion process. These in turn can have implicit influence on landslide occurrence, especially in arid or semi-arid environment (Sidle and Ochiai, 2006). The importance of slope aspect to landslide frequency were clearly evidenced in several previous works; e.g. Dai, Lee and Ngai (2002); Vijith and Madhu (2008); Pradhan and Lee (2010). However, no distinct influence of aspect on landslide frequency was also reported in Oh, Lee, Chotikasathien, Kim, and Kwon (2009); Hasekiogullar and Ercanoglu (2012); Choi et al. (2012), for examples.

(3) Elevation. Elevation is usually associated indirectly to landslides by virtue of other factors like slope gradient, precipitation, erosion, weathering, soil thickness, and land use. Typically, at high elevations, e.g. near mountain top, terrain usually consist of rather solid and stable rocks with low potential to generate immediate landslide while at the intermediate elevations, sloped surfaces tend to be covered by

thin colluvium that make them more prone to landslide. Human activity on the gentle slopes at these levels, like crop plantation, could enhance chances of having landslide occurrence also. On the contrary, at low elevations, landslide frequency is often low because terrain is relatively flat and often covered with thick colluvium or residual soils. These facts are emphasized in works of, for examples, Yilmaz (2009); Yalcin, Reis, Aydinoglu and Yomralioglu (2011); Solaimani, Mousavi and Kaviani (2012). In addition, elevation is also used as primary proxy for average rainfall that increases with height due to orographic effects. In this regard, high elevations are preferentially susceptible to the landslides because they receive greater amounts of rainfall than those at lower elevations.

(4) Lithology. This factor indicates properties of the slope-forming materials such as strength, permeability and weathering potential which, therefore, should affect the likelihood of slope failure (and landslide activity). According to Soralump (2007), observed landslides in Thailand were identified most frequently in the Jurassic granite and sandstone, shale, mudstone, conglomerate, and chert rock groups. Similar result was also found in Intarawichian and Dasananda (2011). As illustrated in work of Tanavud, Yongchalerchai and Navanugraha (2000), mountainous terrain with granite bedrock is more prone to the slope failure as the weathered rock shall be dominantly converted to a thin layer of sandy soil which has little or no cohesion.

(5) Distance from fault (or lineament). This factor is a crucial characteristic one of ground surface which normally indicates highly fractured terrain over which unstable slopes could be developed and encourage landslide formation. As a consequence, areas situating close to prominent fault or lineament (e.g. at < 1000 m) should be potentially

prone to landslide occurrence as reported in, for examples, Lee and Talib (2005); Lee and Sambath (2006); Oh et al. (2009).

(6) Distance from drainage (stream). Stream has become well-known landslide contributing factor as it initiates gully erosion and undercutting of a slope base along the stream bank which can undermine slope stability of the adjacent area. In addition, increasing level of ground water close to the stream body can saturate lower soil layer which makes the affected area more susceptible to slope failure. Furthermore, debris and soil material close to drainage channel are prone to collapse during heavy rainfall. Therefore, landslide occurrence is supposed to be more frequent within an area close to the stream body (e.g. at < 500 m) as shown in, e.g. Lee and Talib (2005); Oh et al. (2009); Jadda, Shafri, Mansor, Sharifikia and Pirasteh (2009). However, some reports have found no conclusive relation on this issue like Lee and Sambath (2006); Pradhan and Lee (2010); Yalcin et al. (2011); Park, Choi, Kim and Kim (2013).

In addition, some works also included stream density, usually defined as ratio of the total length of the stream to the area of stream basin in the analysis, e.g. Yalcin and Bulut (2007); Yalcin (2008). Typically, the higher in stream density indicates the lower in infiltration and the faster in the movement of surface flow.

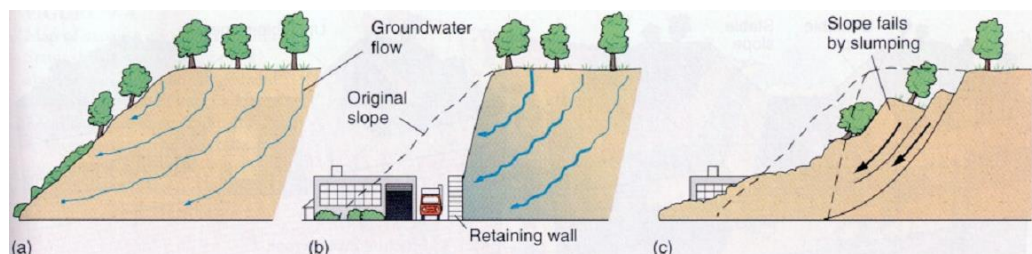


Figure 2.4 Landslide mechanisms due to road construction (van Westen, 2013).

(7) Distance from road or settlement. These factors involve human activities that can influence slope instability and landslide formation. Landslides may occur on slopes adjacent to the roads due to extensive slope excavation for the construction of the roads that greatly reduces load both on the topography and on the slope heel. This change can induce soil instability in the slope layer because of some negative effects such as water ingress (as illustrated in Figure 2.4). The frequent vibrations by vehicle movement can also affect slope stability that eventually leads to landslide incidence. This effect makes areas located fairly close to road network (e.g. at < 100 m distance) more susceptible to landslide occurrence than usual as evidenced in several works, e.g. Mancini, Ceppi, and Ritrovato (2010); Sujartha, Rakamanickam, Kumaravel and Saramathan (2011); Regmi et al. (2010); Solaimani et al. (2012). However, some reports had found different conclusions on this issue like Yalcin et al. (2011); Akgun (2012). For the settlement, proximity to the settlement is typically believed to influence landslide probability also as human activities on vulnerable areas, like fragile hillslopes, might increase chances for slope instability and slope failure. However, this factor was not used much so far, e.g. in Bai, Lu, Wang, Zhou and Ding (2011); Hasekiogullar and Ercanoglu (2012).

(8) Land use and land cover (LULC). In principle, LULC patterns have significant role in determining slope stability as they can influence both the shear stress and shear strength conditions of the natural slope through relevant mechanical and hydrological mechanisms. Focus of the analysis is often on role of the vegetation cover, e.g. forest, in controlling landslide formation over a vulnerable region. Generally, vegetation can increase slope stability through three different processes; (1) the enforcement of soil internal strength by its complex and strong root system, (2) the interception of rainfall which reduces infiltration into the ground, and (3) by removing

soil moisture through evapotranspiration (ET). In this regard, capability of particular vegetation to improve slope stability varies greatly with its type. For examples, trees should be more capable than shrubs, which should be better than grass. Therefore, vegetation clearance for land development or agricultural activities which results in rather exposed soil shall have greater chances for soil erosion and slope instability. However, increasing load on the slope by weight of existing plants or trees can make them less stable than usual at the same time. Commonly, it was often reported that thick forest with strong and large root systems is having less susceptibility from landslide activity than average, for examples, in Kanungo, Arora, Sarkar and Gupta (2006); Dahal et al. (2007); Ercanoglu and Temiz (2011); Sujartha et al. (2011); Yalcin et al. (2011).

In some cases, vegetation abundance might be represented by index called NDVI (normalized difference vegetation index) with original scale of -1 to 1 where positive values closer to 1 indicate more vegetation abundance, for examples, in works of Lee and Talib (2005); Lee and Pradhan (2007); Pradhan and Lee (2010); Intarawichian and Dasanada (2011); Pradhan (2011); Hasekiogullar and Ercanoglu (2012); Choi et al., 2012. However, general conclusion on relationship of NDVI to landslide frequency is still inconclusive based on reviewed literature so far. In some research, characteristics of trees or forest density were integrated explicitly in the preparing process of landslide susceptibility maps, i.e., Young, Jin and Choi (2003).

(9) Soil properties. Soil can influence landslide activity in a particular area through the cohesion strength and some geotechnical properties like porosity, and permeability and grain-size distribution (McKenna, Santi, Amblard and Negri, 2011). In general, each soil type often has different internal strength to hold soil material

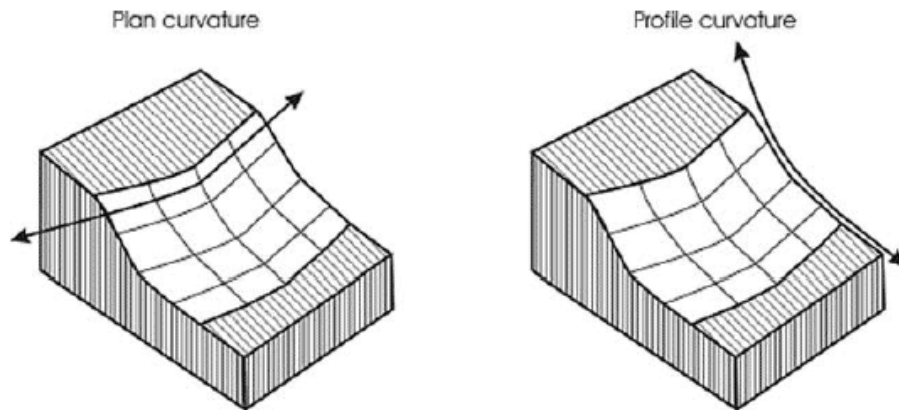
together (called soil cohesion) to resist landsliding. This property for the wet soil is called soil plasticity. The relatively loose soil texture, or ones with low plasticity, should be more susceptible to landsliding, e.g. the loose and unconsolidated alluvial or colluvial soil layer deposited on hillslope. Through, soil properties are necessary for the analysis process of landslide susceptibility by deterministic approach [like SINMAP model described in Eq. (2.2)], but not many reports were appeared to include them for the analysis through different approaches (in terms of soil group, soil texture, soil depth, or soil plasticity); e.g. Wang and Sassa (2005); Lee and Lee (2006); Lee (2007); Lee and Pradhan (2007); Regmi et al. (2010); Oh and Pradhan (2011); Bai et al. (2010). It should be noted that, majority of landslides usually happen within the hilly or remote mountainous areas which often have limited surveyed soil data for the use in the landslide susceptibility analysis. This deficiency can make the analysis procedure less fruitful, e.g. in Pradhan and Lee (2010); Intarawichian and Dasananda (2011).

(10) Landform. Landform is an another variable often used in the quantification of landslide susceptibility at a specific area due to its crucial role in controlling dynamics of the evaluated surface flow (e.g. deceleration, acceleration, convergence, divergence) and, therefore, shall also influence the subsequent gully erosion, deposition, and slope instability resulted from the flow interaction. Inclusion of landform data in the landslide susceptibility analysis in most published reports can be categorized into three different processes as detailed below.

The first one is to apply geomorphology characteristics of the examined area into the analysis process directly as reported in, e.g., Vijith and Madhu (2008); Jadda et al. (2009); Kannan et al. (2012). The second one is processed through the use of defined slope curvature characteristics in which two well-known types are normally

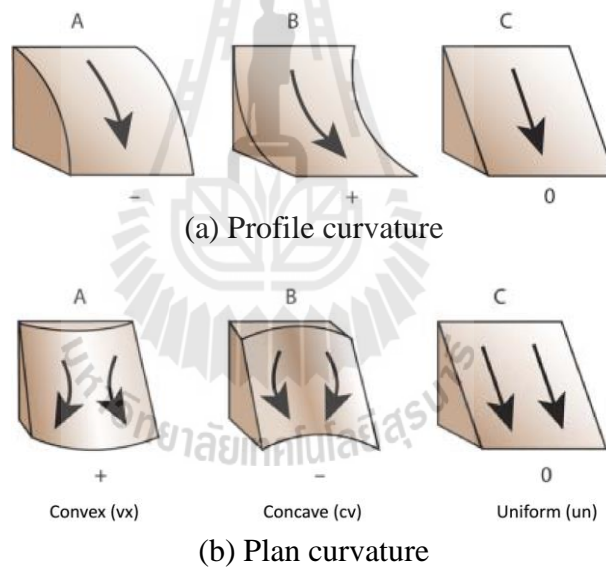
considered: plan curvature and profile curvature (as illustrated in Figure 2.5). Plan curvature might be called contour curvature as it describes rate of change in direction of a hypothetical contour line while passing through a specific location, e.g. an image pixel. The profile curvature is defined by rate of change of the slope along direction of a maximum slope. In addition, their combination to provide total curvature for a given pixel is also useful (Schmidt, Evans and Brinkmann, 2003; ESRI, 2010).

The curvature values describe morphology of the terrain which can be divided into three categories: convex, concave, or flat (as illustrated in Figure 2.6). Typically, the plan curvature influences convergence and divergence of flow across a surface while the profile curvature affects acceleration and deceleration of the surface flow as well as associated erosion and deposition of the landslide material and water along direction of landslide motion. In principle, erosion (and slope instability) should prevail in areas with convex profile curvature and deposition should be favorable over those locations with concave curvature (ESRI, 2010; Regmi et al., 2010). In most studies, the convex curvature areas were found most susceptible to landsliding followed by the concave curvature ones, while flat areas often found much less susceptible if compared to both aforementioned zones, e.g. in Lee and Talib (2005); Lee and Lee (2006); Lee and Pradhan (2006); Lee (2007); Lee and Pradhan (2007); Vijith and Madhu (2008); Pradhan and Lee (2010); Lepore, Kamal, Shanahan and Bras (2012).



Source: Transport Scotland (2008)

Figure 2.5 Visual representation of plan curvature and profile curvature.



Source: ESRI (2010)

Figure 2.6 Three fundamental types of (a) profile and (b) plan, or contour, curvature which are convex, concave and flat (or uniform) (+/- signs are as used in ArcGIS10).

The third approach involves the use of some water-related factors, such as flow accumulation, flow/slope length, runoff, topographic wetness index (TWI) and stream power index (SPI) as predictors for landslide susceptibility. Among these, TWI

and SPI were found most popular in the reviewed literature. These indices are used to describe the wetness and stream power over an area, respectively, and conceptually defined as a function of the slope gradient and upstream contributing area of the flow (through a given pixel) as follows (Yilmaz, 2009);

$$SPI = A \cdot \tan \beta, \quad (2.4)$$

$$TWI = \ln(A / \tan \beta), \quad (2.5)$$

where A is the upslope water contributing area per unit contour length for a particular pixel and $\tan \beta$ is the local slope of that pixel.

By definition, the stream power index (SPI) is a measure for the erosive power of overland flow at a given location of the topographic surface. As a contributing area and slope gradient increase, amount of surface water contributed by the upslope areas and its flow velocity increase, hence the SPI and erosion risk increase (Moore, Grayson and Ladson, 1991). For the topographic wetness index (TWI), it is a measure of the water accumulation potential at a site which correlates to the amount of soil moisture content. Therefore, higher TWI values indicate greater water content (and pore water pressure) in slope material from which soil strength and soil stability shall be diminished, e.g. in Yilmaz (2009); Regmi et al. (2010); Oh and Pradhan (2011). The slope length or flow length; a distance of surface flow from origin till the end, is also attracted more interest, e.g. Vijith and Madhu, 2008; Regmi et al., 2010. Typically, larger slope length indicates more water accumulates at the ending part of the considered flow which probably leads to more erosion and landslide activity.

Systematic combination of these aforementioned contributing factors through an appropriate methodology can lead to production of the landslide susceptibility map as needed. Among these, lithology and slope gradient were usually found to attain top

priority in most works, on the contrary, aspect, distance to stream and distance to road were among the least favourable ones in the analysis. It should be noted here that, as rainfall is categorized as being a triggering factor therefore, in principle, it should not be included in the formulation of the susceptibility map in the first step which should be involved the landslide contributing factor only. However, integration or the annual-mean rainfall data into the analysis shall generate the general hazard map for an area as the resulted map is not only detailed spatial likelihood of slope failure over the area but also the temporal probability as well (from nature of the rainfall data) as evidenced in, for examples, Lee and Pradhan (2006); Pradhan and Lee (2007); Bagherzadeh and Daneshvar (2012); Thanh and Smedt (2012).

2.5 Concept of landslide risk analysis

By definition described in Varnes (1984), landslide risk analysis is a systematic process to determine expected loss in terms of human death or injury, property damage, and disruption of economic activity due to landslide over a particular area and reference period (e.g. a year). These losses can be expressed both in qualitative or quantitative manner. In the qualitative assessment, losses are evaluated and expressed in qualitative terms (e.g. high, medium, low) based on a set of some pre-determined criteria while in quantitative assessment, relevant losses shall be presented in quantitative or numerical terms (e.g. amount of death or injury, or monetary loss from property). Between these, the qualitative method is normally easier to perform but it is rather subjective in nature as the used criteria are traditionally drawn from expert judgment (AGS, 2000).

Conceptually, when dealing with physical losses, risk can be quantified as a direct product of three main factors: probability of occurrence of the concerned

phenomenon (at a given magnitude or intensity), cost or amount of the defined elements at risk, and vulnerability of those elements to impact of the examined phenomenon. According to this definition, total landslide risk (LR) can be determined using following formula,

$$\text{Total landslide risk (LR)} = E \times (H \times V). \quad (2.6)$$

Here, E (Element at risk) often includes population, properties, economic activities and public services at risk within the area, H (Hazard) represents probability of occurrence within a specific period of time (e.g. a year) and within an expected influencing area of landslide phenomenon, and V (Vulnerability) is degree of loss to a specific element at risk resulting from a referred landslide having scale from 0 (no damage) to 1 (total loss). Term $H \times V$ is called specific risk for each individual at-risk element (Varnes, 1984).

Definition of the landslide risk given by Varnes (1984) seems straightforward in essence; however, to implement it fruitfully in reality is still proved rather difficult so far, especially at medium mapping scales between 1:10,000 and 1:50,000 (van Westen, van Asch and Soeters, 2006). The difficulty is arisen mainly from the frequent lack of essential data or information to complete the key tasks required at each step of the risk analysis process, which generally comprises of five main successive works as follows.

The first step is to establish a landslide inventory map to portray locations and areal extent of past landslide occurrences. These acquired inventory data are preferred in the development of landslide susceptibility and its associate hazard maps for the

interested area afterwards. The second step is to establish a landslide susceptibility map to inform spatial probability (or likelihood) of potential future landslide activity in the area based on knowledge of past landslide events and a set of preferred terrain and environmental parameters, e.g. slope, elevation, soil data, lithology or land use pattern.

The third step is to formulate the hazard map that describes probability of landslide occurrence at a specific location within the area during a reference period of time from the referred susceptibility map yielded in the second step. The fourth step is to construct a comprehensive map of an at-risk element along with its associated vulnerability maps for the area. These maps usually include information of population, economic activities, properties (e.g. houses or buildings), and public infrastructure (e.g. roads or bridges) prone to having tangible effect from landslide activity in the area.

And the final step of the process is to develop a preferred landslide risk map which is a direct product of the hazard map and the vulnerability map [as detailed in Eq. (2.6)] to present expected amount, or level, of life loss and damage cost throughout the area during the considered time period (AGS, 2000; Dai, Lee and Ngai, 2002; van Westen et al., 2006; Abella, 2008; van Westen et al., 2008).

Figure 2.7 exhibits general conceptual framework for landslide risk analysis and management expressed in Dai et al. (2002) and Figure 2.8 illustrates main aspects of risk analysis process described earlier. Typically, after having landslide risk map for an area, the found risk value must be taken into process of risk assessment to judge whether it is acceptable or not (based on the reference risk tolerance criteria). And if not, some strategies to control or reduce the known risk should be implemented which is a crucial part of the risk management process (AGS, 2007b).

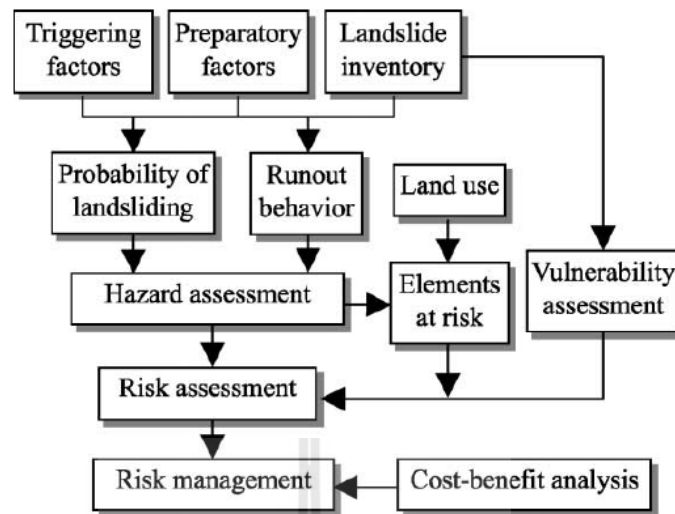


Figure 2.7 General conceptual framework for landslide risk analysis and management (Dai et al., 2002).

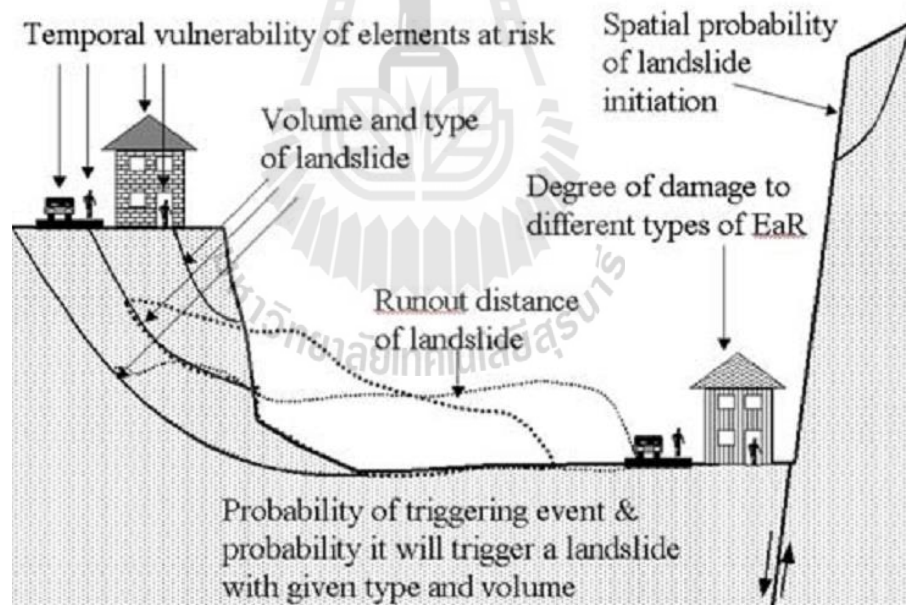


Figure 2.8 Main aspects of risk analysis process (van Westen et al., 2006).

As preparing process of a landslide risk map is still a considerably laborious task, most works seen on landslide zonation analysis are normally focused on the derivation of preferred landslide susceptibility map for a specific area of interest only

(or step 2 of the full process). However, risk mapping at regional scale is still conceptually appealed to attain broad information of the potential at-risk area from landslide activity which is essential for the planning of appropriate land use managing policy as well as effective emergency response strategy (Michael-Leiba, Baynes, Scott and Granger, 2003). In this aspect, according to van Westen et al. (2006), main purpose of the analysis should be to acquire primary data to support site-selection process for the new development over the area (to minimize potential landslide risk), or to identify concerned at-risk locations to aid the proper implementation of risk management policy. Definitions for common terms used in the landslide zoning are given in Appendix A.

The qualitative risk analysis is commonly recommended for work at regional scale due to its less demand in detailed input data and less complex computing procedure in which the eventual risk classification are reported in the form of qualitative terms (e.g. high, moderate and low) based on the pre-determined criteria. In addition, the medium-scale risk map should include a description of its practical implications and it should be prepared for a single type of landslide only each time. It is also further recommended that mapping process should be directed toward the investigation on geomorphological evidences related to aspects that influence the considered risk such as runout distance, size and depth of the landslide, progressive movement of the concerned landslide within a considered environmental setting (van Westen et al., 2006). Information about typical landslide zoning mapping scales and their applications is presented in Table 2.

Table 2.2 Typical landslide zoning mapping scales and the applications (AGS, 2007a).

Scale Category	Scale Range	Examples of Zoning Application	Zoning Area (km ²)
Small (National)	< 1:100,000	Landslide inventory and susceptibility to inform policy makers and the general public	>10,000
Medium (Regional)	1:100,000 to 1:25,000	Landslide inventory and susceptibility zoning for regional and local development or very large scale engineering projects. Preliminary level hazard mapping for local areas.	1,000-10,000
Large (Local)	1:25,000 to 1:5,000	Landslide inventory, susceptibility and hazard zoning for local areas. Preliminary level risk zoning for local areas and the advanced stages of planning for large engineering structures, roads and railways.	10-1,000
Detailed (Site-specific)	> 1:5,000	Intermediate and advanced level hazard and risk zoning for local and site specific areas and for the design phase of large engineering structures, roads and railways.	Several hectares to tens of km ²

2.5.1 Preparation of landslide inventory maps

The first step in processing landslide risk analysis is to develop an appropriate inventory map of past landslides in the study area. Landslide inventories are commonly regarded as the simplest form of landslide mapping in which locations, occurrence dates and types of past landslides that took place and still left discernable traces over an area are assembled (Hansen, 1984; Guzzetti, 2002). These maps could be prepared either by collecting available historical information on individual landslide incidences (making landslide archives), or from rigorous analysis of the aerial photographs or appropriate satellite images, coupled with data acquired from the coverage field surveys of the area (making landslide distribution map). These maps can

be separated into two broad types (Malamud, Donald, Guzzetti and Reichenbach, 2004):

(1) Landslide-event inventory. This consists of all landslide events associated with a single trigger, such as an earthquake, rainstorm or snowmelt.

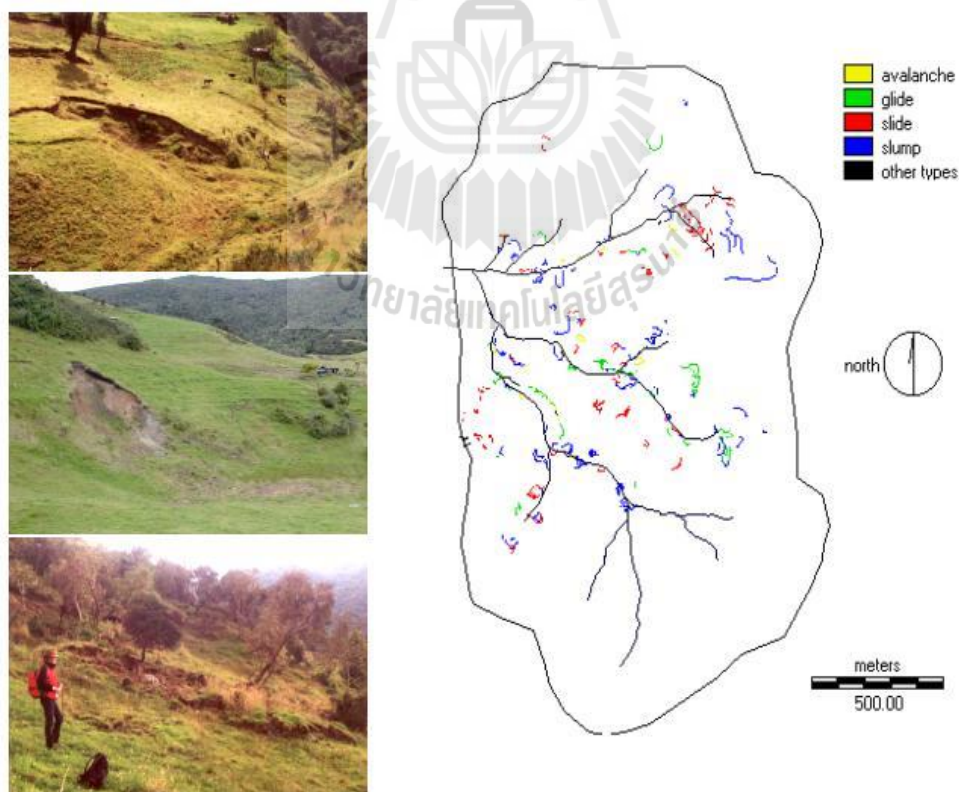
(2) Historical landslide inventory. This includes all observed landslide events over a period of many years, e.g. tens or hundreds years.

If time period of the acquired landslide data is known, e.g. from information of temporal aerial photos or satellite images, “multi-temporal inventory” maps can then be prepared. Similarly, if type of slope failure can be identified, the required map can be prepared separately according to the identified types of landslide (Figure 2.9).

Recent landslide data can be readily acquired from the visual interpretation of apparent landslide-induced scarps on aerial photos or high/very-high resolution satellite images (e.g. those with spatial resolution < 5 m). Among these, the disrupted or absent vegetation cover anomalous with the surrounding terrain is usually an obvious sign of the landslide traces (like those in Figure 1.2). Recently, several automatic classification technique for landslide traces were developed based on knowledge of distinct landslide spectral or spatial characteristics, e.g., change vector analysis, the maximum likelihood classifier, normalized differential vegetation index (NDVI), the principal component analysis, and object-based image analysis (Mondini, Chang and Yin, 2011). However, evidences of old landslides, especially the relatively small ones, might still be difficult to identify straightforwardly as they might be obscured by surface erosion, vegetation, urbanization, or human activities, as time passes (Guzzetti, Cardinali, Reichenbach and Carrara, 2000; Malamud et al., 2004). Knowledge of past landslide data are crucial for the associated susceptibility analysis in three aspects: (1) for calibration of the applied

model, (2) as reference for the operating of used model (quantitative type in particular), and (3) as reference for the validation of the yielded susceptibility map.

For detailed landslide inventory maps, common information should include, for examples, state of the activity, type of slope movement, certainty of identification, primary direction of the movement, estimated volume, size, predominant material, and occurrence date for each individual registered landslide (Wieczorek, 1983). In addition information of the geological structure or relevant environmental characteristics of each mapped landslide location should also be included for further analysis on the potential landslide prone locations over an area through both qualitative approach (expert-based) and quantitative approach (data-based).



Source: <http://serc.carleton.edu/details/images/14949.html>

Figure 2.9 Example of the landslide inventory map.

2.5.2 Preparation of landslide susceptibility maps

Landslide susceptibility mapping is the most popular activity of landslide zoning known so far as it can be carried out straightforwardly using plenty of existing methods. Main purpose of the task is to systematically locate areas that are susceptible to having concerned landslide activities based on knowledge of past landslide events over the area and their mutual relations to a set of reference environmental factors (causative factors). The landslide susceptibility maps normally display spatial probability, or probabilistic likelihood, of the studied area to having slope failures under the assumed relationship of the input predisposing factors and the formation of landslide activity (see for reviews in Aleotti and Chowdhury, 1999; Guzzetti, Carrara, Cardinali and Reichenbach, 1999; Dai, Lee and Ngai, 2002; Kanungo et al., 2009).

Construction of a landslide susceptibility map is fundamentally based on three common assumptions (Varnes, 1984; Kanungo et al., 2009; Guzzetti, 2012):

- (1) landslides are likely to take place over the same areas as seen in the past;
- (2) landslides are likely to originate in places with similar contributing factors; e.g. topographical, geological or hydrological conditions, to past landslide locations;
- (3) landslides activity can be explained through the slope-stability theory which involves complex interaction of several land internal factors known as the causative or contributing factors, e.g. lithology, geography, soil property, and the external factors called triggering factors, such as rainfall or earthquake.

From these assumptions, plenty of techniques were invented and productively implemented to prepare landslide susceptibility maps around the world. Nevertheless, success of the landslide susceptibility zoning might be still limited by some problems

like the location-based nature of landslide occurrence, difficulty in identifying proper causative factors for found landslide activities, and still lack of data about past landslide occurrences over the interested area (Aleotti and Chowdhury, 1999).

Traditionally, landslide susceptibility evaluating methods can be divided into two broad groups: qualitative and quantitative (as detailed in Table 2.3). In qualitative or heuristic methods, final decision on landslide potential over an area is determined based principally on the collective expert opinion (on nature of landslide characteristics experienced within an area). The most common procedure is called geomorphological mapping method in which landslide prone areas are identified by the researchers from sites that have similar properties of contributing factors to those used to have landslide activity before, like topography, geology, or hydrology under some reference criteria (Kanungo et al., 2009). This method is called a direct approach which has been widely-used as a basic methodology to the construction of initial landslide susceptibility zoning by landslide researchers for long time. However, in recent decades, more complicated methods of the qualitative type were introduced to build more sophisticated and realistic susceptibility maps for an interested area like the weighted linear combination (WLC) or analytical hierarchy process (AHP) methods.

These stated methods have improved the decision rule on landslide probability by introducing different numerical influencing weights to each concerned contributing factors and their respective attributes. These weight values are judged by the assessed importance of these factors, or their attributes, on landslide formation within the area. Linear combination of the weight product for each contributing factor and its relevant attribute shall be used as a basis to calculate landslide susceptibility score for each land unit which implicitly indicates susceptible level of the area to landslide initiation. Main

advantage of the qualitative methods is no explicit need for past landslide data but their concept could lead to an uncertainty in the attained outcome due to subjective nature of the expert judgments. This makes the interpretation on actual importance of each factor in use sometimes difficult to achieved (Yalcin, 2008; Kanungo et al., 2009).

For the quantitative methods, their approaches for the formulation of landslide susceptibility maps rely principally on numerical expressions of apparent relationship appeared between a group of contributing factors and data of past landslide occurrences. Generally, there are two broad categories of the quantitative methods: deterministic and statistical (Aleotti and Chowdhury, 1999). Typically, the deterministic methods depend on engineering principles of slope instability expressed in terms of the predefined index called “factor of safety” (FS). This factor is often quantified using some simple models of the groundwater flow in combination with infinite slope stability analysis to estimate potential or instability condition of surface slopes within the region (like the SINMAP model mentioned earlier in Section 2.3). Significant advantage of these methods is their realistic and theoretically-sound working concept which can be directly implemented to perform physically-based landslide susceptibility analysis (for engineering purpose). However, they are normally most effective if applied to small area due to the exhaustive need in physical and hydrological information as input data (Fall, Azam and Noubactep, 2006; Ho, Lee, Chang, Wang and Liao, 2012).

Table 2.3 Classification of well-known landslide susceptibility determination methods (Aleotti and Chowdhury, 1999; Guzzetti et al., 1999; Kanungo et al., 2009).

Category	Sub-category	Prominent methods	
Qualitative or Heuristic (knowledge-based)	Geomorphological analysis (direct approach)	Geomorphological mapping	
	Qualitative map combination (or semi-quantitative)	Weighted linear combination (WLC) Analytical hierarchy process (AHP)	
Quantitative (data-based)	Deterministic	Slope-stability analysis (FS assessment)	
		Information Value (InfoVal)	
	Statistical	Bivariate	Probabilistic frequency ratio (FR)
			Probabilistic weight of evidence (WoE)
		Multivariate	Discriminant Function Analysis
			Multiple logistic regression Artificial neural network (ANN)
Others	Fuzzy logic, neuro-fuzzy, SVM, decision tree		

Comparatively, the statistical methods are more popular than the deterministic ones at present, in which spatial relationship between past landslide activities and their contributing factors is determined through some preferred statistical analysis methods which can be structured into two major groups: bivariate and multivariate. In bivariate statistical analysis, existing relationship of the contributing factors to the formation of past landslides are assessed independently one by one based primarily on distribution pattern in amount of past landslides with respect to the listed attributes of each factor. The most notable methods are frequency ratio (FR) and weight-of-evidences (WOE) methods (Regmi et al., 2010; Yalcin et al., 2011; Lee et al., 2012).

In multivariate statistical analysis, the inherent relationship of past landslides and a set of the contributing factors is assessed through the found optimal interrelation

pattern among all used factors that can satisfactorily predict the occurrence chances of the past landslides. This task can be accomplished through the use of several standard statistical procedures such as discriminant function analysis, multiple linear regression method, multiple logistic regression method, and the artificial neural network analysis (Guzzetti et al., 1999). Among these, the multiple logistic regression analysis is most favored at present due to its ability to include both numerical data and categorical data (as independent variables) in the assessment of landslide occurrence likelihood over an area which is not able in the discriminant analysis or multiple linear regression analysis (Nandi and Shakoor, 2009; Pradhan, 2010). For artificial neural network (ANN), it has gained more interest in recent years due to its distinct ability to identify relationship of past landslide occurrences and a set of the chosen contributing factors automatically in a nonlinear fashion using predefined logic without prior assumption on the distributing pattern of the used input data. This capability makes it theoretically able to analyze complicated relationship between past landslide events and their predisposing factors better than the conventional approaches of this type like discriminant function analysis or multiple logistic regression. Also, ANN can process data at varied measuring scales frequently encountered in practical landslide susceptibility mapping, e.g., continuous, ordinal and categorical data (Kanungo, Arora, Sarkar and Gupta, 2006).

Main superiority of the statistical methods is the straightforward approach to identify appropriate relationships between past landslides and the applied contributing factors which can be applied to develop landslide susceptibility map over large areas, e.g. at regional scale. Their noted inferiority is the critical need for sufficient knowledge of past landslide incidences to produce highly credible susceptibility map. In general, quantitative methods can be used to reduce subjectiveness in weight assessment process

used in the qualitative methods and provide more accountable interpretation on defined importance scale of the used factors (or attributes). In addition, in terms of risk analysis, statistical methods are effective in assessing spatial probability of the hazard occurrence for risk analysis, but might have problems in the evaluation of its temporal probability of the occurrence (van Westen et al., 2006).

Apart from the aforementioned methods, fuzzy logic has been implemented in the production of landslide susceptibility maps also as seen in, for examples, Saboya, Alves and Pinto (2006); Gorsevski and Jankowski (2010); Pourghasemi, Pradhan and Gokceoglu (2012). Fuzzy logic is attractive due to its ability to justify the likelihood of slope failure based on the imprecise determination criteria defined by experts or from knowledge inherited from other relevant methods. Apart from these standard methods, several new landslide susceptibility assessment methods have been introduced in recent years for being an alternative or a comparative approach to the conventional ones, e.g. neuro-fuzzy (Oh and Pradhan, 2011; Pradhan, 2011; Sezer, Pradhan and Gokceoglu, 2011), support vector machine (SVM) (Yao, Tham and Dai, 2008; Yilmaz, 2010; Ballabio and Sterlacchini, 2012); and the decision tree approach (Yeon, Han and Ryu, 2010; Bui et al., 2012). Details of the methods implemented in this study (WLC, AHP, FR, LR, ANN, fuzzy logic) are given in later section. They were chosen due principally to their wide use, well-approved capability, and the rather distinct working concepts to reach the preferred solution (credible landslide susceptibility mapping).

2.5.3 Preparation of landslide hazard maps

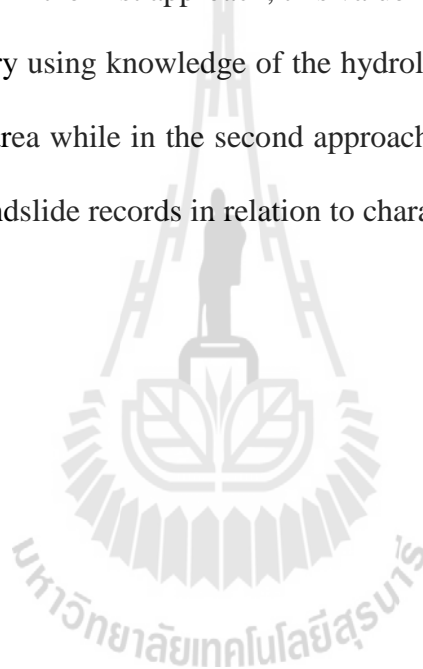
Landslide hazard mapping is a successive process from landslide susceptibility mapping towards the construction of the corresponding landslide risk map for an area (as illustrated in Figure 2.7) According to Varnes (1984), “hazard” is

the probability of occurrence of a potentially damaging phenomenon (such as landslide, flood) within a specified period of time and within a given area of interest. This means the temporal probability of having landslide over an area must be included in the susceptibility map for the formulation of the needed hazard map for the area (AGS, 2007a).

Normally, landslide hazard is usually defined as probability of occurrence for a particular type of the landslide at a certain magnitude, or of a particular type, within a specific period of time (Guzzetti et al., 1999). In this respect, all landslide activities that can affect an area should be considered including those originally initiate outside but might eventually travel into the area during its development. In principle, landslide hazard mapping takes an output from the landslide susceptibility analysis, and assigns an estimated frequency (e.g. annual probability) to the considered landslides. Temporal probability of the landslide occurrence over an area can be evaluated through the use of slope stability analysis to identify probability of slope failure based on knowledge about the recurrent period of the triggering factor (mostly rainfall and earthquake). The other well-known method for this task is the frequency analysis of past landslide incidences (of certain type or magnitude). This analysis may be processed directly through records of the identified landslide seen within the area, or, indirectly through knowledge about the recurrence of triggering events (Corominas and Moya, 2008). However, in reality, determining temporal probability is considerably difficult due to lack of landslide records or information of triggering events (van Westen et al., 2006).

Commonly, the small landslides should happen more often than the large ones which make them have higher occurring frequency. The magnitude-frequency

relation of the landslide incidences is well examined as depicted in Figure 2.10 for example. In case of rainfall-induced landslide, amount of the accumulated rainfall over an area that can trigger typical landslide (of certain type or magnitude) usually varies with locations (Guzzetti, Peruccacci, Rossi and Stark, 2007; 2008; Corominas and Moya, 2008). However, a minimum rainfall threshold that can activate this process can be estimated either by using the process-based methods or the empirical methods (Guzzetti et al., 2007). In the first approach, this value is determined through the slope stability analysis theory using knowledge of the hydrological system and the relevant slope structure of an area while in the second approach, the answer is extracted from the analysis of past landslide records in relation to characteristics of the rainfall events that cause them.



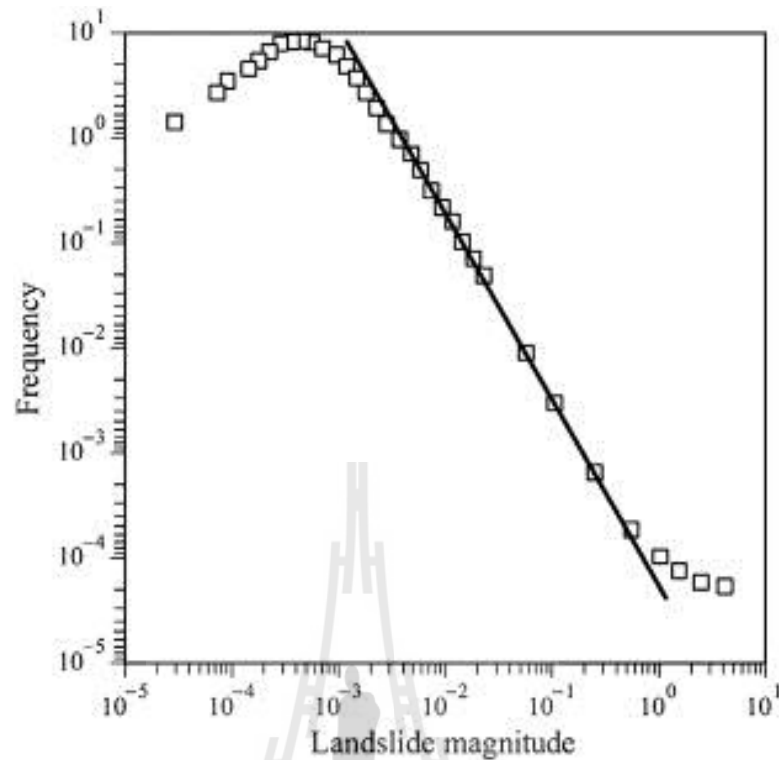


Figure 2.10 Typical found relationship of the magnitude-frequency relation observed in landslide inventories. Magnitude often displays in terms of landslide size (e.g. km²) while frequency (non-cumulative) usually reports based on number of events per year. Note that, the solid line represents theoretical prediction but there is a large deviation from theory at small landslide magnitude (often under 10,000 m²) called a rollover, or inflection, effect. This situation implies that observed number of the relatively small landslides is crucially lower than expected from the adopted theory but actual causes of this phenomenon are still under active investigation (Corominas and Moya, 2008).

Results from these investigations have established the rainfall intensity-duration (ID) threshold for explaining critical situation of the rainfall event that might be able to activate landslide phenomenon over an area of interest which can be written in general form as follows (Guzzetti et al., 2007):

$$I = c + \alpha D^\beta \quad (2.7)$$

where I is the average rainfall intensity, D is the rainfall duration, and $c \geq 0$, α and β are proper parameters of the analysis (in most cases, $c = 0$ is applied). Typical ranges of these variables are about 1 to 200 mm (for intensity) and 1 to 100 hours (for duration).

As described in Guzzetti et al. (2007, 2008) and Corominas and Moya (2008); the rainfall threshold depends significantly on landslide mechanism. High-intensity and short-duration rainfall normally trigger shallow landslides and their associated debris flow for slope covered with permeable materials in which the build-up and dissipation of positive pore pressures is very rapid. Also, the low to moderate intensity rain storms lasting for several days or weeks might trigger landslide and its subsequent debris flow in low permeability soil. In this case, the antecedent rainfall shall have important role in reducing soil cohesion and increasing the positive pore-water pressure that leads to the eventual slope failure. Therefore, thresholds based on the antecedent rainfall were also established in several works, often examined in conjunction with the rainfall data at failure day (see Figure 2.11 for an example). However, the preferred period of rainfall accumulation is still inconclusive.

In theory, hazard map must include areas affected by the landslide runout in its detail also. This requirement needs accurate prediction of the runout behavior of a landslide, e.g. how far and how fast a landslide travels once mobilized. Typically, several parameters related to landslide runout are of interest in the study of risk analysis, e.g. runout distance (a distance from landslide source area to distal toe of the deposition area), damage corridor width (width of an area subjected to landslide damage in the distal part of the landslide path where impact on buildings and other facilities occurs; velocity (within the damage corridor which determines the potential damage to facilities

and the design parameters of any required protective measures), depths of the moving mass and of the deposit (which influence the impact of landslide runout within the damage corridor) (see more details in Dai et al., 2002).

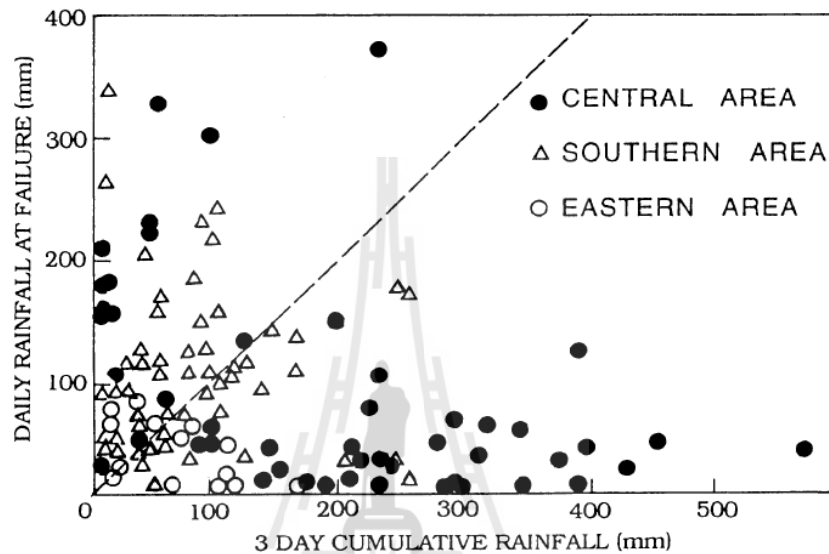


Figure 2.11 Relationship of daily rainfall at the failure and antecedent rainfall in Korea (Kim, Hong and Kim, 1992). Note that, landslides in the central area are influenced by the antecedent rainfall the most while for those southern side is daily rainfall.

2.5.4 Preparation of landslide risk maps

In essence, landslide risk zoning shall take outcomes from the hazard mapping and assess potential damage to each concerned element at risk resided within the area (comprising mainly of people, properties, and services) from a considered hazard, with temporal and spatial probability of the hazard occurrence and vulnerability to the hazard of the at-risk element taken into account (as shown in Figure 2.12). In case of landslide hazard, it might be necessary to formulate susceptibility, hazard and

risk zoning maps separately for different types of the landslides affecting the area; e.g., rock falls, small shallow landslides and deep-seated larger landslides (AGS, 2007a).

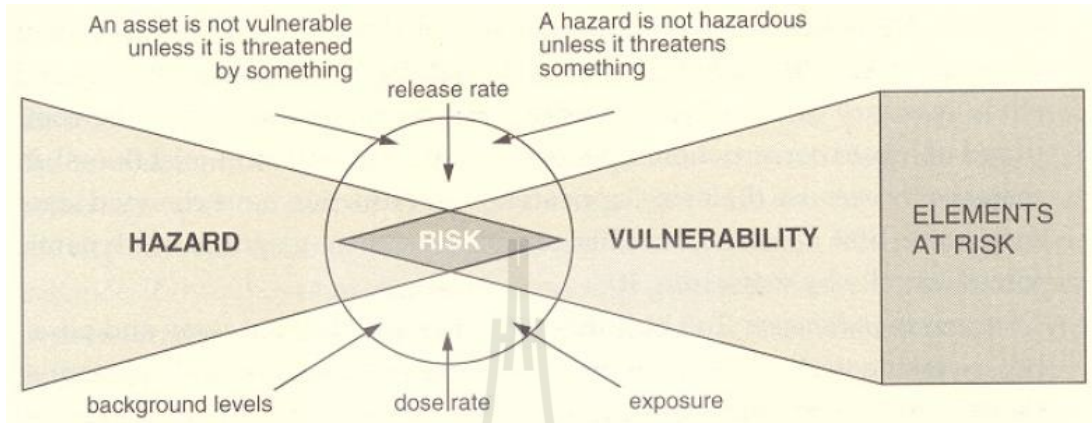


Figure 2.12 Conceptual relationship between hazard, elements at risk, vulnerability and risk (Alexander, 2002).

To prepare the landslide risk map, information of all the elements at risk must be systematically identified and mapped first. These data normally include population, buildings, economic activities, public services, utilities, infrastructure, etc., which are at risk from landslide activities in a considered area. The emphasis is mostly given to population, buildings, and infrastructure. Rapid inventory of the database for elements at risk generally uses high-resolution images. Each of the listed elements has its own characteristics, which can be spatial (the location in relation to the hazard), temporal (such as population amount that might differ in time at a certain location) and thematic characteristics (such as the material type of the buildings/houses, or the age distribution of the population) (van Westen et al., 2006).

The next step of the risk analysis process is quantification of the vulnerability for the elements at risk. The concept is to perform an assessment on degree of damage

that may result from the occurrence of a particular landslide of a given type/volume. Vulnerability is a crucial component in the evaluation of landslide risk often defined as the level of potential damage, or degree of loss, of a particular element (expressed on a scale of 0 to 1) subjected to a landslide event of a given intensity (Varnes, 1984; Crozier and Glade, 2005). The assessment involves understanding of the interaction between the considered landslide and affected elements. Generally, the vulnerability to landslide influence depends mainly on (a) runout distance; (b) volume and velocity of the sliding; (c) elements at risk (buildings and other structures), nature and proximity to the slide; and (d) elements at risk (persons), proximity to the slide, nature of the building/road that they are in, and where they are in. With this method, the vulnerability of an element at risk depends principally on characteristics of the landslide and technical resistance of that element to landslide impact, such as the type, nature, age, etc. (Dai et al., 2002).

Ultimately, combination of hazard and vulnerability information shall define values of a specific risk as preferred (Eq. (2.6)). Combination of the data for one specific type of landslide and one specific type of the elements at risk results in a specific risk. Integration of all specific risks for all landslide types and volumes and all the elements at risk results theoretically in the total risk (Varnes, 1984; van Westen et al., 2006).

2.6 Relevant landslide susceptibility mapping methods

As several landslide susceptibility assessment methods are of interest to be applied in this thesis, therefore, knowledge on general concept and working procedure of these methods are necessary for the appropriate preparation of the subsequent work and this shall be described in this section as follows.

2.6.1 Conventional weighted linear combination (WLC)

Conventional weighted linear combination (WLC) is one of the widely-used qualitative methods for landslide susceptibility analysis, especially at a regional scale (Glade and Crozier, 2005). In this approach, contributing factors and their attributes are directly assessed for their relative importance in the initiation of landslide activity found within the examined area based on assembled expert opinions or from literature review. The comparative importance is normally represented by the assigned numerical values for the relevant factors and their corresponding attributes [e.g. using ordinal scale from 0 (not important) to 9 (most important)]. These values are typically called factor weight (for the factors) and class weight, or rating, (for the attributes). Higher values of weight (or rating) indicate greater influence of the concerned factors (or attributes) on landslide occurrence over the area (Lee, Ryu, Won and Park, 2004). Product of factor weight and corresponding class weight (of a specific attribute) is represented the net contributing weight of that attribute to landslide occurrence therein (see Table 2.4 for example).

To construct the required landslide susceptibility map, the net contributing weight from each input factor (i.e. that of the apparent attribute) are accumulated on a pixel-based basis and the result is called landslide susceptibility index (LSI) which is different for each considered pixel, the higher LSI indicates the greater probability of landsliding. This process can be written as follows:

$$LSI = \sum_{i=1}^n FW_i \cdot CW_i, \quad (2.8)$$

where LSI is a landslide susceptibility score for a considered pixel, FW_i and CW_i are corresponding factor weight and class weight for a contributing factor i of that pixel and n is number of the causative factors in use.

Figure 2.13 shows example of the flow diagram presented in work of Kanungo et al. (2006) which used the WLC method for landslide susceptibility classification in Darjeeling Himalayas hill region. There were six main input factors considered in this case with different preferred factor and attribute weights as detailed in Table 2.3 from which the drainage buffer was given the highest priority (with factor weight of 9) and aspect was considered having lowest priority in the analysis (with factor weight of 1).

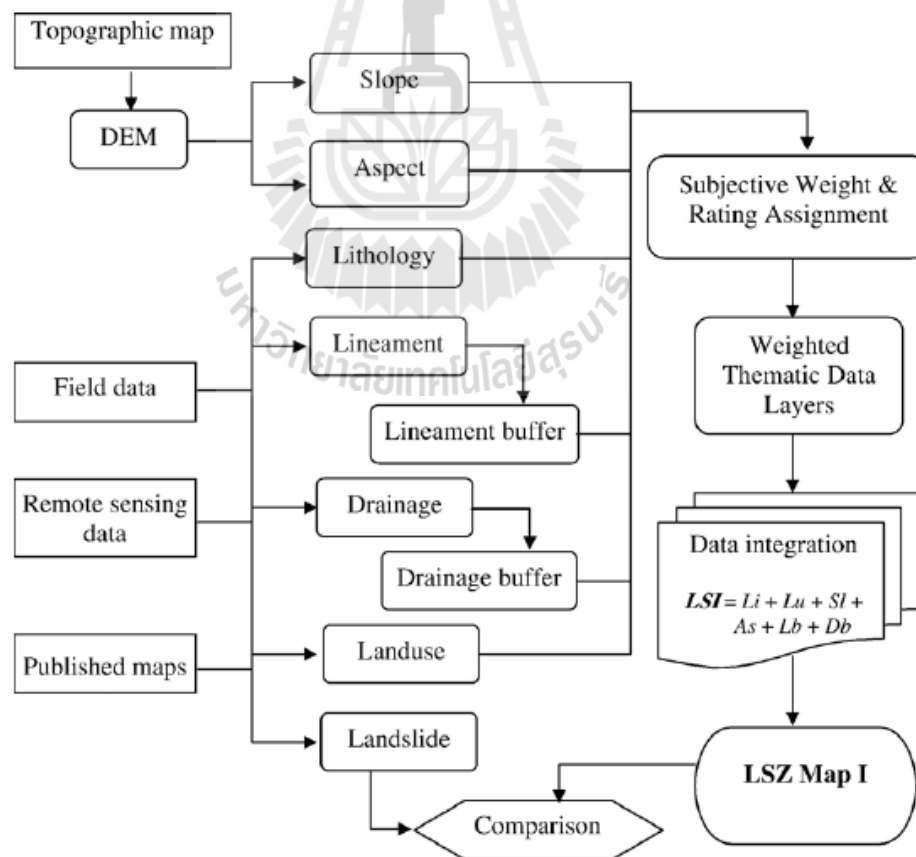


Figure 2.13 Flow diagram for the landslide susceptibility assessment procedure using the conventional weighted linear combination method (Kanungo et al., 2006).

Table 2.4 Examples of factor weights and class weights (or rating) for input thematic layers and their attributes for the WLC method as reported in Kanungo et al. (2006).

Thematic layers	Attributes	Factor weight (FW)	Class weights (CW)	Net contributing weights (FW·CW)
Drainage buffer	First order	9	9	81
	Second order		5	45
Lineament buffer	0-125 m	8	9	72
	125-250 m		7	56
	250-375 m		5	40
	375-500 m		3	24
	>500 m		1	8
Slope	0-15°	7	1	7
	15-25°		3	21
	25-35°		5	35
	35-45°		7	49
	>45°		9	63
Lithology	Darjeeling gneiss	6	7	42
	Feldspathic greywacke		3	18
	Paro gneiss		5	30
	Lingse granite gneiss		9	54
	Paro quartzite		1	6
LULC	Reyang quartzite	4	1	6
	Agriculture land		5	20
	Tea plantation		3	12
	Thick forest		1	4
	Sparse forest		7	28
	Barren land		9	36
	Habitation	2	8	

2.6.2 Analytic hierarchy process (AHP)

Another popular qualitative method in landslide susceptibility evaluation is the analytic hierarchy process (AHP). This method was first developed by Saaty (1977, 1980) as supporting tool for solving of the encountered multi-criteria decision situation. The method has gained broad application so far especially in the research fields of site selection, suitability analysis, regional planning, and landslide

susceptibility analysis (Vaidya and Kumar, 2006; Ho, 2008; Long and De Smedt, 2012).

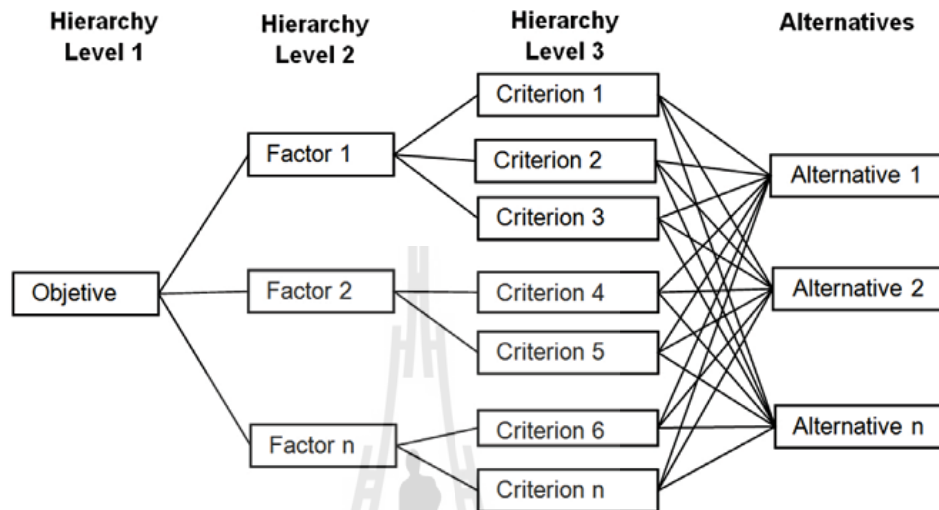


Figure 2.14 A hierarchical structure of the analytic hierarchy process method (AHP) (Cortes, Serna and Martinez, 2012).

According to Malczewski (1999); fundamental concept of the AHP method is based on the three principles: decomposition, comparative judgment, and synthesis of priorities. In the first task, a target problem must be broken down into a conceptual hierarchical order (or successive level) of its decision-making components, beginning with the ultimate objective, or goal, of the decision strategy given at Level 1, followed by details of the applied decision-making components in the subsequent levels, starting with the broadest categories first (at Level 2) followed by the subcategories (or criteria) at higher levels. The final layer comprises a list of the alternative options, or solutions, under consideration (as illustrated in Figure 2.14).

In the second task, the priority score (or weight) for each listed component at a specific level must be determined using a pairwise comparison method in which all considered elements at each hierarchical order are judged for their initial preferences in pair describing by the scale from 1 to 9 (see Table 2.5 for detail). These results are then further processed to identify priority score for each applied element later using the gain pairwise comparison matrix, or the preference matrix. The final task is to rank priority of each potential option based on the total priority score associated to the considered option, i.e., the multiplication of all original scores at each defined level of the hierarchical order (Saaty and Vargas, 2001; Saaty, 2008).

Table 2.5 Scale of preference between pair of factors in pairwise comparison process of the AHP method (Saaty and Vargas, 2001).

Scale	Degree of preference	Explanation
1	Equally	Two activities contribute equally o the objective
3	Moderately	Experience and judgment slightly to moderately favor one activity over another
5	Strongly	Experience and judgment strongly or essentially favor one activity over another
7	Very strongly	An activity is strongly favored over another and its dominance is showed in practice
9	Extremely	The evidence of favoring one activity over another is of the highest degree possible of an affirmation
2,4,6,8	Intermediate	Used to represent compromises between the preference in weight 1,3,5,7 and 9
Reciprocals	Opposites	Used for inverse comparison

AHP has been often applied to landslide susceptibility analysis in which it was used principally to determine appropriate factor weights and class weights for all

included contributing factors, such as, Yoshimatsu and Abe (2006); Yalcin et al. (2011); Intarawichian and Dasananda (2011); Long and De Smedt, (2012); Bagherzadeh and Daneshvar (2012). Clear advantage of the AHP in landslide susceptibility analysis is its capability to include all kinds of contributing factor into the analysis process and the preference order of the factors (and their attributes) can be established automatically through application of used pairwise comparison method. In addition, the consistency of judgment in comparison process can be directly verified to determine credibility of the applied methodology. However, main disadvantage of AHP is its lack of generality in the applied preference judgment rules for each pair of the listed contributing factors due to subjective nature of decision in the standard pairwise comparison method which is usually depended on the collective expert opinion or on the group consensus (Long and De Smedt, 2012). After final weights of all factors and their attributes are known, susceptibility map can be constructed as a consequence from the pixel-based landslide susceptibility index (LSI) computation using Eq. (2.8).

The formal procedure of the AHP method to landslide susceptibility analysis can be summarized in conclusive details as follows (Triantaphyllou and Mann, 1995; Bachri and Shresta, 2010; Long and De Smedt, 2012):

- (1) Construction of the pairwise comparison matrix used for the determination of the preferred factor weights and class weights. In this process, all relevant elements are compared in pair and a preference scale is given to each pair of data ranging from 1 to 9 (as detailed in Table 2.5). These results are then put in order to create a pairwise comparison matrix of size n (n is number of used elements) (like ones in Table 2.6).

(2) Determination for the appropriate factor and class weights. At this step, priority score for each factor (and their listed attributes) are quantified. This can be done through several methods as stated in Gao, Zhang and Cao (2009) but the most popular ones are the eigenvector method, sum method and geometric mean method.

(2.1) Eigenvector method. This one is from the basis of the AHP theory originally described in Satty (1980) where preference vector ω is introduced to fulfill the following relation:

$$A\omega = \lambda_{max} \omega, \quad (2.9)$$

here, A is pairwise comparison matrix of order n denoted by $A = (a_{ij})$ where i and j are the row and column indices, respectively, and n is the number of total contributing factors (or attributes) in use. The matrix member a_{ij} is a preference scale for compared factors (or attributes) i and j with constrains: $a_{ij} = 1/a_{ji}$, for $i \neq j$, and $a_{ii} = 1$, for all i , which make A being a reciprocal matrix. In this case, ω is an eigenvector and λ_{max} is a maximum eigenvalue of matrix A corresponding to ω . By solving Eq. (2.9), members of vector ω could be identified and their normalized values (by dividing the original ones with their sum) shall become respective weight values for the considered factors (or attributes) by matching one by one for each row of A and ω .

(2.2) Sum method. This might be called the normalized-sum-average method as the first task is to normalize all members of the original preference matrix by dividing each matrix element by net sum of all elements found in its column. Then, the priority score for each listed factor (or attribute) is derived from the average

of all elements in a row that the studied factor (or attribute) is belonged. This aforementioned procedure can be written as:

$$\omega_i = \frac{1}{n} \sum_{j=1}^n \frac{a_{ij}}{\sum_{k=1}^n a_{kj}} \quad (i = 1, 2, \dots, n) \quad (2.10)$$

(2.3) Geometric mean method. In this case, the priority scores are first determined by multiplying all elements in each row of the preference matrix and take the n-th root of the product result. These yielded data are then normalized by dividing them with their sum to attain respective weights for each listed element as an outcome (matching row by row). This stated procedure can be written as:

$$\omega_i = \frac{\left(\prod_{j=1}^n a_{ij} \right)^{\frac{1}{n}}}{\sum_{k=1}^n \left(\prod_{j=1}^n a_{kj} \right)^{\frac{1}{n}}} \quad (i = 1, 2, \dots, n) \quad (2.11)$$

(3) Assessment for consistency of the judgment. Before the resulted weights in previous step are put in use, satisfied consistency of the comparison must be ensured. For the ideal performance with a perfect consistency in the comparison, i.e. $a_{ij} \cdot a_{jk} = a_{ik}$, $\lambda_{max} = n$, but for the general cases with some inconsistency in the judgment, $\lambda_{max} > n$. Degree of the inconsistency in the used judgment can be quantified by using an index called the consistent ratio index (CR) defined as:

$$CR = \frac{CI}{RI}, \quad (2.12)$$

where CI is the defined consistency index and RI is called the random index; which is the consistency index of a randomly-generated pairwise comparison matrix. And, as discussed in Saaty (1980), if the CR is significantly low (i.e. $CR \leq 0.1$), this means the overall judgment is rather reliable and the achieved factor (or attribute) weights can be accepted for further use. However, if $CR > 0.1$ (or 10%), it indicates that subjective judgment in use is still too inconsistent and needed to be revised accordingly.

The consistency index (CI) was introduced to be a measure of the consistency of the pairwise comparison preferences in use which is defined as:

$$CI = \frac{\lambda_{\max} - n}{(n-1)}, \quad (2.13)$$

value of λ_{\max} can be identify directly from Eq. (2.9) provided that matrices A and ω are already known form earlier works [as explained in Coyle (2004)] and standard values of random index are listed in Table 2.6 as a function of matrix size.

Table 2.6 Random index (RI) given by Saaty (1980) as a function of matrix size (n).

n	1	2	3	4	5	6	7	8	9	10	11	12
RI	0.00	0.00	0.58	0.90	1.12	1.24	1.32	1.41	1.45	1.49	1.51	1.54
n	13	14	15									
RI	1.56	1.57	1.59									

To illustrate applied procedure of the AHP method to landslide susceptibility analysis in more details, resulted preference matrix reported in work of Thanh and De Smedt (2012) for their study area in central Vietnam is presented here as an example in

Table 2.7. It was found that, among nine factors included in the study; slope angle and precipitation were having top priority at weights of 0.303 and 0.236, respectively. And elevation and drainage distance are the two factors with lowest priority with weights of 0.021 and 0.025 respectively. For the slope category, the highest rank was evidenced at slope $> 35^\circ$ with weight of 0.347 and for land use group, shrubs/bare hills and afforest land were found most important with the total weights of 0.615 and 0.255, respectively. Table 2.8 describes information of essential variables used in the consistency analysis of this work. Note that, half of the preference matrix was left empty but actual members are just a respective reciprocal of the shown preference scale for the same pair of data.

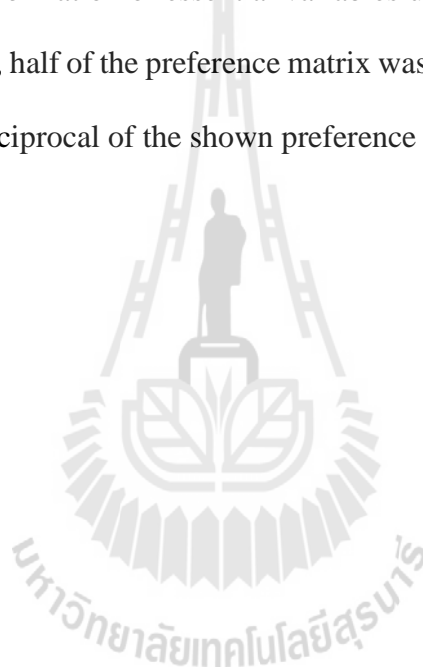


Table 2.7 Example of the pair-wise comparison matrix, or preference matrix, reported in Thanh and De Smedt (2012) along with the corresponding normalized eigenvector (representing factor, or attribute, weights of the analysis).

Causative factors and classes within each factor	Pair-wise comparison matrixes													Eigen-vector:
	[1]	[2]	[3]	[4]	[5]	[6]	[7]	[8]	[9]	[10]	[11]	[12]	[13]	
Factors														
[1] Slope angle	1													0.303
[2] Weathering	1/3	1												0.151
[3] Land use	1/4	1/2	1											0.108
[4] Geomorphology	1/5	1/3	1/2	1										0.078
[5] Fault density	1/7	1/5	1/3	1/3	1									0.045
[6] Geology	1/6	1/4	1/4	1/2	1/2	1								0.033
[7] Drainage distance	1/8	1/6	1/6	1/5	1/3	2	1							0.025
[8] Elevation	1/9	1/7	1/7	1/7	1/4	1/3	2	1						0.021
[9] Precipitation	1/2	2	3	5	7	6	8	9	1					0.236
Slope angle														
[1] <5°	1													0.032
[2] 5°–15°	2	1												0.046
[3] 15°–25°	4	2	1											0.089
[4] 25°–35°	6	4	2	1										0.139
[5] 35°–45°	7	7	4	4	1									0.347
[6] >45°	7	7	4	4	1	1								0.347
Weathering														
[1] Quaternary deposit	1													0.046
[2] Ferrosiallite	3	1												0.093
[3] Silixite mixtures	5	3	1											0.269
[4] Sialferrite	7	5	2	1										0.469
[5] Siallite	3	2	1/3	1/5	1									0.123
Land use														
[1] Cultivated areas	1													0.065
[2] Afforest land	5	1												0.255
[3] Shrubs and bare hills	7	4	1											0.615
[4] Village and built-up area	1	1/5	1/7	1										0.065

Table 2.8 Information of essential variables used in the consistency analysis reported in Thanh and De Smedt (2012).

Causative factors	<i>n</i>	λ_{\max}	CI	RI	CR (%)
All	9	9.75	0.093	1.45	6.4
Slope angle	6	6.23	0.045	1.24	3.6
Weathering	5	5.14	0.035	1.12	3.1
Land use	4	4.14	0.047	0.90	5.2
Geomorphology	8	8.19	0.027	1.41	1.9
Fault density	4	4.11	0.036	0.90	4.0
Geology	13	14.28	0.107	1.56	6.8
Drainage distance	3	3.07	0.033	0.58	5.6
Precipitation	3	3.07	0.033	0.58	5.6
Elevation	4	4.12	0.039	0.90	4.3

Values of CR smaller than 10% indicate consistency of the preference matrix

2.6.3 Frequency ratio (FR)

Frequency ratio (FR) is a popular quantitative approach (of bivariate type) in landslide susceptibility evaluation, e.g. in Lee and Sambath (2006); Vijith and Madhu (2007); Oh et al. (2009); Pradhan and Lee (2010); Intarawichian and Dasananda (2011); Yalcin et al. (2011); Park, Choi, Kim and Kim (2013). This method is famous for its simple concept and straightforward calculation of landslide susceptibility index which can be performed by most widely-used GIS softwares. In principle, it works by finding relative importance of each incorporated factor's attribute (defined as a class weight) in producing past landslides independently and describes it in terms of the FR index. The index is simply defined by a ratio of the landslide occurrence percentage and area occupation percentage for that attribute compared to the whole area, or,

$$FR = \frac{(CLP/TLP)}{(CA/TA)} = \frac{(CLP/CA)}{(TLP/TA)}, \quad (2.14)$$

where CLP is number of landslide pixels seen in a specific class (of a certain factor), TLP is number of total number of the observed landslide pixels, CA is the associated total class area and TA is total study area.

By definition seen in Eq. (2.14), FR shall represent the landslide frequency over a unit area of a considered attribute compared to that of the entire area. In this case, FR can be any number from 0 onwards. For $FR < 1$, it means landslide occurrence per unit area of that factor's attribute (or class) is lower than the determined average value (for the entire area), which implies that it is less important in producing landslide over the area. For $FR > 1$, it means this attribute has higher landslide

frequency than average (indicating greater influence in producing landslide) and $FR = 1$ means the result is comparable to average (Lee, 2005).

After the FR values for all attributes of used factors are determined, they can be applied to quantify landslide susceptibility index (LSI) on a pixel-based basis using the following formula:

$$LSI = \sum_{i=1}^n FR_i , \quad (2.15)$$

where FR_i is the FR value for the corresponding attribute of factor i of the considered pixel and n is the total number of used factors. The accumulated LSI values in a study area can be applied for the formulation of the landslide susceptibility map for the area afterwards using the chosen mapping method of interest.

Though FR model is widely adopted at present for the creation of landslide susceptibility map worldwide, this method still contains some distinct shortcomings in itself. For examples, it evaluates the importance of each causative factor individually and ignores any spatial autocorrelation between them. As a result, some areas might be overemphasized of their proneness to having landslide activity (with higher LSI values) if two or more dominant factors (with relatively high FR score) are highly correlated to each other. In addition, it needs sufficient and well-distributed reference landslide data in order to determine the FR index more realistically (with less bias) (Intarawichian and Dasananda, 2011).

Table 2.9 shows examples of the frequency ratio (FR) value given in work of Vijith and Madhu (2008) for a study area in Western Ghats of Kerala, southern India. The result indicates strong correlation of landslide activity with slope angle of

30-35° (FR = 2.86), slope aspect along the N and W directions (FR = 2.01, 2.22), slope range of > 750 m (FR = 2.06), lithology in the quartzite class (FR = 2.84), and land use in natural vegetation class (FR = 2.51).

Table 2.9 Frequency ratio (FR) index found in work of Vijith and Madhu (2008).

Thematic layer	Class	Number of pixels in the class	Class (%)	Number of landslide pixels within the class	Slide (%)	Frequency ratio
Slope angle (Degree)	0-5	114610	29.58	6	11.76	0.39
	0-10	23809	6.15	3	5.88	0.95
	0-15	39062	10.08	1	1.96	0.19
	15-20	47724	12.32	8	15.68	1.27
	20-25	44228	11.41	7	13.73	1.20
	25-30	36101	9.3	7	13.73	1.47
	30-35	26498	6.84	10	19.61	2.86
	35-40	18965	4.89	4	7.85	1.60
	>40	36521	9.43	5	9.80	1.03
Slope aspect	Flat	83366	21.41	1	1.96	0.09
	N	18913	4.98	5	9.81	2.01
	NE	45792	11.83	4	7.84	0.66
	E	40173	10.36	6	11.76	1.13
	SE	35719	9.21	4	7.85	0.85
	S	39130	10.09	10	19.60	1.94
	SW	48068	12.42	8	15.68	1.26
	W	40976	10.57	12	23.52	2.22
Slope curvature	NW	35381	9.13	1	1.96	0.21
	Concave	56511	14.58	10	19.61	1.34
	Flat	170875	44.10	10	19.61	0.44
Slope length (m)	Convex	160132	41.32	31	60.78	1.45
	<1	122283	31.55	6	11.77	0.37
	1-250	195827	50.53	31	60.78	1.20
Distance from drainage (m)	250-750	36253	9.36	5	9.80	1.04
	>750	33155	8.56	9	17.65	2.06
	0-100	192896	49.78	23	45.10	0.90
	100-200	126235	32.57	22	43.14	1.32
	200-300	50787	13.11	5	9.80	0.74
Distance from lineament (m)	300-400	13414	3.46	1	1.96	0.56
	>400	4186	1.08	0	0.00	0.00
	0-100	73891	19.07	8	15.69	0.82
	100-200	70961	18.31	12	23.52	1.28
	200-300	60329	15.56	10	19.61	1.26
Lithology	300-400	47235	12.18	10	19.61	1.61
	>400	135102	34.86	11	21.57	0.61
	Charnockite	362651	93.59	49	96.08	1.03
	Quartzite	2680	0.69	1	1.96	2.84
	Dolerite	4772	1.24	1	1.96	1.59
Landuse	Biotite gneiss	13911	3.58	0	0.00	0.00
	Granite	3504	0.9	0	0.00	0.00
	Natural vegetation	30177	7.79	10	19.61	2.51
	Grass land	21469	5.64	2	3.92	0.69
	Barren land	23932	6.18	4	7.85	1.27
	Crop land	1790	0.46	0	0.00	0.00
	Rubber	268784	69.36	30	58.82	0.84
	Tea	18817	4.87	0	0.00	0.00
	Cleared area	22080	5.70	5	9.80	1.71
	Built up land	70	0.00	0	0.00	0.00
Water body	399	0.00	0	0.00	0.00	

2.6.4 Logistic regression (LR)

Logistic regression is one of the well-known multivariate analysis methods for making landslide susceptibility maps in recent years, e.g. Nefeslioglu, Gokceoglu and Sonmez (2008); Akgun, Kincal and Pradhan (2011); Ercanoglu and Temiz (2011); Yalzin et al. (2011); Akgun (2012). In essence, the logistic regression is an extension of the ordinary linear regression in which the considered dependent variable is not of a continuous type as usual but becomes a categorical type with some certain number of its possible states (or values). If only two states are possible, e.g., presence/absence, men/women, success/failure, 0/1, this case shall be called a binomial (or binary) logistic regression, but if more states are also an option for being an eventual outcome, this shall be called multinomial logistic regression (Czepiel, 2013).

Logistic regression is superior to the ordinary regression in terms of the able input data (as independent variables) that include both numerical and categorical type. Main objective of the analysis is to identify a suitable regression function (of the used independent variables) that can satisfactorily describe probability of having a certain outcome of the dependent variable. These properties of the logistic regression method suit the landslide susceptibility analysis well, as in this work, the dependent variable is the presence or absence of landslide incidence at a specific pixel over the study area which is assumed to be resulted from the complex interaction of several contributing factors of both numerical and categorical types. Hence, it might be possible to assess landslide occurrence likelihood for each pixel assumed that the relation of independent factors, one that actually determines the absence or presence of the landslide activity in the area, can be evaluated through the binary logistic regression method (Ayalew and Yamagishi, 2005; Lee, 2005; Pradhan, 2010).

Common concept of the method is based on assumption that the probability of having a landslide incidence at a particular pixel (p) can be quantified through the use of a specific function called log-odds or Logit(p) defined as (Lee, 2005):

$$L = \text{Logit}(p) = \ln\left(\frac{p}{1-p}\right). \quad (2.16)$$

This function is conceptually assumed to have linear regression relation with the used dependent variables, or,

$$L = c_0 + c_1x_1 + c_2x_2 + \dots + c_nx_n. \quad (2.17)$$

The crucial task here is to find the proper values of the coefficients c_0 , c_1 , ... c_n from the reference landslide data and their associated contributing factors x_1 , x_2 , ..., x_n . This process is usually achieved by using maximum likelihood estimation technique to solve for appropriate values of parameters that best fit the landslide data as detailed in Dayton (1992) and Czepiel (2013). The known value of L for each pixel can be used to calculate the probability p as follows:

$$p = \frac{e^L}{1+e^L} = \frac{1}{1+e^{-L}}. \quad (2.18)$$

These pixel-based probability values (of 0-1) can be used as landslide susceptibility index (LSI) for making susceptibility map of the area afterwards.

Note that, it is commonly desired that all continuous variables have the same scale in the multivariate statistical analyses. From this reason, all continuous variables (like slope, elevation, and proximity) should be normalized to have values in the range of [0, 1]. And for the categorical data (like land use or soil type), they are expressed in binary format (presence/absence) with respect to each attribute of the referred factor, similar to that of the dependent variable. One of the main requests of the multivariable statistical applications is equal sampling of the training data set (of reference landslide data). This means that the ratio of presence (1) to absence (0) should be equal to 1 in the training data sets (Nefeslioglu et al., 2008).

Table 2.10 presents final results (FR values and logistic regression coefficients) of the landslide hazard analysis using FR and logistic regression methods reported in Lee and Pradhan (2007) for an area in Selangor, Malaysia. From this study, the proper relationship of Logit function L with the used influencing factors was found to be:

$$\begin{aligned}
 L = & 0.0780 \cdot \text{Slope} + \text{Aspect} - 0.0032 \cdot \text{Curvature} - 0.0048 \cdot \text{Drainage} \\
 & + \text{Lithology} + 0.0001 \cdot \text{Lineament} - 1.3633 \cdot \text{NDVI} + \text{Landcover} \quad (2.19) \\
 & + 0.0043 \cdot \text{Precipitation} - 16.4726.
 \end{aligned}$$

Table 2.10 Example landslide susceptibility analysis using FR and logistic regression models by Lee and Pradhan (2007) in Selangor, Malaysia.

Factor	Class	Number of pixels showing landslide occurrence	Percentage of pixels showing Landslide occurrence	Pixels in domain	Pixel %	Frequency ratio	Coefficients of logistic regression
Slope	0~15 degree	67,777,334	82.86	115	35.17	0.42	0.0780
	16~25 degree	8,426,979	10.30	87	26.61	2.58	
	26~35 degree	4,648,328	5.68	68	20.80	3.66	
	35~85 degree	940,212	1.15	57	17.43	15.16	
Aspect	Flat	32,746,440	40.04	0	0.00	0.00	-9.1703
	North	5,541,254	6.77	55	16.82	2.48	-1.9392
	Northeast	6,678,670	8.17	45	13.76	1.69	-1.3081
	East	6,077,711	7.43	27	8.26	1.11	-1.2635
	Southeast	6,181,783	7.56	28	8.56	1.13	-1.9959
	South	5,564,596	6.80	29	8.87	1.30	-1.1984
	Southwest	6,721,149	8.22	35	10.70	1.30	-2.0135
	West	6,105,258	7.46	46	14.07	1.88	-2.0177
	Northwest	6,175,992	7.55	62	18.96	2.51	0.0000
Curvature	Concave	13,288,765	16.25	66	20.18	1.24	-0.0032
	Flat	55,283,859	67.59	15	4.59	0.07	
	Convex	13,220,229	16.16	246	75.23	4.65	
Distance from drainage	0~20 m	8,269,740	10.11	34	10.40	1.03	-0.0048
	21~50 m	10,004,084	12.23	88	26.91	2.20	
	51~80 m	8,281,601	10.13	64	19.57	1.93	
	81~120 m	8,714,376	10.65	54	16.51	1.55	
	121~183 m	7,870,547	9.62	52	15.90	1.65	
	184~357 m	7,731,050	9.45	32	9.79	1.04	
	358~804 m	7,737,710	9.46	3	0.92	0.10	
	805~1,546 m	7,730,045	9.45	0	0.00	0.00	
	1,547~2,765 m	7,730,365	9.45	0	0.00	0.00	
	2,766~9,912 m	7,723,339	9.44	0	0.00	0.00	
	Geology	Acid intrusives (undifferentiated)	18,064,989	22.27	197	60.24	
Add intermediate volcanics		6,352,018	7.83	30	9.17	1.17	-6.1941
Basic intrusives, mainly gabbro		20,480,378	25.25	0	0.00	0.00	-9.2067
Clay and silt (marine)		6,947,667	8.57	19	5.81	0.68	-12.8382
Clay and silt, sand and gravel		11,351,353	13.99	1	0.31	0.02	6.6926

2.6.5 Artificial neural network (ANN)

An artificial neural network (ANN) is generally defined as a computational mechanism able to acquire, represent, and compute a mapping from one multivariate space of information to another, given a set of data representing that mapping (Garrett 1994). ANN works by finding optimal paths to connect several input data to a trained correct output and uses them as a reference to predict correct output for a given set of input afterwards. Therefore, there are two stages involved in using ANN for multi-source classification: the training stage and the classifying stage (Figure 2.16).

The structure of ANN is comprised of a multi-layered neural network, which consists of an input layer, hidden layers, and an output layer (Figure 2.15). Input data are fed through the complex hidden layer that will process them to gain most correct output during the training session of the system. In the process, the hidden and output layer neurons shall process their inputs by multiplying each input by a corresponding weight, summing up the product, then processing the sum using a nonlinear transfer function to produce a definite result. This network gradually learn to know the proper weights (for each input factor) that lead to the correct results by adjusting the internal weights between neurons to reduce errors between actual output values and the target output values. At the end of this training phase (after a large number of tries), the neural network provides an appropriate model that is able to predict a target value correctly from a given input value. Typically, the back-propagation algorithm is applied to train the network where the training session continues until some targeted minimal error is achieved between the desired and actual output values of the network. Once the training is complete, the network is used as a feed-forward structure to produce a classification for the entire data (Paola and Schwengerdt, 1995).

The ANN approach for landslide susceptibility mapping has attracted more attention in recent years, e.g. in Kanungo et al. (2006); Lee and Evangelista (2006), Yilmaz (2009); Pradhan, Lee and Buchroithner (2010); Paval, Nelson and Fannin (2011), due to its distinct ability to identify a nonlinear relationship of the past landslide data and a set of the chosen contributing factors automatically which cannot be achieved by the conventional methods like the FR or logistic regression. And, due to the ability of the ANN method to incorporate the imprecise and fuzzy data, hence, they can work with numerical, categorical and binary data without violating any prior assumptions.

Generally, a three-layer feed-forward network consisting of an input layer, one hidden layer and one output layer was found appropriate as an ANN structure for the analysis of landslide susceptibility for an interested area (Yilmaz, 2009).

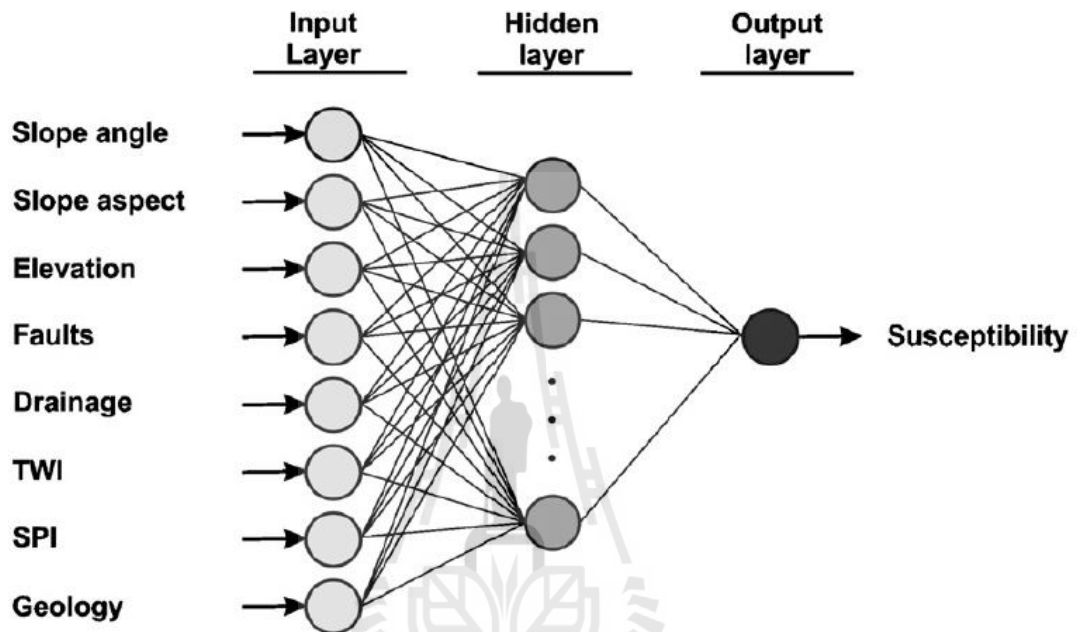


Figure 2.15 Typical ANN architecture for landslide classification (Yilmaz, 2009).

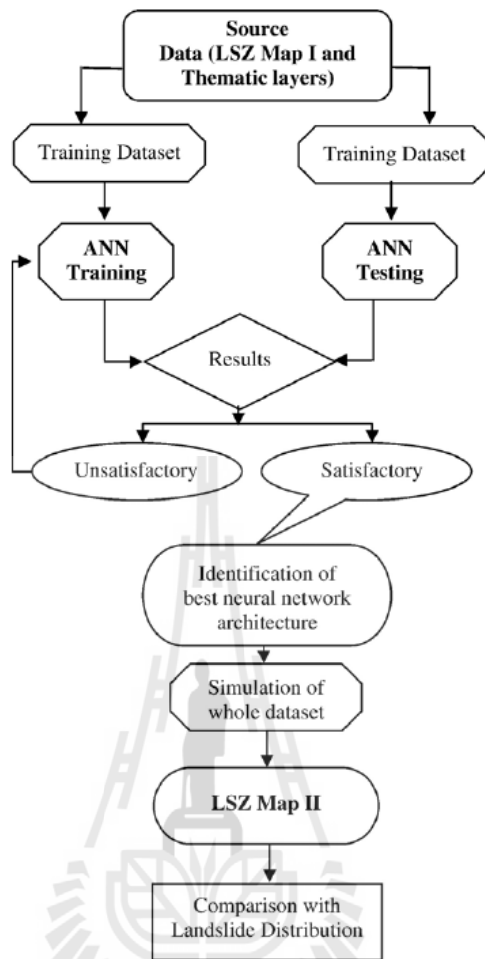


Figure 2.16 Typical ANN work flowchart for landslide susceptibility classification comprising of two steps; training and classifying (Kanungo et al., 2006).

2.6.6 Fuzzy logic approach

The fuzzy set theory proposed by Zadeh (1965) is one of the standard tools for solving complex problem containing vague information. The most notable aspect of this methodology is its possibility of capturing, in a mathematical model, the intuitive concepts which are the base of consistent judgment (Saboya, Alves and Pinto, 2006). The method has been widely applied for many scientific studies in different disciplines including landslide susceptibility analysis, such as, Saboya et al. (2006); Lee

(2007); Gorsevski and Jankowski (2010); Guettouche (2012); Pourghasemi et al. (2012). Fuzzy logic is attractive due to its capability to justify likelihood of the slope failure based on the imprecise determination criteria defined by experts or from the knowledge inherited from other relevant methods.

Main concept of this theory is based on a mathematical theory of fuzzy sets, which is an extension of the classical sets to sets defined imprecisely. A fuzzy set can be described as a set containing elements that have varying degrees of membership in the set whose corresponding mathematical expression can be written as follows (Ross, 1995; Ercanoglu and Temiz, 2011):

$$A = \{(x, \mu_A(x))\}; x \in X, \quad (2.20)$$

where A is a given fuzzy set, μ is a membership function, and x is the element of X universe. The fuzzy set theory is different from the classical set theory as in the latter case, membership values of an element for a specific set are either 1 (being a member) or 0 (not being a member), but in the first case (fuzzy set), possible membership values of an element regarding to that set have a continuous scale from 1 (for full membership) to 0 (for full non-membership), reflecting degree of certainty of being membership (see the illustration in Figure 2.17 for example).

For the landslide susceptibility analysis, an attribute of a specific contributing factor shall be considered as being a member of the landslide producer set with a certain fuzzy-membership value. These values can be assessed by some data-driven methods, such as the frequency ratio (FR) model mentioned earlier (e.g. Lee,

2007; Regmi et al., 2010; Aksoy and Ercanoglu, 2012) or the cosine amplitude method (e.g. Ercanoglu and Gokceoglu, 2004; Kanungo et al., 2006; Ercanoglu and Temiz, 2011), or by the expert-based judgments through the application of the defined if-then rules (e.g. Saboya, Alves and Pinto, 2006; Pourghasemi et al., 2012). Table 2.11 gives examples of the FR-based fuzzy membership values of attributes presented in works of Lee (2007); Bui, Pradhan, Lofman, Revhaug and Dick (2012), respectively.

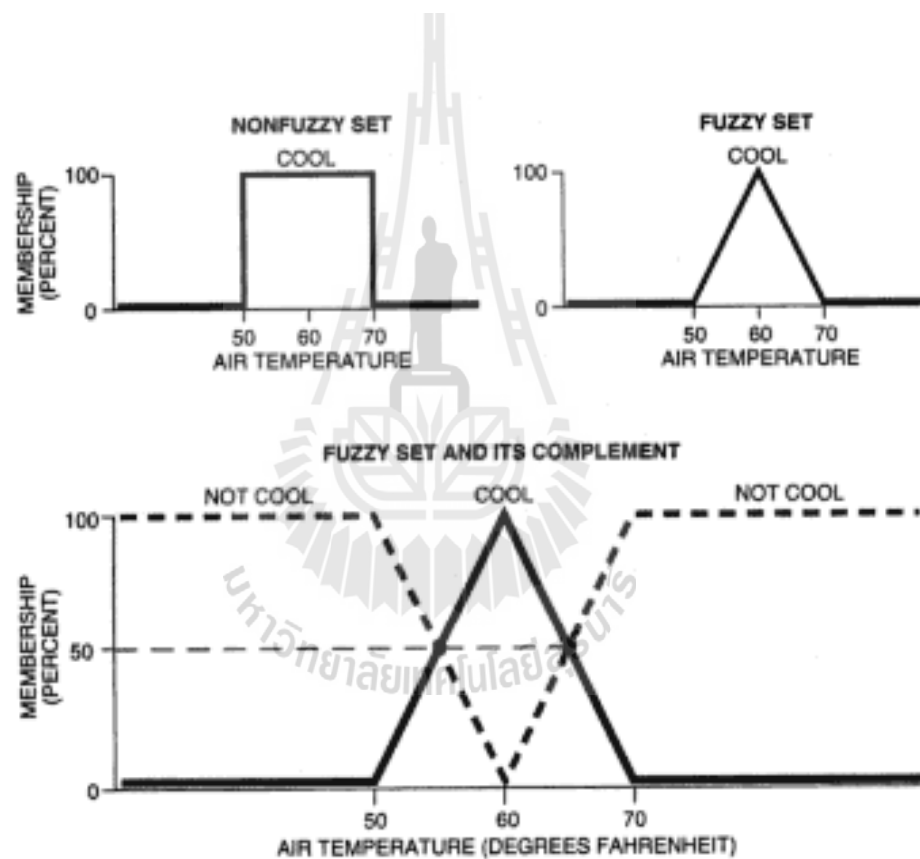


Figure 2.17 Example of the fuzzy set and its complement with the membership values of 0 to 100% (for “cool” and “not cool” conditions) (Fano, 2011).

To produce a susceptibility map, the fuzzy membership values from each used factor (i.e., that of a corresponding attribute for a considered pixel) are then integrated to yield a landslide susceptibility index (LSI) outcome for each unit area (or a pixel). This task can be accomplished by using five fuzzy operators: fuzzy-OR, fuzzy-AND, fuzzy algebraic sum, fuzzy algebraic product, and fuzzy-gamma, which can be written mathematically as follows (Regmi et al., 2010):

$$\text{FuzzyOR} : \mu_{OR} = \text{MAX}(\mu_A, \mu_B, \mu_C, \dots)$$

$$\text{FuzzyAND} : \mu_{AND} = \text{MIN}(\mu_A, \mu_B, \mu_C, \dots)$$

$$\text{Fuzzy algebraic sum} : \mu_{sum} = 1 - \prod_{i=1}^n (1 - \mu_i) \quad ,$$

$$\text{Fuzzy algebraic product} : \mu_{product} = \prod_{i=1}^n \mu_i$$

$$\text{Fuzzy gamma} : \mu_{gamma} = [\text{Fuzzy algebraic sum}]^\lambda \times [\text{Fuzzy algebraic product}]^{1-\lambda}$$

where μ_i is the fuzzy-membership function for the i -th factor map, and $i = 1, 2, 3, \dots, n$ and $\lambda = [0, 1]$.

From these standard definitions, it is obvious that, for the fuzzy-OR operator, the yielded result at any particular location is controlled by the maximum input fuzzy membership function. On the contrary, for the fuzzy-AND operator, this output result is controlled by the smallest value of the input data. These operators are appropriate if the landslide activity at a particular location is controlled mostly by a single dominant contributor, otherwise, the other three operators (sum, product, and gamma) should be more suitable for the application. Note that, operation gamma is a compromise between the increase tendency of the fuzzy algebraic sum and the decrease tendency of the fuzzy algebraic product in which $\lambda = 0$ is giving pure fuzzy product and $\lambda = 1$ is giving actual fuzzy sum operator (Figure 2.18) (Lee, 2007; Regmi et al.,

2010). In literature review, the gamma and product operators often found most effective in formulating the credible landslide susceptibility map compared to the other operators (Table 2.12); e.g. in Lee (2007); Regmi et al. (2010); Ercanoglu and Temiz (2011).

Table 2.11a Examples of the FR-based fuzzy membership values for the respective attributes of a specific contributing factor presented in Lee (2007).

Factor	Class	No. of pixels in domain	Percentage of domain	No. of landslide	Percentage of landslide	Frequency ratio	Fuzzy membership values
Slope	0-5	336,945	17.57	0	0.00	0.00	0.00
	6-10	204,758	10.68	2	0.59	0.06	0.01
	11-15	311,658	16.25	13	3.86	0.24	0.04
	16-20	362,062	18.88	46	13.65	0.72	0.13
	21-25	322,133	16.80	78	23.15	1.38	0.24
	26-30	217,740	11.36	97	28.78	2.53	0.44
	31-35	108,568	5.66	67	19.88	3.51	0.61
	36-40	39,827	2.08	20	5.93	2.86	0.49
	41-90	13,783	0.72	14	4.15	5.78	1.00
Aspect	Flat	82,385	4.30	0	0.00	0.00	0.00
	North	226,606	11.82	18	5.34	0.45	0.25
	Northeast	292,155	15.24	39	11.57	0.76	0.42
	East	299,541	15.62	56	16.62	1.06	0.58
	Southeast	247,143	12.89	33	9.79	0.76	0.42
	South	165,431	8.63	53	15.73	1.82	1.00
	Southwest	169,659	8.85	35	10.39	1.17	0.64
	West	209,333	10.92	57	16.91	1.55	0.85
	Northwest	225,221	11.75	46	13.65	1.16	0.64
Curvature	Concave	557,948	29.10	99	29.38	1.01	0.44
	Flat	785,003	40.94	91	27.00	0.66	0.00
	Convex	574,523	29.96	147	43.62	1.46	1.00
Distance from drainage	Buffer (100 m)	1,421,849	74.15	243	72.11	0.97	0.85
	Buffer (200 m)	374,666	19.54	74	21.96	1.12	0.98
	Buffer (300 m)	86,849	4.53	14	4.15	0.92	0.80
	Buffer (400 m)	29,718	1.55	6	1.78	1.15	1.00
	Buffer (>400 m)	4,392	0.23	0	0.00	0.00	0.00

Table 2.11b Examples of the FR-based fuzzy membership values for the respective attributes of a specific contributing factor presented in Bui et al. (2012).

Data layers	Class	Number of class pixels	Landslide pixels	Frequency ratio	Fuzzy value
Slope ($^{\circ}$)	0–10	4,919,804	2	0.007	0.102
	10–20	3,346,950	222	1.114	0.435
	20–30	2,326,636	368	2.657	0.900
	30–40	785,451	92	1.968	0.692
	40–50	106,715	0	0.000	0.100
	>50	4750	0	0.000	0.100
Aspect ($^{\circ}$)	Flat (-1)	6556	0	0.000	0.100
	North (0–22.5; 337.5–360)	1,380,854	27	0.328	0.251
	Northeast (22.5–67.5)	1,672,941	82	0.823	0.478
	East (67.5–112.5)	1,385,498	44	0.533	0.345
	Southeast (112.5–157.5)	1,383,072	106	1.287	0.691
	South (157.5–202.5)	1,482,483	138	1.564	0.818
	Southwest (202.5–247.5)	1,677,042	174	1.743	0.900
	West (247.5–292.5)	1,299,469	65	0.840	0.486
	Northwest (292.5–337.5)	1,202,391	48	0.671	0.408
Relief Amplitude (m)	0–50	3,101,843	6	0.032	0.100
	50–100	2,753,898	228	1.391	0.843
	100–150	2,640,812	235	1.495	0.900
	150–200	1,694,502	126	1.249	0.766
	200–250	811,634	53	1.097	0.682
	250–532	487,617	36	1.240	0.761

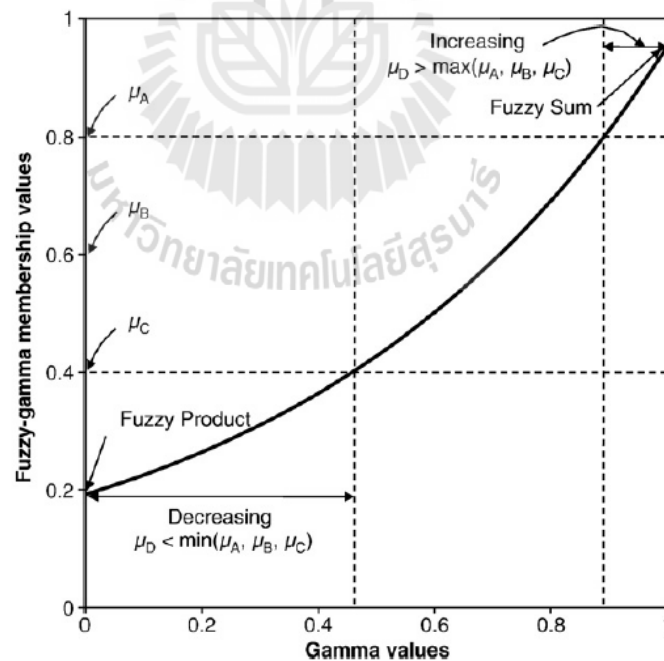


Figure 2.18 Graph showing example of the combination of three fuzzy factors

($\mu_A = 0.8$, $\mu_B = 0.6$, $\mu_C = 0.4$) by fuzzy-gamma operation (Regmi et al., 2010).

Table 2.12 Report of accuracy scales for used fuzzy logic operators in Lee (2007).

Fuzzy operator	Prediction accuracy (%)
Fuzzy and	66.79
Fuzzy or	66.50
Fuzzy algebraic sum	78.92
Fuzzy algebraic product	84.58
Gamma (λ) = 0.025	84.57
Gamma (λ) = 0.05	84.58
Gamma (λ) = 0.1	84.55
Gamma (λ) = 0.2	84.55
Gamma (λ) = 0.3	84.55
Gamma (λ) = 0.4	84.55
Gamma (λ) = 0.5	84.55
Gamma (λ) = 0.6	84.56
Gamma (λ) = 0.7	84.57
Gamma (λ) = 0.8	84.58
Gamma (λ) = 0.9	84.61
Gamma (λ) = 0.95	84.63
Gamma (λ) = 0.975	84.68

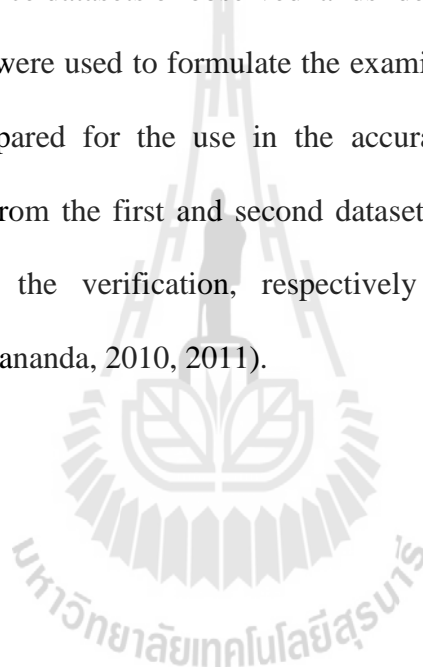
2.7 Accuracy assessment of yielded susceptibility maps

All attained susceptibility maps from each preferred method were eventually assessed for their accuracy with two popular methods: The Area-Under-Curve (AUC) and Receiver Operating Characteristic (ROC) curves analysis. The acquired degree of accuracy shall be taken as primary indicator of efficiency for each evaluated model in the construction of the credential susceptibility map for the study area.

2.7.1 The Area-Under-Curve (AUC) method

The AUC works by creating a specific rate curve illustrating percentage of known landslides that falls into each defined level of the susceptibility rank (LSI values) and displays it as cumulative frequency diagram. To build the rate curve, the LSI values of all pixels on the assessed map are sorted in descending order (from high to low) and divided into 100 classes with equal number of member for each defined class. The rate curve can be produced as a plot between the defined LSI rank

(i.e., 1-100) on the x-axis (higher rank means lower LSI values) and the accumulated percentage of the reference landslide pixels at each LSI rank on the y-axis (see Figure 2.19 for example). Total area under a rate curve (AUC) is used to determine prediction accuracy of the susceptibility map qualitatively in which larger area means higher accuracy achieved. And, in order to compare results quantitatively, the AUC data are typically re-scaled to have total area of 1 (means perfect prediction, or 100% accuracy). There were two reference datasets of observed landslides being used in this assessment process: (1) data that were used to formulate the examined susceptibility map before, (2) other dataset prepared for the use in the accuracy assessment process only. Accuracies acquired from the first and second dataset are called “success rate” and “prediction rate” of the verification, respectively (Vijith and Madhu, 2008; Intarawichian and Dasananda, 2010, 2011).



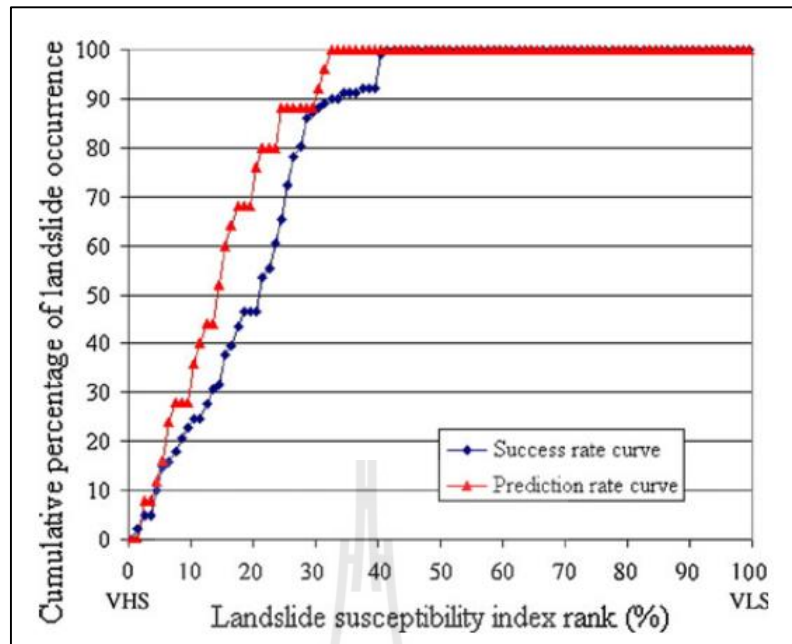


Figure 2.19 Examples of the cumulative frequency diagram in AUC method showing landslide susceptibility index rank (x-axis) in relation to the cumulative percent of landslide occurrence (y-axis) (Intarawichian and Dasananda, 2011)

2.7.2 Receiver Operating Characteristic (ROC) curves

Basically, the ROC curve is introduced and used as a measure of performance of a predictive rule. The graphs provide a diagnostic that might be used to distinguish between two classes of events, and to visualize classifier performance (Swets, 1988). In essence, the ROC curve is a plot of the probability of having a true positive versus the probability of having a false positive. For example, on the landslide prediction issue, a true positive is a prediction of having a slide for a location whereupon a slide actually occurred, while a false positive is a prediction of a slide for location where no slide did occur. An ideal model would have an area equal to 1 (100% accuracy), because in this case the probability of the true-positive case is 1 and of the false-positive is 0 regardless of the cutoff point (Williams et al., 1999).

Each point on the ROC curve may be related to a specific decision criterion for how much risk that a user is willing to take regarding the accuracy of the prediction. This referred point might vary among observers because their decision criteria can vary even when their concerned ROC curves are the same (Swets, 1988).

Table 2.13 Contingency table for ROC curve analysis method.

		Reference data	
		In class of interest (1)	Not in class of interest (0)
Simulated data	In class of interest (within threshold)	A (true positive)	B (false positive)
	Not in class of interest (not with threshold)	C (false negative)	D (true negative)

ROC is a summary statistic extracted from a comparison of simulated data with the reference data (as described in Table 2.13). Practically, ROC curve can be derived by computing the True Positive (TP) and False Positive (FP) rates from the contingency tables (for both dataset) associated to different proposed cut off values using following formulas (SafeLand- FP7, 2011):

$$\text{True positive rate (TP) = sensitivity} = \frac{TP}{TP + FN} = \frac{TP}{P}, \quad (2.21)$$

$$\text{False positive rate (FP) = 1- specificity} = \frac{FP}{FP + TN} = \frac{FP}{N}, \quad (2.22)$$

where specific meaning of all relevant parameters are as detailed in Table 2.14.

The primary goal of using ROC curve analysis is to find a cutoff value that will, in some way, minimize number of false predictions (positive/negative), or, maximizing the sensitivity and specificity of the prediction.

Table 2.14 Symbol description of ROC curves on landslide prediction issue.

Symbol	Measuring	Description
TP	True Positive rate	Proportion of pixels correctly predicted as landslide occurrences
TN	True Negative rate	Proportion of pixels correctly predicted as non-landslide occurrences
FP	False Positive rate	Proportion of pixels incorrectly predicted as landslide occurrences
FN	False Negative rate	Proportion of pixels incorrectly predicted as non-landslide occurrences
P	Positive	Proportion of pixels correctly predicted as landslide occurrences
N	Negative	Proportion of pixels correctly predicted as non-landslide occurrences

On landslide prediction issue, “sensitivity” is the probability that a landslide cell is correctly identified, and is plotted on the y-axis, while “specificity” is the probability that a non-slide cell is correctly classified, and is displayed along the x-axis of the curve. Hence, 1-specificity then defines the false positive rate. The area under the ROC curve in this case represents the probability that the gained susceptibility value for a randomly chosen landslide cell would exceed result for a randomly chosen non-landslide cell.

Similar to the AUC, The area under ROC curve can be approximated by adding areas of polygons between thresholds. Eq. (2.23) use integral calculus’ trapezoidal rule to compute the area (Pontius and Schneider, 2001).

$$AUC = \sum_{i=1}^n (x_{i+1} - x_i) (y_i + y_{i+1}) / 2, \quad (2.23)$$

where x_i is the rate of false positives for the threshold i , y_i is the rate of true positive for threshold i , and n is number of thresholds. By changing the cut off values, it is possible to obtain different contingency tables which correspond to different points in the ROC curve (Figure 2.20).

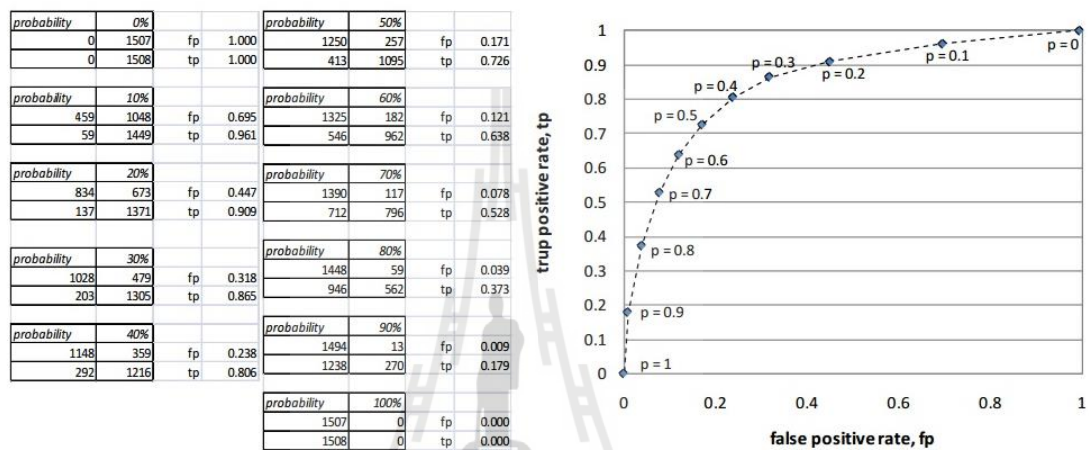


Figure 2.20 Example of contingency tables for different values (cut off) of membership probability of a landslide susceptibility assessing model and the associated ROC curve (of the true/false positive rates) (SafeLand - FP7, 2011).

2.8 Concept of the landslide-induced runout analysis

Landslide-induced runout has often become fundamental source of destruction for people's lives and properties of the affected community, therefore, knowledge of its development and resulted debris flow is crucial for preventing or reducing such losses. Runout is typically defined by means of the debris flow source which makes up of soil, rock, and water. As such, the reduction of potential losses can be pursued by prediction of their velocities and the runout distances. Indeed, runout prediction provides a mean of defining the realistic susceptible areas through the estimation of debris flow intensity

and its expansion over gentle terrain (which are necessary for conduction risk analysis). This knowledge is important for working design of the appropriate protective measures and, at the same time, the reliable predictions of runout characteristics can help avoiding exceedingly conservative or sensitive decisions regarding the pro-urban development of the potentially at-risk areas (Cascini et al., 2005).

Generally, the debris flow characteristics depend on the water content, sediment size and/or sorting, and on the dynamic interaction between the solid and fluid phases where modelling of such interaction still becomes a quite difficult task which relies on the use of some advanced empirical or numerical models (Pirulli and Sorbino, 2008). In this study, the runout hazard analysis was carried out through the application of high popularity Flow-R (Flow path assessment of gravitational hazards at a Regional scale) model. Flow-R is a distributed empirical model for regional susceptibility assessments of debris flows, developed at the University of Lausanne and was successfully applied worldwide so far. Flow-R is a free software with no limitation in scope of use that was built to process GIS-based regional susceptibility assessments of debris flows in which the identification of potential source areas and corresponding propagation extent are allowed. Marked characteristics of the software are (1) limited requirement of datasets (Figure 2.21) and (2) customization of inputs, algorithms, and the parameters, through a graphical user interface (Horton et al., 2013).

To fulfil its main objectives, two distinctive steps are needed for the application of the model (Iverson and Denlinger, 2001):

- (1) Identification of source area (based on topography and user-defined criteria),

(2) Analysis on the propagation mechanism of the induced debris flows from their sources on basis of frictional laws and flow direction algorithms.

Generally, two types of algorithms are necessary in the propagation assessment (Huggel et al., 2003):

- (1) Spreading algorithms for the identification of path/spreading of debris flows,
- (2) Friction laws for the determination of the runout distance.

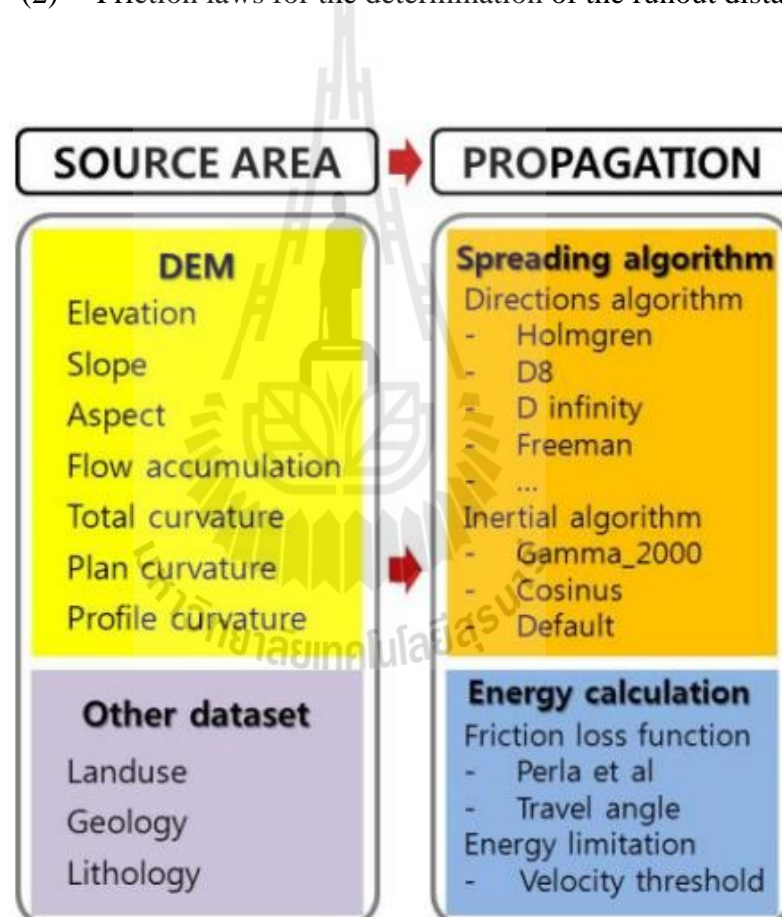


Figure 2.21 Conceptual diagram of the Flow-R model (Park et al., 2013).

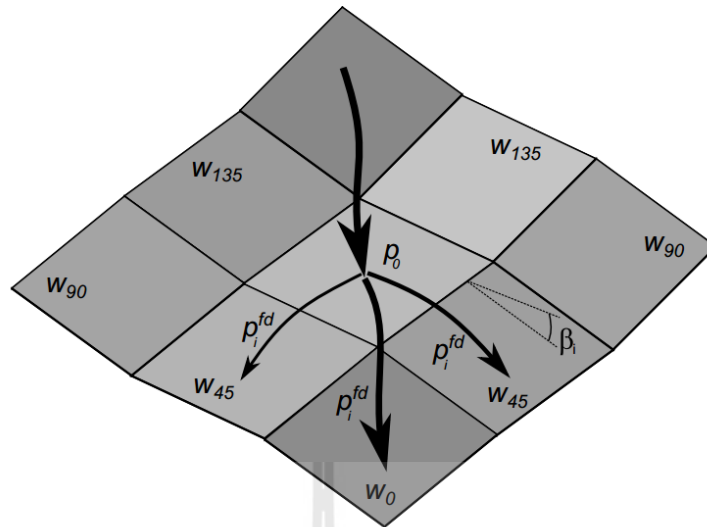


Figure 2.22 Illustration of the spreading of susceptibility value to the neighboring cells (Horton et al., 2013).

2.8.1 Algorithms for the spreading assessment

Typically, path and spreading of the debris flow are under control of the flow direction algorithms and persistence functions as detailed below.

(1) Flow direction algorithms

Flow direction algorithms determine the direction of the flow from one cell to its eight neighboring cells. Concerning the angle of spreading, Holmgren (1994) adds a parameter to multiple flow direction algorithms as an exponent which controls the convergence of the flow that can be expressed as follows:

$$P_i^{fd} = \frac{(\tan \beta_i)^x}{\sum_{j=1}^8 (\tan \beta_j)^x} \quad \text{for all } \tan \beta > 0, \quad (2.23)$$

where i, j are the defined flow directions (1-8), p_i^{fd} is susceptibility proportion (0-1) in direction i , $\tan \beta_i$ is slope gradient between the central cell and cell in direction i , and x is the variable exponent. Higher exponent indicates more convergent of the flow. When $x = 1$, it turns into basic multiple flow direction, and when $x \rightarrow \infty$, it becomes a single flow direction.

(2) Persistence function

Based on Gamma (2000), the persistence function aims at reproducing behavior of inertia, and weights the flow direction based on the change in direction with respect to the previous direction (see Figure 2.22) using the following formula:

$$p_i^p = w_{\alpha(i)}, \quad (2.24)$$

where i is flow direction (1-8), p_i^p is flow proportion (0-1) in direction i and $\alpha(i)$ is the angle between the former direction and the direction from the central cell to other cell i . Three implementations of the persistence were chosen (Table 2.15): the first is called proportional, the second one uses a cosine, and the third one is based on Gamma (2000). In every persistence distribution, the cell opposed to the given flow direction is nulled ($w_{180} = 0$) to avoid eventual backward propagation, and thus to save computing time.

Table 2.15 Implemented weightings of the persistence function in the assessment of the flow spreading.

	w0	w45	w90	w135	w180
Proportional	1	0.8	0.4	0	0
Cosines	1	0.707	0	0	0
Gamma (2000)	1.5	1	1	1	0

(3) Overall susceptibility

The values given by the flow direction algorithm and the weighting of the persistence are combined according as follows:

$$p_i = \frac{p_i^{fd} p_i^p}{\sum_{j=1}^8 p_j^{fd} p_j^p} p_0, \quad (2.25)$$

where i, j are flow directions (1-8), p_i is the susceptibility value (0-1) in direction i , p_i^{fd} is flow proportion from flow direction algorithm, p_i^p is flow proportion according to the persistence, and p_0 is previously determined flow proportion value of the central cell.

2.8.2 Runout distance assessment

Runout distance algorithm is based on simple frictional laws; as the source mass is unknown, the energy balance is unitary (Eq. (2.26)). The processing takes place at cell level and controls which other cells the flow would be able to reach. Thus, these algorithms control runout distance and, in addition, may reduce lateral

spreading (when a cell on the border of the spreading cannot be reached because of insufficient energy).

Structure of the relevant energy balance scenario can be expressed as follows:

$$E_{kin}^i = E_{kin}^0 + \Delta E_{pot}^i - E_f^i, \quad (2.26)$$

where E_{kin}^i is the kinetic energy of the cell in direction i , E_{kin}^0 is the kinetic energy of the central cell, ΔE_{pot}^i is the change in potential energy to cell in direction i , and E_f^i is the energy lost in friction to the cell in direction i .

Two main algorithms are available for the friction loss: the two parameters friction model by Perla et al. (1980) and a simplified friction-limited model (SFLM). Both can result in similar propagation areas, depending on the parameters choice.

(1) Perla's two parameters friction model

The friction model from Perla et al. (1980) was developed for avalanches, but has also been used for debris flows.

$$V_i = \left(a_i \omega (1 - \exp b_i) + v_0^2 \exp b_i \right)^{\frac{1}{2}} \quad (2.27)$$

$$\text{with } a_i = g(\sin \beta_i - \mu \cos \beta_i) \text{ and } b_i = \frac{-2L_i}{\omega},$$

where μ is the friction parameter, ω is mass-to-drag ratio, originally expressed as M/D, β_i is the slope angle of the segment, V_0 is the velocity at the beginning of the segment, L_i is the length of the segment, and g the acceleration due to gravity.

(2) Simplified friction-limited model

The simplified friction-limited model is based on the maximum possible runout distance, which is characterized by a minimum travel angle, also called angle of reach. It is the angle of the line connecting the source area to the outmost distant point reached by the debris flow, along its path:

$$E_i^f = g\Delta x \tan \varphi, \quad (2.28)$$

where E_i^f is the energy lost in friction from the central cell to other cell in direction i , Δx is the increment of horizontal displacement, $\tan \varphi$ is the gradient of the energy line, and g is the acceleration due to gravity.

This approach may result in improbable runout distances in steep catchments due to unrealistic energy amounts reached during the propagation. To keep the energy within reasonable values, a maximum limit can be introduced to ensure not to exceed realistic velocities (Figure 2.23), which can be expressed as follows:

$$V_i = \min\{ \sqrt{V_0^2 + 2g\Delta h - 2g\Delta x \tan \varphi}, V_{\max} \}, \quad (2.29)$$

where Δh is the difference in elevation between the central cell and the cell in direction i , V_{\max} is the given velocity limit.

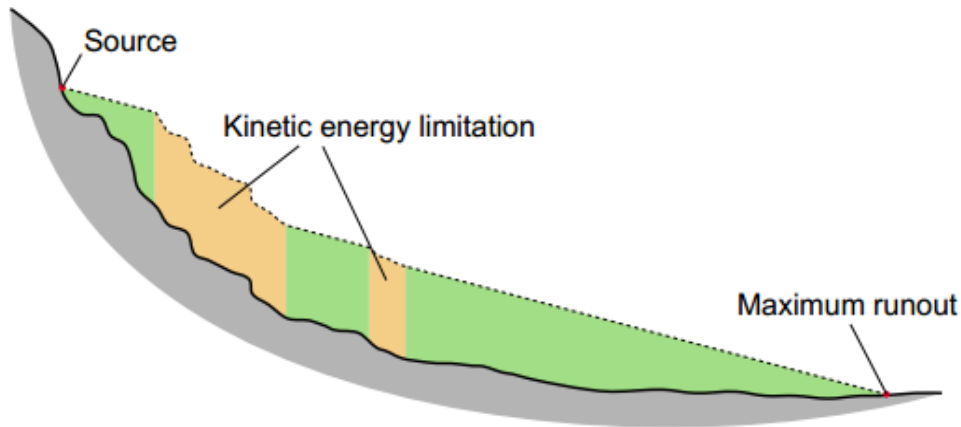


Figure 2.23 Illustration of the travel angle and the velocity limitation of the simplified friction-limited model (SFLM) (Horton et al., 2013).

The probable maximum runout is characterized by an average slope angle or shadow angle which is the average slope between the starting and end points, following the debris flow path. A constant friction loss has been considered, corresponding to this angle, which would result in a runout distance equal to the probable maximum runout.

2.9 Roles of GIS and remote sensing in landslide risk analysis

In recent decades, remote sensing (RS) and Geographic Information Systems (GIS) technologies have played an important role in rapid advance of landslide research field which mainly involves three following aspects (van Westen et al., 2006):

- (1) Detection, classification, and mapping of past landslides,
- (2) Monitoring occurrences of new landslides and activity of the existing ones,
- (3) Analysis and prediction of the prone areas to landslide activity in terms of both spatial distribution (space) and temporal distribution (time).

These three broad groups of activities are of great interest to landslide researchers where both RS and GIS tools were frequently applied to fulfill these tasks. Brief details of their roles are summarized here for an example.

2.9.1 Applications of GIS technology

In the past three decades, the rapid advance in landslide mapping methodology (i.e. inventory mapping, susceptibility mapping, hazard mapping and risk mapping) is contributed tremendously to the advent of the Geographic Information Systems (GIS) (van Westen et al., 2006; Chacon, Irigaray, Fernandez, and Hamdouni, 2006). GIS was defined by Burrough (1986) as “powerful set of tools for collecting, storing, retrieving at will, transforming, and displaying spatial data from the real world for particular set of purposes”, by Star and Estes (1990) as “an information system designed to work with data referenced by spatial or geographic co-ordinates”, and by Bonham-Carter (1996) as “a computer system for managing spatial data”. This means GIS is a specifically-built geographic-data processing system with an intention to extract useful information from its processed data which can be separated into two general types: vector (for those existed in point, line, and polygon format) and raster (for those of the contiguous data) (as illustrated for examples in Figures 2.24). Traditionally, a GIS structure shall consist of five processing components, i.e., (1) data collection; (2) data input and verification; (3) data storage, database manipulation and data management; (4) data transformation and analysis; and (5) data output and presentation (Sgzen, 2002).

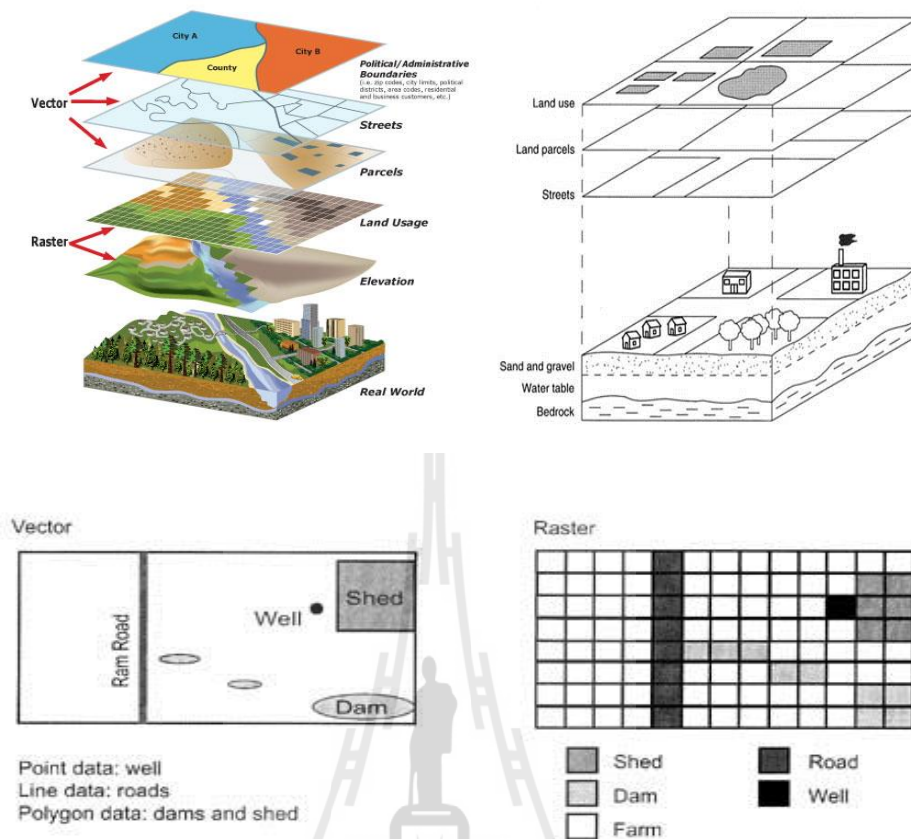


Figure 2.24 Examples of the geographic input data (vector/raster types) for the GIS operation (Schuurman 2004; NOAA, 2013). Vector structure is preferable for data with definite location (point) like house position, direction (line) like street/water channels, or boundary (polygon), like land parcel while raster structure is appropriate for spatial data with continuous values in space such as elevation or land use information.

GIS powerful capability in processing spatial data of most kinds and also in simulating specific interaction among them was found crucially benefit for the landslide risk analysis as initiation of slope failure often depends on complex interactions among several contributing factors themselves as well as with the associated triggering factors, in which the GIS can have crucial role in extracting that relationship information using its powerful data processing technology. This makes GIS become an essential tool for

facilitating landslide susceptibility or hazard mapping regardless of the methods in use. In addition, landslide runout data can also be extracted from the GIS-based simulation models (Chacon et al., 2006; van Westen et al., 2006).

According to Guzzetti et al. (2012), GIS has become an excellent platform for constructing of detailed landslide inventory maps in which landslide locations along with their descriptions (or attributes) crucial for the landslide susceptibility mapping; e.g. size, volume, age, type, environmental condition, can be conveniently recorded, modified, and displayed as an individual GIS-based data layer by the able GIS software. This ability has solved several persistent problems related to the production, update and visualization of landslide maps often encountered in the traditional approach. Similarly, GIS efficiency can be effectively implemented to produce detailed map of the elements at risk from landslide activities over an area, which is very necessary for the preparation of the vulnerability and risk maps afterwards (through the integration with hazard map). General reviews about GIS applications to the research field of landslide mapping are seen in, e.g., Carrara and Guzzetti (1995); Carrara, Guzzetti, Cardinali and Reichenbach (1999); van Westen (2000); Huabin, Gangiun, Weiya and Gonghui (2005).

2.9.2 Applications of remote sensing technology

In general, RS data have been widely utilized at all steps of landslide risk analysis stated earlier (i.e., inventory mapping, susceptibility/hazard/risk assessment). In the landslide inventory preparation, high resolution aerial photos (usually in the form of orthophoto) or satellite images (like those from the IKONOS, QuickBird, or GeoEye satellites) are normally employed to identify location and spatial distribution of existing landslide evidences in a particular area (see Figure 2.25 as example) based on the direct visual interpretation or the developed automatic

classifying method (Malamud, Donald, Guzzetti and Reichenbach, 2004; Duman et al., 2005; Mondini et al., 2011; Rau, Chang, Shao and Lau, 2012).



Source: <http://earthobservatory.nasa.gov/NaturalHazards/view.php?id=49976>

Figure 2.25 Satellite image of the 2011 landslide evidences in Krabi Province, southern Thailand from the NASA-Advanced Land Imager (ALI) sensor aboard EO-1 satellite.

In recent years, the advanced technologies of radar observing system called “InSAR” (Interferometric Synthetic Aperture Radar) system (Richard, 2007; Ferretti, Monti-Guarnieri, Prati and Rocca, 2007) and the “LiDAR” system (LiDAR-UK, 2013) operating onboard surveying airplane or earth-observing satellites were also applied to identify small-scale landslides in several works, e.g. Colesanti and Wasowski (2006); Strozzi, Ambrosi and Raetzo (2013); Ghuffar, Szekely, Roncat and Pfeifer (2013).

Remote sensing data have also become a primary source for the extraction of several landslide contributing factors, for examples:

(1) Topography and landform properties. These data can be acquired from the original DEM (digital elevation model) data generated from the InSAR or LiDAR systems (both airborne and space-borne types). For examples, the InSAR radar system in SRTM project (NASA-Shuttle Radar Topographic Mission) can be used to generate DEM data around the world at good spatial resolution of 90 meters (CGIAR-CSI, 2013) which is noticeably useful for landslide susceptibility mapping at the regional to global scales (Hong, Adler and Huffman, 2007; Kirschbaum et al., 2011).

(2) LULC data, especially those related to vegetation like forest or plantation. These data can be found through visual interpretation of aerial photos or high-resolution satellite images, or from automatic classification of medium-resolution satellite images (like those from Landsat or SPOT satellites). Similarly, vegetation indices (like NDVI) can be derived from suitable satellite images (both high and medium resolution types). The importance of LULC as a prominent landslide contributing factor and influence of LULC changes over a particular area on landslide activity were highlighted in several works, e.g. Glade (2003); van Beek and van Asch (2004); Fell et al. (2008); Karsli et al. (2009); Chen and Huang (2013).

(3) Precipitation data. At present rainfall characteristics (in both spatial and temporal aspects) can be estimated from the ground-based or satellite-based weather radar, like those in the Tropical Rainfall Measuring Mission (TRMM) satellite (NASA-TRMM, 2013). Knowledge of the immediate rainfall information provided by advanced radar systems can support rapid evaluation of potential landslide danger area

introduced by that rainfall event (in corporation with the known landslide susceptibility locations of the area) (Kirschbaum et al., 2012).

Reviews on roles of remote sensing on landslide analysis are provided in, e.g. Zhang, Gong, Zhao and Zhang (2005); Metternicht, Hurni and Goru (2005); Joyce, Bellis, Samsonov, McNeill and Glassey (2009); Zhong, Li, Xiang, Su and Huang (2012); Tofani, Gegoni, Agostini, Catani and Casagli (2013).

2.9.3 Landslide activity in Thailand

Landslide is a recurrent and devastated incidence commonly encountered in Thailand especially within the mountainous regions in the northern and southern parts of the country (GERD, 2006; Soralump, 2010b). Generally, the predominant types of landslides over high areas with thick residual soil layer are mostly the debris avalanche and rotational slide but for areas having relatively shallow residual soil, the translational slide is prevalent (DMR, 2010). And as massive landslides evidenced in Thailand were induced mostly by the prolonged heavy rainfall in rainy season, this can result in rapid movement of soil cover downhill to the surrounded lowland area in forms of earth flow or debris flow. During this period, the landslide might transform itself into a destructive debris avalanche, with increasing velocity and volume. If the debris flows move down to a gully at the hill's base, then the runout of their material could move over fairly long distance (up to several kilometers) (Revellino, Hungr, Guadagno and Evans, 2004).

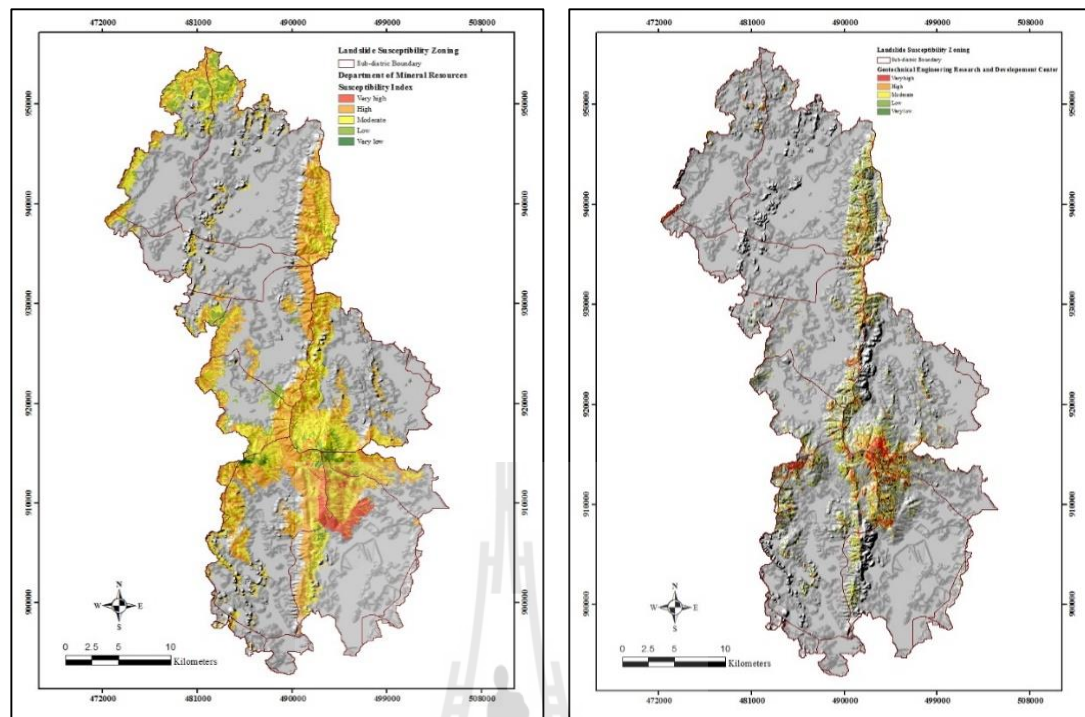
According to DMR (2010, 2011), landslide activity in Thailand is controlled by four important factors: geology (lithology and lineament in particular), topography (slope, elevation, and aspect in particular), rainfall intensity (amount and duration) and environment (vegetation, land-use type/activity, and agricultural practice

in particular). For lithology, it was found that the most susceptible rock type to landslide occurrence (in average) is the Jurassic granite. This is followed by a group of the sedimentary rock (e.g. sandstone, mudstone, shale) while the least susceptible one is the Carboniferous-Permian granite (Soralump, 2007). For rainfall intensity, the general triggering rates (for warning purpose) were set to be 100 mm/day, or 300 mm/3-day. In conclusion, the most susceptible areas for landsliding were found to be steep slope in hilly regions with relatively thick and loose residual soil layer and without vegetation cover.

Due to the catastrophic nature of the recurrent massive landslide in Thailand especially for people who live in the vulnerable area, the preparation of a strategic plan for the prevention and mitigation of landslide risk and impacts has become a declared priority of the recent Thai governments (NESDB, 2011). Some of the notable activities are the derivation and implementation of the landslide susceptibility maps nationwide, especially for the mountain-dominated provinces in the northern and the southern parts of the country DMR (2010, 2011), and the application of an effective landslide warning system to numerous areas with high landslide potential (DWR, 2013). These maps were synthesized qualitatively based on crucial knowledge of susceptible geologic structure, slope gradient, and vegetation cover in combination over an area from which the highly-concerned ones are those areas with comprising of the thick residual soil, lack of root cohesion, and steep slope (i.e. $> 30^\circ$). In general, researches on landslide activity in Thailand were usually focused on the production of the susceptibility and hazard maps (with inclusion of the annual rainfall data). However, the applied methods are still considerably limited among which the most widely-used ones are the simple weighted linear combination (WLC), e.g. in

Tanavud et al. (2000); Soralump (2007); Soralump, Pungsuwan, Chantasorn, Inmala and Alambepola (2010), the systematic factor overlay method, e.g. in Akkrawintawong, Chotikasathien, Daorerk and Charusiri (2008); DMR (2011); and the slope stability analysis (or the deterministic approach), e.g. in Mairiang and Thaiyuenwong (2010); Soralump et al. (2010); Tanang, Sarapirome and Plaiklang (2010), Ono, Kazama, and Ekkawatpanit (2014). Some other methods previously reported are the frequency ratio (FR), logistic regression, and the analytical hierarchy process (AHP) as illustrated in works of Oh et al. (2009); Intarawichian and Dasananda (2010, 2011), for examples.

Figure 2.26 presents two distributed susceptibility maps developed by DMR and GERD based at Kasetsart University (KU). The DMR map was originally derived based on presumed conditions of potential slope instability within the area derived from knowledge of four main causative components: lithology, topography, rainfall amount, and predominant LULC aspect, while the GERD map was built from the engineering principles of slope instability which expressed in terms of the “factor of safety” (FS), or the deterministic method, as explained in Section 2.3.



(a) DRM susceptibility map

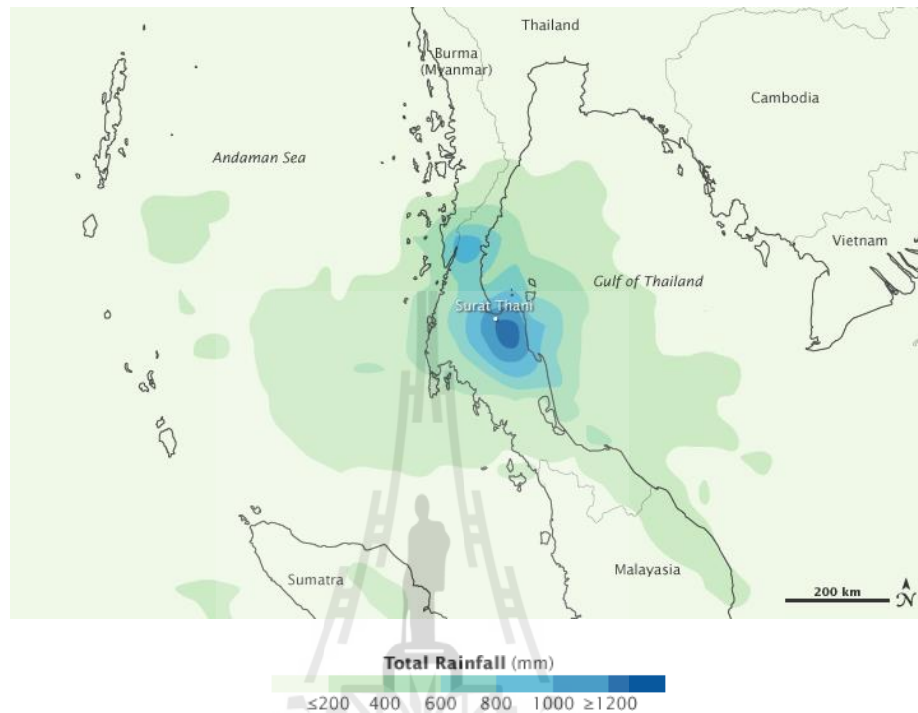
(b) GERD susceptibility map

Figure 2.26 Classified landslide susceptibility maps prepared by the DMR and GERD using equal-interval classification technique.

The case study of March 2011 event

The most recent occurrence of deadly landslide incidence at Khao Phanom Bencha Watershed was taken place in late March 2011 due to the unseasonably heavy rainfall happening over a week earlier which led to several tragic deaths and expansive damage to the properties and infrastructures in the area. This unusual phenomenon was initiated by the powerful storm from an active low pressure cell over southern Thailand, bringing up to 1,200 mm of rain in just over a week over some places (Figure 2.27) and introducing widespread torrential floods, massive landslide, and powerful debris flow, within an area of the eight southern provinces of Thailand, including, Chumphon, Surat

Thani, Nakhon Si Thammarat, Songkhla, Patthalung, Narathiwat, Yala, Trang, Phang Nga, Krabi, and Satun.



Source: <http://earthobservatory.nasa.gov/NaturalHazards/view.php?id=49929>

Figure 2.27 TRMM map of accumulated rainfall data over southern Thailand during period of 23th-30th March 2011.

As a consequence, more than 20 people were reported dead and nearly a million people were in need of immediate help (reliefwep, 2014). In Krabi Province, especially in the vicinity of Khao Phanom Bencha mountain range, the large landslide patches and devastated outcome from strong floods and debris flows were obviously evidenced over the area from which several villages were partly destroyed and at least 10 people were reported dead. Therein, expansive deposition area of flow material were experienced with flow length of about 2.5-3.0 km were encountered with maximum width of up to 500 meters (as illustrated in Figures 1.2 and 1.3).

CHAPTER III

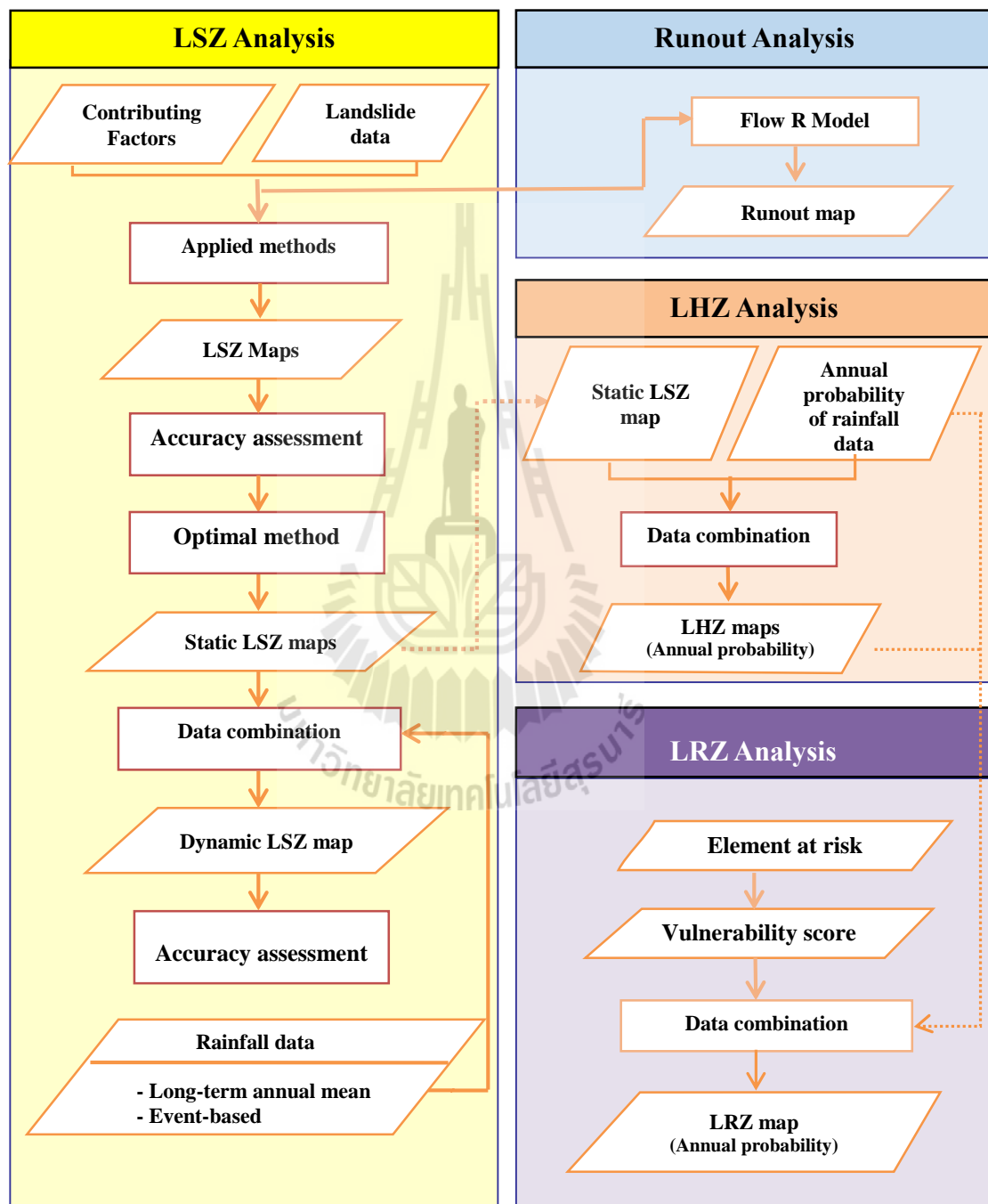
RESEARCH METHODOLOGY

The entire thesis work has been divided into 4 principal parts in accordance with the two objectives described in Chapter I involving the systematically construction and evaluation of the landslide inventory map, susceptibility map, hazard map and risk map consecutively as illustrated by the work flowchart shown in Figure 3.1. Comprehensive description of the work process can be summarized as follows.

3.1 Data preparation

3.1.1 The necessary data were acquired from the responsible agencies and from other relevant resources (as detailed in Table 3.1) and then restructured to have a proper format for further use (in form of a GIS-based dataset). Ten notable contributing factors for landslide occurrence in tropical zone were included in the construction of the needed susceptibility map: elevation, slope gradient, slope aspect, slope curvature, topographic wetness index (TWI), distance from drainage, distance from lineament, lithology, soil texture, and land use/land cover (LULC) (Figures 3.2a-j). These factors can be separated into three broad categories: geological, topographical, and environmental groups. Here, elevation and all slope-related maps (Figures 3.2a-e) were created from digital elevation model (DEM) data of the area. This map was built using

triangular irregular network (TIN) system based on the 20-m interval contours extracted from the official 1:50,000-scale topographic map acquired from the RTSD.



Note: LSZ ≡ Landslide susceptibility zoning; LHZ ≡ Landslide hazard zoning;
LRZ ≡ Landslide risk zoning.

Figure 3.1 Conclusive work flowchart.

Table 3.1 List of necessary data and their respective sources.

Classification		GIS	Scale or	Original	
Data category	Details	Data Type	Resolution	sources	Note
Past landslide data	Field survey	Point	-	GPS	Fig.3.8
	THEOS	Grid	2m x 2m	GISTDA	Fig.3.4a
	EO-1	Grid	10m x 10m	NASA	Fig.3.4b
	Google Earth	Grid	-	Google Earth	Fig.3.4c
	Bing Map	Grid	-	Bing Map	Fig.3.4d
Land use / Land cover	LULC-2009	Polygon	1:25,000	LDD	Fig.3.2j
Topography	Elevation	Point/Line	1:50,000	RTSD	Fig.3.2a
	Slope gradient				Fig.3.2b
	Slope aspect				Fig.3.2c
	Slope curvature				Fig.3.2d
Landform	TWI				Fig.3.2e
Stream	Stream network				Fig.3.2f
Geology	Lithology	Polygon	1 : 250,000	DMR	Fig.3.2h
	Lineament	Line	1 : 250,000	DMR	Fig.3.2g
Soil	Soil texture	Polygon	1 : 100,000	LDD	Fig.3.2i
Triggering factor	Rainfall	Point	-	TMD, RID,	Fig.3.10
				DMR	Fig.3.11
Socio-economics	Building	Point	-	Google Earth	Fig.3.12a
	Subsidy		-	MOAC	Fig.3.14
Administrative data	Administrative boundary	Polygon	1:50,000	RTSD	Fig.1.4

Note: DMR ≡ Department of Mineral Resources; GISTDA ≡ Geo-informatics and Space Technology Development Agency; LDD ≡ Land Development Department; MOAC ≡ Ministry of Agriculture and Cooperatives; RID ≡ Royal Irrigation Department; RTSD ≡ Royal Thai Survey Department; TMD ≡ Thai Meteorological Department.

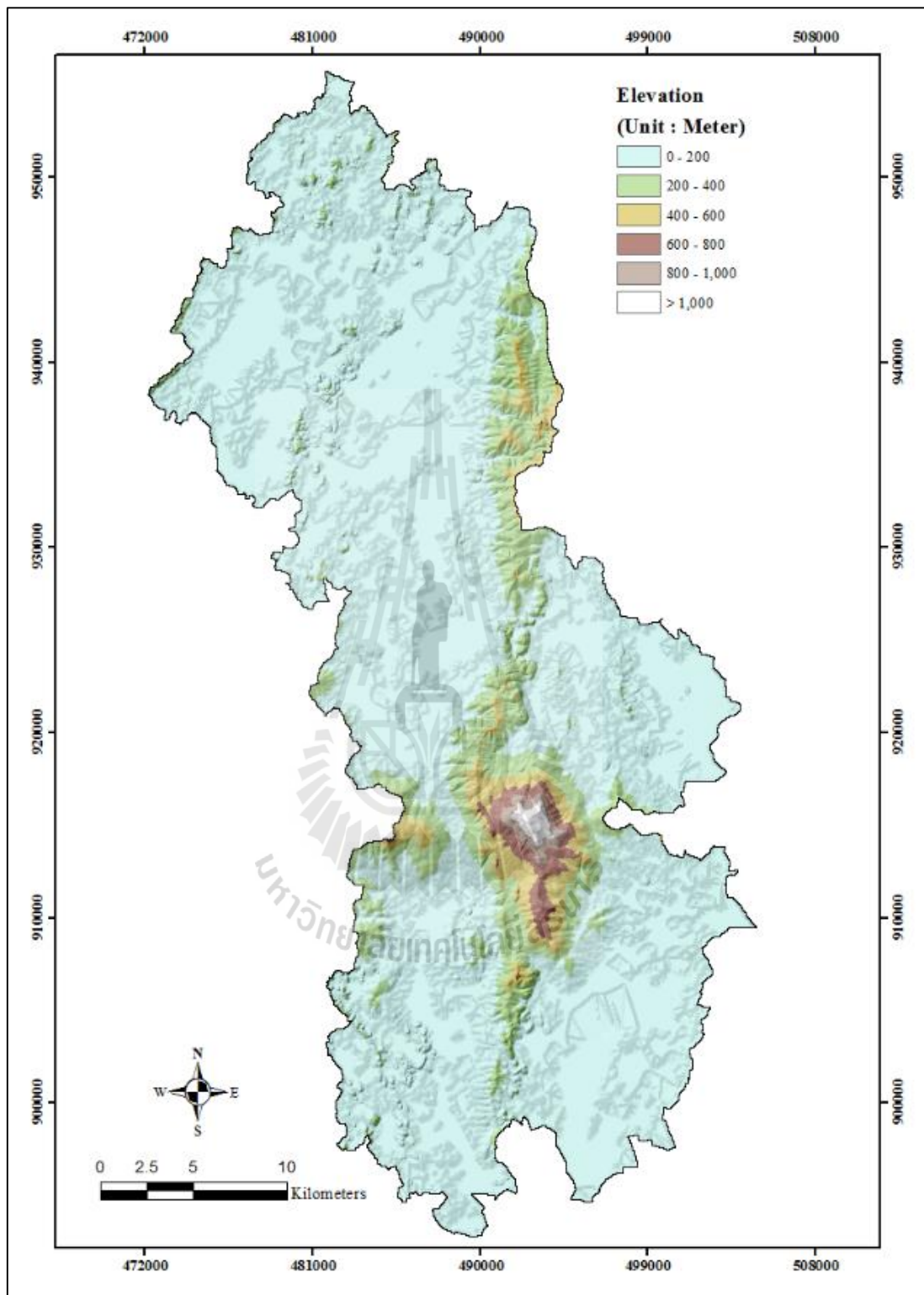


Figure 3.2a Elevation map of the study area based on DEM data from topographic map of 1:50,000 scale.

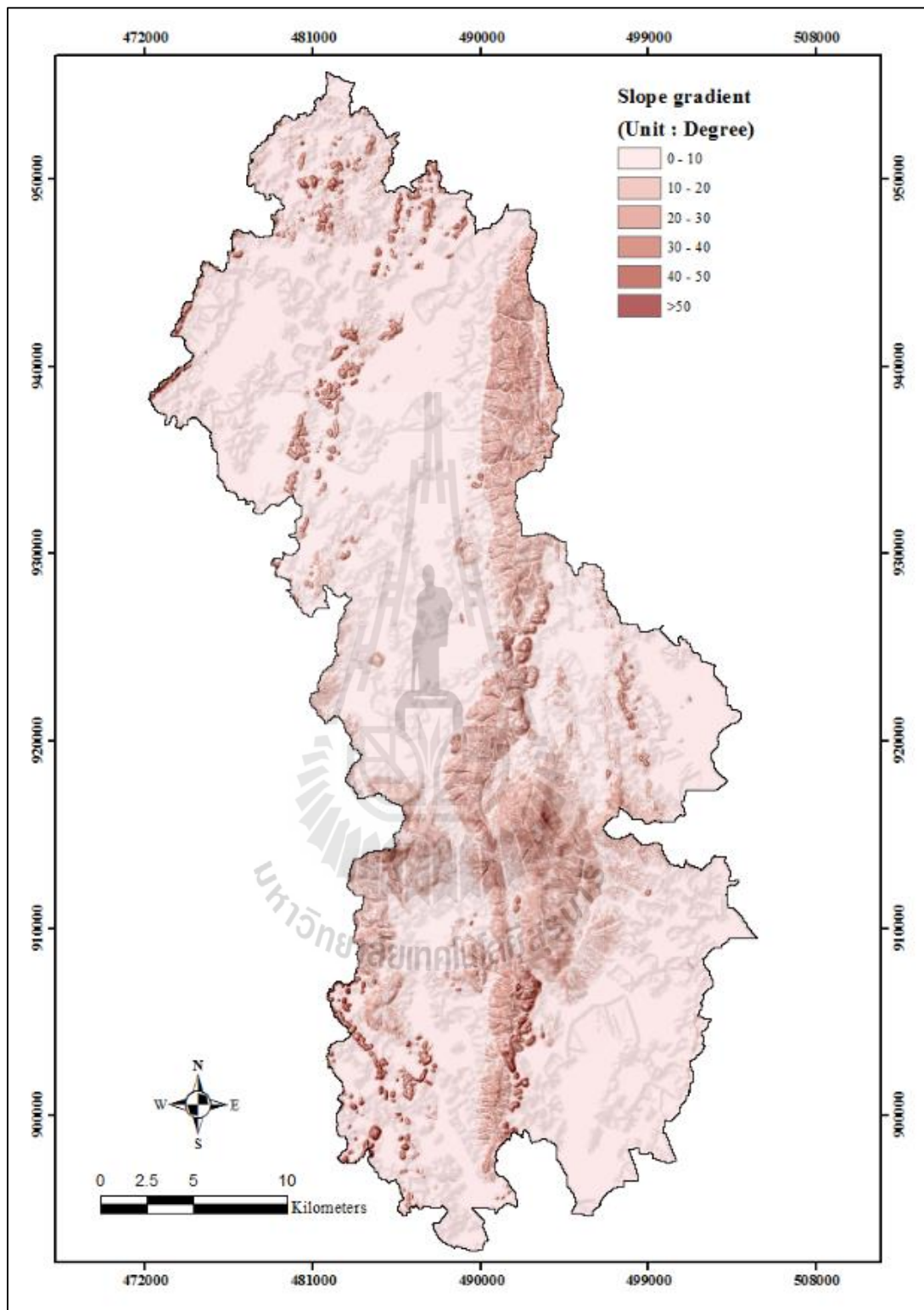


Figure 3.2b Slope gradient map of the study area based on DEM data from topographic map of 1:50,000 scale.

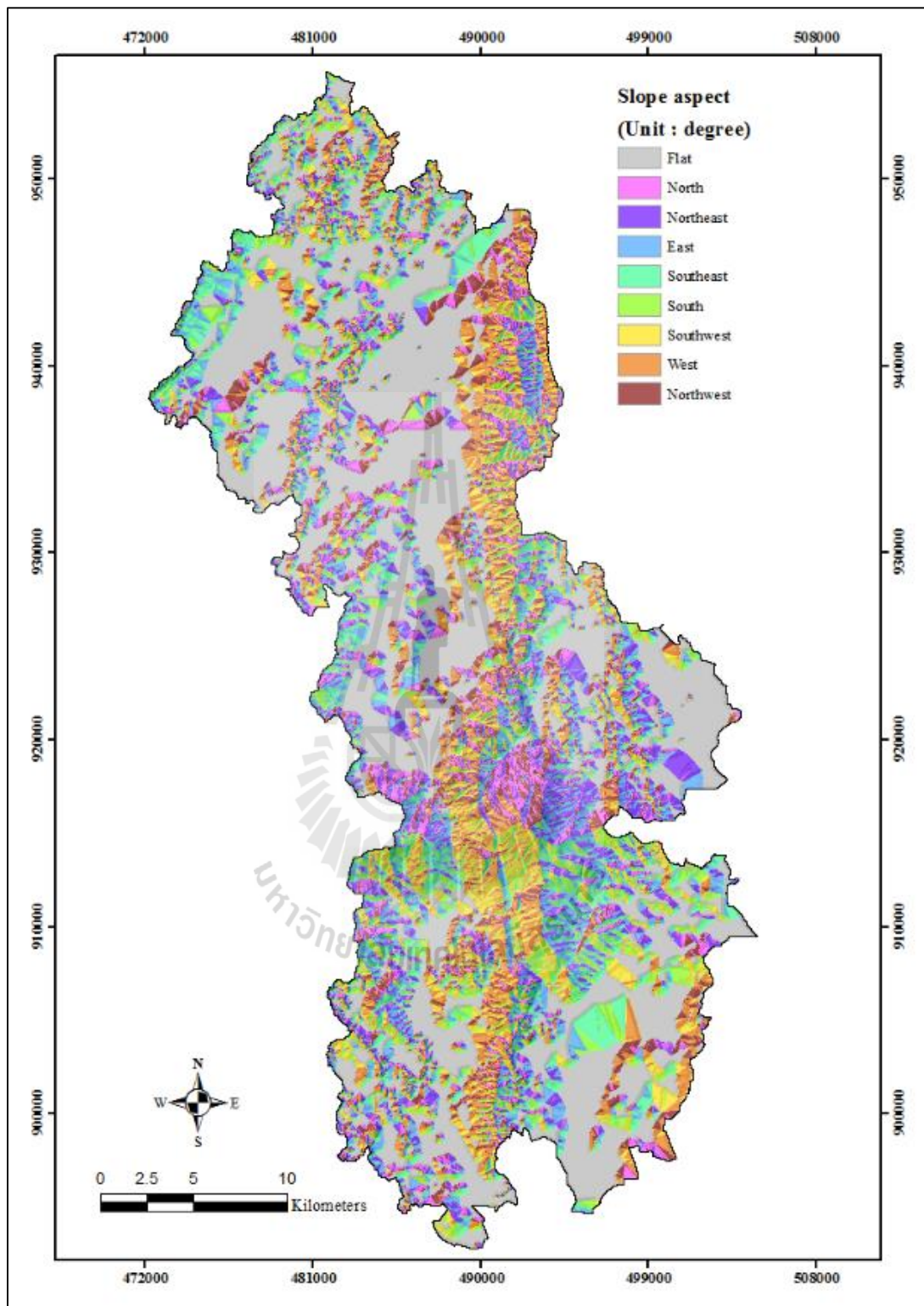


Figure 3.2c Slope aspect map of the study area based on DEM data from topographic map of 1:50,000 scale.

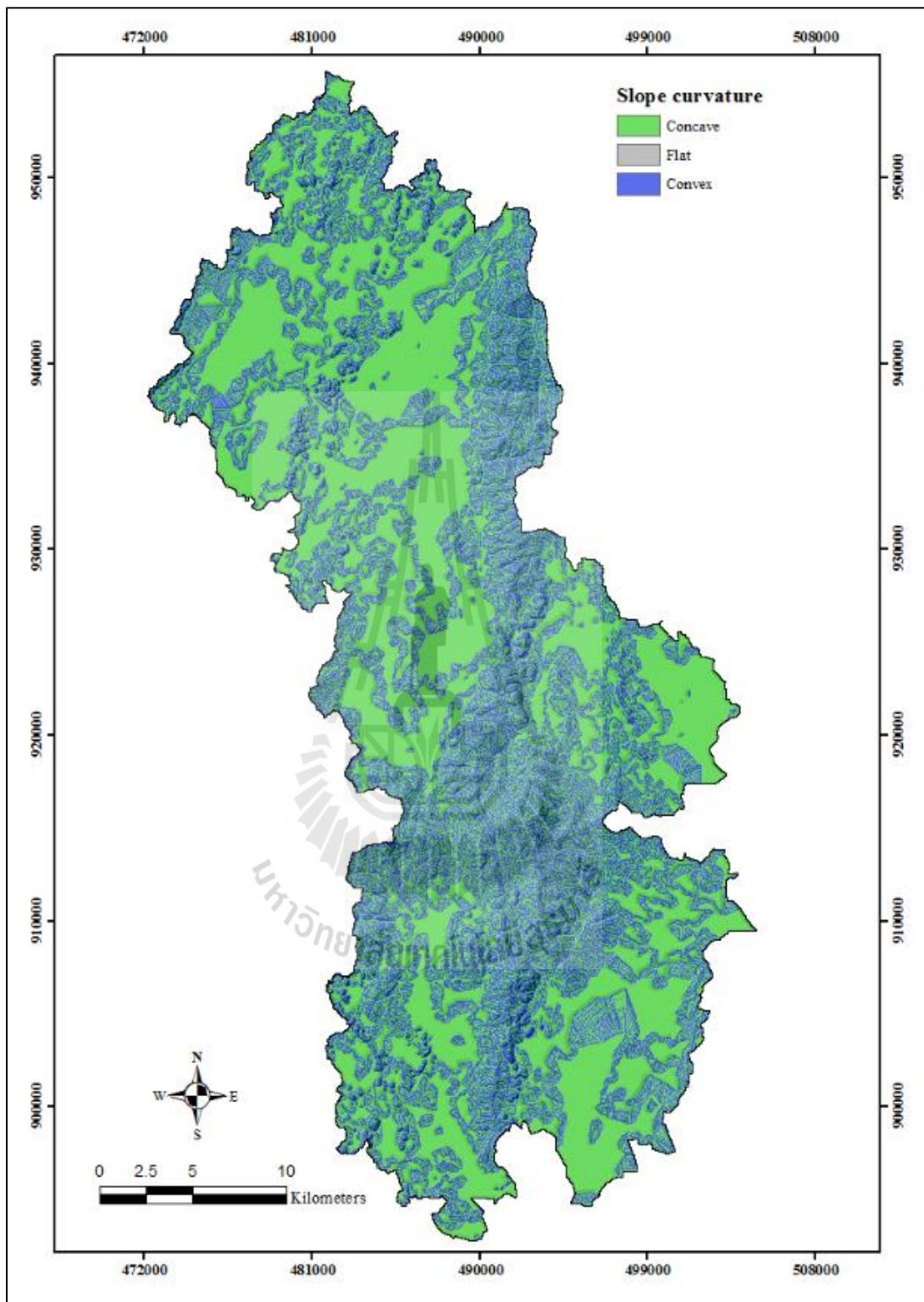


Figure 3.2d Slope curvature map of the study area based on slope data of topographic map of 1:50,000 scale.

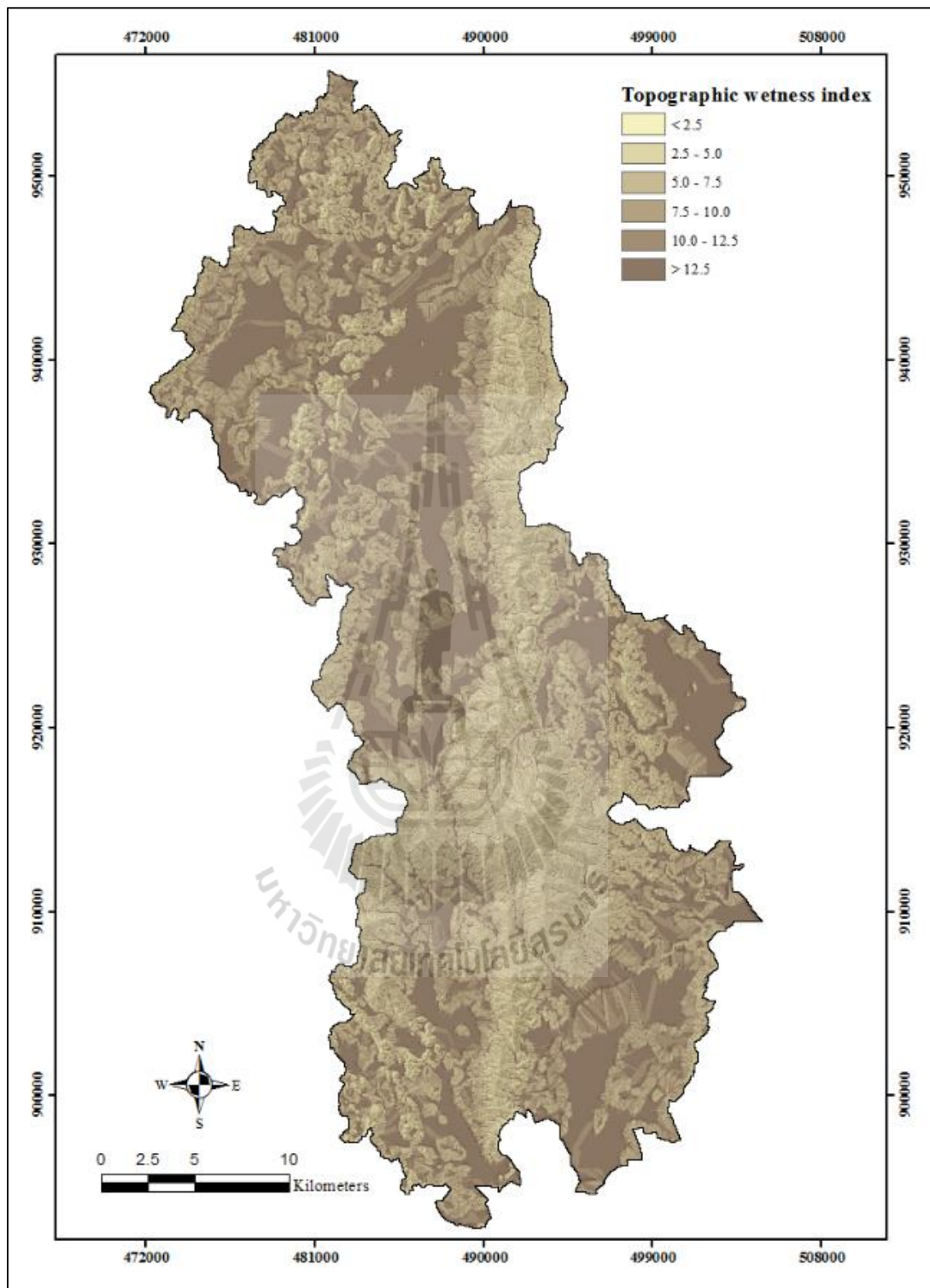


Figure 3.2e Topographic wetness index (TWI) map of the study area based on the slope and water accumulation data from the topographic map of 1:50,000 scale.

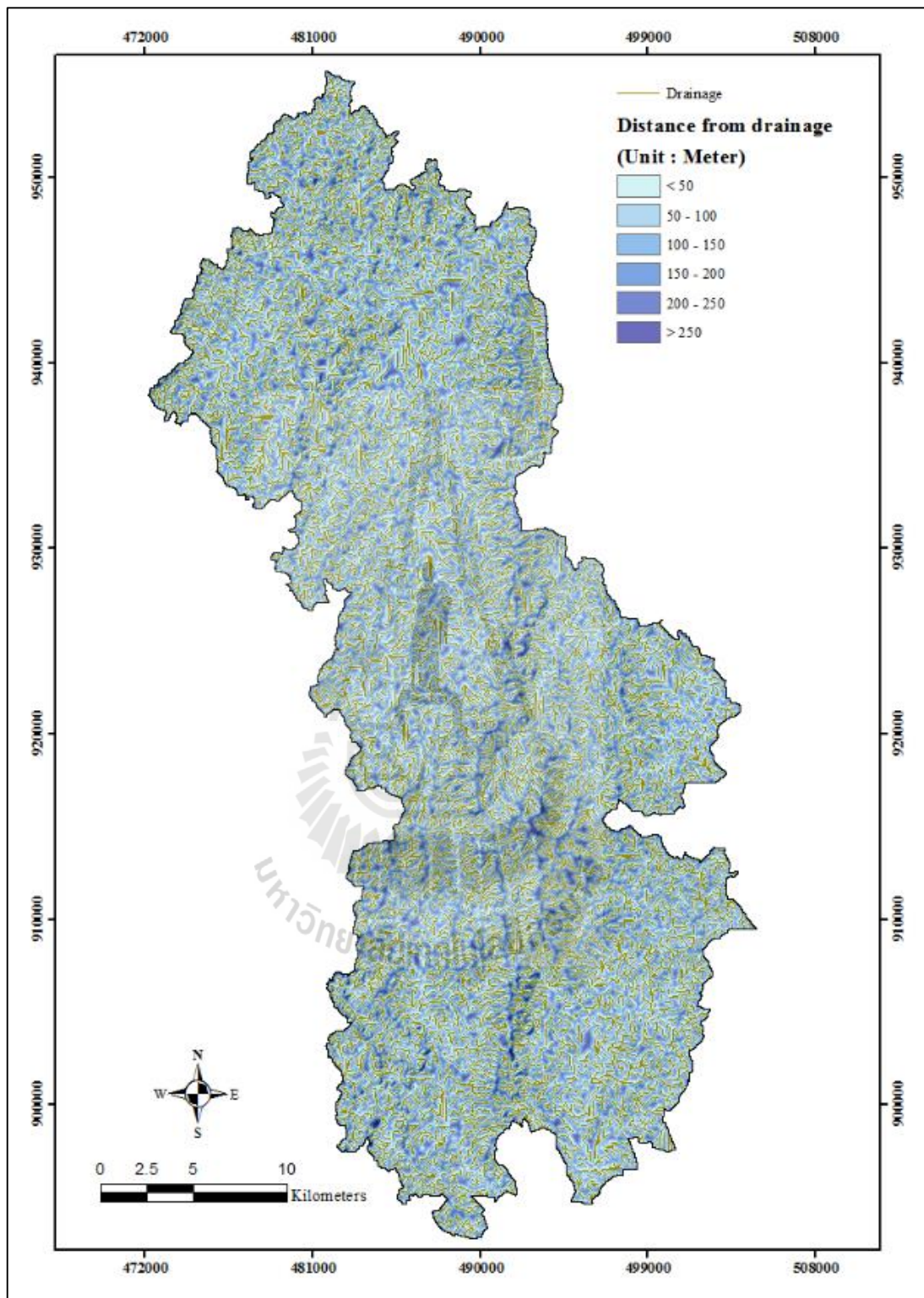


Figure 3.2f Distance-from-drainage map of the study area based on DEM data from the topographic map of 1:50,000 scale.

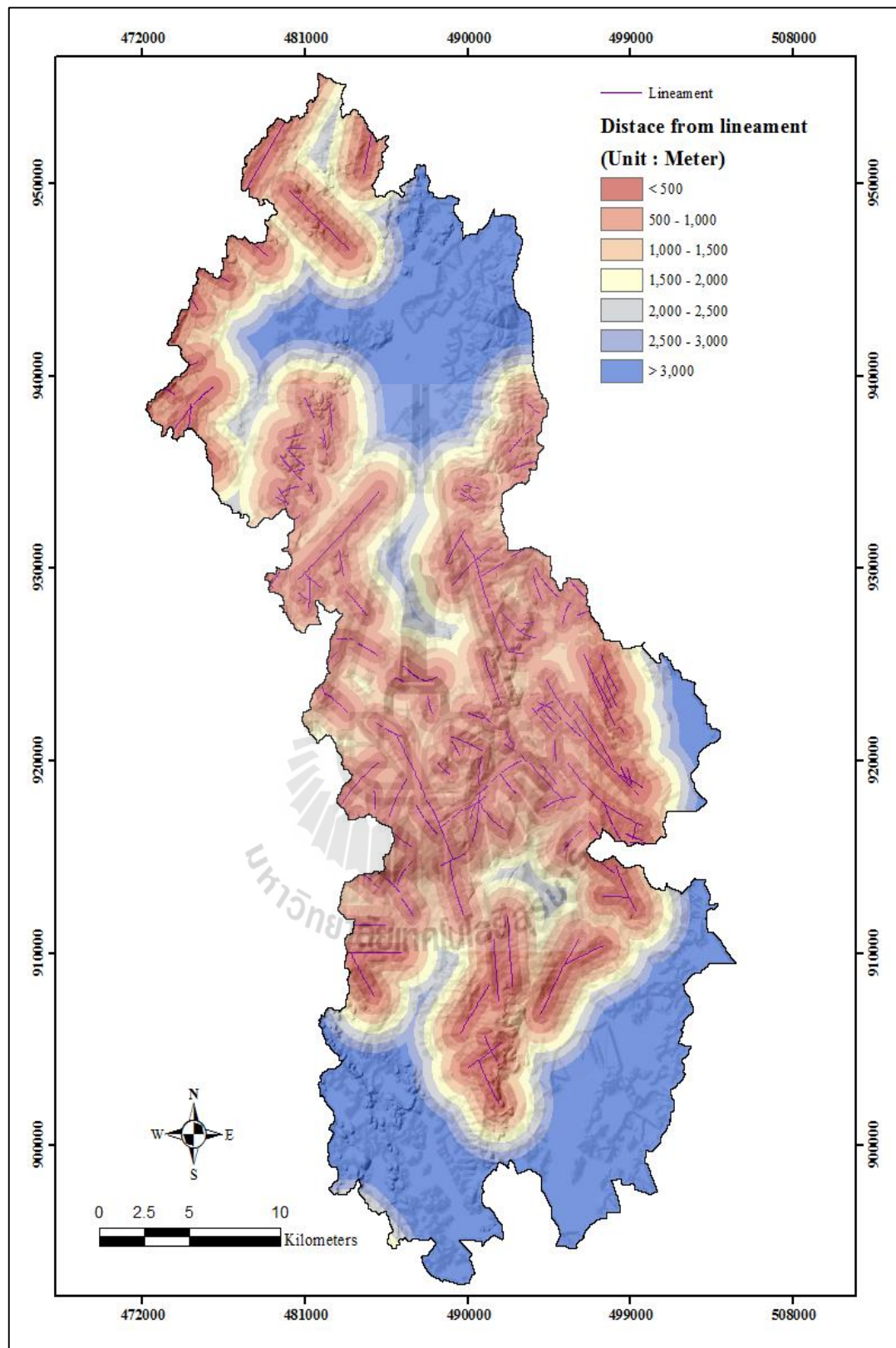


Figure 3.2g Distance from lineament map of the study area (at 1:250,000 scale).

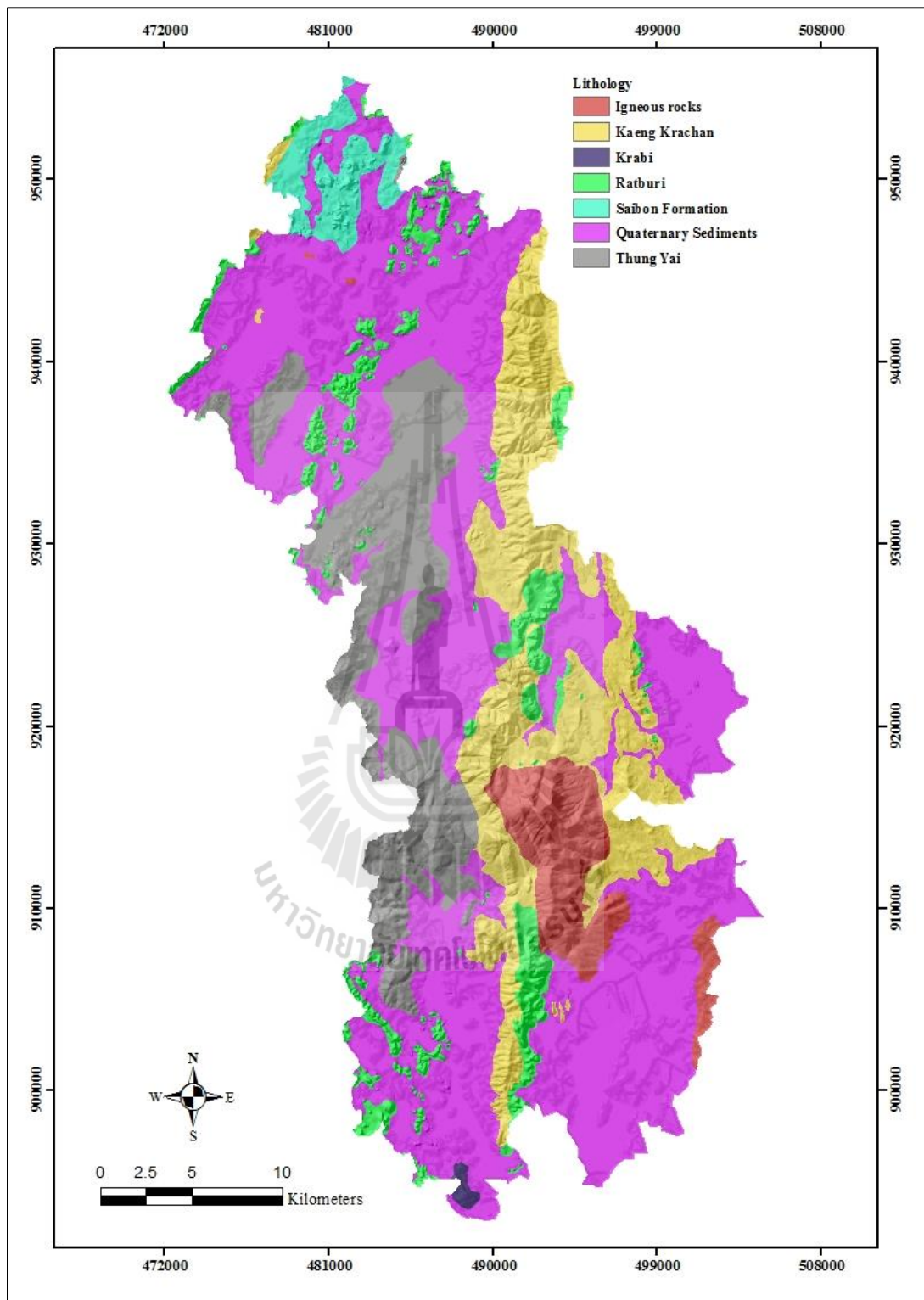


Figure 3.2h Lithology map of the study area at 1:250,000 scale. Detailed explanation of each listed lithological type is given in Table 3.2.

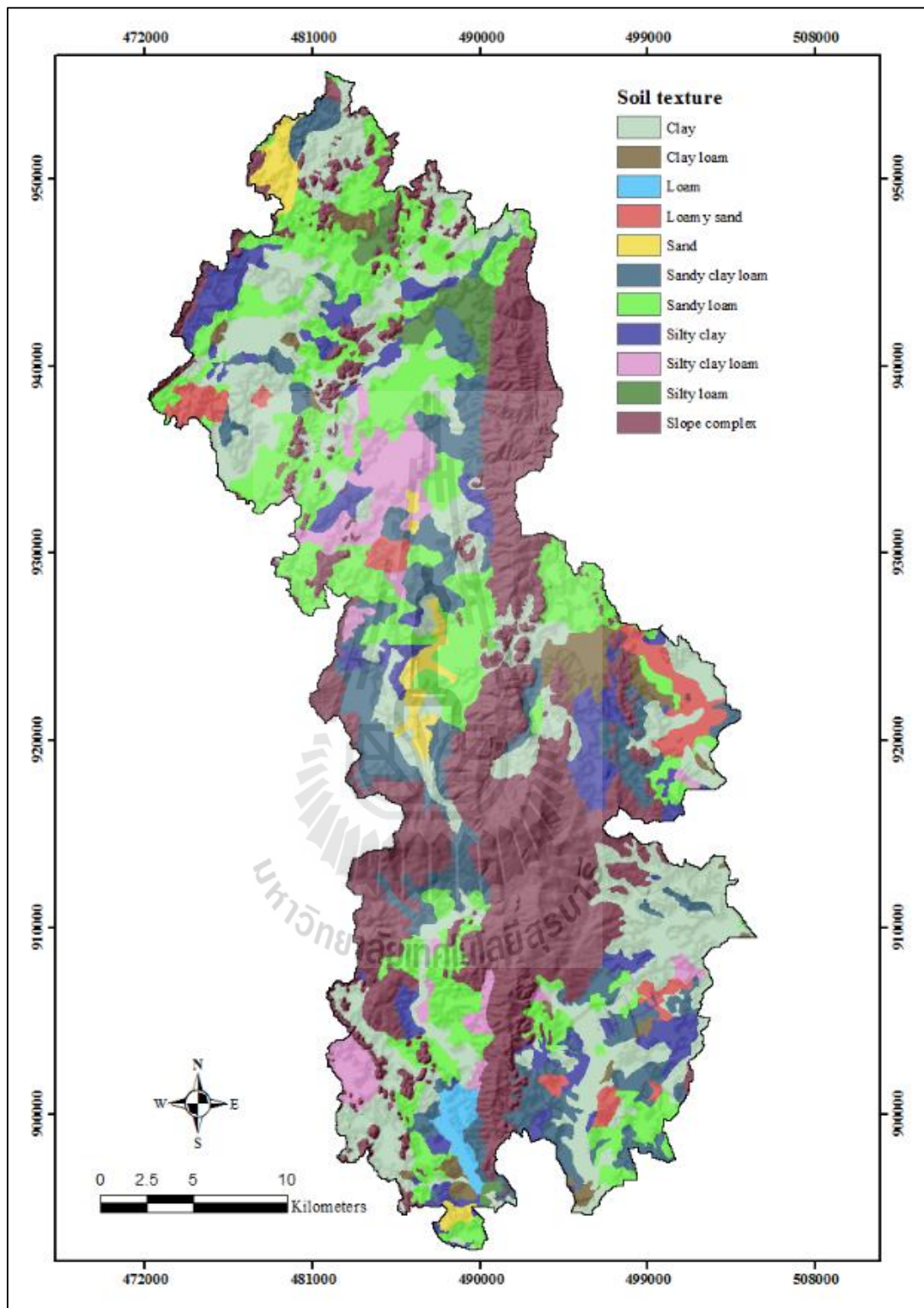


Figure 3.2i Soil texture map of the study area modified from LDD soil data at 1:100,000 scale.

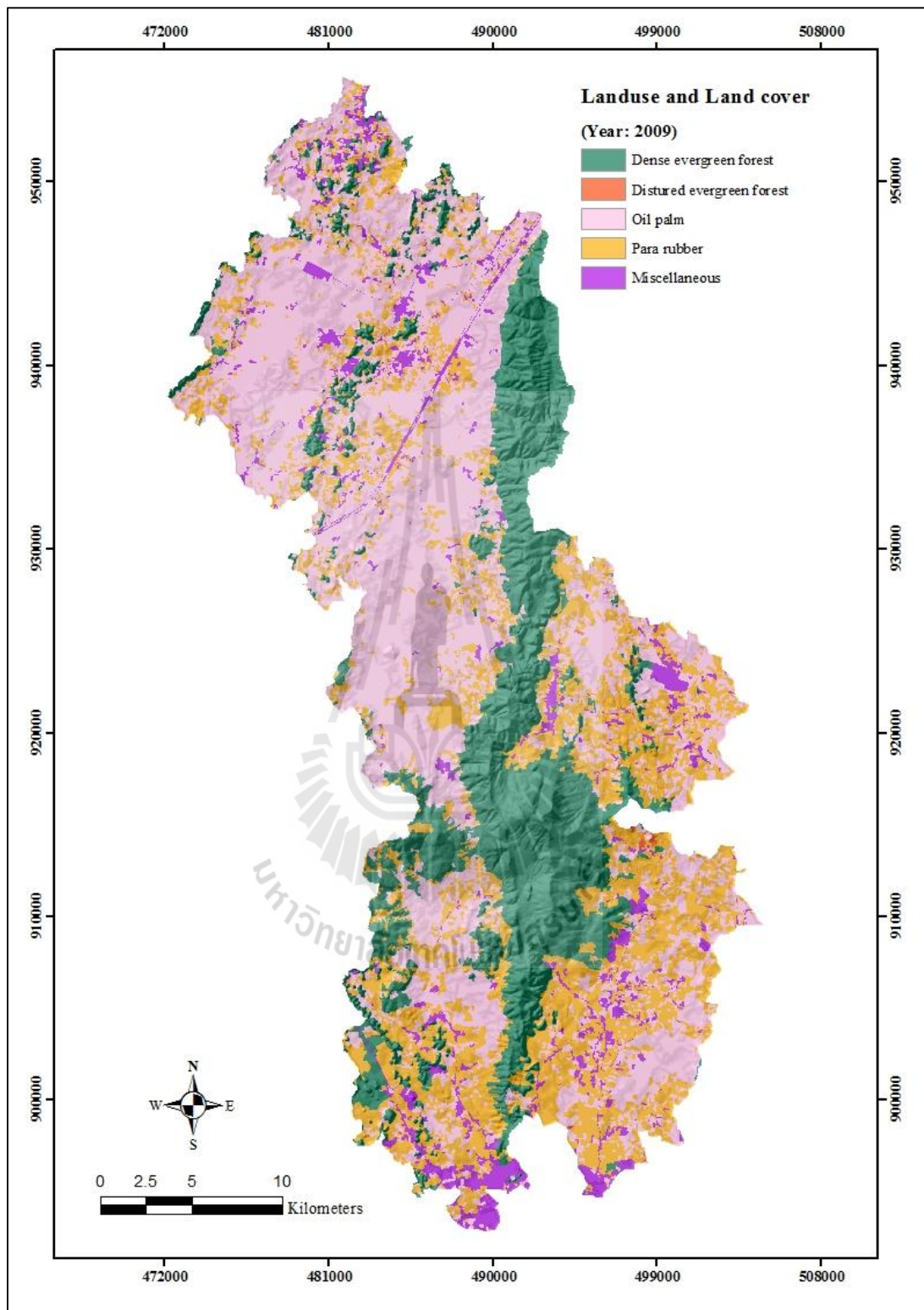


Figure 3.2j LULC map of the study area in 2009 modified from the original LDD data at 1:25,000 scale.

All maps displayed in Figure 3.2 were prepared mainly through the appropriate functions of the ArcGIS software in which slope gradient was determined from steepest downhill slope for a location on surface calculated for each triangle unit in TIN and for each referred raster cell. For TIN, this is the maximum rate of change in elevation across each triangle unit. For raster cell, this is the maximum rate of change in elevation found towards its eight surrounding neighbors. Typically, slope gradient can be presented in degrees from horizontal (0-90), or in percent slope [defined by ratio of the terrain rise (or vertical distance) to the run (or horizontal distance), multiplied by 100]. In this case, a slope of 45 degrees equals 100 percent slope (vertical distance = horizontal distance). Lower slope gradient means flatter terrain; the higher one indicates steeper terrain.

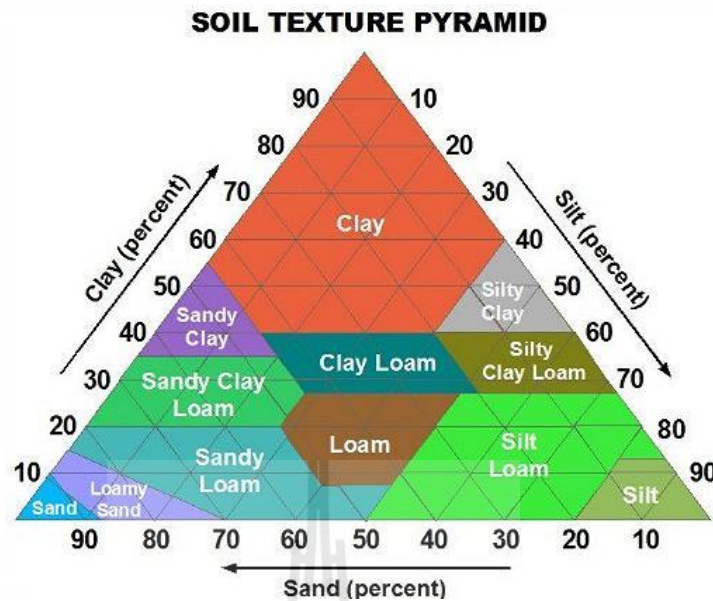
Slope aspect was referred to the steepest downslope direction for each raster cell towards its neighbor cells (one with maximum rate of change in slope value). The aspect output was defined based on the known closest compass direction measured clockwise in degrees, which are, 0 (north), 45 (northeast), 90 (east), 135 (southeast), 180 (south), 225 (southwest), 270 (west), 315 (northwest), and 360 (north). However, for flat areas with no exact downslope direction, they are usually given a specific aspect value of -1. Slope curvature was defined from the 2nd derivative of a surface, or the rate of change of slope values over a unit area of interest. It represents the combination of two main types of the curvature: the profile curvature (along the direction of the maximum slope), and the plan curvature (along direction perpendicular to direction of maximum slope). The curvature values describe terrain morphology in three forms: convex, concave, flat. The positive value indicates the surface is upwardly convex at

that cell while a negative one indicates an upwardly concave, and 0 indicates flat surface (Figures 2.5-2.6).

Topographic Wetness Index (TWI) for a raster cell was calculated from Eq. (2.5). It is normally used to define influence of the water accumulation on ground stability at a specific location. Higher TWI values indicate greater amount of existing water content (and pore water pressure) in slope material from which soil strength and soil stability shall be diminished which potentially support the occurrence of landslide over the area. Drainage lines were extracted from the topographical sheet used for DEM generation. The ordering of the drainage has been performed on the basis of Strahler's classification scheme Drainages up to 5th order have been observed in the study area and buffered at 50-meter interval while distance from lineament was buffered at 500-meter interval.

The lithology map was made from original data prepared by the Department of Mineral Resources (DMR) for Krabi Province. Eventually, seven principal lithological types were identified and shown on the output map (Figure 3.2h): Igneous rocks, Kaeng Krachan, Krabi, Ratburi, Saibon Formation, Quaternary Sediments, Thung Yai (more information is given in Table 3.2).

The soil textural classes from lower soil classification category is not bring to use but the soil-texture identification process began with the quantification of soil plasticity and depth from the LDD soil series based on the relevant in each soil description profile data provided in the LDD Soil Information Reference and in website: <http://www.mcc.cmu.ac.th/dinhai/layers.asp>. Knowledge of plasticity property and soil profile led to the estimation of sand, silt, clay combination and soil texture, eventually (as described in the USDA's soil texture pyramid below).



Source: <http://www.todayshomeowner.com/diy-soil-texture-test-for-your-yard/>

Figure 3.2k Soil texture pyramid chart.

The soil texture map (Figure 3.2i) was prepared from the LDD's 1:100,000 scale soil data map of the from which 11 types of soil texture were found: Clay, Clay loam, Loam, Loamy sand, Sand, Sandy loam, Sandy clay loam, Silty clay, Silty clay loam, Silty loam, and Slope complex area (i.e., one with slope gradient > 35%).

The LULC map was derived based on the original 1:25,000 LULC map in 2009 of the province prepared by the LDD (before the referred landslide incidence in March 2011 taking place). Five LULC classes were identified and mapped as an output: dense evergreen forest, disturbed evergreen forest, oil palm, para rubber, and miscellaneous (paddy field, water body, and built-up area).

3.1.2 The mapped data were converted to have a raster-grid format with pixel size of 30m × 30m for further use in the landslide susceptibility evaluating process based on several chosen susceptibility mapping methods of interest.

According to data reported in Table 3.3, predominant topography of the study area is flat terrain which occupies about 36.47% of the total area whereas about 73.38% of land has slope gradient of $< 10^\circ$. In addition, most areas situate at low land of altitude < 200 meters above mean sea level (about 83.64%) with only 5.34% of land that locates at altitude greater ≥ 400 meters, mostly in area of Khao Phanom Bencha mountain range (as illustrated in Figure 3.2a). About half of the total area (52.94%) is classified as being “Quaternary Sediments” lithological type and three types of soil textures; clay, sandy loam, slope complex, were commonly found over an area with proportion of 20.99%, 19.58%, and 28.11%, respectively. Major types of the identified LULC data in 2009 are oil palms (44.36%), para rubber (25.94%), and dense evergreen forest (23.83%).

Table 3.2 Lithological description of Krabi Province (DMR).

Formation/ Group	Symbol	Explanation	Period	Age (my.)
Sediment, Sedimentary and metamorphic rocks				
-	Q _a	Alluvial and flood plain deposits: sand, silt, gravel and clay	Quaternary	0.01 - 1.6
-	Q _b	Beach deposits: loose sand, fine-grained, well sorted, abundant plant remains and shell fragments		
-	Q _{mc}	Mangrove clay deposits; Peaty clay, silt clay, grey or greenish-grey, cover with mangrove		
-	Q _t	Terrace deposits: coarse sand and fine gravel intercalated with clay, silt and fine sand		
-	Q _c	Colluvial deposits: silt, sand, clay, laterite and rock fragment		
Krabi Gp.	T _{kb}	Mudstone, peaty mudstone, thin-bedded, calcareous; fossiliferous mudstone; marlstone; lignite; and semi-consolidated sandstone	Paleocene	1.6 - 66.4
Phum Phin Fm., Thung Yai Gp.	K _p	Sandstone, brick-red, fine to medium grained, arkosic and micaceous, medium bedded, through cross bedding and intercalation	Cretaceous	66.4 - 140
Sam Chom Fm., Thung Yai Gp.	K _{sc}	Conglomerate and sandstone, coarse grained, thick bedded, cross bedding, mudstone, reddish-brown, plant remains		
Lam Thap Fm., Thung Yai Gp.	K _{lt}	Sandstone, light brown, reddish-brown, fine/medium-grained, arkosic, thin to medium bedded, cross bedding, mudstone, reddish-brown		

Table 3.2 (Continued).

Formation/ Group	Symbol	Explanation	Period	Age (my.)
Khlong Min Fm., Thung Yai Gp.	J _{km}	Sandstone, siltstone, shale, and limestone, greenish gray, pale green, reddish purple to dark gray, thin to medium bedded, ripple mark, burrows, fossils of bivalve, <i>Pavamusium</i>	Jurassic	140 - 210
Saibon Formation Fm.	TR _{sb}	Siltstone, brick-red, thin bedded, dolomitic limestone lenses, with fossil of pelecypods and plants remains; sandstone, light brown, fine-to- medium grained, quartzitic, thin to medium bedded	Triassic	210 - 245
Um Luk Fm., Ratburi Gp.	P _{ul}	Limestone, dolomitic limestone, gray and dark grey, massive, with chert lenses	Permian	245 - 286
Phap pha Fm., Ratburi Gp.	P _{pp}	Limestone, dolomitic limestone, gray and dark gray, thin to medium bedded with fossils of bryozoas, fusulinids, corals and crinoids, partly chert lenses intercarate		
Ratburi Gp.	P	Shale, gray; sandstone, yellowish-brown and limestone. Gray lense or bedded; with fossils of fusulinids, brachiopods and corals and plant remains	Permian to Carboni- ferous	245 - 360
Khao Chao Fm., Kaeng Krachan Gp.	CP _{kc}	Arkosic sandstone, white to light gray, good sorted, medium-grained, thin bedded, with <i>Posidnomya</i> sp.		
Khao Phra Fm., Kaeng Krachan Gp.	CP _{kp}	Sandstone, siltstone, greenish gray, massive to laminated bedded, bioturbated, silt to fine-sized, angular to subrounded, poor to moderate sorting; mudstone, greenish-gray, thin bedded to massive, limestone lenses, fossil of bryozoa		
Ko He Fm., Kaeng Krachan Gp.	CP _{kh}	Pebbly sandstone, pebbly mudstone, greenish gray to gray, with clasts of quartz, sandstone, siltstone, granite, shale, schist and limestone, subangular to round, matrixes of clay mineral, chlorite, sericite, feldspar, biotite, quartz, calcite and iron oxide		
Laem Mai Phai Fm., Kaeng Krachan Gp.	CP _{ip}	Mudstone, dense, black, thin bedded, well bedded, with silt lamination, intercalated with lithic sandstone; quartzitic sandstone, siltstone and pebbly mudstone, black, reddish brown and gray, thin bedded to massive		
Kaeng Krachan Gp.	CP _k	Shale, light brown, thin-bedded; sandstone, arkosic, light brown, fine to coarse grained, thick-bedded; siltstone and chert with bryozoas, foraminiferous, crinoid and gastropods, limestone were found in the upper part		
-	gy	Igneous rocks Geyserite, milky white, cryptocrystalline quartz and feldspar, brecciated	Quaternary	0.01- 1.6
-	sy	Syenite, dark gray, porphyritic, mainly feldspar, quartz and hornblende, crystalline feldspars, maximum 2 cm., with shallow extrusive rock	Tertiary	1.6 - 66.4
-	k _{gr}	Khao Phanom granite: granite, porphyry, consisting of quart, feldspar, and biotite, feldspar phenocryst, subhedral, 2-5 cm, some foliation	Cretaceous	66.4 - 140

Table 3.3 Proportion of land for each type of the input factor.

Factors	Class	Area		Factors	Class	Area	
		m ²	%			m ²	%
Elevation	< 200 m	825,963.3	83.64	Slope gradient	0° - 10°	724,701.6	73.38
	200 m - 400 m	108,863.1	11.02		10° - 20°	121,362.3	12.29
	400 m - 600 m	33,528.6	3.40		20° - 30°	91,974.6	9.31
	600 m - 800 m	11,840.4	1.20		30° - 40°	36,180.0	3.67
	800 m - 1,000 m	4,388.4	0.44		40° - 50°	10,846.8	1.10
	> 1,000 m	2,946.6	0.30		> 50°	2,465.1	0.25
Slope aspect	Flat	360,195.3	36.47	Slope curvature	Concave (-)	646,574.4	65.47
	North	59,090.4	5.98		Flat (0)	0.0	0.00
	Northeast	78,685.2	7.97		Convex (+)	340,956.0	34.53
	East	92,162.7	9.33				
	Southeast	94,161.6	9.54				
	South	65,843.1	6.67				
	Southwest	78,502.5	7.94				
	West	86,49.9	8.81				
Topographic wetness index (TWI)	0 - 2.5	6.3	0.00	Drainage (Distance from drainage)	< 50 m	380,292.3	38.51
	2.5 - 5.0	86,101.2	8.72		50 m - 100 m	309,343.5	31.33
	5.0 - 7.5	288,927.9	29.26		100 m - 150 m	203,735.7	20.63
	7.5 - 10.0	184,322.7	18.66		150 m - 200 m	69,272.1	7.01
	10.0 - 12.5	146,898.0	14.88		200 m - 250 m	21,922.2	2.22
	> 12.5	281,274.3	28.48		> 250 m	2,964.6	0.30
Lineament (Distance from lineament)	< 500 m	246,398.4	24.95	Lithology	Thung Yai	136,994.4	13.87
	500 m - 1000 m	186,186.6	18.85		Ratburi	70,267.5	7.12
	1000 m - 1500 m	113,625.9	11.51		Quaternary Sediments	522,804.6	52.94
	1500 m - 2000 m	83,300.4	8.43		Kaeng	168,712.2	17.08
	2000 m - 2500 m	67,513.5	6.84		Krachan	57,576.6	5.83
	2500 m - 3000 m	46,690.2	4.73		Igneous rocks	2,121.3	0.22
	> 3000 m	243,815.4	24.69		Krabi	29,053.8	2.94
					Saibon Formation		
Soil texture	Clay	207,291.6	20.99	LULC	Para rubber	256,185.9	25.94
	Silty clay	64,061.1	6.49		Oil palm	438,069.6	44.36
	Loamy sand	27,146.7	2.75		Dense evergreen forest	235,363.5	23.83
	Sandy loam	193,401.0	19.58				
	Silty clay loam	40,239.9	4.07		Disturbed evergreen forest	640.8	0.07
	Sand	17,924.4	1.82				
	Sandy clay loam	113,548.5	11.50		Miscellaneous	57,270.6	5.80
	Clay loam	23,261.4	2.36				
	Silty loam	15,800.4	1.60				
	Loam	7,281.0	0.74				
Slope complex	277,574.4	28.11					

Note: Total amount of the study area is 987.53 km².

3.2 Construction of landslide inventory map

3.2.1 The landslide inventory map was made based on accumulated data of past landslide occurrences within the area, mainly from the devastated incidences reported in March 2011 (see Figure 3.3 for a work flowchart). These data were visually extracted from distinctive landslide scars found in the high-resolution satellite imagery like those of the THEOS (or Thaichote) satellite recorded on 15th April 2011 (at spatial resolution of 2.0 meters) or NASA's EO-1 satellite taken on 4th April 2011 (at spatial resolution of 10 meters). Also, the distributed satellite imagery recorded over the area around that time (with landslide traces evidenced) from the Google Earth and Bing Map websites were also incorporated in the analysis. Figure 3.4 demonstrates compared examples of several distinctive landslide scars on the used satellite imagery assembled from those four aforementioned sources. Only cloud-free satellite images were used for this task.

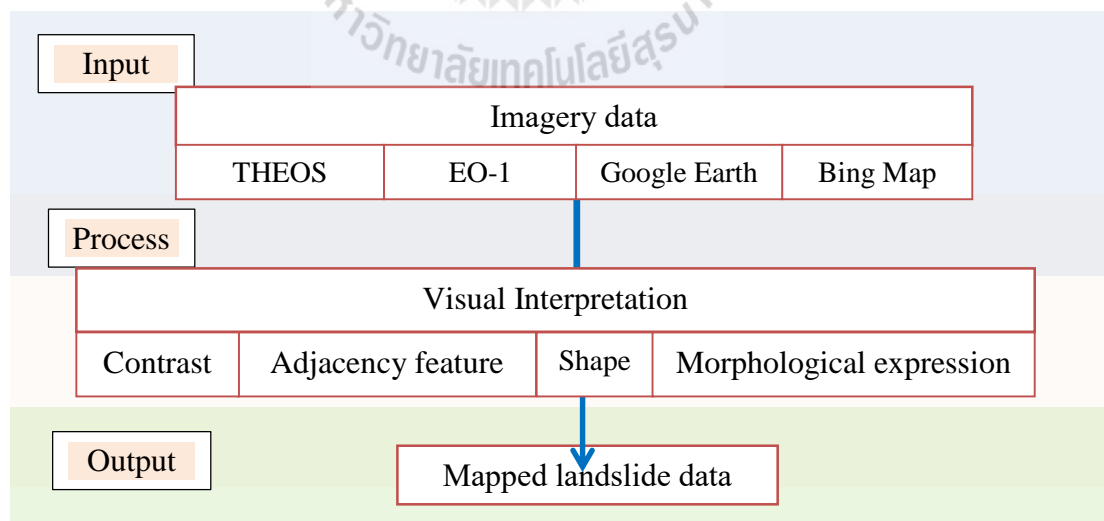
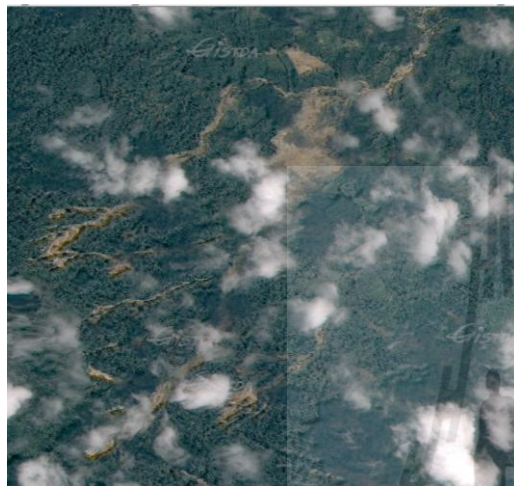


Figure 3.3 Work flowchart of the landslide inventory mapping process.

The identification of potential landslide trace on the applied satellite images was achieved principally through rigorous examination of the distinct terrain properties like contrast, adjacency feature, shape, and the morphological expression that might signify the existing landslide trace. The contrast means the difference in spectral characteristics between the landslides and the surrounding areas. Normally, fresh landslide is usually well recognized based on its sharp outer edge and bright appearance (compared to its background environment) due critically to explicit exposure of its soil or rock content. Older slope failures may have degraded features such as rounded head scarps and worn edges along with evidences of ongoing weathering and erosional processes (Figure 3.5). The landslide axis is normally parallel to general flow direction. Type of the movement was assigned using shape criteria, such as length/width ratio and asymmetry. Upstream landslide can be transformed into debris flow that is often resulted in large runout over flat downstream area (Figure 1.3). In addition, landslide traces can also be located by their distinctive fan shape or sharp lines of break in topography, and sometimes a local drainage anomaly. For morphological features, appearance such as clear breaks on steep scarps, disrupted/disordered forest cover and bare soil can be used to identify landslide.

3.2.2 The located landslide evidences over the area gained from all four sources of high-resolution satellite imagery mentioned earlier (THEOS, EO-1, Google Earth, and Bing Map) were eventually merged to formulate an integrated landslide inventory map of the area which contains information of all notes landslide locations (uppermost part of each individual landslide scarp) along with their approximated extent boundary (like in Figure 3.6). The underlined assumption was that each individual landslide scarp was originated from large land subsidence at the uppermost

part and descended as flow downward by gravity towards, or along, the adjacent drainage routes. This inventory map (in raster format) was built to accommodate evaluation of landslide susceptibility zone afterwards.



(a) THEOS



(b) EO-1



(c) Google Earth



(d) Bing Map

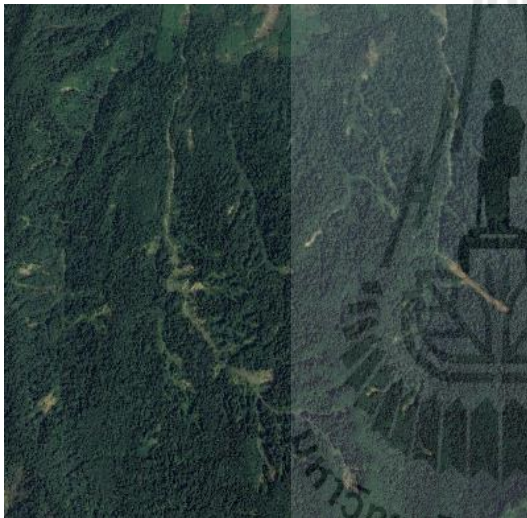
Figure 3.4 Examples of the high-resolution satellite images from four different sources; (a) THEOS satellite, (b) EO-1 satellite, (c) Google Earth website, (d) Bing Map website, showing landslide traces within the study area (from the incidence in late March 2011).



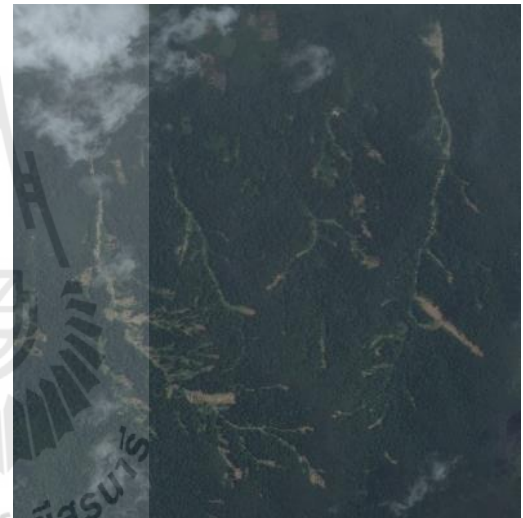
(a) THEOS



(b) EO-1



(c) Google Earth



(d) Bing Map

Figure 3.4 Examples of the high-resolution satellite images from four different sources; (a) THEOS satellite, (b) EO-1 satellite, (c) Google Earth website, (d) Bing Map website, showing landslide traces within the study area (from the incidence in late March 2011) (Continued).



(a) THEOS



(b) EO-1

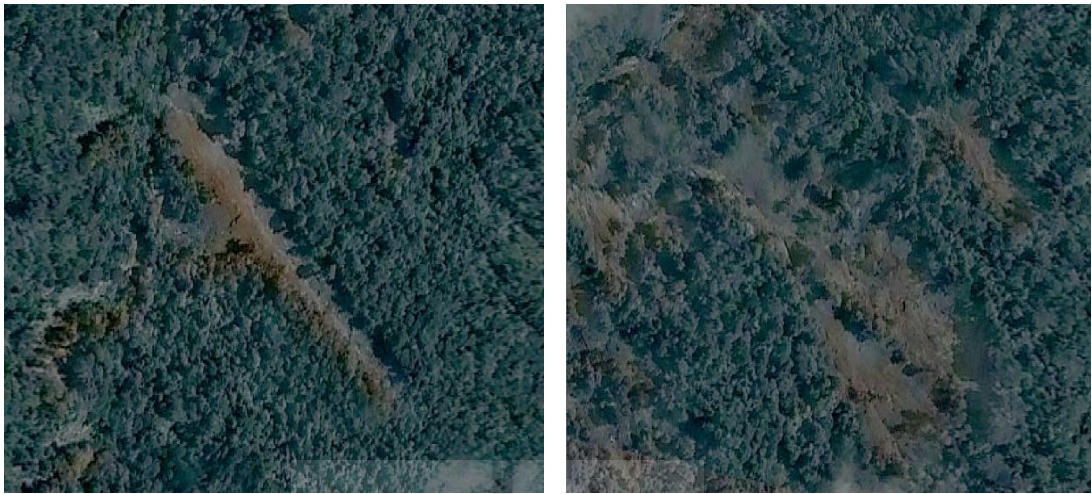


(c) Google Earth

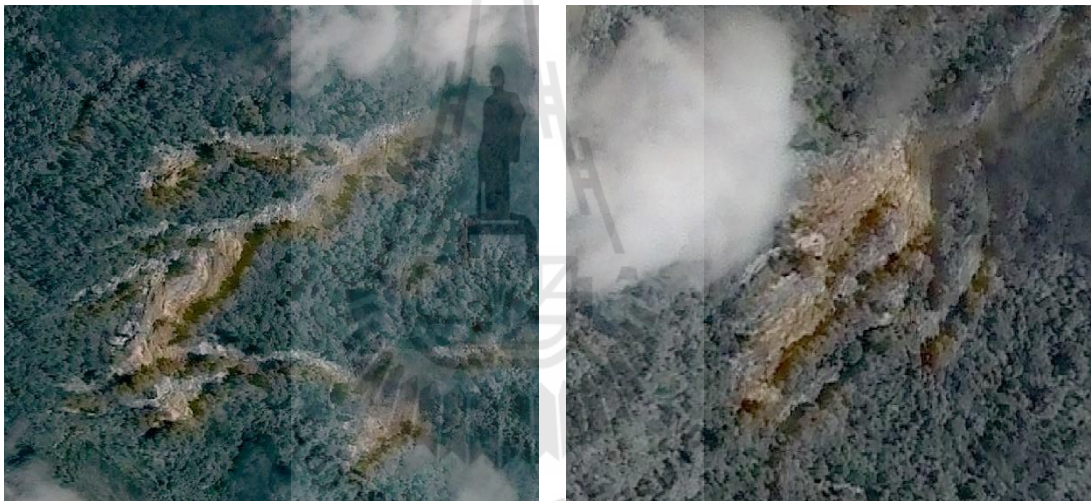


(d) Bing Map

Figure 3.4 Examples of the high-resolution satellite images from four different sources; (a) THEOS satellite, (b) EO-1 satellite, (c) Google Earth website, (d) Bing Map website, showing landslide traces within the study area (from the incidence in late March 2011) (Continued).



(a) Fresh landslide



(b) Old landslide

Figure 3.5 Different characteristics between fresh and old landslide scars as shown on the THEOS satellite imagery.

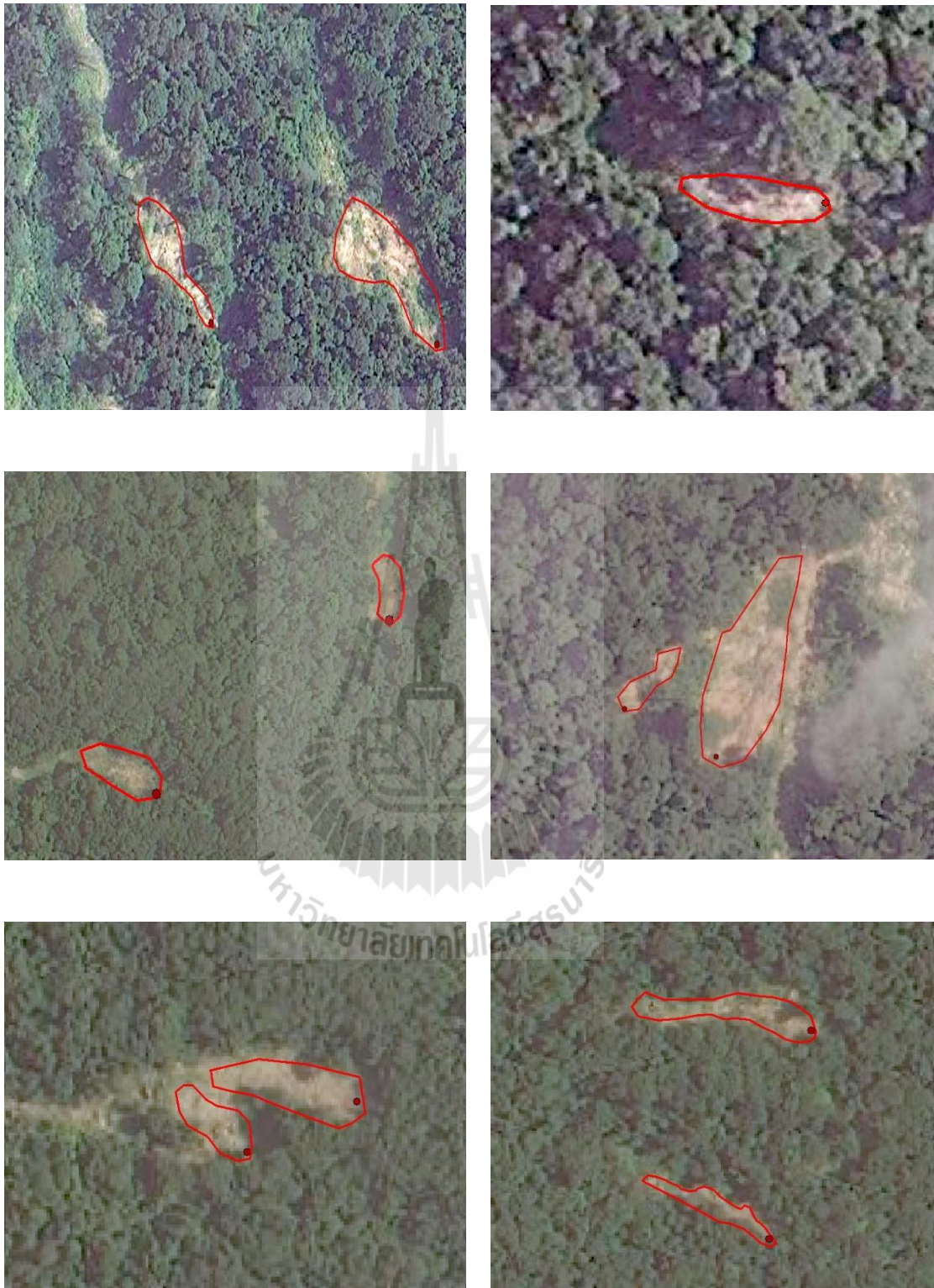


Figure 3.6 Examples of the evidenced landslide inventory map of the area.

Finally, a total of 700 landslide incidences (location and extent) were identified and mapped. Most of them were found concentrated in Khao Phanom Bencha mountain range, especially in the middle portion close to the summit (as depicted in Figure 3.7) due to the highly susceptible land characteristics for slope failures of the area. Records of this landslide inventory data were then split into 70% (or 490 locations) for modeling of the desired susceptibility maps and 30% (or 210 locations) for the validation of those derived maps. This 70:30 proportion was recommended in Huberty (1994).

Note that, field surveys of landslide prone area in the vicinity of Khao Phanom Bencha mountain network were also managed but exact positions of the seen landslide scars were difficult to justify then due to their frequently inaccessible locations (situated mostly at high elevation and on the steep terrain) (Figure 3.8). Also, mapped locations of landslide incidences in the area compiled by the Department of Disaster Prevention and Mitigation (DDPR) and the Department of Mineral Resources (DMR) were considered but were not directly put in use due to the still uncertainty in their validity.

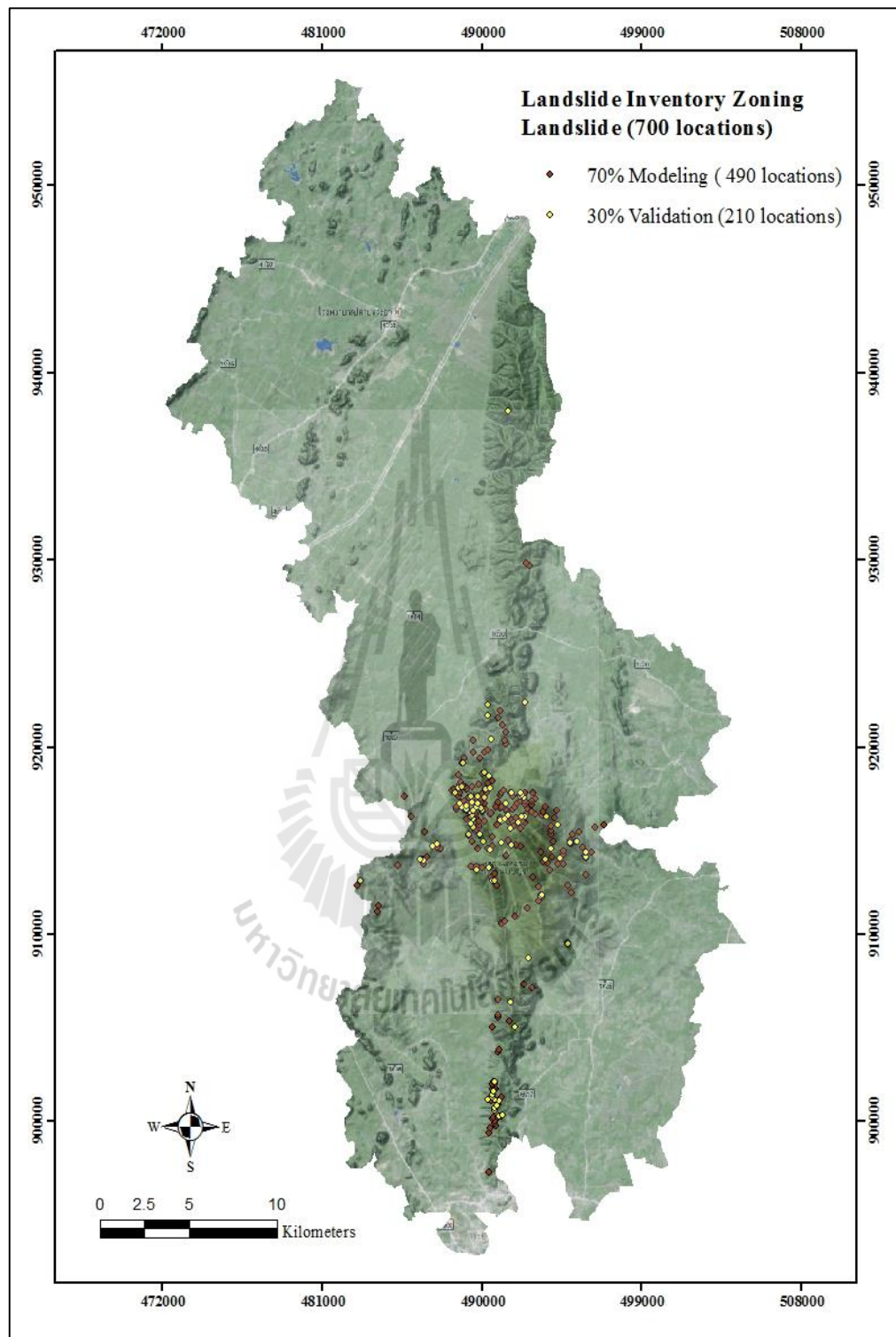


Figure 3.7 Location map of the 700 identified landslide spots within the study area.

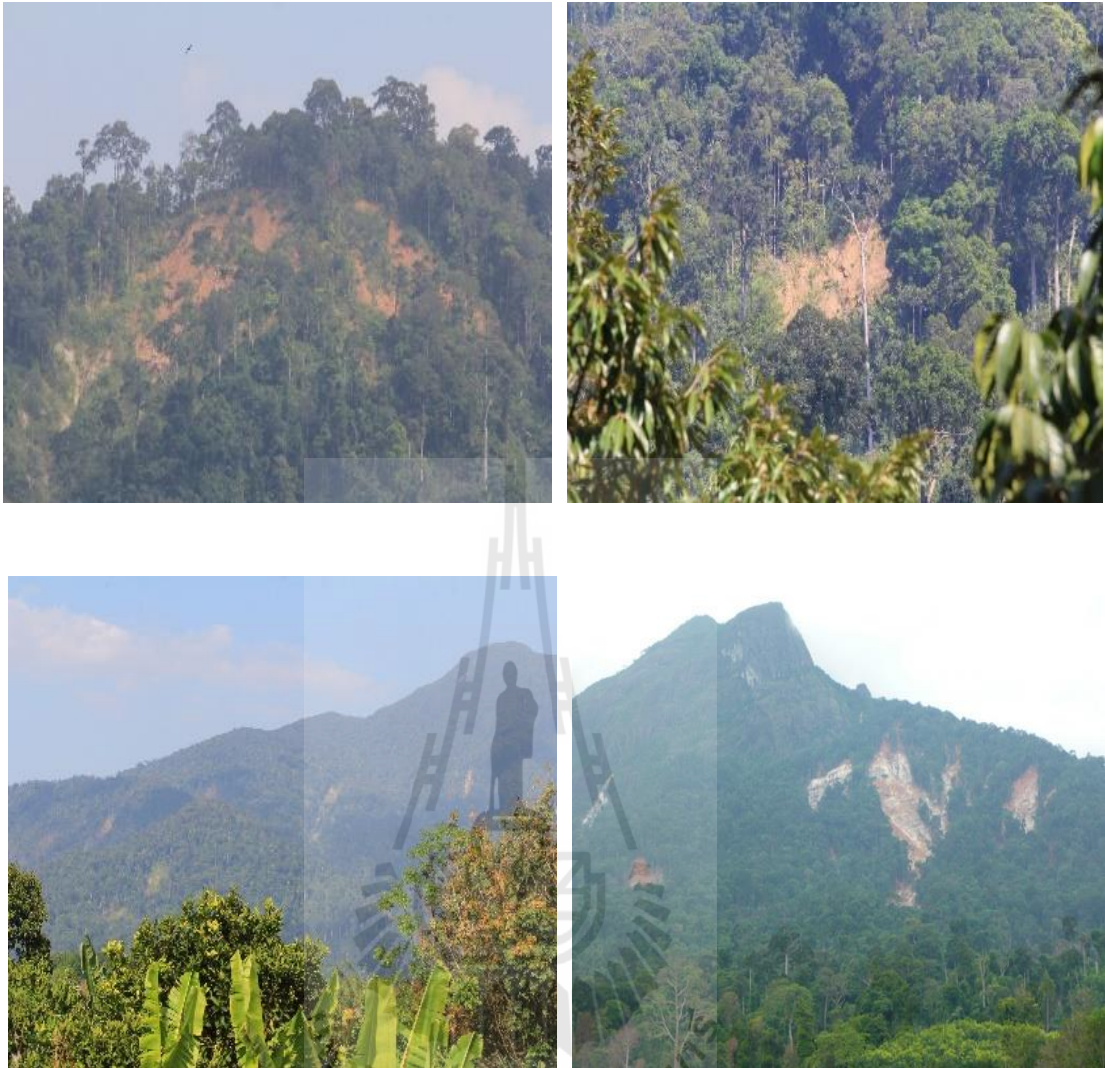


Figure 3.8 Examples of photos taken during the field survey of the study area in which evidences of landslide occurrences over the mountain's terrain are clearly visible.

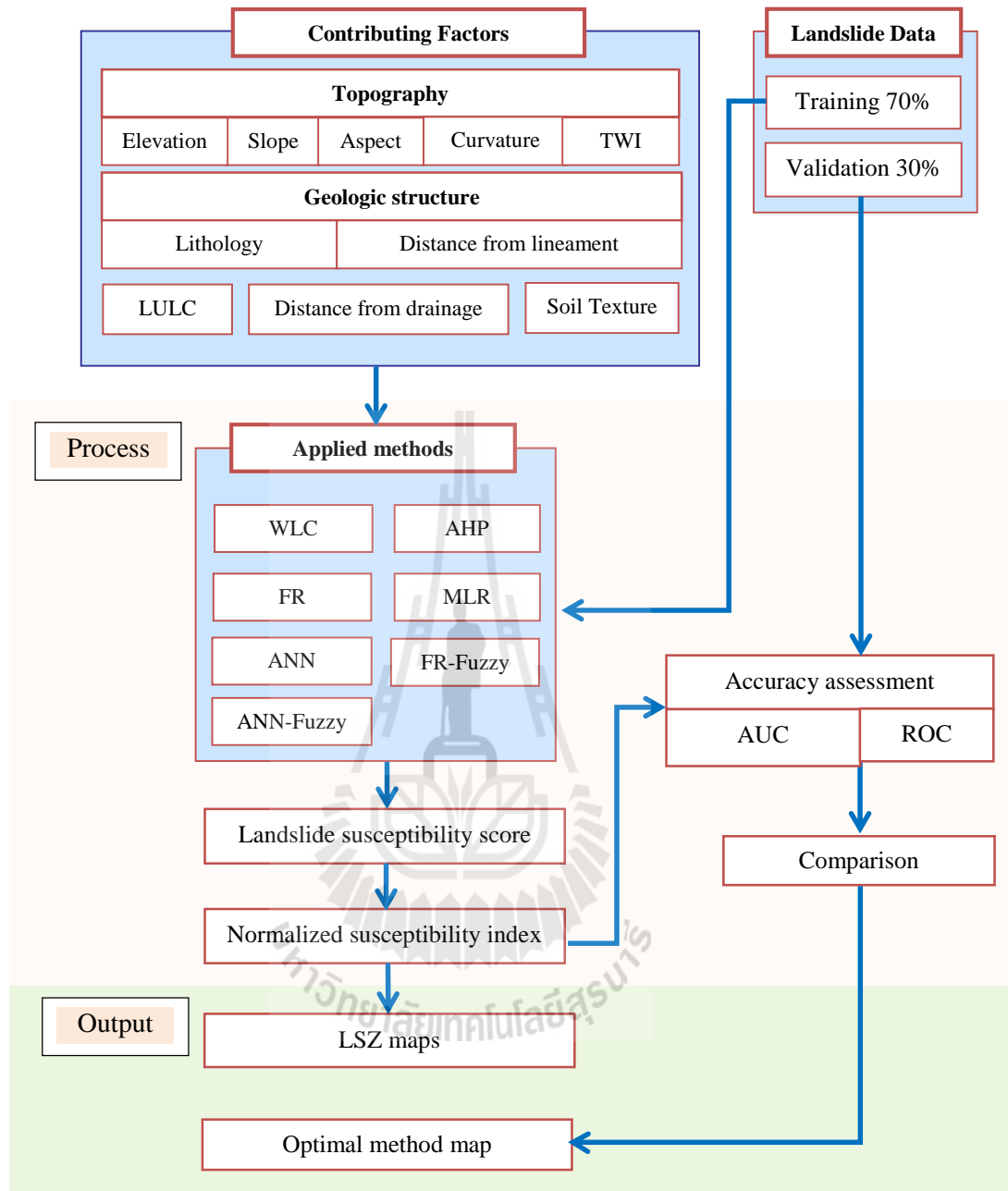


Figure 3.9 Work flowchart for the construction and verification of the susceptibility maps to find an optimal method for further application in subsequent work.

3.3 Construction and verification of the landslide susceptibility maps

This part consists of two principal tasks. The first one is to formulate the landslide susceptibility maps for the area using several chosen methods (both of the qualitative and quantitative types). The second task is to assess for accuracy of resulted maps gained from each applied method and determine the optimal one for further use in the subsequent work (hazard and risk mapping). Flowchart of main work in this part is shown in Figure 3.9.

All output susceptibility maps were established based on knowledge of the normalized susceptibility score (NSS), ranging from 0 to 1, in which five main classes (for five different susceptibility zones) were established. These include (1) very low susceptibility (VLS) for $NSS = 0.0-0.2$, (2) low susceptibility (LS) for $NSS = 0.2-0.4$, (3) moderate susceptibility (MS) for $NSS = 0.4-0.6$, (4) high susceptibility (HS) for $NSS = 0.6-0.8$, and (5) very high susceptibility (HS) for $NSS = 0.8-1.0$. Note that, the equal-interval classification technique (of NSI data) was applied as a standard for the making of all output maps regardless of the method involved. NSS data for each corresponding pixel on the map was quantified based on its original landslide susceptibility score (LSS), or probability, obtained for each pixel by each preferred method. The analysis process carried out in this part was mostly achieved through the use of the ArcGIS and Weka softwares (Hall et al., 2009).

3.3.1 Necessary input data for each preferred susceptibility mapping method were prepared in form of the appropriate GIS dataset in raster format as described earlier. These stated methods can be separated into 2 groups, which are,

- (1) the qualitative type, including,

- (1.1) Conventional weighted linear combination (WLC),
- (1.2) Analytical hierarchy process (AHP),
- (2) the quantitative type, including,
 - (2.1) Frequency ratio (FR) model,
 - (2.2) Integrated FR-fuzzy model,
 - (2.3) Multiple logistic regression (MLR),
 - (2.4) Artificial neural network (ANN),
 - (2.5) Integrated ANN-fuzzy model.

3.3.2 Suitable factor and class (or attribute) weights for the two qualitative methods, WLC and AHP, were determined from the independent judgment of 8 experts in this field collected through the reply of distributed questionnaires for each stated method (as detailed in Appendices B-D). Net contributing weight [= factor weight (FW) x class weight (CW)], or *NCW*, for each attribute of a considered factor was then assessed (for each method) and used as a basis for the generation of landslide susceptibility score (*LSS*) and the normalized susceptibility score (*NSS*) for a specific pixel as follows (for 10 contributing factors):

$$LSS_i = \sum_{j=1}^{10} NCW_{ij} , \quad (3.1a)$$

$$NSS_i = \frac{LSS_i - LSS_{\min}}{LSS_{\max} - LSS_{\min}} , \quad (3.1b)$$

where LSS_i is the LSS value for pixel i^{th} on the map, LSS_{max} and LSS_{min} are the maximum and minimum values of LSS found on the map, respectively.

3.3.3 For the frequency ratio (FR) method, the corresponding FR values (for each attribute of each identified factor) were computed (through Eq. (2.14)) and used to determine the landslide susceptibility score (LSS) for each pixel on the final map (through Eq. (2.15)). The LSS dataset was then changed to be the equivalent NSS dataset for classifying purpose using similar conversion formula illustrated in Eq. (3.1b).

3.3.4 An attribute of a specific contributing factor shall be considered as being a member of the landslide producer set with a certain fuzzy-membership value. These values can be assessed by some data-driven methods, such as the frequency ratio (FR) model (e.g. Lee, 2007; Regmi et al., 2010; Aksoy and Ercanoglu, 2012) or the cosine amplitude method (e.g. Ercanoglu and Gokceoglu, 2004; Kanungo et al., 2006; Ercanoglu and Temiz, 2011), or by the expert-based judgments through the application of the defined if-then rules (e.g. Saboya, Alves and Pinto, 2006; Pourghasemi et al., 2012). Here, the fuzzy-membership values were found based on the FR method instead of the traditional expert-based if-then rules as it is more convenient and might be more suitable in this case as most reference landslides were originated from unusually heavy rainfall over an area which is not often experienced by the experts in the field, therefore, the evidence-based like FR might be more effective in evaluating the incidence.

The FR dataset obtained in the earlier analysis (in Step 3.3.3) were then used as proxy for the determination of the membership value through the linearly transformation function expressed below (for the use in the FR-Fuzzy mapping model):

$$MV(C_{ij}) = \frac{FR_{ij} - \text{Min}(FR_{ij})}{\text{Max}(FR_{ij}) - \text{Min}(FR_{ij})} [\text{Max}(MV(C_{ij})) - \text{Min}(MV(C_{ij}))] + \text{Min}(MV(C_{ij})), \quad (3.2)$$

where $MV(C_{ij})$ is the fuzzy membership value, $\text{Max}(MV(C_{ij}))$ and $\text{Min}(MV(C_{ij}))$ are the upper and lower normalization bounds, respectively.

This transformation shall result in membership values in the range of 0.1-0.9 similar to methodology used in Bui et al. (2012). Susceptibility maps in this case were synthesized through the utilization of five main fuzzy operators detailed in Section 2.6.6: OR, AND, algebraic sum, algebraic product, and gamma with varying values of λ function (0-1). The corresponding NSS dataset was gained through conversion of output from each operation (pixel-based) using the formula likes that of Eq. (3.1b). Final map with the highest obtained accuracy was then used as a representative of the output resulted from this method.

3.3.5 For the MLR method, input data to the model were separated into 2 groups: (1) the continuous data (e.g., slope, elevation, or proximity), which were normalized to have new values in the range of [0, 1], and (2) the categorical data (e.g., land use or soil type), which were administrated in basic binary format (i.e., presence = 1/absence = 0) for each respected attribute of the referred factor (like input landslide incidence data). All 490 locations of the known landslide incidences were used as training samples along with another 490 locations of the landslide-free pixels found by random sampling. After initial processing, proper relationship of the Logit function L, as expressed in Eq. (2.17), for all input factors was established along with knowledge of probability (p) of landslide occurrence for a pixel (through Eq. (2.18)). This

parameter “p” was then used as a proxy of the *NSS* for the preparation of the susceptibility map afterwards.

3.3.6 For the ANN mapping method, the input data were prepared like those done for the MLR method explained earlier (30 layers in total of independent data and 1 layer of the dependent data). These data were then systematically processed to gain the appropriate weights (or coefficient) for each included input layer. These weights were then integrated and applied in the form of their equivalent absolute values. These obtained weights were then normalized (using formula similar to that described in Eq. (3.2)) to aid the determination of the *LSS* value for each pixel on the map through this linear combination format:

$$LSS = w_1x_1 + w_2x_2 + \dots + w_nx_n. \quad (3.3)$$

The coefficients w_0, w_1, \dots, w_n ($n = 1-30$) are the normalized weights (NW) of each used factor (for the numerical type) or attribute (for categorical type) while x_1, x_2, \dots, x_n are their associated input values, respectively (real data for the numerical type and binary-format data for the categorical type). The equivalent *NSS* dataset was finally generated through the use of the following formula:

$$NSS_i = \frac{LSS_i}{\sum_{i=1}^{30} (LSS_i)}, \quad (3.4)$$

where LSS_i is the *LSS* value for pixel i^{th} on the map.

3.3.7 For the ANN-fuzzy method, the normalized weights obtained for each layer of input data in the ANN method were applied, along with the known membership value for each attribute (or each layer of input data) from the FR-fuzzy method, to determine the final net contributing weight (NCW) like that of the MLR or AHP methods [NCW = normalized weight (w) x membership value (MV)], similar to that reported in Kanungo et al. (2006). The susceptibility map could then be made straightforwardly through the yielded datasets of LSS and NSS (from NCW data) through the use of formulas detailed in Eq. (3.1a and b), respectively. The susceptibility maps in this case were prepared like those done for the FR-fuzzy method explained earlier.

3.3.8 All derived landslide susceptibility maps (from each preferred method) were then compared and evaluated about the similarity or differences in terms of featured general characteristics and contents. In this regard, the obtained landslide susceptibility maps built by the responsible government agencies, or the relevant research groups, for the study area were also taken into the consideration and discussion.

3.3.9 To validate for their credential, accuracy assessment of all susceptibility maps were carried out based on two popular methods: the Area-Under-Curve (AUC) method and the Receiver Operating Characteristic (ROC) method detailed in Chapter II.

3.3.10 An optimal method for landslide susceptibility mapping for the area was finally identified based primarily on the obtained accuracy of each generated map (from each method). However, as levels of the found accuracy for the top methods in average were rather comparable (i.e. < 3% in the difference), therefore, other criteria were added

to judge for the preferred choice of optimal method, which are, the ease in their similar application and the superiority in the interpretability of the output.

3.3.11 Two different datasets of rainfall amount (i.e., the long-term annual mean record during 1951-2012 period and the event-based record during 27-29 March 2011) seen at 17 rainfall stations operated both in and nearby the provincial area (Figure 3.10) were used to prepare rainfall maps for the area using kriging interpolation method (as shown in Figure 3.11). Noted that, rainfall map over an area might be established from the satellite data (like TRMM satellite) or from the radar observations during the chosen time period, however, due to their relatively coarse solutions (if compared to actual size of the study area), they were then not included in this analysis. The original rainfall data of interest were gained from Thai Meteorological Department (TMD), Royal Irrigation Department (RID) and the Department of Mineral Resources (DMR) (Table 3.4-3.6). These built rainfall maps were then used as an additional layer of input data for making a new susceptibility map by the optimal method identified earlier, followed by accuracy assessment process of the achieved maps regarding to this action to evaluate influence of the integrated rainfall data on the yielded susceptibility map for the area in terms of the average accuracy from all assessing methods in use.

Table 3.4 Statistics of rainfall at the nearby rainfall station (data for 1951-2012).

ID	Station name	Province	Annual average (millimeter)
551006	Phrasaeng	Surat thani	1,766.9
551011	Phanom	Surat thani	1,706.0
552008	Thung Yai	Nakhon si thammarat	1,544.2
561001	Phang nga	Phang nga	2,352.4
561002	Thap Put	Phang nga	2,126.5
561006	Takua Thung	Phang nga	2,886.9
561008	Ko Yao	Phang nga	2,174.6

Source: The Thai Meteorological Department, Office of Water Management and Hydrology, Royal Irrigation Department.

Table 3.5a List of rainfall stations in Krabi Province and their annual mean of rainfall.

ID	Rainfall station			Annual mean : millimeter		
	Station	District	Number of year	Total rain	Wet season	Dry season
15012	Krabi	Mueang	48	1,807.3	1,171.5	635.8
15022	Khlong Thom	Khlong Thom	45	2,092.1	1,356.7	735.4
15032	Ao Luek	Ao Luek	33	2,184.1	1,439.2	744.9
15042	Ko Lanta	Ko Lanta	45	2,168.1	1,479.4	688.6
15052	Todlongyangnaichong	Ao Luek	52	2,564.5	1,638.5	926.0
15060	Pakasai Dam	Mueang	33	1,830.7	1,189.1	641.6
15070	Sai Kao Dam	Khlong Thom	32	2,016.4	1,338.1	678.3
15080	Nam Daeng Dam	Khao Phanom	24	1,556.5	1,009.5	547.0
15093	Ko Lanta Meteorology	Ko Lanta	23	2,170.9	1,475.5	695.5
15123	Krabi Meteorology	Mueang	8	2,119.7	1,402.9	716.8

Table 3.5b Statistics of monthly mean rainfall of Krabi Province at the listed stations.

Station ID	Monthly mean rainfall : millimeter											
	Apr	May	Jun	Jul	Aug	Sep	Oct	Nov	Dec	Jan	Feb	Mar
15012	112.8	203.6	217.2	217.6	231.3	283.2	246.4	146.9	46.1	24.0	23.2	55.0
15022	128.4	253.0	244.0	246.4	279.4	313.1	271.2	185.6	61.1	23.8	19.4	66.9
15032	130.7	220.5	249.6	292.9	294.1	323.0	283.5	184.0	61.7	34.5	35.7	73.9
15042	95.0	261.7	254.8	296.3	319.6	373.1	306.6	138.9	45.0	12.8	25.6	38.7
15052	189.9	289.1	278.9	314.0	337.7	385.7	337.7	194.4	69.0	36.3	36.7	95.0
15060	113.9	235.6	191.3	206.7	238.1	254.1	242.7	172.8	74.7	25.2	16.0	59.6
15070	110.4	245.9	233.8	261.3	269.8	314.6	268.2	163.5	60.7	29.8	17.4	41.0
15080	92.8	198.0	136.5	145.2	180.1	203.8	215.5	191.5	73.4	30.5	25.6	63.5
15093	118.1	260.8	226.1	285.4	306.3	345.9	322.5	166.6	48.7	13.4	21.3	55.8
15123	167.4	180.2	229.5	202.9	308.6	267.3	359.2	183.9	81.0	28.9	54.5	56.3

Source: Office of Water Management and Hydrology, Royal Irrigation Department.

Table 3.6 Statistics of rainfall during 2011 landslide event (during 27th-29th March).

ID	Station name	Province	Daily rainfall data for 27 th -29 th March 2011			
			27 th	28 th	29 th	3 days
551202	Surat Thani	Surat Thani	6.00	148.20	241.50	395.7
551301	Surat Thani Agromet		7.80	250.00	247.30	505.1
551401	Phra Sang		2.80	61.40	0.00	64.2
552201	Nakhon Sri Thammarat	Nakhon	6.8	249.4	91.4	347.6
552401	Chawang	Sri	1.5	70.8	104.2	176.5
27013	Ban Bangpu	Thammarat	-	61.8	44.9	106.7
27401	Ban Hua Na		0	234.5	148.7	383.2
27551	Ban Wang Sai		13.3	128.7	146.2	288.2
-	Waag Aai Wow		2.8	43.6	55.8	102.2
-	Tha Lao Tha lone		1.2	49	100.8	151.0
566001	Krabi	Krabi	20.6	130.8	161.4	312.8
566002	Ko Lanta		6	45.6	12	63.6
-	Thub Prik		-	60.0	200.0	260.0
-	Kao Phanom		21.0	131.0	161.0	313.0
-	Kao Khram		-	-	320.0	320.0
567201	Trang	Trang	1.9	121.1	108.4	231.4
561004	Takua Pa	Phang nga	33.1	74.2	105.2	212.5
34052	Khukkhak Sub-district		33.1	74.2	105.2	212.5

Source: Thai Meteorological Department; Department of Mineral Resources; Royal Irrigation Department (RID).

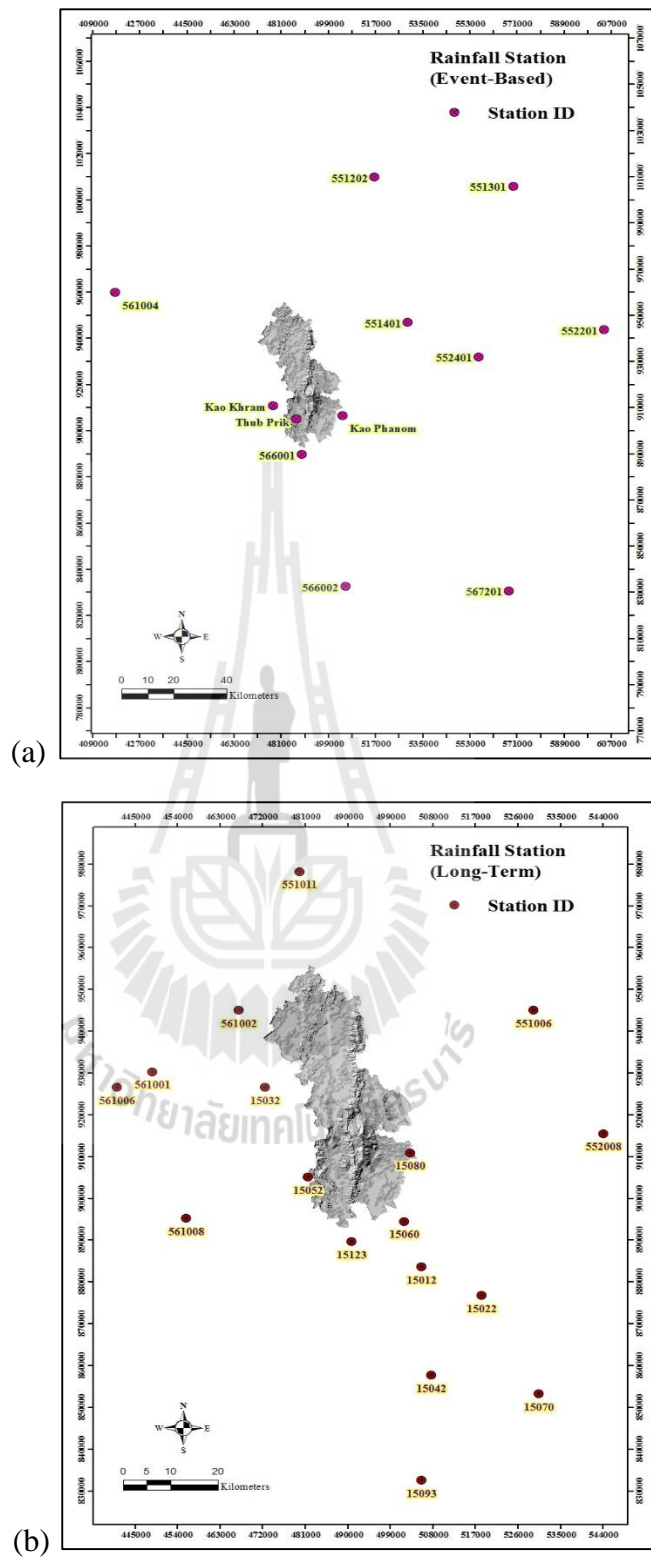


Figure 3.10 Location maps of the applied rainfall stations for (a) during 27th-29th March 2011 and (b) long-term average for the period 1951-2012.

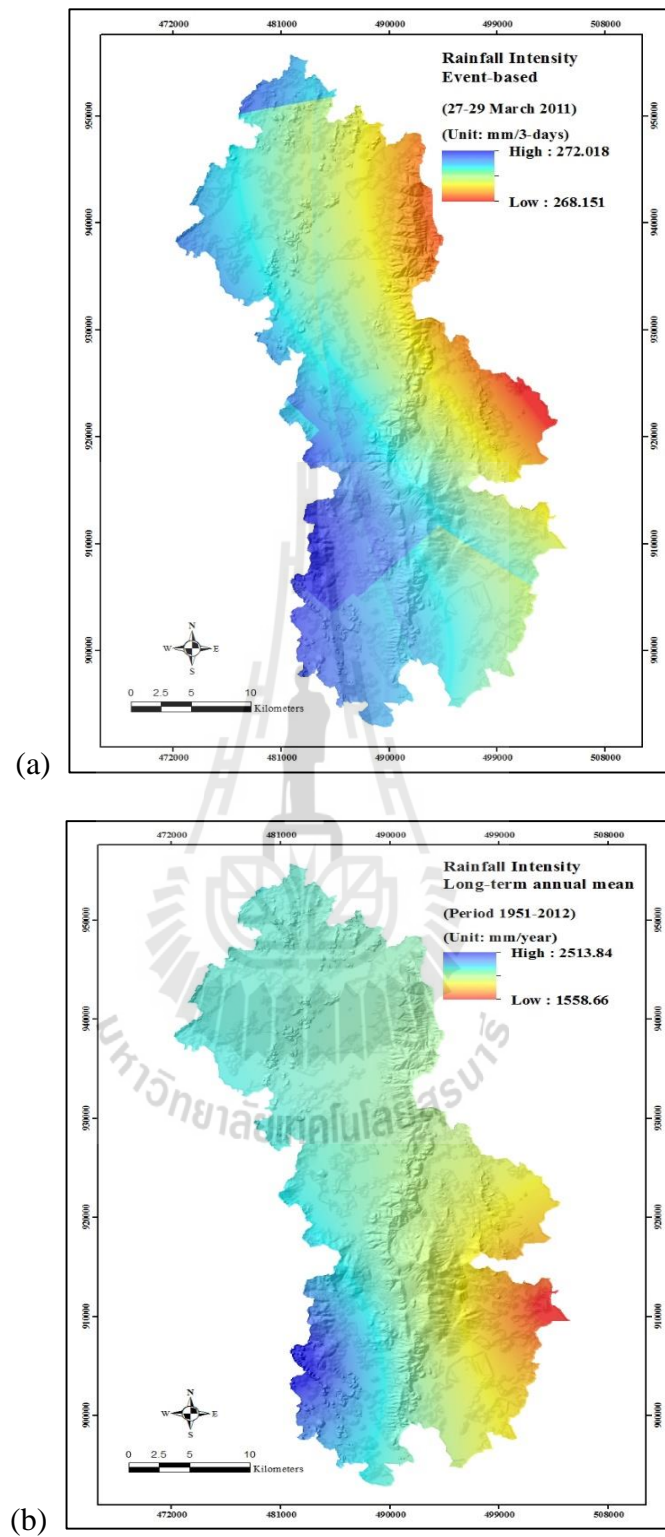


Figure 3.11 Representative rainfall maps of the area for (a) during 27th-29th March 2011 and (b) long-term average for the period 1951-2012.

3.4 Construction of the hazard, vulnerability, and risk maps

3.4.1 The landslide hazard maps for the study area were produced by integrating annual rainfall probability (ARP) data for the critical rainfall values of 100 mm/day and 300 mm/3-days (DMR, 2011) (Table 3.7a and Figure 3.12). These threshold values are specific for the study area but for the other areas different values might be more suitable.

These ARP data were extracted from known return-period data of those rainfall criteria for the area (given by the RID) (Table 3.7b), with the original landslide susceptibility score (*LSS*) data (not the normalized data, or *NSS*):

$$\text{Hazard index (HI)} = \text{ARP} \times \text{LSS}. \quad (3.4)$$

The hazard maps (for each rainfall criterion) were then established based on application of the equal-interval method on the known values of the HI on the map.

3.4.2 The concerned elements at risk within the identified hazard areas (in both cases), which are building and economic LULC components like paddy field, field crop (maize), horticulture (coffee, rambutan, durain, oil palm, coconut, mangosteen, mixed orchard, mixed perennial, and orange) and para rubber were mapped (Figure 3.13).

3.4.3 The vulnerability map was then derived based on data of the normalized vulnerability score (NVS) defined for each group of the defined elements at risk based on their estimated economic values of loss per unit area by the responsible government agency (mainly for the compensation purpose).

3.4.4 The landslide risk maps were then constructed through the combination of the hazard map (from each considered source) and the vulnerability map yielded earlier based on the following calculation of the risk index (pixel-based):

$$\text{Risk index (RkI)} = \text{HI} \times \text{NVS}. \quad (3.5)$$

The equal-interval technique was applied to classify risk data (RkI) existing on the map into five different zones: very high; high; moderate; low; and very low, respectively.

Table 3.7a Statistics of annual rainfall probability at measuring stations in Krabi Province.

ID	Rainfall station		Number of year	Annual rainfall probability	
	Station	District		100 mm/day	300 mm/3-days
15012	Krabi	Mueang	54	0.33	0.003
15022	Khlong Thom	Khlong Thom	47	0.50	0.013
15032	Ao Luek	Ao Luek	35	0.33	0.100
15042	Ko Lanta	Ko Lanta	49	0.50	0.100
15052	Tod Long Yang	Ao Luek	52	0.50	0.020
15060	Pakasai Dam	Mueang	33	0.33	0.003
15070	Sai khao Dam	Khlong Thom	33	0.33	0.013
15080	Nam Dang Dam	Khao Phanom	26	0.20	0.002
15093	Ko Lanta Meteorology	Ko Lanta	23	0.50	0.013
15123	Krabi Meteorology	Mueang	8	0.50	0.100

Source: Office of Water Management and Hydrology, Royal Irrigation Department.

Table 3.7b Statistics of return period for maximum rainfall at measuring stations in Krabi Province.

ID	Rainfall station		Number of year	Max.rainfall day	Return period (year) for rainfall in millimeter /year												
	Station	District			2	3	5	10	25	50	75	100	200	300	500	750	1000
15012	Krabi	Mueang	54	1	94.2	107.9	123.2	142.4	153.2	166.6	184.6	195.0	202.4	225.9	243.7	254.1	261.4
				2	118.2	133.0	149.4	170.1	181.7	196.2	215.6	226.8	234.8	260.1	279.3	290.4	298.4
				3	140.3	157.3	176.2	200.0	213.4	230.0	252.2	265.2	274.3	303.4	325.4	338.3	347.4
15022	Khlong Thom	Khlong Thom	47	1	100.8	115.3	131.5	151.8	163.3	177.5	196.6	207.7	215.5	240.4	259.2	270.2	278.0
				2	139.7	160.6	183.9	213.1	229.6	250.1	277.5	293.4	304.7	340.6	367.6	383.4	394.6
				3	168.5	193.3	220.9	255.6	275.2	299.4	332.0	350.9	364.2	406.7	438.8	457.6	470.9
15032	Ao Luek	Ao Luek	35	1	98.2	113.6	130.9	152.5	164.7	179.9	200.2	211.9	220.3	246.8	266.8	278.5	286.8
				2	139.5	166.7	196.9	234.9	256.4	283.0	318.6	339.4	354.0	400.6	435.8	456.3	470.9
				3	171.0	214.1	262.1	322.4	356.5	398.7	455.2	488.1	511.4	585.3	641.1	673.7	696.9
15042	Ko Lanta	Ko Lanta	49	1	114.8	134.5	156.5	184.1	199.7	219.1	245.0	260.0	270.7	304.6	330.1	345.1	355.7
				2	157.0	187.2	220.9	263.2	287.1	316.7	356.4	379.4	395.8	447.6	486.8	509.6	525.9
				3	185.5	220.3	259.0	307.6	335.0	369.1	414.6	441.1	459.9	519.5	564.5	590.8	609.4
15052	Tod Long Yang	Ao Luek	52	1	102.9	119.9	138.8	162.6	176.1	192.7	215.0	228.0	237.2	266.4	288.4	301.3	310.4
				2	148.0	169.5	193.5	223.5	240.5	261.5	289.7	306.1	317.7	354.5	382.3	398.6	410.1
				3	182.6	209.3	238.9	276.2	297.2	323.3	358.2	378.5	392.9	438.6	473.0	493.2	507.5
15060	Pakasai Dam	Mueang	33	1	90.3	104.2	119.7	139.1	150.1	163.7	181.9	192.5	200.0	223.8	241.8	252.3	259.8
				2	118.9	134.9	152.7	175.1	187.7	203.3	224.3	236.5	245.1	272.5	293.2	305.3	313.9
				3	142.4	159.4	178.4	202.3	215.8	232.5	254.9	268.0	277.2	306.5	328.6	341.5	350.6
15070	Sai khao Dam	Khlong Thom	33	1	97.4	114.7	134.0	158.1	171.8	188.7	211.3	224.5	233.8	263.5	285.8	298.9	308.2
				2	139.3	160.1	183.2	212.2	228.6	248.9	276.2	292.0	303.2	338.8	365.6	381.3	392.5
				3	160.4	182.1	206.2	236.5	253.7	274.9	303.3	319.8	331.5	368.6	396.7	413.1	424.7
15080	Nam Dang Dam	Khao Phanom	26	1	80.4	89.7	100.0	112.9	120.2	129.3	141.4	148.4	153.4	169.3	181.2	188.2	193.2
				2	106.5	122.4	140.2	162.5	175.0	190.6	211.5	223.7	232.3	259.6	280.2	292.3	300.8
				3	128.7	146.3	166.0	190.8	204.8	222.1	245.3	258.8	268.3	298.7	321.6	334.9	344.4
15093	Ko Lanta Meteorology	Ko Lanta	23	1	118.5	134.3	151.9	174.1	186.6	202.0	222.8	234.9	243.4	270.5	291.0	303.0	311.5
				2	147.9	168.8	192.1	221.4	237.9	258.4	285.8	301.7	313.0	348.9	375.9	391.8	403.0
				3	173.5	196.0	221.1	252.6	270.4	292.5	322.0	339.2	351.4	390.0	419.2	436.2	448.3
15123	Krabi Meteorology	Mueang	8	1	101.8	119.2	138.6	163.0	176.7	193.7	216.6	229.8	239.2	269.1	291.6	304.8	314.1
				2	143.0	171.1	202.3	241.6	263.7	291.1	327.9	349.3	364.5	412.6	448.9	470.1	485.2
				3	177.0	222.8	273.8	337.8	374.0	418.8	478.8	513.7	538.4	616.9	676.2	710.8	735.4

Source: Office of Water Management and Hydrology, Royal Irrigation Department.

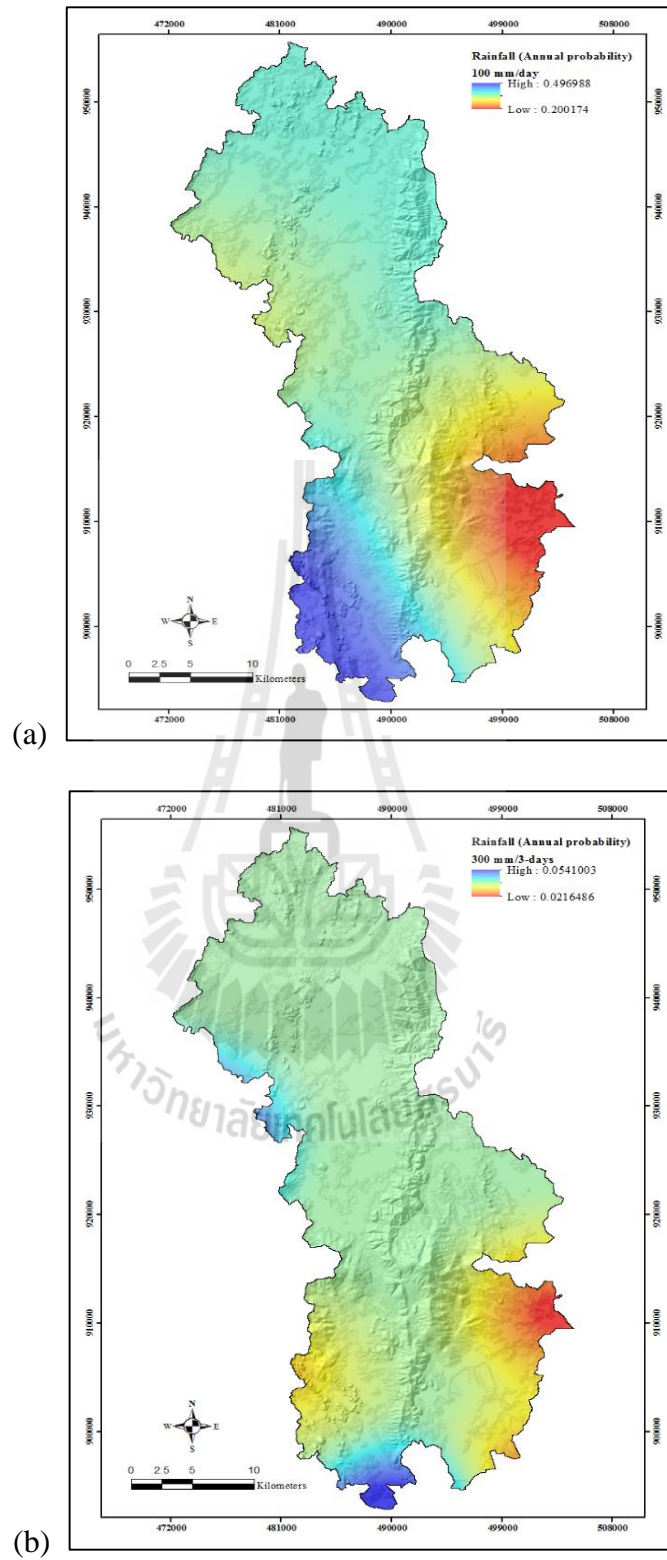


Figure 3.12 Annual rainfall probability maps: (a) 100 mm/day and (b) 300 mm/3-days.

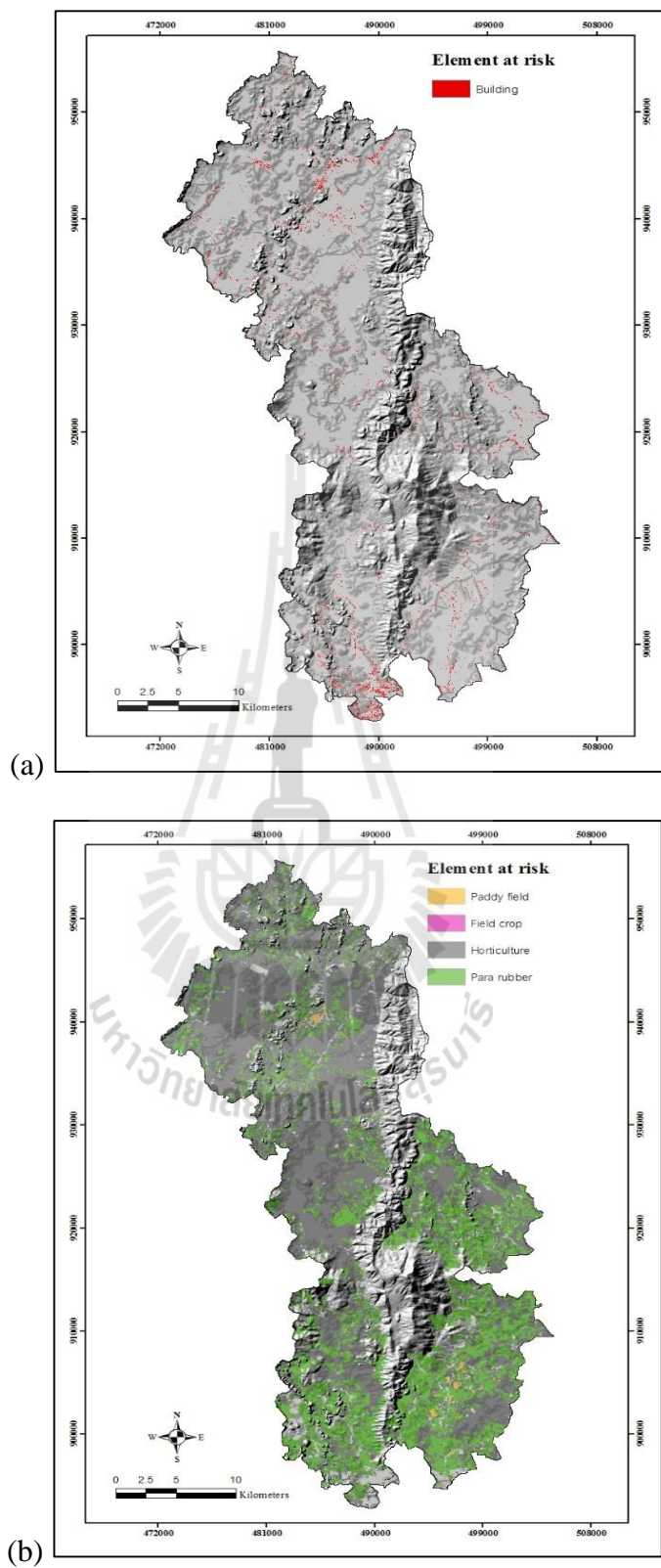


Figure 3.13 Element at risk maps for (a) building (houses) and (b) LULC.

3.5 Construction of the runout map

The additional susceptibility map originating from the subsequent runout caused by the occurrence of massive landslides upstream was also formulated from knowledge of the runout susceptibility (RS) of debris flow integrated in the Flow-R model (as detailed in Chapter II). All input data were in the ASCII format and landslide scare data were recorded in binary format as 0 (no scare) and 1 (scare). The mapping process comprised of three main distinct steps (as outlined in the framework shown in Figure 3.14):

(1) The directions of flow were identified on the basis of DEM and user-defined datasets while the propagation of their masses (as debris flow) over the topography was determined using a probabilistic and energy approach, respectively.

(2) Spreading area of the flow was determined based on probabilistic spreading (by means of the flow direction algorithms), and also on a basic energy balance which defines maximal runout distance.

(3) The yielded runout prediction map was compared to the satellite-based one for identifying the distinctive similarities or differences.

To calibrate the maximum probable debris flow runout, the March 2011 event that affected Phanom Bencha Mountain was used as a reference. THEOS satellite imagery in late March 2011 were used to calibrate the possible maximum runout using the edge of alluvial fans where previous debris flows were observed and historical events from DMR in form of GIS shape file. In this research, main input data included DEM, slope gradient, flow accumulation, and the landslide scare data. The propagation assessment comprises of two crucial parts: spreading algorithm and energy analysis. In

the first part, models involved are direction algorithm modified from Holmgren (1999) and inertial algorithm with weight of the persistence function in the assessment of flow spreading defined from Gamma (2000) type. In the second part, the simplified friction-limited model was used for the determination of runout distance based on the maximum possible runout distance characterized by a minimum travel angle, also called angle of reach. In case of energy limitation, maximum limit of the potential energy was defined to ensure the realistic outcome of the flow velocity (see Figure 3.15 for an example of the model's main user interface).

Propagation parameters were taken from the literature in case of well supported by both physical and empirical backgrounds. For examples, velocity threshold of 15 m/s and the friction loss function: SFLM, with a travel angle of 11° .

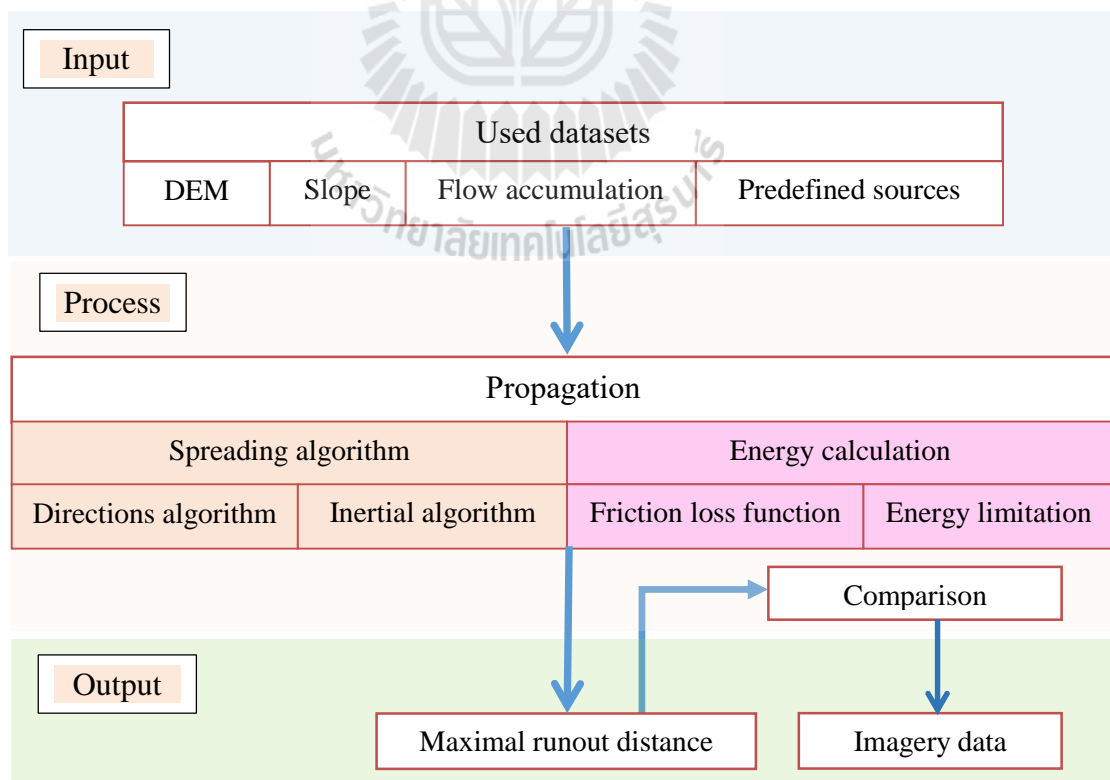


Figure 3.14 Flowchart of the runout analysis work.

Flow-R 0.9.6 (UNIL)

Options Tools Help

Working directories

Directory to store data: D:\Landslide\Khaopanom\Hazard\flow\wr\ Select

Directory to save resulting files: D:\Landslide\phanombenja\flow\result Select

Run definition

1. Choice of the study area: khaopanom

2. Choice of the rivers layer: khaopanom_no_river

3. Enter run name: panombenja

Source areas

Include the following data: + Backup intermediate grids (not recommended)

Distance to rivers (buffer) Buffer: Select...

DEM dem Criteria: above_0100m

Predefined sources scararea Criteria: boolean

Slope slope Criteria: above_15_deg

Flow accumulation accumulate Criteria: DF_rare_events_f...

Select... Select... Criteria: Select...

Select... Select... Criteria: Select...

Source value: Binary (0/1) Use the value of DEM

Propagation

Propagation calculation Additional results: Sum of probabilities

Sources triggering mode: Connected areas

Calculation method: Quick: energy based discrimination (recommended)

Spreading algorithm: Holmgren (1994) modified dh=02.0m_exp=15.0

Directions algorithm: weights Gamma_2000

Inertial algorithm: Gamma_2000

Energy calculation: Friction loss function: travel angle 11.0_deg

Energy limitaion: velocity < 15_mps

Display options

Display the source areas

Display the propagation extent

Run

Figure 3.15 Example of the main user interface of the Flow-R model.



CHAPTER IV

RESULTS AND DISCUSSION

This chapter reports conclusive results of the overall thesis work in accordance with the objectives stated in Chapter I and research procedure illustrated in Chapter III. Content of the report is separated into three main consecutive parts which focus on three main tasks. These are, (1) the construction of landslide susceptibility maps (using seven proposed methods) and the identification of the optimal method, (2) the formulation of hazard maps (from the output landslide susceptibility map of the named optimal method and the annual rainfall probability maps) and risk maps (from the vulnerability map of the identified elements at risk located in the area and the formulated hazard maps), and (3) the analysis on potential risk arisen from the landslide-induced runout phenomenon on the mapped element at risks over the area. The associated discussion on the presented results of each aforementioned issue of interest is also given accordingly therein.

4.1 Establishment of landslide susceptibility maps

Work in this part was planned in respect to the first stated objective of the thesis which is to identify optimal method for the construction of landslide susceptibility map for the study area (the Khao Phanom Bencha Watershed, Krabi Province) from a set of the preferred methods, which are, (1) weighted linear combination (WLC), (2) analytical hierarchy process (AHP), (3) frequency ratio (FR), (4) integrated FR-fuzzy,

(5) multiple logistic regression (MLR), (6) artificial neural network (ANN), and (7) integrated ANN-fuzzy. The accomplished results are as follows.

4.1.1 Application of the weighted linear combination (WLC) method

The WLC method was chosen as a representative of the widely-used qualitative approach (along with the AHP method) whose decision is relied mainly on the surveyed opinion of experts in the field, rather than on objective evidence of the concerned issue itself. For this method, the appropriate preference score (or weight) for each input factor and its associated attributes were identified based on independent judgment of 8 experts in this field collected through the reply of distributed questionnaires (detailed in Appendix C). The primary scores were prescribed in order from 1 (not important) to 5 (most important) and the average values were put in use, which include, factor weight (FW), class weight (CW) and net contributing weights (NCW = FW·CW) (as detailed in Table 4.1).

According to this definition, possible values of NCW rank from 1 to 25 from which higher value indicates greater contribution towards the landslide occurrence over the area. From data given in Table 4.1, in terms of priority, slope gradient, lithology, and soil texture were rated highest by the associated experts with FW of 4.50, 4.29, and 3.88, respectively. Meanwhile, elevation, slope aspect, and slope curvature were given the lowest priority ones with FW of 2.38, 2.38, and 2.75, respectively. And, at attribute level, the preferable areas for the landslide incidence (with $CW \geq 4.00$) were those with elevation > 800 m, slope gradient > 40°, TWI > 10.0, distance from drainage < 200 m and from lineament < 1,000 m, and igneous rocks as their foundation. Two top favorites for the aspects here are the southwest and west directions with equal CW of

3.63. Also, for the LULC, para-rubber planting was considered most significant cause of landsliding found in the area (with CW = 4.00). Eventually, in terms of NCW, igneous rock, slope gradient of $> 50^\circ$, and slope gradient of 40° - 50° , were considered the most important ones in this respect with the NCW values of 21.45, 19.71, and 18.58, respectively.

Table 4.1 Expert-based factor and class (attribute) weights for the WLC method.

Thematic layers	Attributes	Factor weight (FW)	Class weights (CW)	Net contributing weights (FW·CW)
Elevation	< 200 m	2.38	1.25	2.9750
	200 m – 400 m		2.13	5.0694
	400 m – 600 m		2.88	6.8544
	600 m – 800 m		3.88	9.2344
	800 m – 1,000 m		4.63	11.0194
	> 1,000 m		4.50	10.7100
Slope gradient	0° – 10°	4.50	1.00	4.5000
	10° – 20°		2.00	9.0000
	20° – 30°		3.00	13.5000
	30° – 40°		3.88	17.4600
	40° – 50°		4.13	18.5850
	$> 50^\circ$		4.38	19.7100
Slope aspect	Flat	2.38	1.00	2.3800
	North		1.50	3.5700
	Northeast		2.50	5.9500
	East		2.88	6.8544
	Southeast		2.50	5.9500
	South		3.00	7.1400
	Southwest		3.63	8.6394
	West		3.63	8.6394
	Northwest		2.25	5.3550
	Slope curvature		Concave (-)	2.75
Flat (0)		1.38	3.7950	
Convex (+)		3.50	9.6250	
Topographic wetness index (TWI)	0 – 2.5	2.88	1.00	2.8800
	2.5 – 5.0		2.00	5.7600
	5.0 – 7.5		3.00	8.6400
	7.5 – 10.0		3.75	10.8000
	10.0 – 12.5		4.75	13.6800
	> 12.5		5.00	14.4000
Drainage (Distance from drainage)	< 50 m	2.88	4.88	14.0544
	50 m – 100 m		4.13	11.8944
	100 m – 150 m		3.25	9.3600
	150 m – 200 m		2.25	6.4800
	200 m – 250 m		1.38	3.9744
	> 250 m		1.00	2.8800

Table 4.1 (Continued).

Thematic layers	Attributes	Factor weight (FW)	Class weights (CW)	Net contributing weights (FW·CW)
Lithology	Thung Yai		3.14	13.4706
	Ratburi		1.57	6.7353
	Quaternary sediments		1.57	6.7353
	Kaeng Krachan	4.29	3.71	15.9159
	Igneous rocks		5.00	21.4500
	Krabi		3.00	12.8700
	Saibon Formation		3.00	12.8700
Lineament (Distance from lineament)	< 500 m		5.00	15.0000
	500 m – 1,000 m		4.13	12.3900
	1,000 m – 1,500 m		2.88	8.6400
	1,500 m – 2,000 m	3.00	2.13	6.3900
	2,000 m – 2,500 m		1.63	4.8900
	2,500 m – 3,000 m		1.25	3.7500
	> 3,000 m		1.13	3.3900
Soil Texture	Clay		1.88	7.2944
	Silty clay		2.13	8.2644
	Loamy sand		3.25	12.6100
	Sandy loam		3.13	12.1444
	Silty clay loam		3.00	11.6400
	Sand	3.88	3.25	12.6100
	Sandy clay loam		3.13	12.1444
	Clay loam		2.38	9.2344
	Silty loam		2.63	10.2044
	Loam		2.88	11.1744
	Slope complex area		3.63	14.0844
LULC	Dense evergreen forest		1.38	4.1400
	Disturbed evergreen forest		2.88	8.6400
	Oil palm	3.00	3.50	10.5000
	Para rubber		4.00	12.0000
	Miscellaneous		3.50	10.5000

The factor's order of priority (in terms of the factor weight) found in this work was rather similar to that presented in several WLC-based works reported earlier, especially on the top two candidates (slope gradient and lithology) and the usual bottom members (slope aspect, slope curvature, distance to drainage), e.g., in Tanavud et al. (2000), Wachal and Hudak (2000), Sarkar and Kanung (2004), Matori et al. (2011), and Kayastha et al. (2013). For the attribute's merit (in terms of the attained class weight) of each listed factors, it often conforms well to conventional believes or prevalent theories. For examples, areas with higher slope gradient should be more susceptible to

the slope failure as well as those located closer to the drainage or lineament. Also, areas with igneous-rock foundation and those situated in slope complex area are believed to most prone to landslide occurrence.

Figure 4.1 exhibits the final classified landslide susceptibility map resulted from the WLC method in which five levels of the susceptible states were presented from very low (VLS) to very high (VHS). Proportion of land belonged to each classified category of this susceptibility map is described in Table 4.2 from which about 43% were situated in the very low to low susceptibility zones and about 17% were in the high to very high susceptibility zones (mostly at Khao Phanom Bencha mountain network).

Table 4.2 Landslide susceptibility classification of land based on the WLC method.

Landslide susceptibility classes	LSS values	NSS values	Area	
			%	km ²
Very low susceptibility (VLS)	54.59 - 68.50	0.00-0.20	2.11	20.84
Low susceptibility (LS)	68.50 - 82.40	0.20-0.40	40.75	402.39
Moderate susceptibility (MS)	82.40 - 96.30	0.40-0.60	39.66	391.61
High susceptibility (HS)	96.30 - 110.31	0.60-0.80	16.28	160.79
Very high susceptibility (VHS)	110.31 - 124.12	0.80-1.00	1.21	11.91

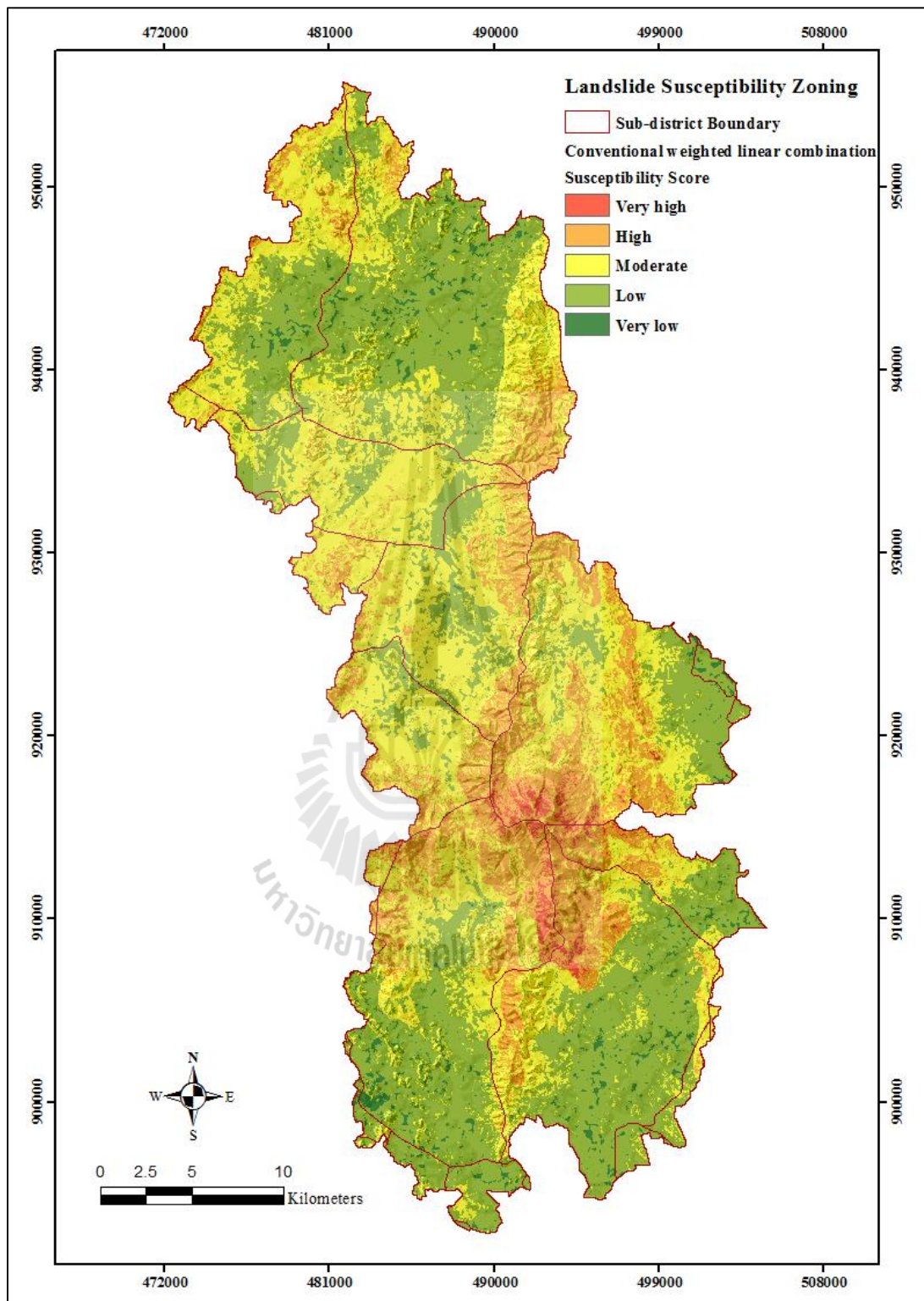


Figure 4.1 Classified landslide susceptibility map yielded from the WLC method.

4.1.2 Application of the analytical hierarchy process (AHP) method

Similar to the WLC method, the AHP method is also a very popular qualitative approach in decision-making analysis. However, apart from the expert-based judgment on value of the possible option, the consistency of this judgment by an individual expert is also examined. In this method, the pair-wise comparison matrix was established first from the comparative judgment of each corresponding expert, to attain preference scale of these factors (and their respective attributes) given in terms of the normalized weight between 0 and 1. In this case, validity of each given judgment was determined and those with $CR < 0.10$ were included in the further analysis (see more details in Appendix D). Tables 4.3 and 4.4 presents the output normalized weights for all input factors and their respective set of attributes, while Table 4.5 summarizes yielded values of the factor and class weights (FW and CW) reported earlier in Tables 4.3 and 4.4.

From data shown in Table 4.3, slope gradient, lithology, and soil texture were still on top in terms of the preference, like in the WLC method, with FW of 0.1733, 0.1756 and 0.1184, respectively, while the three least scores now were aspect, drainage, and elevation with FW of 0.0517, 0.0545, and 0.0550, respectively. And at attribute level, the favorite areas for landslide activity were found resemble to those of the WLC method, e.g., ones with high elevation, steep slope, close distance to lineament and drainage system, high TWI, or igneous rocks as their foundation. Two most preferred candidates for the aspect were still the southwest and west, and for LULC, these were oil palm and para-rubber planting. The eventual output of the AHP approach are reported in Figure 4.2 (classified susceptibility map) and Table 4.6 (proportion of

coverage area). And, similar to that of the WLC-based map, about 56% of land on the AHP-based map were found situating in the very low to low susceptibility zones and only about 9% were resided in the high to very high susceptibility categories (mostly in the mountainous regions).

Table 4.3 Factor weights from pair-wise comparison matrix yielded from 8 experts.

Factors (Input layer)	Factor weights from individual expert's judgment								Mean weights (CR < 0.1)
	1	2	3	4	5	6	7	8	
Elevation	0.0227	0.0735	0.0460	0.0551	0.0206	0.0181	0.0802	0.0200	0.0550
Slope gradient	0.2796	0.2431	0.2652	0.0468	0.2601	0.2807	0.2015	0.1101	0.1733
Slope aspect	0.0600	0.0171	0.0276	0.0776	0.1790	0.0194	0.0692	0.0671	0.0517
Slope curvature	0.0297	0.1179	0.0295	0.0806	0.1292	0.0346	0.0355	0.1127	0.0752
TWI	0.0415	0.0332	0.0718	0.0692	0.0271	0.0933	0.0423	0.1807	0.0794
Drainage	0.1625	0.0170	0.0918	0.0702	0.0457	0.0626	0.0395	0.0540	0.0545
Lithology	0.1014	0.2511	0.1646	0.1663	0.1327	0.0986	0.0211	0.2750	0.1756
Lineaments	0.0675	0.1513	0.1815	0.0522	0.0413	0.0813	0.0478	0.0908	0.1047
Soil texture	0.1529	0.0588	0.1011	0.1481	0.1047	0.1498	0.2314	0.0526	0.1184
LULC	0.0820	0.0370	0.0211	0.2339	0.0595	0.1617	0.2314	0.0370	0.1121
Consistency ratio	0.15	0.07	0.09	0.09	0.14	0.12	-0.03	0.07	

Note: Only judgments with CR < 0.1 were used to calculate mean weight.

Table 4.4 Class weights from pair-wise comparison matrix based on expert opinions.

Factors	Class weights (of each factor) from individual expert's judgment								Mean weight (CR < 0.1)
	1	2	3	4	5	6	7	8	
Elevation (m)									
(1) < 200	0.0408	0.0260	0.0499	0.0469	0.0372	0.0434	0.0580	0.0268	0.0387
(2) 200 – 400	0.0633	0.0471	0.1656	0.0677	0.0478	0.0655	0.0872	0.0498	0.0724
(3) 400 – 600	0.1344	0.0886	0.1937	0.1132	0.0971	0.1024	0.1226	0.0864	0.1165
(4) 600 – 800	0.4186	0.1660	0.3159	0.1132	0.1684	0.1604	0.1677	0.1824	0.2179
(5) 800 – 1,000	0.1965	0.3362	0.1523	0.2140	0.2532	0.2488	0.2302	0.2077	0.2298
(6) > 1,000	0.1464	0.3362	0.1225	0.4449	0.3962	0.3794	0.3344	0.4469	0.3246
Consistency ratio	0.08	0.05	0.03	0.10	0.03	0.02	0.11	0.05	
Slope gradient									
(1) 0° – 10°	0.0484	0.0269	0.0464	0.0458	0.0361	0.0309	0.0379	0.0301	0.0378
(2) 10° – 20°	0.0731	0.0488	0.1658	0.0712	0.0549	0.0428	0.0591	0.0567	0.0733
(3) 20° – 30°	0.1868	0.1137	0.3998	0.1018	0.0767	0.0720	0.1001	0.0707	0.1459
(4) 30° – 40°	0.3730	0.1875	0.2452	0.1636	0.1397	0.1564	0.1562	0.1323	0.1997
(5) 40° – 50°	0.1494	0.3116	0.0956	0.1636	0.2543	0.2759	0.2464	0.2503	0.2144
(6) > 50°	0.1693	0.3116	0.0472	0.4541	0.4384	0.4219	0.4003	0.4599	0.3289
Consistency ratio	0.06	0.02	0.04	0.10	0.06	0.07	0.13	0.05	
Slope aspect									
(1) Flat	0.0372	0.0208	0.0271	0.0358	0.0230	0.0252	0.0340	0.0141	0.0298
(2) North	0.0432	0.0345	0.0362	0.0358	0.0317	0.0252	0.0404	0.1801	0.0386
(3) Northeast	0.2485	0.0695	0.1945	0.0674	0.0718	0.0566	0.0471	0.2047	0.1399
(4) East	0.1879	0.0336	0.0530	0.1678	0.0742	0.2243	0.0471	0.0996	0.0804
(5) Southeast	0.0849	0.0336	0.1945	0.0843	0.2001	0.1948	0.0814	0.0396	0.0986
(6) South	0.0503	0.2054	0.0530	0.1662	0.2998	0.0793	0.1263	0.1369	0.1087
(7) Southwest	0.1696	0.3730	0.1945	0.0843	0.1486	0.0564	0.2533	0.2293	0.2476
(8) West	0.1181	0.1960	0.0530	0.2523	0.0832	0.2762	0.2533	0.0727	0.1551
(9) Northwest	0.0603	0.0336	0.1945	0.1061	0.0676	0.0621	0.1172	0.0231	0.1014
Consistency ratio	0.07	0.04	0.04	0.20	0.18	0.21	0.05	0.22	
Slope curvature									
(1) Concave (-)	0.5247	0.1749	0.2521	0.1285	0.1062	0.2605	0.4286	0.2605	0.2691
(2) Flat (0)	0.1416	0.0472	0.0726	0.2766	0.2605	0.1062	0.1429	0.1062	0.1544
(3) Convex (+)	0.3338	0.1113	0.6752	0.5949	0.6333	0.6333	0.4286	0.6333	0.4812
Consistency ratio:	0.05	0.10	0.11	0.00	0.03	0.03	0.00	0.03	
Topographic wetness index									
(1) < 2.5	0.3915	0.0248	0.0563	0.0469	0.0408	0.3451	0.0379	0.0249	0.0387
(2) 2.5 – 5.0	0.0638	0.0435	0.4276	0.0677	0.0530	0.2093	0.0591	0.0439	0.1271
(3) 5.0 – 7.5	0.0739	0.0789	0.3305	0.1132	0.0920	0.1474	0.1001	0.0956	0.1420
(4) 7.5 – 10.0	0.1031	0.1385	0.0933	0.1132	0.1522	0.1132	0.1562	0.1574	0.1309
(5) 10.0 – 12.5	0.1502	0.2330	0.0487	0.2140	0.2475	0.1044	0.2464	0.3904	0.2267
(6) > 12.5	0.2176	0.4814	0.0436	0.4449	0.4144	0.0805	0.4003	0.2879	0.3344
Consistency ratio	0.14	0.10	0.05	0.10	0.07	0.15	0.13	0.10	
Drainage									
Distance from drainage (m)									
(1) < 100	0.3425	0.4625	0.4996	-	0.3598	0.4467	0.0249	0.3763	0.3408
(2) 100 – 200	0.2067	0.2550	0.2944	-	0.2154	0.1893	0.0439	0.2959	0.2223
(3) 200 – 300	0.1448	0.1403	0.0872	-	0.1514	0.1408	0.0956	0.1542	0.1193
(4) 300 – 400	0.1260	0.0736	0.0409	-	0.1013	0.1033	0.1574	0.1011	0.0932
(5) 400 – 500	0.1003	0.0343	0.0389	-	0.0911	0.0728	0.3904	0.0455	0.1273
(6) > 500	0.0798	0.0343	0.0389	-	0.0810	0.0471	0.2879	0.0270	0.0970
Consistency ratio:	0.17	0.05	0.06	-	0.2	0.12	0.10	0.08	

Note: Only judgments with CR < 0.1 were used to calculate mean weight.

Table 4.4 (Continued).

Factors	1	2	3	4	5	6	7	8	Mean weight (CR < 0.1)
Lithology									
(1) Thung Yai	0.1660	0.0672	0.0977	0.1075	0.2016	0.1030	-	0.1980	0.1362
(2) Ratburi	0.0328	0.0626	0.0217	0.0742	0.0685	0.0525	-	0.0540	0.0602
(3) Quaternary sediments	0.0578	0.0626	0.0219	0.0433	0.0319	0.0348	-	0.1170	0.0650
(4) Kaeng Krachan	0.1185	0.1195	0.2323	0.1228	0.0905	0.1773	-	0.0785	0.1262
(5) Igneous rocks	0.3778	0.4019	0.4135	0.2267	0.3622	0.3383	-	0.3614	0.3088
(6) Krabi	0.1309	0.2241	0.0828	0.2128	0.0959	0.1919	-	0.0217	0.1421
(7) Saibon Formation	0.1162	0.0620	0.1300	0.2128	0.1494	0.1023	-	0.1694	0.1615
Consistency ratio	0.20	0.28	0.17	0.02	0.12	0.02	-	0.08	
Lineament									
Distance from lineament (m)									
(1) < 500	0.3231	0.3176	0.5302	0.1692	0.2952	0.3817	0.4007	0.3515	0.3455
(2) 500 – 1,000	0.2482	0.3176	0.1864	0.2429	0.1897	0.2486	0.1772	0.2367	0.2467
(3) 1,000 – 1,500	0.1644	0.1675	0.1100	0.2376	0.1391	0.1349	0.1371	0.1630	0.1629
(4) 1,500 – 2,000	0.1152	0.0944	0.0450	0.1776	0.1232	0.0860	0.1059	0.0933	0.1019
(5) 2,000 – 2,500	0.0614	0.0515	0.0433	0.0576	0.1012	0.0792	0.0804	0.0893	0.0637
(6) 2,500 – 3,000	0.0495	0.0257	0.0475	0.0576	0.0844	0.0441	0.0587	0.0456	0.0450
(7) > 3,000	0.0382	0.0257	0.0376	0.0576	0.0672	0.0256	0.0399	0.0206	0.0342
Consistency ratio	0.07	0.04	0.06	-0.02	0.14	0.02	0.12	0.07	
Soil Texture									
(1) Clay	0.0224	0.0155	0.0314	0.0783	0.2734	0.1318	0.0218	0.0174	0.0494
(2) Silty clay	0.0722	0.0155	0.2020	0.0939	0.3119	0.0701	0.0332	0.0311	0.0743
(3) Loamy sand	0.1155	0.1817	0.0372	0.0511	2.8293	0.0585	0.1367	0.0873	0.0921
(4) Sandy loam	0.1341	0.1817	0.0387	0.0567	2.1233	0.0561	0.1103	0.1438	0.0979
(5) Silty clay loam	0.0514	0.0532	0.1683	0.0991	1.7464	0.1038	0.0491	0.0532	0.0878
(6) Sand	0.2871	0.1817	0.0317	0.0318	1.0172	0.0262	0.2161	0.2175	0.1175
(7) Sandy clay loam	0.1125	0.0946	0.1620	0.0991	0.8624	0.0488	0.0888	0.0356	0.0882
(8) Clay loam	0.0400	0.0155	0.0344	0.1512	0.5413	0.1252	0.0483	0.0995	0.0790
(9) Silty loam	0.0779	0.0256	0.0405	0.1512	0.4499	0.0772	0.0562	0.1624	0.0855
(10) Loam	0.0550	0.0532	0.0403	0.1512	0.4898	0.0731	0.0562	0.0831	0.0762
(11) Slope complex area	0.0317	0.1817	0.2135	0.0365	3.3229	0.2292	0.1833	0.0692	0.1522
Consistency ratio	0.11	0.03	0.04	-0.28	0.14	0.08	0.08	-0.29	
LULC									
(1) Dense evergreen forest	0.1106	0.0299	0.3512	0.0661	0.5158	0.0494	0.0912	0.0334	0.1439
(2) Disturbed evergreen forest	0.2052	0.0855	0.1613	0.2303	0.0858	0.0806	0.1280	0.0679	0.0896
(3) Oil palm	0.2339	0.3600	0.0542	0.2910	0.2133	0.4561	0.3548	0.1748	0.3118
(4) Para rubber	0.4002	0.3600	0.1939	0.2773	0.1422	0.2616	0.3548	0.2508	0.2739
(5) Miscellaneous	0.0501	0.1646	0.2394	0.1352	0.0428	0.1523	0.0713	0.4731	0.1808
Consistency ratio	0.11	0.05	0.14	0.19	0.09	0.04	0.08	0.04	

Table 4.5 Factor and class (attribute) weights of all input factors from the AHP method.

Thematic layers	Attributes	Factor weight (FW)	Class weights (CW)	Net contributing weights (FW·CW)
Elevation	< 200 m	0.0550	0.0387	0.0021
	200 m – 400 m		0.0724	0.0040
	400 m – 600 m		0.1165	0.0064
	600 m – 800 m		0.2179	0.0120
	800 m – 1,000 m		0.2298	0.0126
	> 1,000 m		0.3246	0.0179
Slope gradient	0° – 10°	0.1734	0.0378	0.0066
	10° – 20°		0.0733	0.0127
	20° – 30°		0.1459	0.0253
	30° – 40°		0.1997	0.0346
	40° – 50°		0.2144	0.0372
	> 50°		0.3289	0.0570
Slope aspect	Flat	0.0517	0.0298	0.0015
	North		0.0386	0.0020
	Northeast		0.1399	0.0072
	East		0.0804	0.0042
	Southeast		0.0986	0.0051
	South		0.1087	0.0056
	Southwest		0.2746	0.0142
	West		0.1551	0.0080
Slope curvature	Northwest	0.0753	0.1014	0.0052
	Concave (-)		0.2691	0.0203
	Flat (0)		0.1544	0.0116
Topographic wetness index (TWI)	Convex (+)	0.0794	0.4812	0.0362
	0 – 2.5		0.0387	0.0031
	2.5 – 5.0		0.1271	0.0101
	5.0 – 7.5		0.1420	0.0113
	7.5 – 10.0		0.1309	0.0104
	10.0 – 12.5		0.2267	0.0180
Drainage (Distance from drainage)	> 12.5	0.0545	0.3344	0.0266
	< 50 m		0.3408	0.0186
	50 m – 100 m		0.2223	0.0121
	100 m – 150 m		0.1193	0.0065
	150 m – 200 m		0.0932	0.0051
	200 m – 250 m		0.1273	0.0069
Lithology	> 250 m	0.1756	0.0970	0.0053
	Thung Yai		0.1362	0.0239
	Ratburi		0.0602	0.0106
	Quaternary sediments		0.0650	0.0114
	Kaeng Krachan		0.1262	0.0222
	Igneous rocks		0.3088	0.0542
	Krabi		0.1421	0.0250
Saibon Formation	0.1615	0.0284		

Table 4.5 (Continued).

Thematic layers	Attributes	Factor weight (FW)	Class weights (CW)	Net contributing weights (FW·CW)
Lineament (Distance from lineament)	< 500 m	0.1047	0.3455	0.0362
	500 m – 1,000 m		0.2467	0.0258
	1,000 m – 1,500 m		0.1629	0.0171
	1,500 m – 2,000 m		0.1019	0.0107
	2,000 m – 2,500 m		0.0637	0.0067
	2,500 m – 3,000 m		0.0450	0.0047
	> 3,000 m		0.0342	0.0036
Soil Texture	Clay	0.1184	0.0493	0.0058
	Silty clay		0.0743	0.0088
	Loamy sand		0.0721	0.0085
	Sandy loam		0.0979	0.0116
	Silty clay loam		0.0878	0.0104
	Sand		0.1175	0.0139
	Sandy clay loam		0.0882	0.0104
	Clay loam		0.0790	0.0094
	Silty loam		0.0855	0.0101
	Loam		0.0762	0.0090
	Slope complex area		0.1522	0.0180
LULC	Dense evergreen forest	0.1121	0.1439	0.0161
	Disturbed evergreen forest		0.0896	0.0100
	Oil palm		0.3118	0.0350
	Para rubber		0.2739	0.0307
	Miscellaneous		0.1808	0.0203

Table 4.6 Landslide susceptibility classification of land based on the AHP method.

Landslide susceptibility classes	LSS values	NSS values	Area	
			%	km ²
Very low susceptibility (VLS)	0.08 – 0.12	0.00 – 0.20	7.37	72.75
Low susceptibility (LS)	0.12 – 0.15	0.20 – 0.40	48.48	478.73
Moderate susceptibility (MS)	0.15 – 0.18	0.40 – 0.60	35.37	349.29
High susceptibility (HS)	0.18 – 0.22	0.60 – 0.80	8.03	79.30
Very high susceptibility (VHS)	0.22 – 0.26	0.80 – 1.00	0.76	7.46

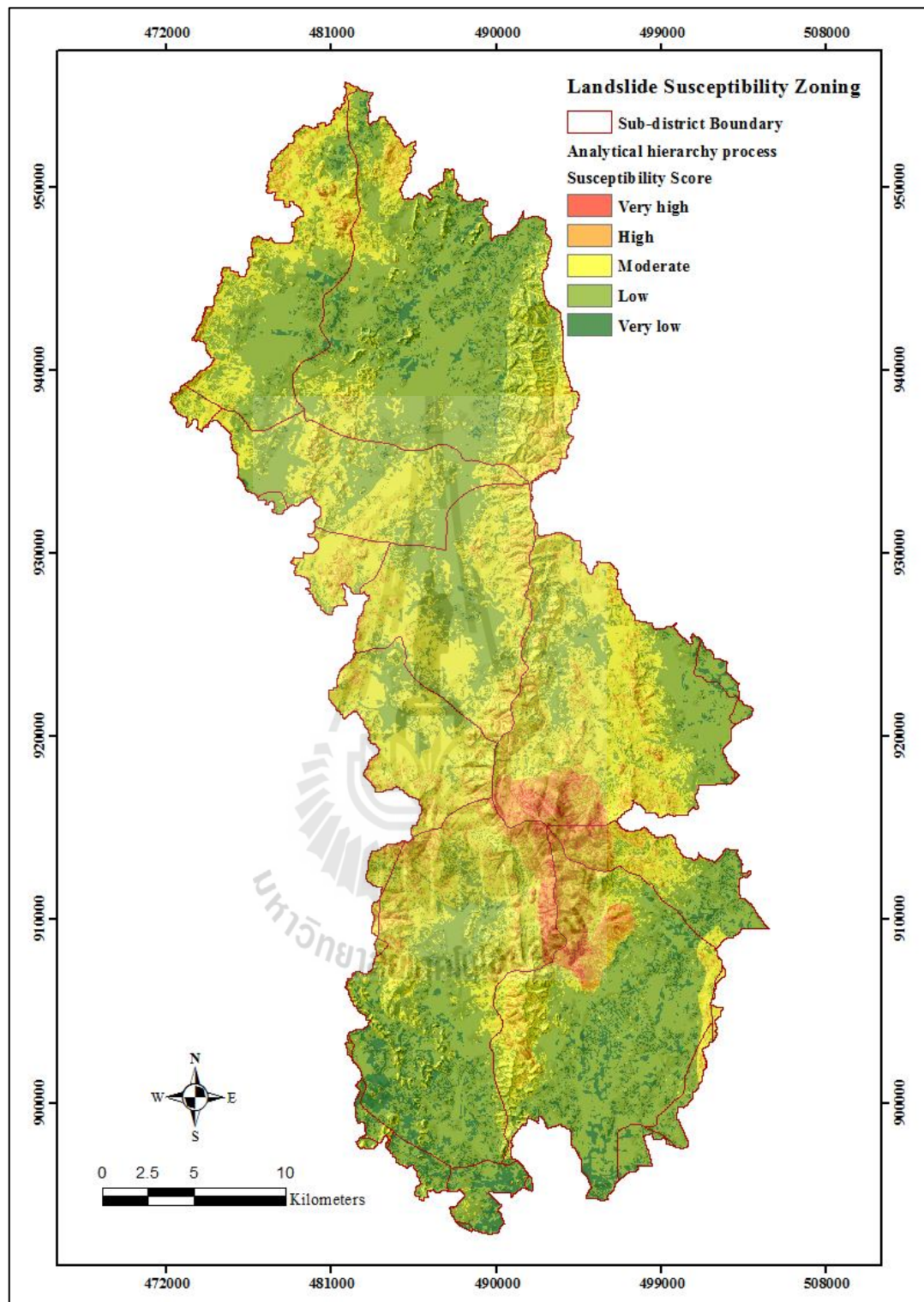


Figure 4.2 Classified landslide susceptibility map yielded from the AHP method.

4.1.3 Application of the frequency ratio (FR) method

As mentioned in Chapter II, the frequency ratio (FR) method has become one of the well-known quantitative approaches for building landslide susceptibility maps worldwide due mainly to its simple concept and straightforward determination of the susceptibility index through most GIS software. In this work, the appropriate FR values for a set of associated attributes of each individual input factor were determined based on Eq. (2.14) and obtained results are displayed in Table 4.7. Initial analysis of these results indicated that order of the priority at attribute level of many factors found in the FR method were rather dissimilar from that encountered in the WLC and AHP methods due significantly to the difference in fundamental concepts of weight assessment (expert judgment-based and evidence-based). For examples, for slope gradient, the two outstanding peak values were evidenced at 20°-40° instead of at steeper slopes previously suggested in the WLC and AHP methods. Or, for the TWI, the two most favorites were remarked at the ranges of 2.5-5.0 (FR = 3.7451) and 5.0-7.5 (FR = 2.0786), while at the higher ranges of TWI, the discovered FR values were appeared to drop dramatically (to be much less than 1.0). And for the LULC, only one feature was found to be notably far superior than the others in this group as main landslide contributor in the area which was dense evergreen forest (FR = 3.9817) while para rubber and palm oil had much lower scores with FR of 0.1337 and 0.0368, respectively. Though this finding might seem to contradict the conventional believe held by most corresponding experts as reported in the WLC and AHP methods, however, this result should not be interpreted literally to diminish potential contribution of these tree plantations on landslide proneness over the area as in this case the planting

places should also be taken into serious consideration (e.g. not on physically vulnerable areas per se like on the highly-sloped or high elevation area).

Apart from the aforementioned results, many accomplished findings did support usual believes about the should-be landslide susceptible locations in the evaluated area (as indicated by the associated FR values), such as ones with the westward slope-facing, convex-type slope curvature, and igneous rock basis, also those situate at high altitude, close to the lineament, and in the classified slope complex area.

Table 4.7 Frequency ratio (FR) and associated membership value (MV) in fuzzy logic.

Factors	Class	Total number of pixels		Landslide occurrence point		Frequency ratio (FR)	Membership value (FR-Fuzzy)
		Number	%	Number	%		
Elevation	< 200 m	917737	83.6393	53	10.8163	0.1293	0.1000
	200 m – 400 m	120959	11.0238	184	37.5510	3.4064	0.2921
	400 m – 600 m	37254	3.3952	140	28.5714	8.4152	0.5857
	600 m – 800 m	13156	1.1990	69	14.0816	11.7446	0.7808
	800 m – 1,000 m	4876	0.4444	30	6.1224	13.7775	0.9000
	> 1,000 m	3274	0.2984	14	2.8571	9.5755	0.6537
Slope gradient	0° – 10°	805224	73.3852	13	2.6531	0.0362	0.1000
	10° – 20°	134847	12.2895	102	20.8163	1.6938	0.3174
	20° – 30°	102194	9.3136	280	57.1429	6.1354	0.9000
	30° – 40°	40200	3.6637	90	18.3673	5.0134	0.7528
	40° – 50°	12052	1.0984	4	0.8163	0.7432	0.1927
	> 50°	2739	0.2496	1	0.2041	0.8176	0.2025
Slope aspect	Flat	400217	36.4744	0	0.0000	0.0000	0.1000
	North	65656	5.9837	63	12.8571	2.1487	0.7894
	Northeast	87428	7.9679	77	15.7143	1.9722	0.7328
	East	102403	9.3326	59	12.0408	1.2902	0.5140
	Southeast	104624	9.5351	17	3.4694	0.3639	0.2167
	South	73159	6.6675	23	4.6939	0.7040	0.3259
	Southwest	87225	7.9494	60	12.2449	1.5404	0.5942
	West	96611	8.8048	102	20.8163	2.3642	0.8586
	Northwest	79933	7.2848	89	18.1633	2.4933	0.9000
Slope curvature	Concave (-)	718416	65.4747	181	36.9388	0.5642	0.3471
	Flat (0)	0	0.0000	0	0.0000	0.0000	0.1000
	Convex (+)	378840	34.5261	309	63.0612	1.8265	0.9000
Topographic wetness index (TWI)	0 – 2.5	7	0.0006	0	0.0000	0.0000	0.1000
	2.5 – 5.0	95668	8.7188	160	32.6531	3.7451	0.9000
	5.0 – 7.5	321031	29.2576	298	60.8163	2.0786	0.5440
	7.5 – 10.0	204803	18.6650	25	5.1020	0.2733	0.1584
	10.0 – 12.5	163220	14.8753	6	1.2245	0.0823	0.1176
	> 12.5	312527	28.4826	1	0.2041	0.0072	0.1015
Drainage (Distance from drainage)	< 50 m	422547	38.5094	176	35.9184	0.9327	0.5422
	50 m – 100 m	343715	31.3250	152	31.0204	0.9903	0.5695
	100 m – 150 m	226373	20.6308	87	17.7551	0.8606	0.5080
	150 m – 200 m	76969	7.0147	58	11.8367	1.6874	0.9000
	200 m – 250 m	24358	2.2199	17	3.4694	1.5629	0.8409
	> 250 m	3294	0.3002	0	0.0000	0.0000	0.1000

Table 4.7 (Continued).

Factors	Class	Total number of pixels		Landslide occurrence point		Frequency ratio (FR)	Membership value (FR-Fuzzy)	
		Number	%	Number	%			
Lithology	Thung Yai	152216	13.8724	80	13.3265	1.1769	0.2470	
	Ratburi	78075	7.1155	9	1.8367	0.2581	0.1322	
	Quaternary sediments Kaeng Krachan	580894	52.9406	0	0.0000	0.0000	0.1000	
	Igneous rocks	187458	17.0843	218	44.4898	2.6041	0.4252	
	Krabi	63974	5.8304	183	37.3469	6.4056	0.9000	
	Saibon Formation	2357	0.2148	0	0.0000	0.0000	0.1000	
			32282	2.9421	0	0.0000	0.0000	0.1000
Lineament (Distance from lineament)	< 500 m	273776	24.9510	242	49.3878	1.9794	0.9000	
	500 m – 1,000 m	206874	18.8538	125	25.5102	1.3531	0.6238	
	1,000 m – 1,500 m	126251	11.5061	38	7.7551	0.6740	0.3243	
	1,500 m – 2,000 m	92556	8.4352	35	7.1429	0.8468	0.4005	
	2,000 m – 2,500 m	75015	6.8366	19	3.8776	0.5672	0.2772	
	2,500 m – 3,000 m > 3,000 m	51878 270906	4.7280 24.6894	11 20	2.2449 4.0816	0.4748 0.1653	0.2365 0.1000	
Soil texture	Clay	230324	20.9909	0	0.0000	0.0000	0.1000	
	Silty clay	71179	6.4870	0	0.0000	0.0000	0.1000	
	Loamy sand	30163	2.7489	0	0.0000	0.0000	0.1000	
	Sandy loam	214890	19.5843	0	0.0000	0.0000	0.1000	
	Silty clay loam	44711	4.0748	0	0.0000	0.0000	0.1000	
	Sand	19916	1.8151	0	0.0000	0.0000	0.1000	
	Sandy clay loam	126165	11.4982	9	1.8367	0.1597	0.1366	
	Clay loam	25846	2.3555	0	0.0000	0.0000	0.1000	
	Silty loam	17556	1.6000	0	0.0000	0.0000	0.1000	
	Loam	8090	0.7373	0	0.0000	0.0000	0.1000	
	Slope complex area	308416	28.1079	481	98.1633	3.4924	0.9000	
	LULC	Dense evergreen forest	261515	23.8335	465	94.8980	3.9817	0.9000
		Disturbed evergreen forest	712	0.0649	0	0.0000	0.0368	0.1074
Oil palm		486744	44.3601	8	1.6327	0.1337	0.1269	
Para rubber		284651	25.9421	17	3.4694	0.0000	0.1000	
Miscellaneous		63634	5.79994	0	0.0000			

Note: Total number of pixels in study area: 1,097,256. Number of landslide occurrence points: 490.

FR = % Landslide occurrence points / % Number of pixels

Table 4.8 Landslide susceptibility classification of land based on the FR method.

Landslide susceptibility classes	LSS values	NSS values	Area	
			%	km ²
Very low susceptibility (VLS)	0.90 – 9.77	0.00 – 0.20	67.31	664.69
Low susceptibility (LS)	9.77 – 18.63	0.20 – 0.40	13.09	129.25
Moderate susceptibility (MS)	18.63 – 27.50	0.40 – 0.60	12.70	125.40
High susceptibility (HS)	27.50 – 36.36	0.60 – 0.80	5.39	53.23
Very high susceptibility (VHS)	36.36 – 45.23	0.80 – 1.00	1.51	14.95

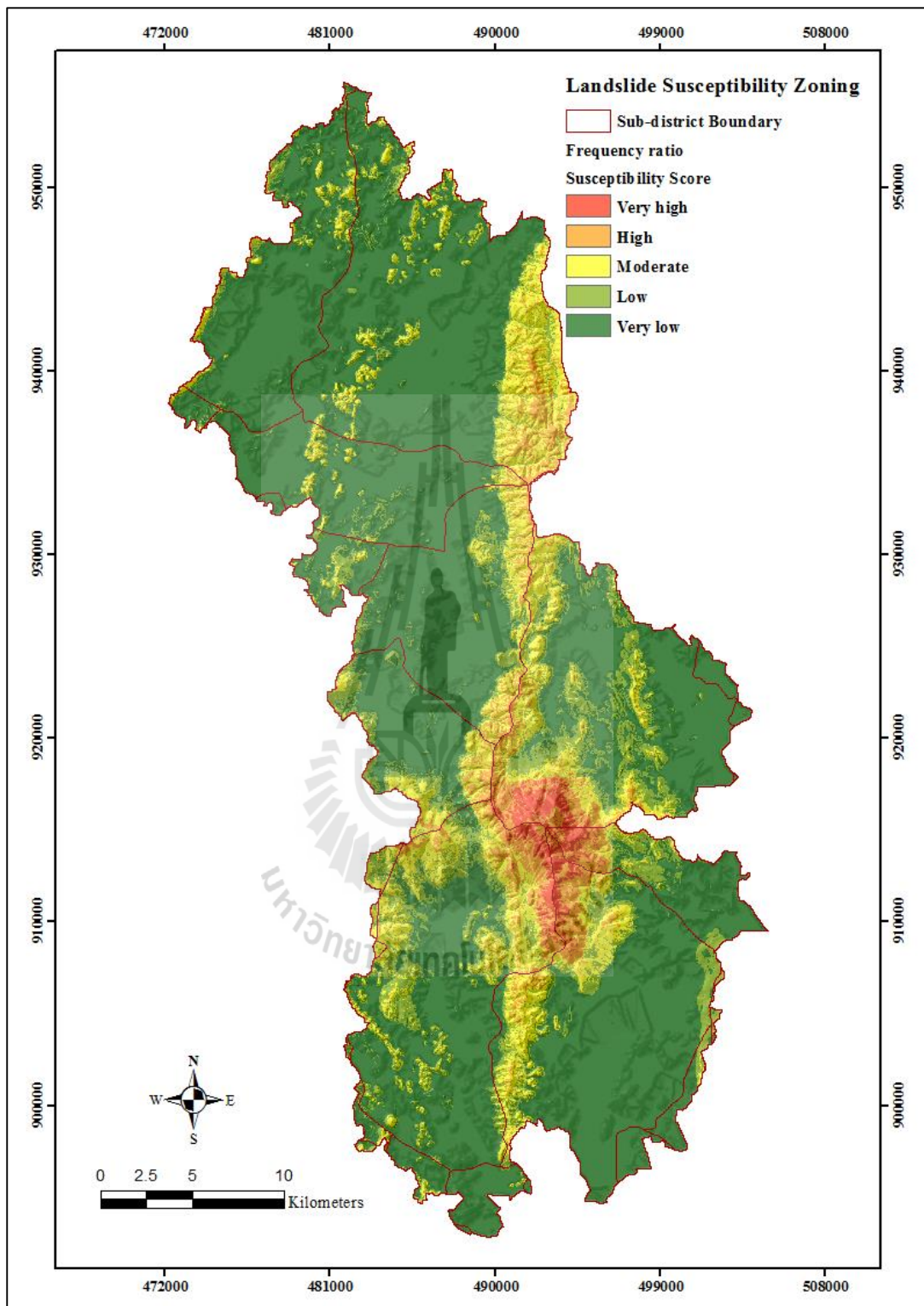


Figure 4.3 Classified landslide susceptibility map yielded from the FR method.

The FR-based landslide susceptibility map is displayed in Figure 4.3 along with its data on covering area of each susceptibility degree in Table 4.8. Though the overall outlook of the derived map seemed resemble to those of the WLC and AHP methods, especially on areas with high and very high probability to having landslide formation (6.90% in total, mostly in mountainous regions). However, in this case, areas belonged to the very low susceptibility category were notably large compared to the other existing classes (67.31%) that led to a stark contrast in the predominant tones of the susceptible classes on the presented map (high/very high against low/very low portions).

4.1.4 Application of the integrated FR and fuzzy logic (FR-Fuzzy method)

As described in Chapter II, fuzzy logic has been applied in some previous works to improve capability of the FR model in the formulation of landslide susceptibility map for an interested area (e.g. Lee, 2007; Regmi et al., 2010; Aksoy and Ercanoglu, 2012). In this study, its benefit in this regard was also examined by integrating its membership value (MV) concept to the FR model as detailed in Chapter III. First, the proper MV data for all affiliated attributes of each input factor were assessed from the original FR values using Eq. (3.2) whereupon the final MV scores shall be in the range of 0.1-0.9 as outlined in Bui et al. (2012) from which gained results are presented in Table 4.7.

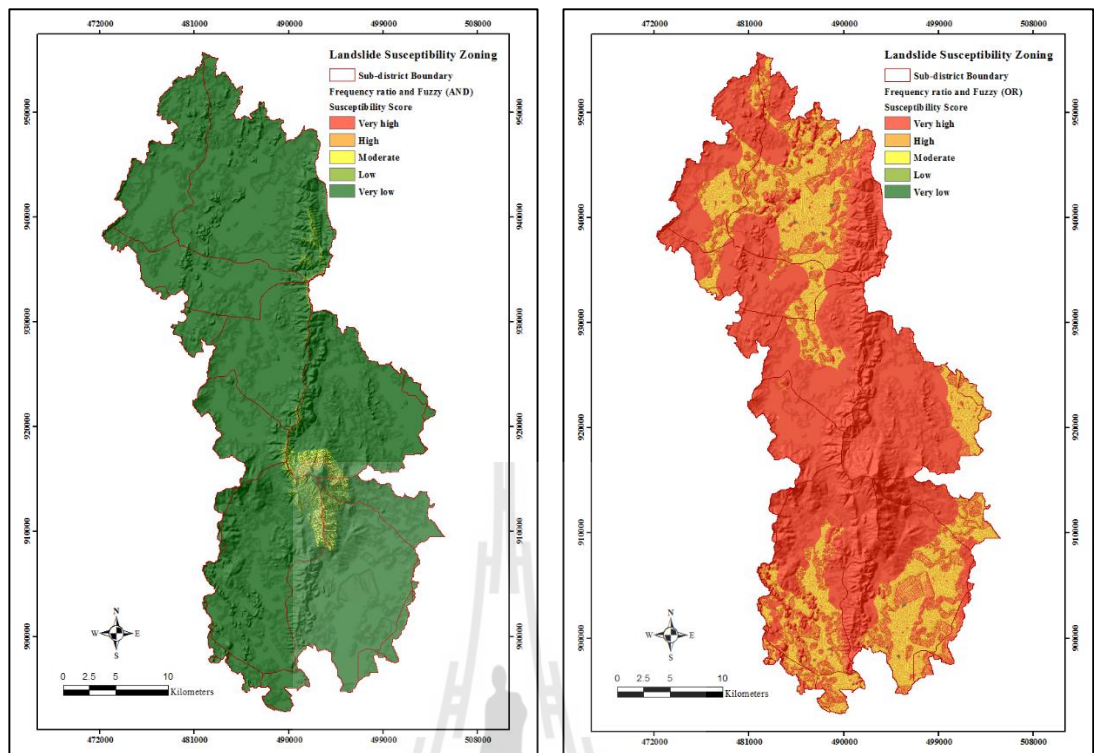
To build a susceptibility map, the candidate MV data from all factors were then integrated to yield a landslide susceptibility score (LSS) for each unit area (pixel basis) on the map through five fuzzy operators: OR, AND, algebraic sum, algebraic product, and fuzzy-gamma for λ values between 0.0-1.0 (see mathematical details in Chapter II).

The yielded susceptibility maps for each examined case of an operator mentioned above are shown in Figure 4.4 along with the achieved accuracy detailed in Table 4.9.

As seen in Table 4.9, the gamma operator ($\lambda = 0.9$) was found most effective in the preparation of landslide susceptibility map for the study area with average accuracy of 92.77%, hence, it was chosen to be a candidate operator for the FR-Fuzzy approach. This finding was similar to what reported earlier in several papers that the most efficient fuzzy operators for this task is gamma operator with notably high λ values (close to 1), e.g. Lee (2007); Regmi et al. (2010); Ercanoglu and Temiz (2011), and Pradhan (2011). The optimal susceptibility map yielded in this case is presented in Figure 4.4(n) along with its relevant details of classified land proportion shown in Table 4.10. Note that, general map outlook in this case quite resembles that of the FR method (in Figure 4.3) as well as reported proportion of area for each classified susceptibility class (Table 4.8).

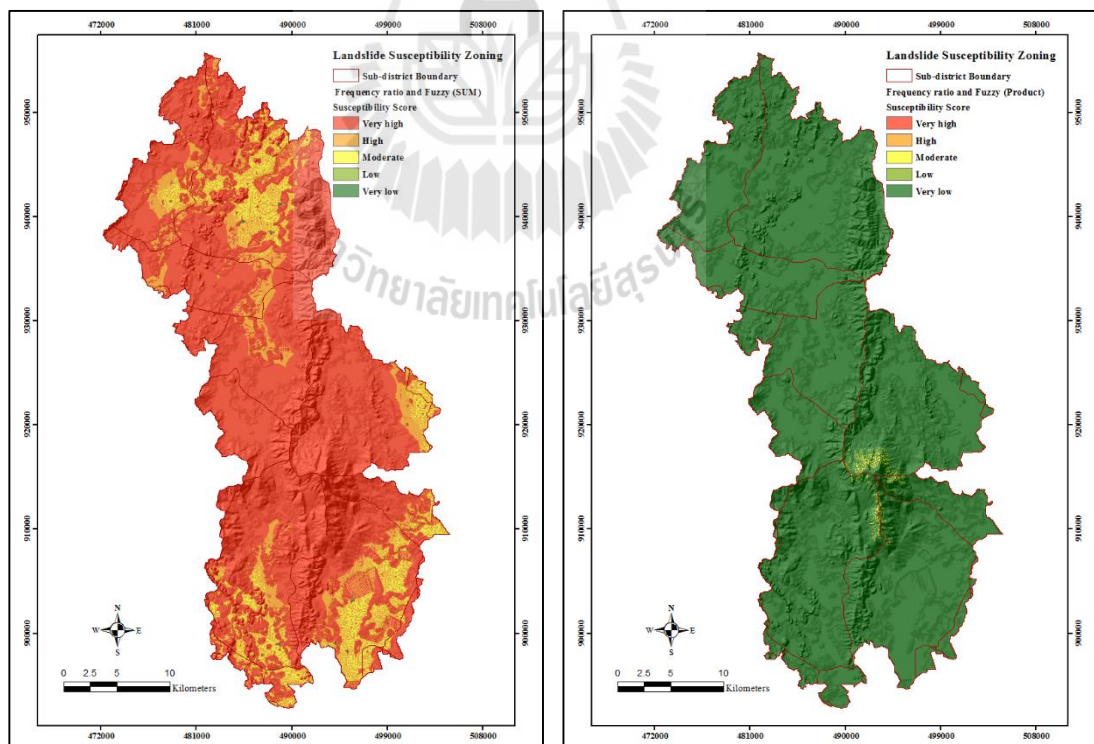
Table 4.9 Achieved map accuracies of the considered fuzzy operators (FR-Fuzzy).

Fuzzy operation	Success accuracy (%)	Prediction accuracy (%)	ROC (%)	Average (%)
AND	53.88	45.40	61.30	53.53
OR	99.50	99.50	66.10	88.37
Algebraic sum	98.35	98.26	62.50	86.37
Algebraic product	88.11	82.79	55.80	75.57
Gamma (λ) = 0.00	89.45	82.66	55.80	75.97
Gamma (λ) = 0.10	90.15	85.05	56.80	77.33
Gamma (λ) = 0.20	91.08	87.28	58.30	78.89
Gamma (λ) = 0.30	92.01	89.79	60.30	80.70
Gamma (λ) = 0.40	92.40	90.07	62.30	81.59
Gamma (λ) = 0.50	91.66	89.07	67.60	82.78
Gamma (λ) = 0.60	91.64	89.07	74.40	85.04
Gamma (λ) = 0.70	91.64	88.08	83.60	87.77
Gamma (λ) = 0.80	92.63	91.07	92.00	91.90
Gamma (λ) = 0.90	92.64	91.08	94.60	92.77
Gamma (λ) = 0.99	92.62	91.07	90.60	91.43
Gamma (λ) = 1.00	95.72	97.27	62.50	85.16



(a) FR-Fuzzy (AND)

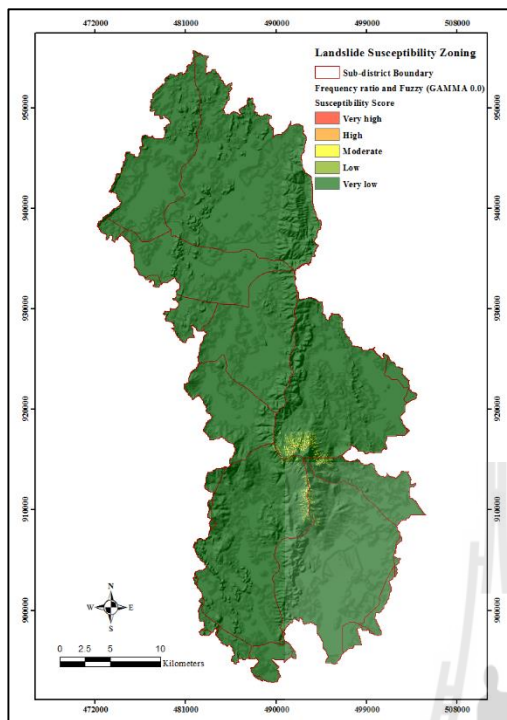
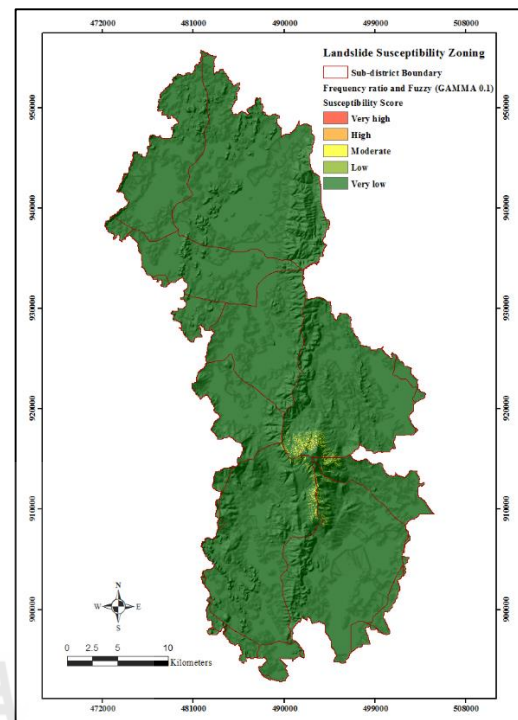
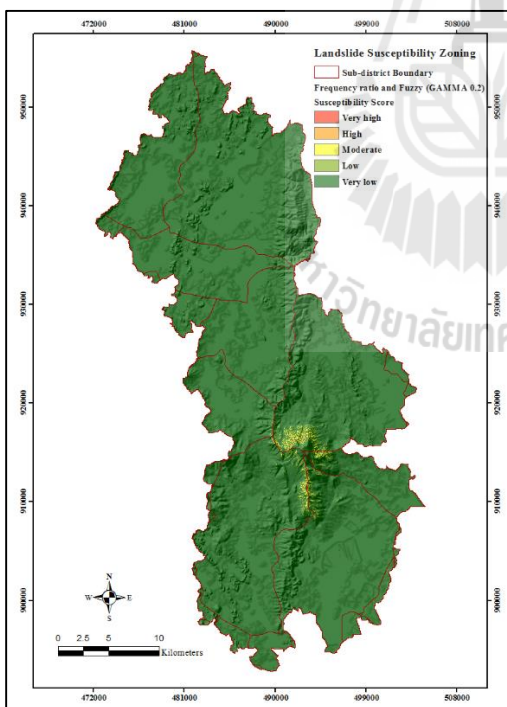
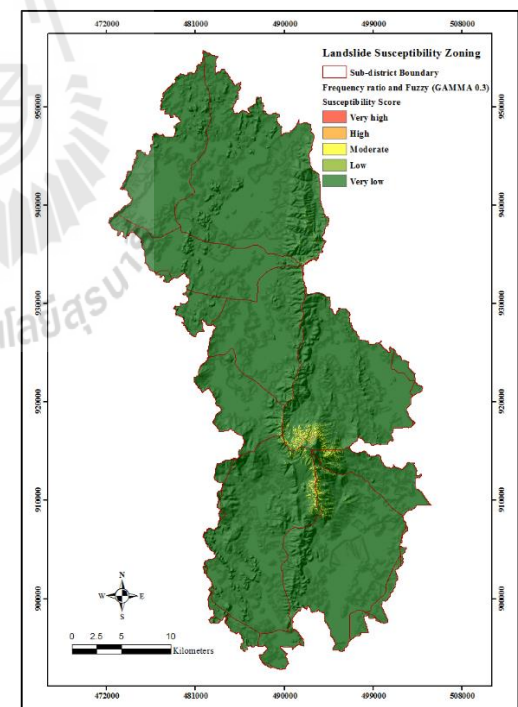
(b) FR-Fuzzy (OR)



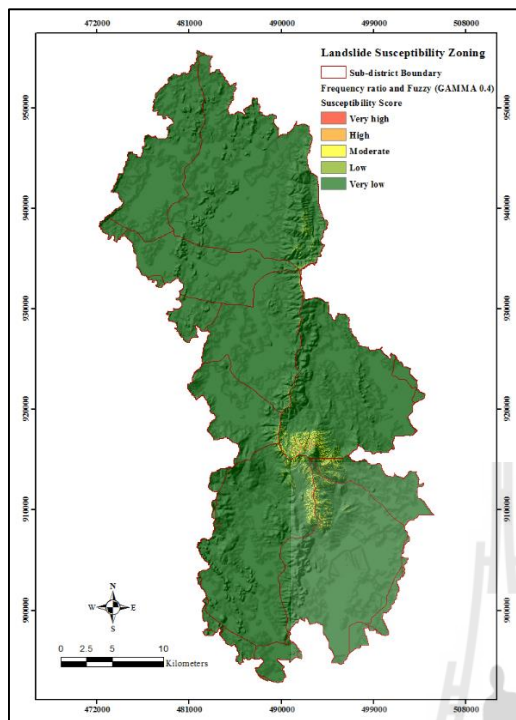
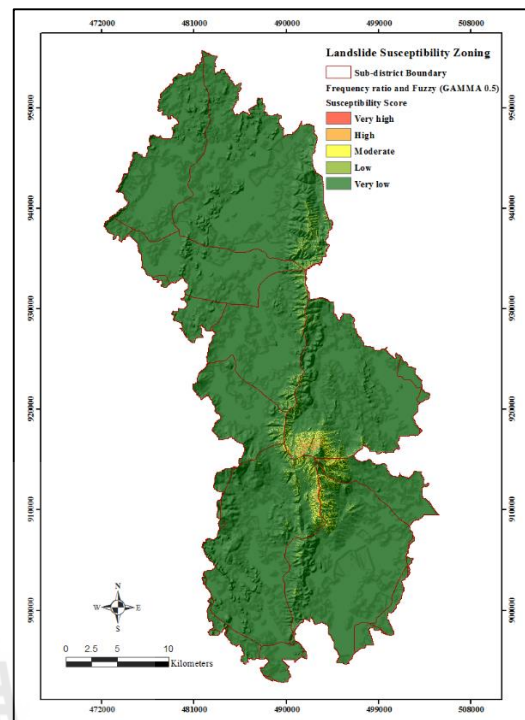
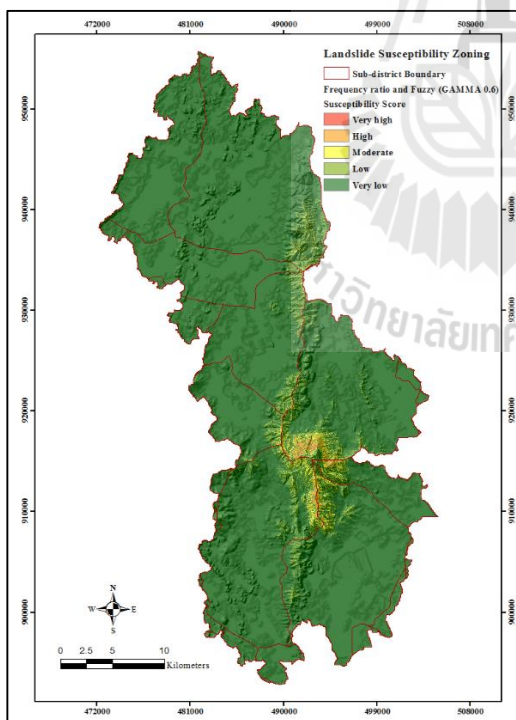
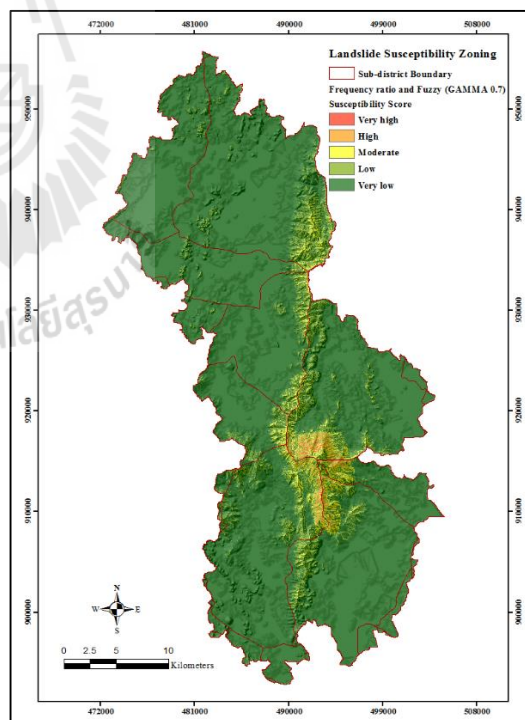
(c) FR-Fuzzy (algebraic sum)

(d) FR-Fuzzy (algebraic product)

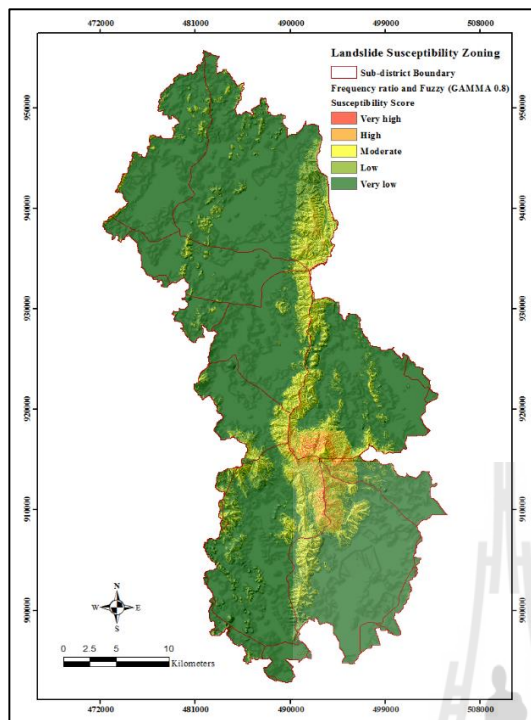
Figure 4.4 Classified landslide susceptibility maps yielded from the FR-Fuzzy method.

(e) FR-Fuzzy ($\lambda = 0.0$)(f) FR-Fuzzy ($\lambda = 0.1$)(g) FR-Fuzzy ($\lambda = 0.2$)(h) FR-Fuzzy ($\lambda = 0.3$)**Figure 4.4** Classified landslide susceptibility maps yielded from the FR-Fuzzy method

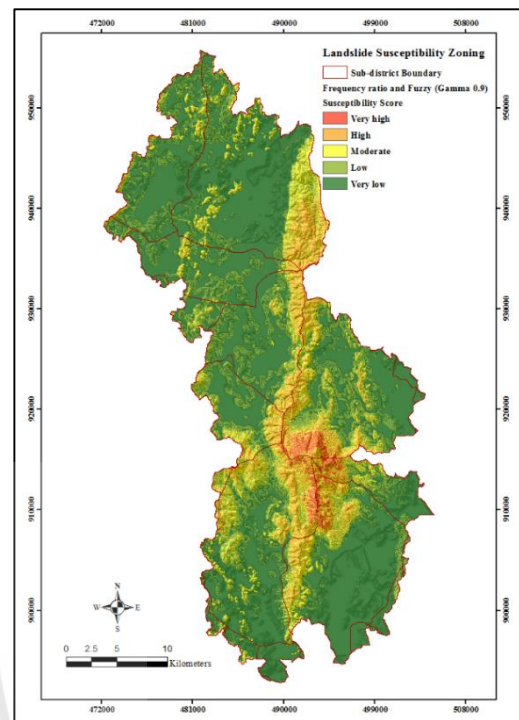
(Continued).

(i) FR-Fuzzy ($\lambda = 0.4$)(j) FR-Fuzzy ($\lambda = 0.5$)(k) FR-Fuzzy ($\lambda = 0.6$)(l) FR-Fuzzy ($\lambda = 0.7$)**Figure 4.4** Classified landslide susceptibility map yielded from the FR-Fuzzy method

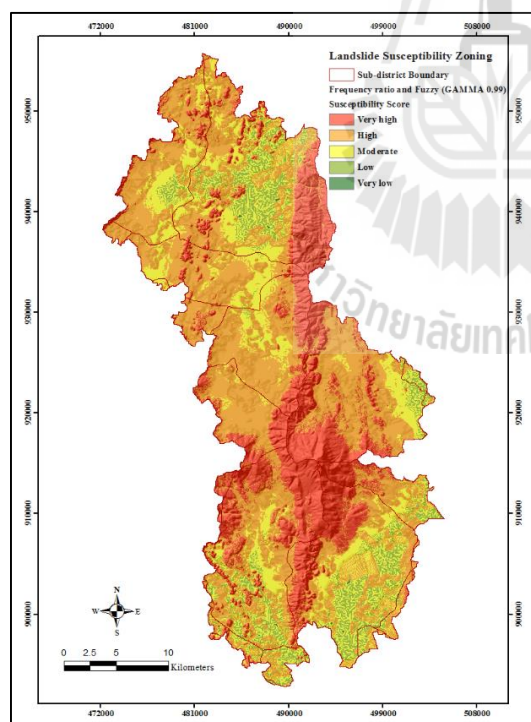
(Continued).



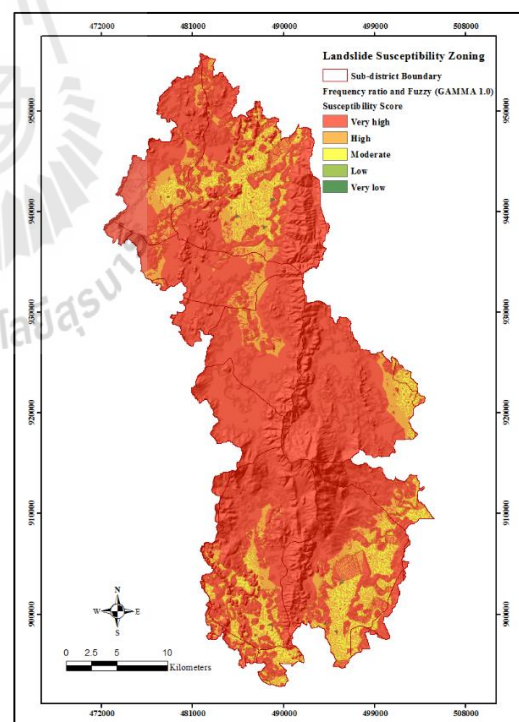
(m) FR-Fuzzy ($\lambda = 0.8$)



(n) FR-Fuzzy ($\lambda = 0.9$)



FR-Fuzzy ($\lambda = 0.99$)



(p) FR-Fuzzy ($\lambda = 1.0$)

Figure 4.4 Classified landslide susceptibility maps yielded from the FR-Fuzzy method
(Continued).

Table 4.10 Landslide susceptibility classification of land (FR-Fuzzy method: $\lambda = 0.90$).

Landslide susceptibility classes	LSS values	NSS values	Area	
			%	km ²
Very low susceptibility (VLS)	0.07 – 0.23	0.00 – 0.20	59.13	583.97
Low susceptibility (LS)	0.23 – 0.40	0.20 – 0.40	20.62	203.65
Moderate susceptibility (MS)	0.40 – 0.56	0.40 – 0.60	12.36	122.02
High susceptibility (HS)	0.56 – 0.73	0.60 – 0.80	6.84	67.52
Very high susceptibility (VHS)	0.73 – 0.90	0.80 – 1.00	1.05	10.38

Table 4.11 Coefficients of each input parameter in the MLR and ANN methods.

Factors	Attributes (class)	MLR coefficients	ANN Normalized weight
Elevation		8.8295	0.1856
Slope gradient		8.2866	0.1407
Slope aspect		0.9868	0.0130
Slope curvature		-18.4705	0.1710
Topographic wetness index		-3.9702	0.0106
Distance from drainage		-2.0935	0.0479
Distance from lineament		3.2612	0.0241
Lithology	Krabi	0.0379	0.0085
	Kaengkrachan	4.9638	0.0409
	Thungyai	5.4886	0.0218
	Igneous rocks	4.9266	0.0171
	Quaternary sediments	-10.5122	0.0232
	Saibon formation	-13.1543	0.0543
	Ratburi	1.7239	0.0351
Soil texture	Clay	-2.4604	0.0221
	Silty clay	-22.3430	0.0210
	Loamy sand	1.2647	0.0097
	Sandy loam	-1.3786	0.0158
	Silty clay loam	-49.7757	0.0116
	Sand	-8.1044	0.0090
	Sandy clay loam	14.7247	0.0111
	Clay loam	-117.5437	0.0083
	Silty loam	12.5615	0.0080
	Loam	-197.1351	0.0080
LULC	Slope complex area	14.8102	0.0299
	Dense evergreen forest	1.3958	0.0016
	Disturbed evergreen forest	0.0000	0.0001
	Oil palm	0.5037	0.0123
	Para rubber	0.7696	0.0074
	Miscellaneous	-17.2292	0.0128

4.1.5 Application of multiple logistic regression (MLR) method

Similar to the FR method, the multiple logistic regression (MLR) method is also highly popular for landslide susceptibility mapping worldwide due mainly on its ability to include both numerical and categorical types of contributing factor into its analysis fairly conveniently. The first task on this issue was to establish the appropriate log-odds or login function L in a linear regression form as detailed in Eq. (2.17) to further quantify the needed pixel-based landslide occurrence probability p for the area through Eq. (2.18).

These referred probability values (of 0-1) were then used as representative of landslide susceptibility score (LSS) for making susceptibility map of the area afterwards.

Regarding to this stated process, the proper relationship of logit function L with the preferred causative factors (30 layers in total as listed in Table 4.11) was given as:

$$\begin{aligned}
 L = & [-10.8212 + (8.8295 \cdot \text{elevation}) + (8.2866 \cdot \text{slope gradient}) + (0.9868 \cdot \text{slope aspect}) \\
 & - (18.4705 \cdot \text{slope curvature}) - (3.9702 \cdot \text{TWI}) - (2.0935 \cdot \text{distance from drainage}) \\
 & + (3.2612 \cdot \text{distance from lineament})] + [(24.8784 \cdot \text{krabi}) + (4.9638 \cdot \text{kaengkrachan}) \\
 & + (5.4886 \cdot \text{thungyai}) + (4.9266 \cdot \text{igneous rocks}) - (10.5122 \cdot \text{quaternary sediments}) \\
 & - (13.1543 \cdot \text{saibon formation}) + (1.7239 \cdot \text{ratburi}) + (12.5615 \cdot \text{silty loam}) \\
 & - (49.7757 \cdot \text{silty clay loam}) - (22.3430 \cdot \text{silty clay}) - (1.3786 \cdot \text{sandy loam}) \\
 & + (14.7247 \cdot \text{sandy clay loam}) - (8.1044 \cdot \text{sand}) + (14.8102 \cdot \text{slope complex area}) \\
 & + (1.2647 \cdot \text{loamy sand}) + (33.3336 \cdot \text{sandy clay}) - (197.1351 \cdot \text{loam}) \\
 & - (117.5437 \cdot \text{clay loam}) - (2.4604 \cdot \text{clay}) + (0.5037 \cdot \text{oil palm}) + (0.7696 \cdot \text{para rubber}) \\
 & - (17.2292 \cdot \text{miscellaneous}) + (1.3958 \cdot \text{dense evergreen forest})]. \tag{4.1}
 \end{aligned}$$

Herein the first bracket contains all numerical-type data (7 layers) and the second one gathers all relevant categorical data (22 layers). In principle, positive coefficients tend to support more landslide activity (higher probability of occurrence) while the negative ones signify the opposite outcome (Ayalew and Yamagishi, 2005).

Table 4.12 Landslide susceptibility classification of land based on the MLR method.

Landslide susceptibility classes	LSS values	NSS values	Area	
			%	km ²
Very low susceptibility (VLS)	0.00 – 0.20	0.00 – 0.20	76.30	753.51
Low susceptibility (LS)	0.20 – 0.40	0.20 – 0.40	3.76	37.12
Moderate susceptibility (MS)	0.40 – 0.60	0.40 – 0.60	3.35	33.07
High susceptibility (HS)	0.60 – 0.80	0.60 – 0.80	4.34	42.84
Very high susceptibility (VHS)	0.80 – 1.00	0.80 – 1.00	12.25	121.00

According to the coefficient data listed in Table 4.11, strong positive influences of several well-known predisposing factors and attributes stated earlier, e.g. elevation, slope gradient, distance from lineament, igneous rock, slope complex property, were still noticeably acknowledged in the derived logit function L (Eq. (4.1)) while the marked negative influencing factors or attributes were slope curvature, TWI, clay or clay-loam types of soil texture, distance from drainage, quaternary sediments or saibon formation of bedrock. Note that, in LULC group, relatively weak positive influence was evidenced for dense evergreen forest, oil palm and para-rubber plantations. Also, several extreme values might be difficult to explain true meaning (e.g. Krabi formation or clay loam).

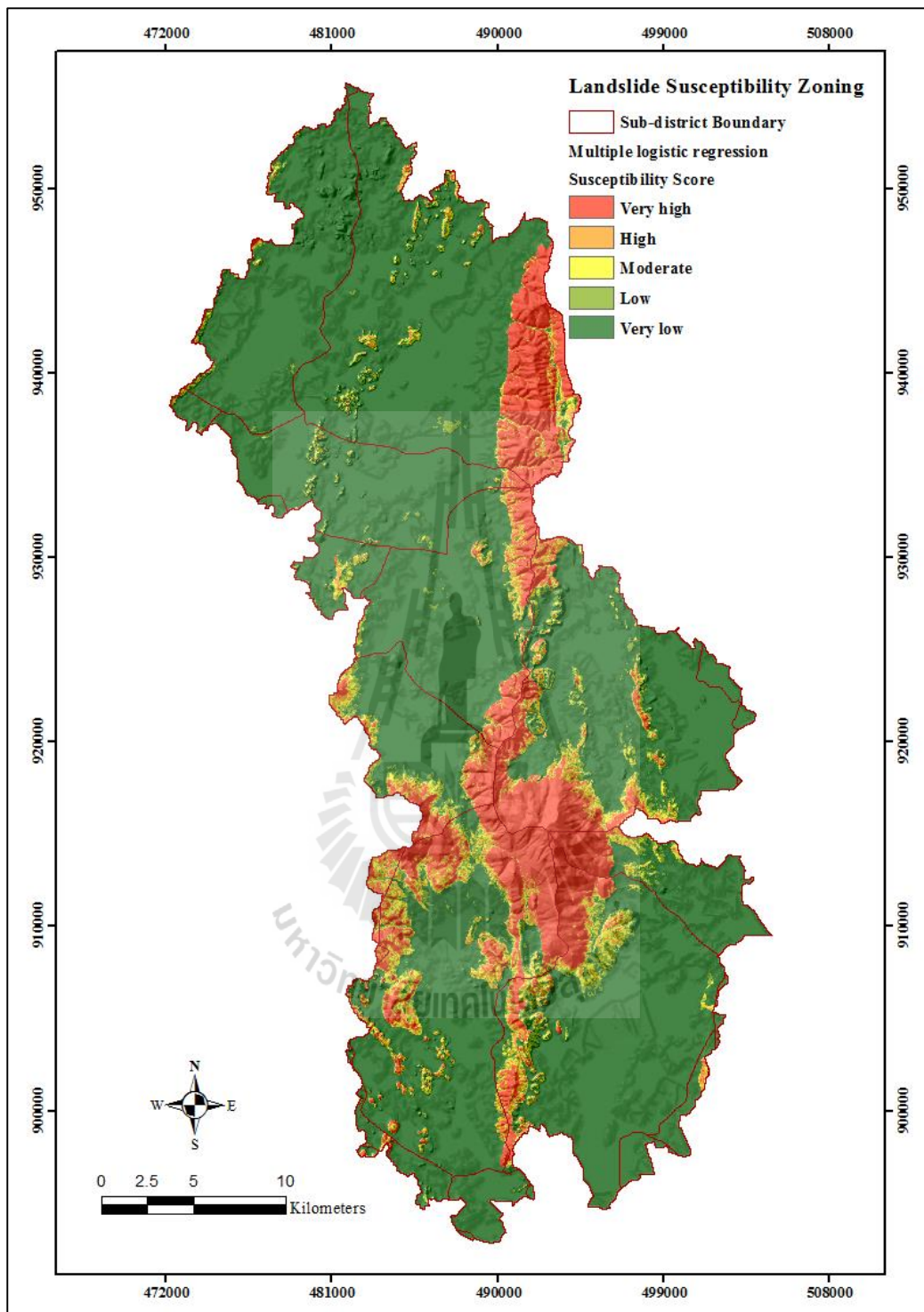


Figure 4.5 Classified landslide susceptibility map yielded from the MLR method.

Figure 4.5 and Table 4.12 shows results of the obtained landslide susceptibility maps from the MLR method described earlier. In general, though conclusive outlook of the established map was somewhat similar to those of the FR and F-Fuzzy methods reported earlier, however, the most distinguish appearance on the MLR-based map was the expansive coverage of land with very high susceptibility status (12.25%) compared with only 1.0-1.5% in cases of FR and FR-Fuzzy methods. This finding implies more work must be utilized to identify the actual should-be concerned areas (e.g. village or important facilities/services) from landslide hazard if this map is to be implemented.

4.1.6 Application of the artificial neural network (ANN) method

The artificial neural network (ANN) method has advantage in its distinct ability to identify existing nonlinear relationship of past landslide data and a set of the chosen causative factors automatically which is still lack in the conventional methods like FR or logistic regression (as addressed in Chapter II). In this work, ANN model was applied to find appropriate weights of the input data (30 layers in total as listed in Table 4.11) and then proceed to build the preferred susceptibility map of the entire study area from knowledge of these output weights based on the linear combination stated in Eq. (3.3). Here, a three-layer system consisting of input layer (30 neurons), one hidden layer (17 neurons) and one output layer was used as a network structure of 30-16-1 in which 980 training samples (490 landslide locations and 490 landslide-free locations) were used as reference dataset in the weight adjustment process.

Tables 4.13 summarizes the input-hidden-output weights at each gradual stage of the experimented working process. These are (1) Input-Hidden connection

weights, (2) Hidden-Output connection weights, and (3) Connection weight products defined as $WP = (1) \times (2)$. Absolute value from the combination of these weight products for each incorporated input layer (called the “absolute weight”: AW) was then applied as a basis to determine corresponding normalized weights (NW) using the following procedure:

$$AW_i = \left| \sum WP_i \right| \quad \text{and} \quad NW_i = \frac{AW_i}{\sum_{i=1}^{30} AW_i} . \quad (4.1)$$

Table 4.13c shows the corresponding NW data for all layers (I1-I30) of input data based on its known absolute weight (AW) along with ranking in terms of weight's priority.

Regarding to the accomplished NW dataset, elevation and slope curvature were considered having top priority with given weights of 0.1856 and 0.1710. For lithology, saibon formation type was most valued with weight of 0.0543 while that of igneous rocks was just 0.0171 which seems rather contrary to conventional believe as reflected in the WLC and AHP method (Tables 4.1 and 4.4) and also to what found in the FR method (Table 4.7). Strong roles of slope gradient and distance from drainage were also found with relatively high weights of 0.1407 and 0.0479, in their respective groups.

To produce the preferred landslide susceptibility map, the pixel-based landslide susceptibility scores (LSS) were determined from this linear function (from Eq. (3.3)):

$$\begin{aligned}
\text{LSS} = & [(0.1856 \cdot \text{elevation}) + (0.1407 \cdot \text{slope gradient}) + \\
& (0.0130 \cdot \text{slope aspect}) + (0.1710 \cdot \text{slope curvature}) + \\
& (0.0280 \cdot \text{TWI}) + (0.0479 \cdot \text{distance from drainage}) + \\
& (0.0241 \cdot \text{distance from lineament})] + [(0.0085 \cdot \text{krabi}) + \\
& (0.0409 \cdot \text{kaengkrachan}) + (0.0218 \cdot \text{thungyai}) + \\
& (0.0171 \cdot \text{igneous rocks}) + (0.0232 \cdot \text{quaternary sediments}) + \\
& (0.0543 \cdot \text{saibon formation}) + (0.0351 \cdot \text{ratburi}) + (0.0080 \cdot \text{silty loam}) + \\
& (0.0116 \cdot \text{silty clay loam}) + (0.0210 \cdot \text{silty clay}) + (0.0158 \cdot \text{sandy loam}) + \\
& (0.0111 \cdot \text{sandy clay loam}) + (0.0090 \cdot \text{sand}) + (0.0299 \cdot \text{slope complex}) + \\
& (0.0097 \cdot \text{loamy sand}) + (0.0080 \cdot \text{loam}) + (0.0083 \cdot \text{clay loam}) + \\
& (0.0221 \cdot \text{clay}) + (0.0123 \cdot \text{oil palm}) + (0.0074 \cdot \text{para rubber}) + \\
& (0.0001 \cdot \text{disturb evergreen forest}), \tag{4.2}
\end{aligned}$$

where the first bracket contains all numerical-type data (7 layers) and the second one gathers all relevant categorical data (23 layers). The obtained LSS data for the whole area were then transformed to be equivalent NSS data for the productions of landslide susceptibility map as depicted in Figure 4.6 whereas amount of classified land for each defined susceptibility class of land is illustrated in Table 4.14.

Table 4.13a Input-hidden-output connection weights (ANN method).

[1] Input (I)-Hidden (H) connection weights																
Factor	H1	H2	H3	H4	H5	H6	H7	H8	H9	H10	H11	H12	H13	H14	H15	H16
I1	0.0323	-1.8739	4.3677	0.0803	0.5449	2.2436	-3.8683	5.8515	5.2228	0.0346	0.0564	-3.8490	9.0584	-5.0653	-1.6500	-0.6350
I2	0.1190	1.5979	-3.7399	0.1146	-1.1949	-3.2912	2.9885	-2.0954	1.6510	5.4760	0.3090	10.9592	-8.9873	2.2625	2.3403	2.9341
I3	0.0329	7.3274	-4.0271	0.0517	2.4779	-0.2931	3.7725	2.9316	-2.2348	4.6067	1.6977	-7.5454	-11.0484	13.7005	3.5283	0.1055
I4	-0.1694	4.5383	-2.6979	0.0178	2.4729	9.1058	-5.7405	-8.5303	5.2137	8.0244	-2.0186	-2.9513	-1.6892	8.2052	-5.0892	-1.5668
I5	0.0134	1.7370	2.2134	0.0369	-1.0067	-0.1153	2.8838	1.4845	-1.2230	-2.7571	-3.1611	-2.0702	1.0825	-0.9476	3.2278	-2.5587
I6	0.4125	-7.1486	0.7399	0.1368	-2.3372	-9.0484	0.6383	4.1667	-10.5820	-5.9454	6.1185	2.0298	-8.8467	-3.8444	0.5291	4.8745
I7	0.0443	-5.5308	-6.4394	0.0346	0.6776	11.8575	-9.5417	-3.0525	8.8666	-3.5933	3.7371	-2.6576	-1.2823	2.2225	-9.9219	0.8453
I8	0.1148	-0.1316	0.1083	0.1910	-0.0304	-0.8248	0.4354	0.2948	-0.8113	-0.4549	0.4182	0.5436	-0.0617	0.1434	0.3745	0.0692
I9	0.1628	-0.3713	0.2809	0.1413	-0.1667	-1.1522	0.6469	0.4020	-1.0336	-0.8081	0.4194	0.9943	-0.4232	-0.2607	0.5465	0.2470
I10	0.0884	0.3050	-0.2246	0.0832	0.2128	1.0948	2.2049	-1.2782	0.3109	1.9796	0.0097	2.3369	1.7409	2.5653	1.7511	-0.1015
I11	0.0823	-0.0538	-0.0167	0.1088	0.0668	-0.6672	0.2980	0.1310	-0.6956	-0.3934	0.3098	0.4052	0.0928	0.2146	0.3131	-0.0772
I12	0.1533	-0.5190	3.6152	0.1142	-0.2678	-2.6315	-2.0981	0.9228	-2.8742	0.4749	-0.2105	-0.4311	-4.1418	-0.6283	-1.4306	1.5082
I13	-0.1003	-0.1097	-0.5300	-0.0415	-0.3037	-1.0621	-2.6410	0.3612	-1.4284	-2.8126	-0.3452	-1.5660	-0.3399	-1.2546	-1.2106	-0.3453
I14	0.1426	-0.6482	1.5157	0.1659	-0.4066	-1.6578	2.3278	2.1137	-1.8093	-1.2049	0.7923	1.4235	-0.9923	-1.5223	1.1790	0.6079
I15	0.0195	-0.0011	-0.0373	0.0464	0.0397	0.0168	-0.0411	0.0318	0.0088	-0.0405	0.0298	0.0469	0.0205	0.0342	0.0480	0.0062
I16	0.1066	-0.3136	0.3622	0.0918	-0.1591	-1.0821	0.8319	0.5212	-1.1265	-0.6529	0.4744	0.8944	-0.3397	-0.3050	0.7395	0.1776
I17	0.0539	0.3489	-0.7737	0.1217	0.2263	0.5542	0.6096	-0.8654	1.4175	0.2499	0.1038	1.1255	2.7543	1.3560	0.7517	-0.1527
I18	0.1304	0.2054	0.0682	0.1166	0.4560	2.9948	0.2886	2.6479	3.4164	0.5870	0.3377	-2.9791	3.7748	-1.7582	0.8769	-1.1594

Table 4.13a (Continued).

[1] Input (I)- Hidden (H) connection weights (continued)																
Factor	H1	H2	H3	H4	H5	H6	H7	H8	H9	H10	H11	H12	H13	H14	H15	H16
I19	-0.1748	0.5784	-4.6710	0.0106	0.4893	-0.8946	-0.8143	-4.6197	-1.7236	-0.9263	-0.0197	1.5609	-0.3715	3.8750	-1.1340	-1.2084
I20	0.0548	-0.0941	0.0440	0.1642	0.0479	-0.7425	0.2773	0.2099	-0.6172	-0.3182	0.2989	0.3574	0.0804	0.2010	0.2248	0.0121
I21	0.1422	-0.0637	-0.0161	0.1755	0.0554	-0.7017	0.2774	0.1403	-0.6369	-0.3633	0.3101	0.3591	0.0886	0.1992	0.2565	-0.0512
I22	0.0821	-0.1917	0.7346	0.1581	0.2300	-0.5519	0.5921	1.0464	0.5556	0.6299	0.5796	-0.6496	-1.0964	-0.8642	-0.4583	0.3952
I23	0.1382	-0.0740	0.0613	0.1253	0.0396	-0.7642	0.3414	0.1764	-0.7096	-0.4123	0.3150	0.3934	0.0873	0.1659	0.3511	-0.0207
I24	-0.1136	-0.2895	-1.1802	-0.0670	-0.4444	-0.9031	-0.5416	-1.5058	0.7973	-0.2141	-0.3208	-2.4192	0.7965	1.6299	-1.7170	-0.5085
I25	0.0764	-0.0692	-0.0024	0.2023	0.0238	-0.6937	0.3607	0.1624	-0.6912	-0.4042	0.3260	0.3750	0.1117	0.1807	0.3380	-0.0326
I26	0.0279	0.8521	0.2918	0.1382	1.1023	2.0916	-0.7379	0.5920	0.2839	1.2287	-0.0109	0.8508	0.6178	-0.1958	0.4057	-0.1570
I27	0.0954	-0.1650	0.1665	0.1129	-0.0635	-0.9422	0.5503	0.3852	-0.8914	-0.5078	0.4231	0.6264	-0.1512	0.0463	0.4884	0.0668
I28	0.1049	-0.1956	0.3122	0.1071	-0.0651	-1.1132	0.7571	0.5200	-0.9938	-0.5425	0.4901	0.8294	-0.2311	-0.1874	0.7159	0.1610
I29	0.1371	-0.1402	0.1248	0.1038	-0.0172	-0.8164	0.4297	0.2021	-0.7188	-0.3985	0.3143	0.5205	0.0481	0.1139	0.3982	-0.0162
I30	0.1342	-0.0948	0.0466	0.1766	0.0892	-0.7070	0.2801	0.1331	-0.6185	-0.3423	0.3478	0.3781	0.1086	0.2447	0.2216	-0.0515
[2] Hidden-Output connection weights																
	H1	H2	H3	H4	H5	H6	H7	H8	H9	H10	H11	H12	H13	H14	H15	H16
output	-0.3349	4.3524	-6.6676	-0.1745	1.6852	5.7799	-6.0184	-7.2152	3.0076	4.6310	-3.2303	-4.9782	6.0578	3.4103	-6.1401	-0.9885

Table 4.13b Connection weight products (WP) for each input layer and their associated absolute weight (AW) (ANN method).

Factor	[3] Connection weight products (WP): [1]x[2]																AW = $ \sum WP $
	H1	H2	H3	H4	H5	H6	H7	H8	H9	H10	H11	H12	H13	H14	H15	H16	
I1	-0.0108	-8.1562	-29.1221	-0.0140	0.9183	12.9677	23.2809	-42.2196	15.7082	0.1603	-0.1821	19.1611	54.8745	-17.2739	10.1309	0.6277	40.8507
I2	-0.0399	6.9547	24.9359	-0.0200	-2.0136	-19.0227	-17.9858	15.1190	4.9656	25.3598	-0.9982	-54.5568	-54.4437	7.7156	-14.3696	-2.9003	81.2998
I3	-0.0110	31.8919	26.8507	-0.0090	4.1757	-1.6939	-22.7047	-21.1519	-6.7215	21.3336	-5.4842	37.5620	-66.9297	46.7221	-21.6638	-0.1043	22.0623
I4	0.0567	19.7525	17.9882	-0.0031	4.1672	52.6303	34.5488	61.5481	15.6808	37.1612	6.5205	14.6921	-10.2327	27.9819	31.2479	1.5487	315.2892
I5	-0.0045	7.5601	-14.7580	-0.0064	-1.6965	-0.6662	-17.3558	-10.7108	-3.6783	-12.7685	10.2111	10.3060	6.5574	-3.2314	-19.8192	2.5292	47.5319
I6	-0.1382	-31.1137	-4.9334	-0.0239	-3.9385	-52.2987	-3.8418	-30.0634	-31.8268	-27.5332	-19.7644	-10.1047	-53.5919	-13.1104	-3.2489	-4.8183	290.3501
I7	-0.0148	-24.0722	42.9351	-0.0060	1.1419	68.5350	57.4261	22.0244	26.6673	-16.6408	-12.0719	13.2300	-7.7680	7.5793	60.9214	-0.8355	239.0511
I8	-0.0384	-0.5729	-0.7224	-0.0333	-0.0513	-4.7673	-2.6201	-2.1272	-2.4399	-2.1065	-1.3508	-2.7061	-0.3736	0.4891	-2.2993	-0.0684	21.7885
I9	-0.0545	-1.6159	-1.8729	-0.0247	-0.2808	-6.6593	-3.8935	-2.9003	-3.1087	-3.7423	-1.3548	-4.9500	-2.5640	-0.8890	-3.3553	-0.2442	37.5100
I10	-0.0296	1.3276	1.4974	-0.0145	0.3586	6.3278	-13.2701	9.2223	0.9351	9.1677	-0.0312	-11.6333	10.5462	8.7483	-10.7522	0.1003	12.5004
I11	-0.0275	-0.2342	0.1116	-0.0190	0.1125	-3.8566	-1.7936	-0.9449	-2.0922	-1.8218	-1.0008	-2.0171	0.5620	0.7319	-1.9224	0.0763	14.1357
I12	-0.0513	-2.2590	-24.1048	-0.0199	-0.4513	-15.2097	12.6271	-6.6581	-8.6445	2.1995	0.6799	2.1463	-25.0905	-2.1426	8.7838	-1.4908	59.6860
I13	0.0336	-0.4774	3.5338	0.0072	-0.5117	-6.1390	15.8947	-2.6059	-4.2960	-13.0255	1.1152	7.7960	-2.0589	-4.2786	7.4333	0.3413	2.7623
I14	-0.0478	-2.8214	-10.1057	-0.0290	-0.6852	-9.5816	-14.0095	-15.2505	-5.4417	-5.5799	-2.5594	-7.0865	-6.0111	-5.1913	-7.2392	-0.6009	92.2408
I15	-0.0065	-0.0047	0.2489	-0.0081	0.0669	0.0970	0.2477	-0.2296	0.0264	-0.1878	-0.0964	-0.2333	0.1244	0.1165	-0.2947	-0.0062	0.1394
I16	-0.0357	-1.3649	-2.4148	-0.0160	-0.2680	-6.2544	-5.0069	-3.7609	-3.3882	-3.0237	-1.5323	-4.4525	-2.0578	-1.0400	-4.5405	-0.1755	39.3322
I17	-0.0180	1.5187	5.1589	-0.0212	0.3814	3.2033	-3.6687	6.2437	4.2632	1.1573	-0.3354	-5.6030	16.6851	4.6244	-4.6158	0.1509	29.1246
I18	-0.0437	0.8941	-0.4545	-0.0204	0.7684	17.3094	-1.7368	-19.1051	10.2753	2.7185	-1.0908	14.8302	22.8669	-5.9960	-5.3844	1.1460	36.9773

Table 4.13b (Continued).

Factor	[3] Connection weight products (WP): [1]x[2]																AW = $ \sum WP $
	H1	H2	H3	H4	H5	H6	H7	H8	H9	H10	H11	H12	H13	H14	H15	H16	
I19	0.0586	2.5175	31.1443	-0.0018	0.8246	-5.1705	4.9010	33.3317	-5.1840	-4.2896	0.0635	-7.7703	-2.2504	13.2147	6.9626	1.1944	69.5464
I20	-0.0184	-0.4097	-0.2932	-0.0287	0.0807	-4.2914	-1.6689	-1.5147	-1.8565	-1.4735	-0.9655	-1.7793	0.4871	0.6853	-1.3806	-0.0120	14.4392
I21	-0.0476	-0.2772	0.1073	-0.0306	0.0933	-4.0557	-1.6693	-1.0126	-1.9156	-1.6825	-1.0016	-1.7878	0.5364	0.6792	-1.5747	0.0506	13.5884
I22	-0.0275	-0.8345	-4.8982	-0.0276	0.3877	-3.1900	-3.5634	-7.5497	1.6709	2.9173	-1.8723	3.2336	-6.6415	-2.9472	2.8140	-0.3906	20.9189
I23	-0.0463	-0.3222	-0.4085	-0.0219	0.0667	-4.4171	-2.0546	-1.2730	-2.1343	-1.9093	-1.0175	-1.9583	0.5290	0.5656	-2.1559	0.0205	16.5371
I24	0.0380	-1.2599	7.8689	0.0117	-0.7490	-5.2198	3.2597	10.8648	2.3981	-0.9916	1.0361	12.0433	4.8251	5.5582	10.5424	0.5027	50.7287
I25	-0.0256	-0.3011	0.0163	-0.0353	0.0401	-4.0097	-2.1707	-1.1718	-2.0788	-1.8720	-1.0531	-1.8669	0.6766	0.6161	-2.0753	0.0322	15.2791
I26	-0.0094	3.7088	-1.9458	-0.0241	1.8575	12.0894	4.4412	-4.2715	0.8538	5.6901	0.0352	-4.2355	3.7425	-0.6676	-2.4909	0.1552	18.9289
I27	-0.0319	-0.7180	-1.1102	-0.0197	-0.1069	-5.4456	-3.3122	-2.7796	-2.6809	-2.3518	-1.3667	-3.1181	-0.9160	0.1580	-2.9987	-0.0660	26.8645
I28	-0.0351	-0.8511	-2.0816	-0.0187	-0.1096	-6.4344	-4.5566	-3.7519	-2.9889	-2.5124	-1.5830	-4.1287	-1.3998	-0.6390	-4.3956	-0.1591	35.6456
I29	-0.0459	-0.6101	-0.8324	-0.0181	-0.0289	-4.7184	-2.5863	-1.4581	-2.1620	-1.8456	-1.0152	-2.5912	0.2911	0.3885	-2.4450	0.0160	19.6614
I30	-0.0449	-0.4127	-0.3105	-0.0308	0.1503	-4.0866	-1.6857	-0.9605	-1.8603	-1.5850	-1.1236	-1.8821	0.6578	0.8344	-1.3605	0.0509	13.6500

Table 4.13c Normalized weight (NW) data for each input attribute layer based on the known absolute weight (AW) (ANN method).

Factor	AW	NW	Rank	Factor	AW	NW	Rank	Factor	AW	NW	Rank
I1	40.8507	0.0241	10	I11	14.1357	0.0083	25	I21	13.5884	0.0080	26
I2	81.2998	0.0479	5	I12	59.6860	0.0351	7	I22	20.9189	0.0123	19
I3	22.0623	0.0130	17	I13	2.7623	0.0016	28	I23	16.5371	0.0097	22
I4	315.2892	0.1856	1	I14	92.2408	0.0543	4	I24	50.7287	0.0299	8
I5	47.5319	0.0280	9	I15	0.1394	0.0001	29	I25	15.2791	0.0090	23
I6	290.3501	0.1710	2	I16	39.3322	0.0232	11	I26	18.9289	0.0111	21
I7	239.0511	0.1407	3	I17	29.1246	0.0171	15	I27	26.8645	0.0158	16
I8	21.7885	0.0128	18	I18	36.9773	0.0218	13	I28	35.6456	0.0210	14
I9	37.5100	0.0221	12	I19	69.5464	0.0409	6	I29	19.6614	0.0116	20
I10	12.5004	0.0074	27	I20	14.4392	0.0085	24	I30	13.6500	0.0080	26

Note:

I1	≡	Distance from lineament	I11	≡	Clay loam	I21	≡	Loam
I2	≡	Distance from drainage	I12	≡	Ratburi	I22	≡	Oil palm
I3	≡	Slope aspect	I13	≡	Dense evergreen forest	I23	≡	Loamy sand
I4	≡	Elevation	I14	≡	Saibon formation	I24	≡	Slope complex area
I5	≡	Topographic wetness index	I15	≡	Disturb evergreen forest	I25	≡	Sand
I6	≡	Slope curvature	I16	≡	Quaternary sediments	I26	≡	Sandy clay loam
I7	≡	Slope gradient	I17	≡	Igneous rock	I27	≡	Sandy loam
I8	≡	Miscellaneous	I18	≡	Thungyai	I28	≡	Silty clay
I9	≡	Clay	I19	≡	Kaengkragan	I29	≡	Silty clay loam
I10	≡	Para rubber	I20	≡	Krabi	I30	≡	Silty loam

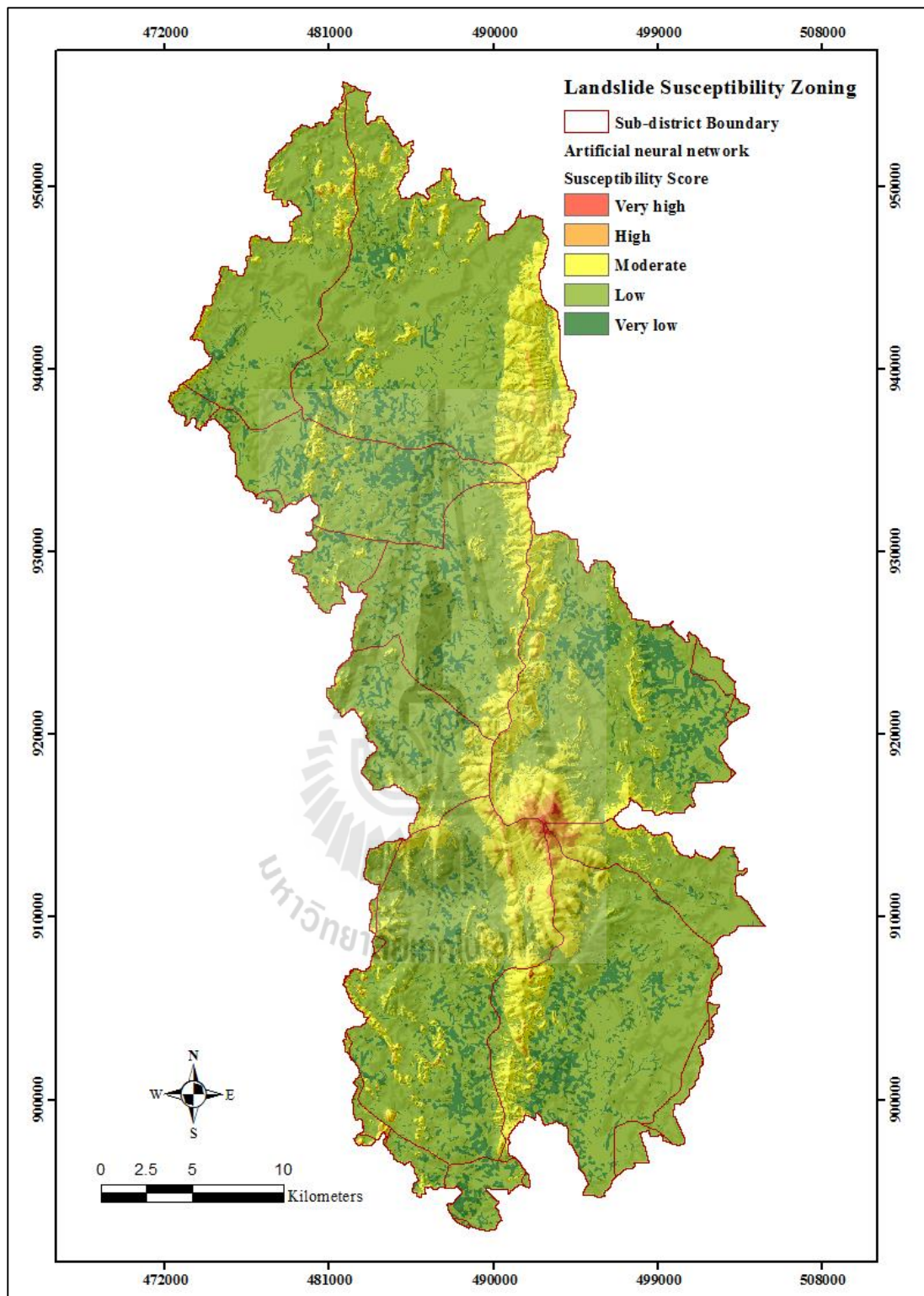


Figure 4.6 Classified landslide susceptibility map yielded from the ANN method.

Table 4.14 Landslide susceptibility classification of land based on the ANN method.

Landslide susceptibility classes	LSS values	NSS values	Area	
			%	km ²
Very low susceptibility (VLS)	0.11 – 0.19	0.00 – 0.20	12.60	124.46
Low susceptibility (LS)	0.19 – 0.26	0.20 – 0.40	69.71	688.42
Moderate susceptibility (MS)	0.26 – 0.33	0.40 – 0.60	16.29	160.86
High susceptibility (HS)	0.33 – 0.41	0.60 – 0.80	1.32	13.03
Very high susceptibility (VHS)	0.41 – 0.49	0.80 – 1.00	0.08	0.77

The highly distinguish appearances on this developed map were the predominant of lands in low susceptibility category (69.71%) and the noticeably small proportion of area with very high susceptibility condition (0.08%) as well as the very low one (1.32%). Therefore, unlike the seen MLR-based map (Figure 4.5) which promoted dominance of the very low and very high susceptibility portions of the examined area, the ANN method seemed to be biased towards output map without notably high or low landslide susceptibility scores.

4.1.7 Application of the integrated ANN and fuzzy logic (ANN-Fuzzy model)

Integration of fuzzy logic and ANN model to formulate landslide susceptibility map for an interested area was also reported in some previous works with encouraging results on the improvement in accuracy of map derived through the ANN model alone, e.g. in Kanungo et al. (2006) and Gupta, Kanungo, Arora, and Sarkar (2008). To assess capability of the fuzzy logic on this stated matter, integration of the achieved FR-Fuzzy MV scores (in Table 4.7) and the ANN-based normalized weights (in Table 4.11) was implemented to establish a new set of MV data for the ANN-Fuzzy method as detailed in Table 4.15. These data were then supplied as input to several types of fuzzy operators as listed in Table 4.16 through which the landslide

susceptibility maps could be derived as end product (like that of the FR-Fuzzy method carried out earlier in Section 4.1.4).

All these maps are displayed in Figure 4.7 whereas their average accuracies are reported in Table 4.16 from which the Gamma operator (with $\lambda = 0.90$) was considered the most effective candidate due to its highest average accuracy of 90.03%. Therefore, susceptibility map of this case as seen in Figure 4.7n was used as representative product from the ANN-Fuzzy method whereas proportion data of the occupied land by each susceptibility class on this map are provided in Table 4.17.

Table 4.15 Membership values at attribute level in the ANN-Fuzzy method.

Thematic layers	Weight (ANN)	Membership value (FR-Fuzzy)	Membership value (ANN-Fuzzy)
Elevation	0.1856		
(1) < 200 m		0.1000	0.0186
(2) 200 m – 400 m		0.2921	0.0542
(3) 400 m – 600 m		0.5857	0.1087
(4) 600 m – 800 m		0.7808	0.1449
(5) 800 m – 1,000 m		0.9000	0.1670
(6) > 1,000 m		0.6537	0.1213
Slope gradient	0.1407		
(1) 0° – 10°		0.1000	0.0141
(2) 10° – 20°		0.3174	0.0447
(3) 20° – 30°		0.9000	0.1266
(4) 30° – 40°		0.7528	0.1059
(5) 40° – 50°		0.1927	0.0271
(6) > 50°		0.2025	0.0285
Slope curvature	0.0728		
(1) Concave (-)		0.3471	0.0253
(2) Flat (0)		0.1000	0.0073
(3) Convex (+)		0.9000	0.0655
Slope aspect	0.0264		
(1) Flat		0.1000	0.0026
(2) North		0.7894	0.0208
(3) Northeast		0.7328	0.0193
(4) East		0.5140	0.0136
(5) Southeast		0.2167	0.0057
(6) South		0.3259	0.0086
(7) Southwest		0.5942	0.0157
(8) West		0.8586	0.0227
(9) Northwest		0.9000	0.0238

Table 4.15 (Continued).

Thematic layers	Weight (ANN)	Membership value (FR-Fuzzy)	Membership value (ANN-Fuzzy)
TWI	0.0106		
(1) < 2.5		0.1000	0.0011
(2) 2.5 – 5.0		0.9000	0.0095
(3) 5.0 – 7.5		0.5440	0.0058
(4) 7.5 – 10.0		0.1584	0.0017
(5) 10.0 – 12.5		0.1176	0.0012
(6) > 12.5		0.1015	0.0011
Distance from drainage			
(1) < 50 m	0.0646	0.5422	0.0350
(2) 50 m – 100 m		0.5695	0.0368
(3) 100 m – 150 m		0.5080	0.0328
(4) 150 m – 200 m		0.9000	0.0581
(5) 200 m – 250 m		0.8409	0.0543
(6) > 250 m		0.1000	0.0065
Lithology			
(1) Krabi	0.0085	0.1000	0.0009
(2) Kaeng Krachan	0.0409	0.4252	0.0174
(3) Thung Yai	0.0218	0.2470	0.0054
(4) Igneous rocks	0.0171	0.9000	0.0154
(5) Quaternary sediments	0.0232	0.1000	0.0023
(6) Saibon Formation	0.0543	0.1000	0.0054
(7) Ratburi	0.0351	0.1322	0.0046
Distance from lineament	0.0241		
(1) < 500 m		0.9000	0.1364
(2) 500 m – 1,000 m		0.6238	0.0945
(3) 1,000 m – 1,500 m		0.3243	0.0491
(4) 1,500 m – 2,000 m		0.4005	0.0607
(5) 2,000 m – 2,500 m		0.2772	0.0420
(6) 2,500 m – 3,000 m		0.2365	0.0358
(7) > 3,000 m		0.1000	0.0152
Soil Texture			
(1) Silty loam	0.0080	0.1000	0.0008
(2) Silty clay loam	0.0116	0.1000	0.0012
(3) Silty clay	0.0210	0.1000	0.0021
(4) Sandy loam	0.0158	0.1000	0.0016
(5) Sandy clay loam	0.0116	0.1366	0.0016
(6) Sand	0.0090	0.1000	0.0009
(7) Slope complex area	0.0299	0.9000	0.0269
(8) Loamy sand	0.0097	0.1000	0.0010
(9) Loam	0.0080	0.1000	0.0008
(10) Clay	0.0221	0.1000	0.0022
(11) Clay loam	0.0083	0.1000	0.0008
LULC			
(1) Dense evergreen forest	0.0016	0.9000	0.0014
(2) Disturbed evergreen forest	0.0001	0.1000	0.0000
(3) Oil palm	0.0123	0.1074	0.0013
(4) Para rubber	0.0074	0.1269	0.0009
(5) Miscellaneous	0.0128	0.1000	0.0013

Table 4.16 Achieved map accuracies of the considered fuzzy operators (ANN-Fuzzy).

Fuzzy operation	Success accuracy (%)	Prediction accuracy (%)	ROC (%)	Average (%)
AND	57.56	53.03	85.30	65.30
OR	63.72	60.30	89.10	71.04
Algebraic sum	87.21	83.17	94.70	88.36
Algebraic product	89.43	82.95	56.50	76.29
Gamma (λ) = 0.00	79.00	69.41	11.70	55.37
Gamma (λ) = 0.10	82.78	75.46	57.00	71.75
Gamma (λ) = 0.20	85.59	80.04	57.80	74.48
Gamma (λ) = 0.30	88.82	83.03	60.00	77.28
Gamma (λ) = 0.40	89.70	85.43	63.50	79.54
Gamma (λ) = 0.50	89.98	86.64	68.00	81.54
Gamma (λ) = 0.60	90.16	87.01	72.70	83.29
Gamma (λ) = 0.70	90.24	86.94	80.10	85.76
Gamma (λ) = 0.80	90.20	86.71	87.50	88.14
Gamma (λ) = 0.90	90.05	86.13	94.30	90.16
Gamma (λ) = 0.99	88.29	82.99	89.60	86.96
Gamma (λ) = 1.00	89.12	83.08	89.20	87.13

Table 4.17 Landslide susceptibility classification for the ANN-Fuzzy method ($\lambda = 0.90$).

Landslide susceptibility classes	LSS values	NSS values	Area	
			%	km ²
Very low susceptibility (VLS)	0.0000 - 0.0024	0.00 - 0.20	72.99	720.77
Low susceptibility (LS)	0.0024 - 0.0049	0.20 - 0.40	15.07	148.77
Moderate susceptibility (MS)	0.0049 - 0.0074	0.40 - 0.60	8.24	81.42
High susceptibility (HS)	0.0074 - 0.0099	0.60 - 0.80	3.25	32.10
Very high susceptibility (VHS)	0.0099 - 0.0125	0.80 - 1.00	0.45	4.47

From Table 4.17 and Figure 4.7n, the ANN-Fuzzy based landslide susceptibility map was dominated by the very low susceptibility portion of land (72.99%) while very small proportion was identified as the high and very high susceptibility zones (3.70%). Therefore, the ANN-Fuzzy method seems to suppress the proneness to landslide hazard over the area significantly if compared with obtained maps of other previous methods. Also, an integration of fuzzy logic to the ANN model did transform general outlook of the yielded map greatly (to be in great favor of the low to very low susceptibility states).

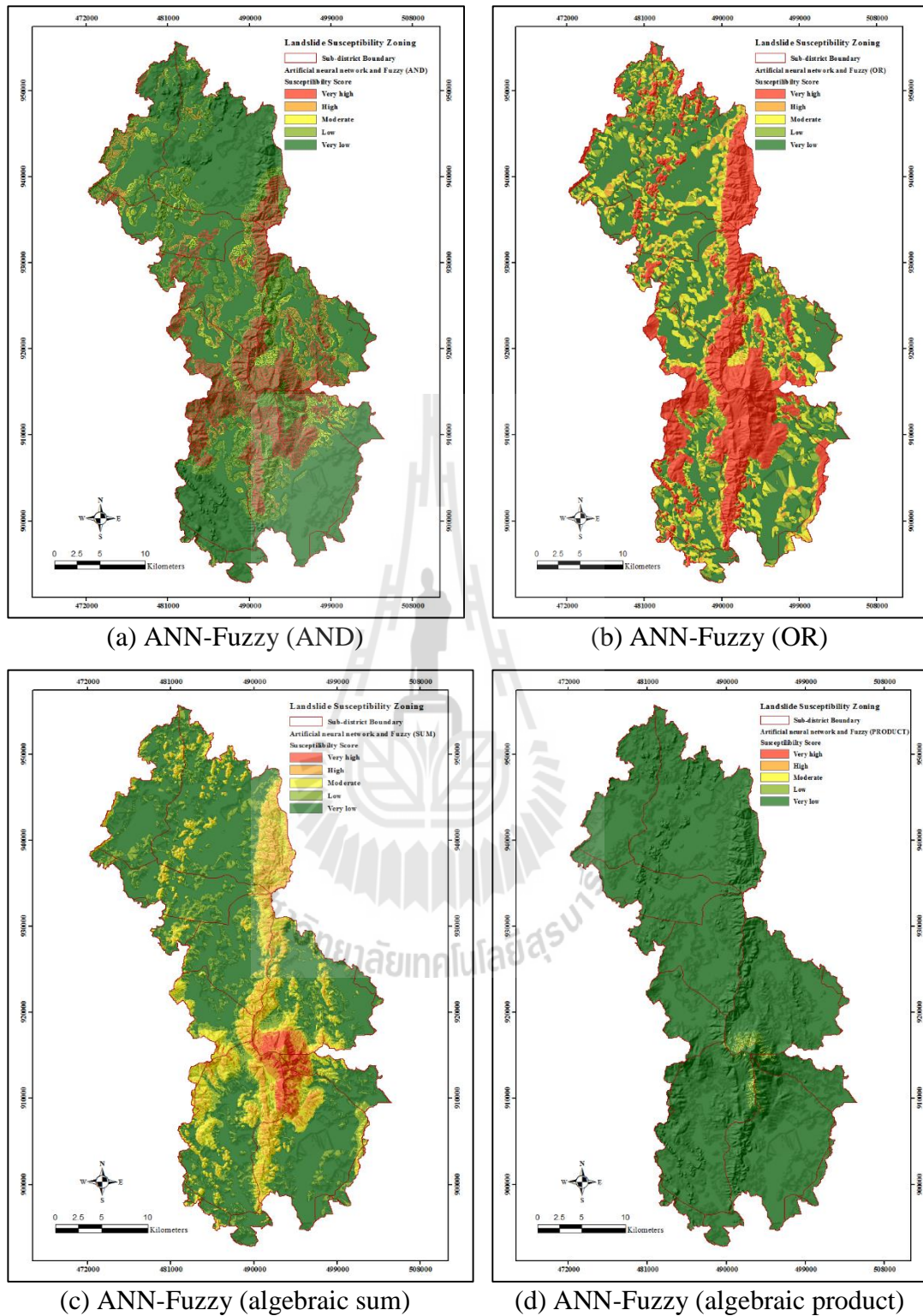
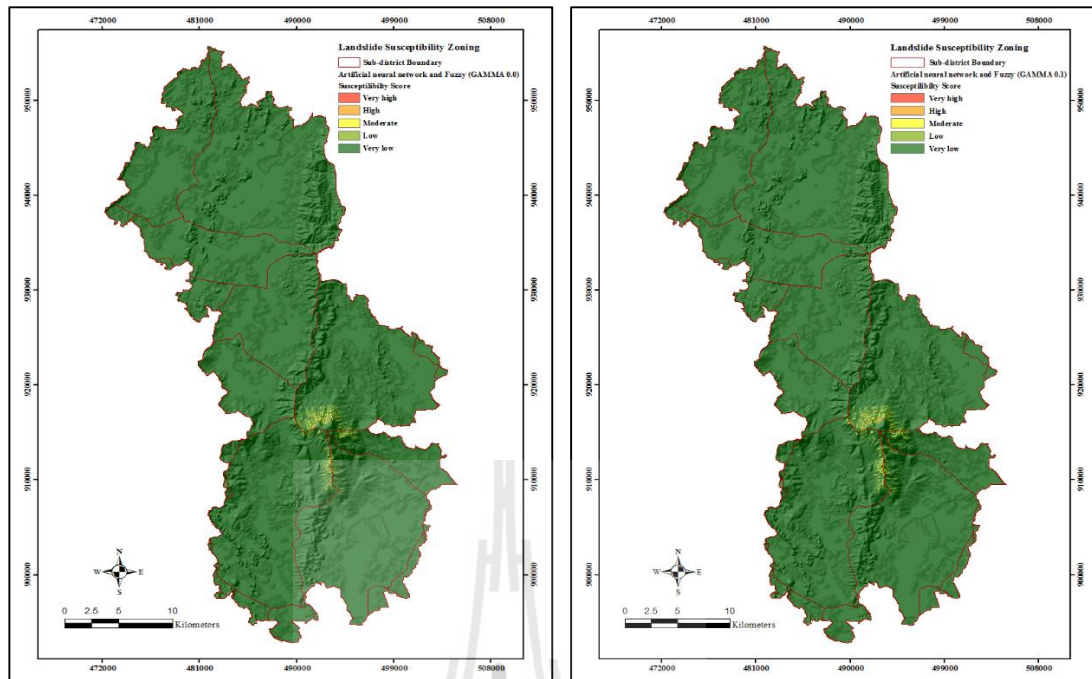
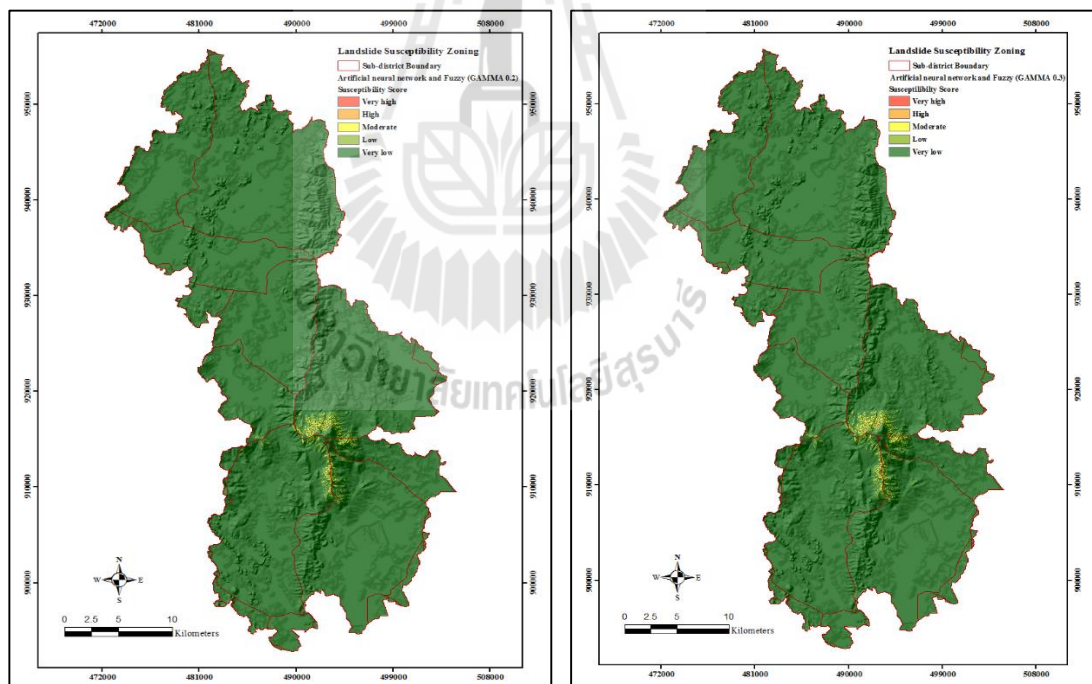
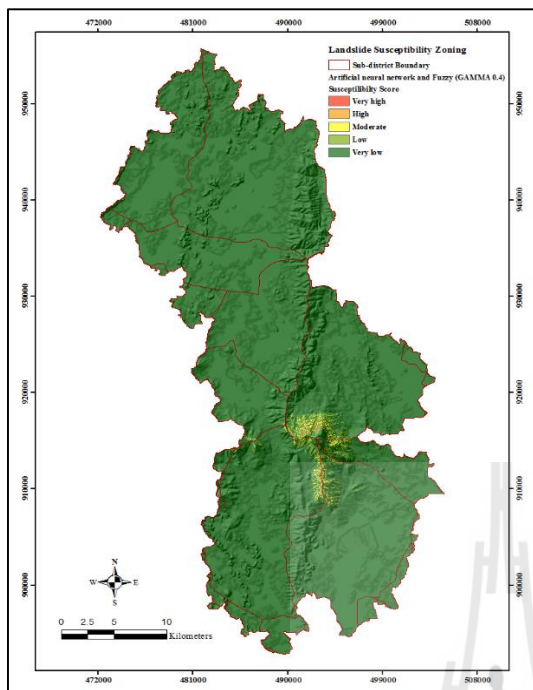


Figure 4.7 Classified landslide susceptibility maps from the ANN-Fuzzy method

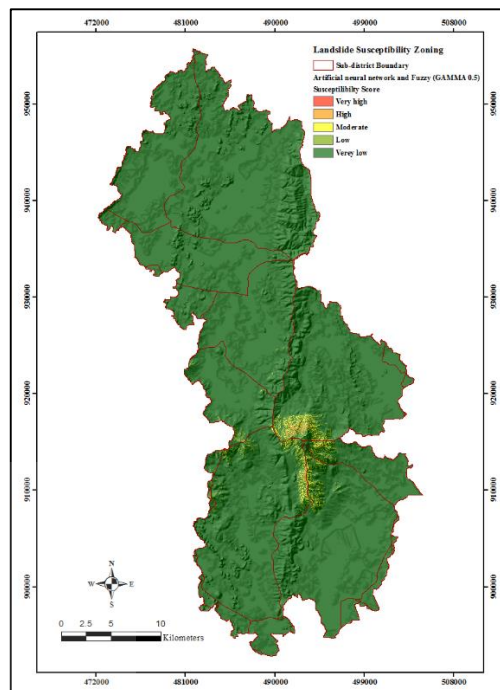
(Continued)

(e) ANN-Fuzzy ($\lambda = 0.0$)(f) ANN-Fuzzy ($\lambda = 0.1$)(g) ANN-Fuzzy ($\lambda = 0.2$)(h) ANN-Fuzzy ($\lambda = 0.3$)**Figure 4.7** Classified landslide susceptibility maps from the ANN-Fuzzy method

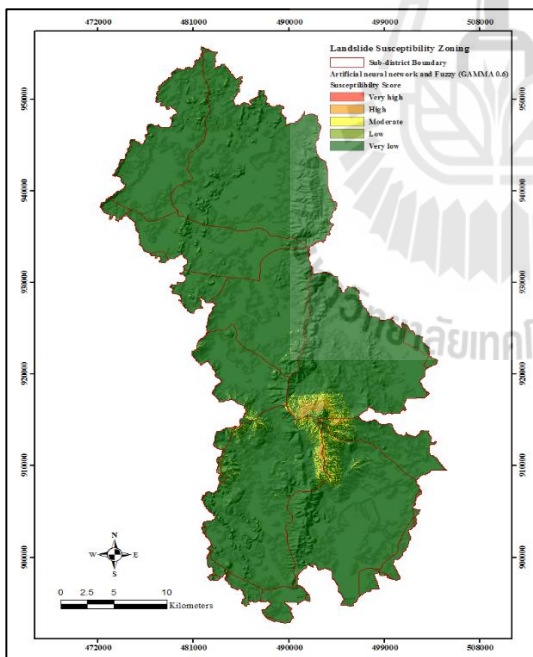
(Continued).



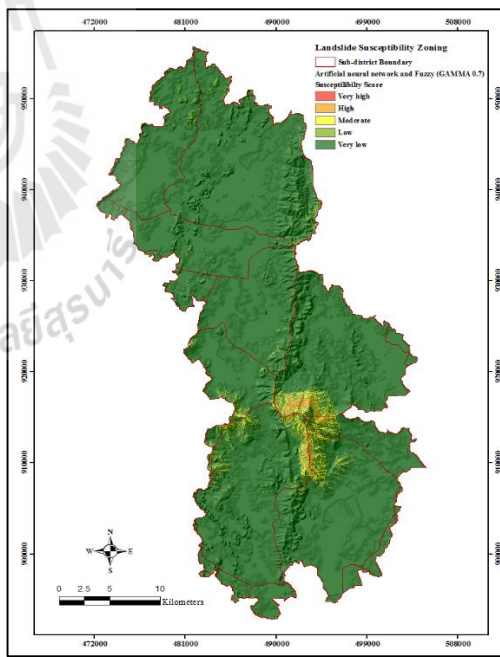
(i) ANN-Fuzzy ($\lambda = 0.4$)



(j) ANN-Fuzzy ($\lambda = 0.5$)



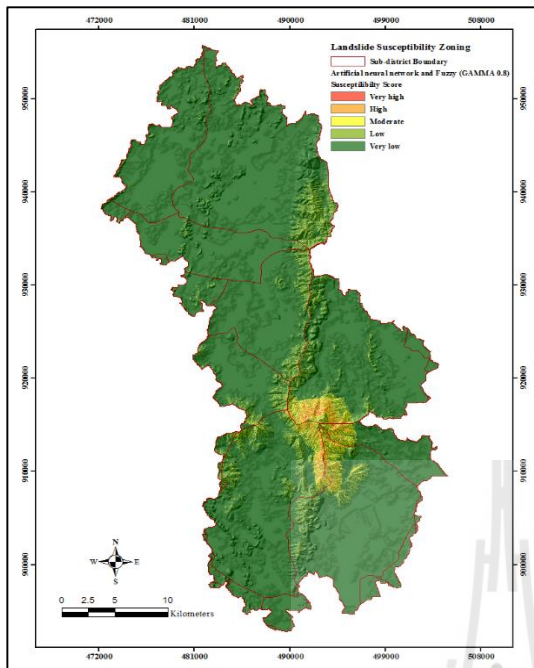
(k) ANN-Fuzzy ($\lambda = 0.6$)



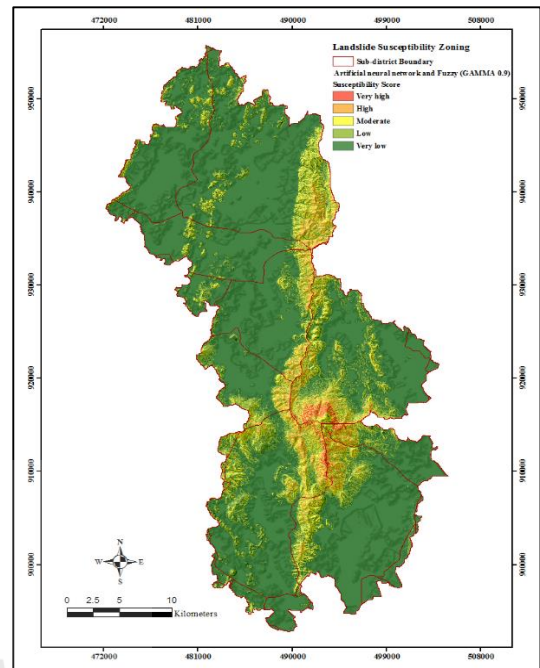
(l) ANN-Fuzzy ($\lambda = 0.7$)

Figure 4.7 Classified landslide susceptibility maps from the ANN-Fuzzy method

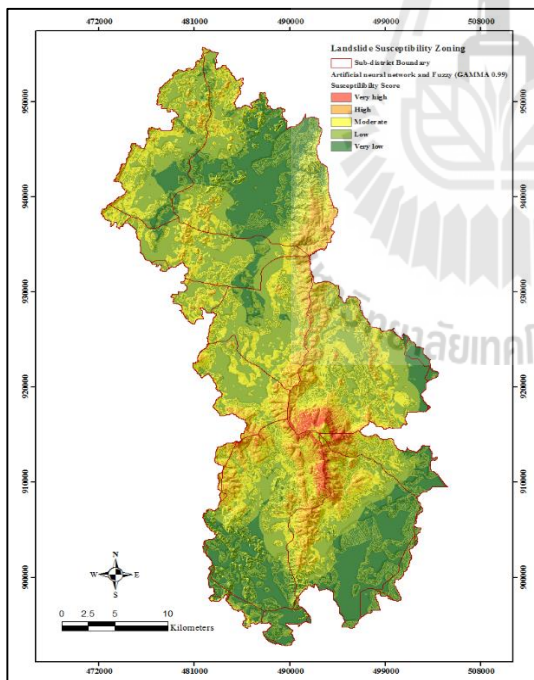
(Continued).



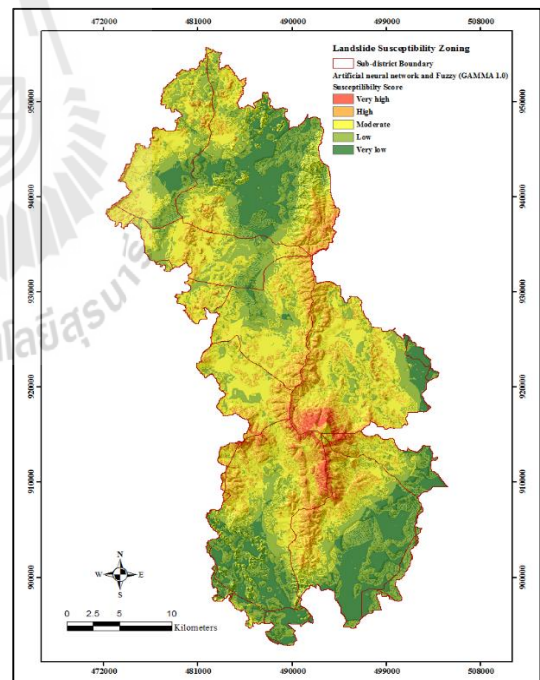
(m) ANN-Fuzzy ($\lambda = 0.8$)



(n) ANN-Fuzzy ($\lambda = 0.9$)



(o) ANN-Fuzzy ($\lambda = 0.99$)



(p) ANN-Fuzzy ($\lambda = 1.0$)

Figure 4.7 Classified landslide susceptibility map from the ANN-Fuzzy method

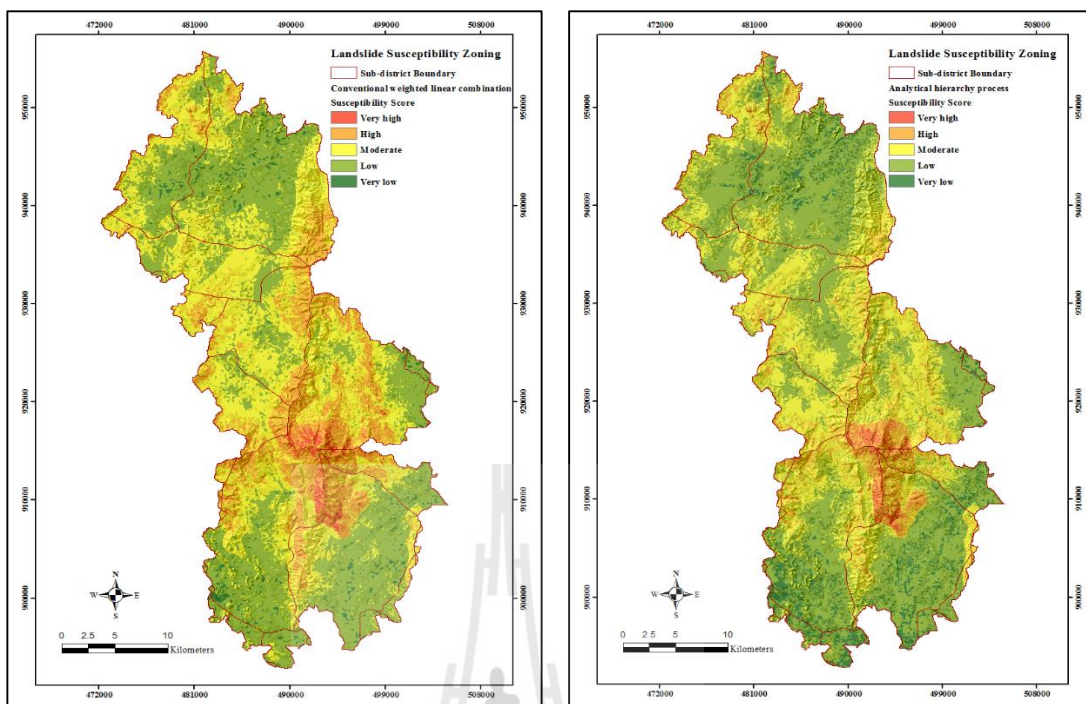
(Continued).

4.2 Comparison and verification of the yielded susceptibility maps

In this part, all derived landslide susceptibility maps as the output products from seven listed methods reported earlier (Figures 4.1-4.7) were compared with each other. Accuracy assessment of obtained maps was also performed independently according to the two popular methods, i.e., the AUC and ROC methods to aid the decision on optimal approach of interest.

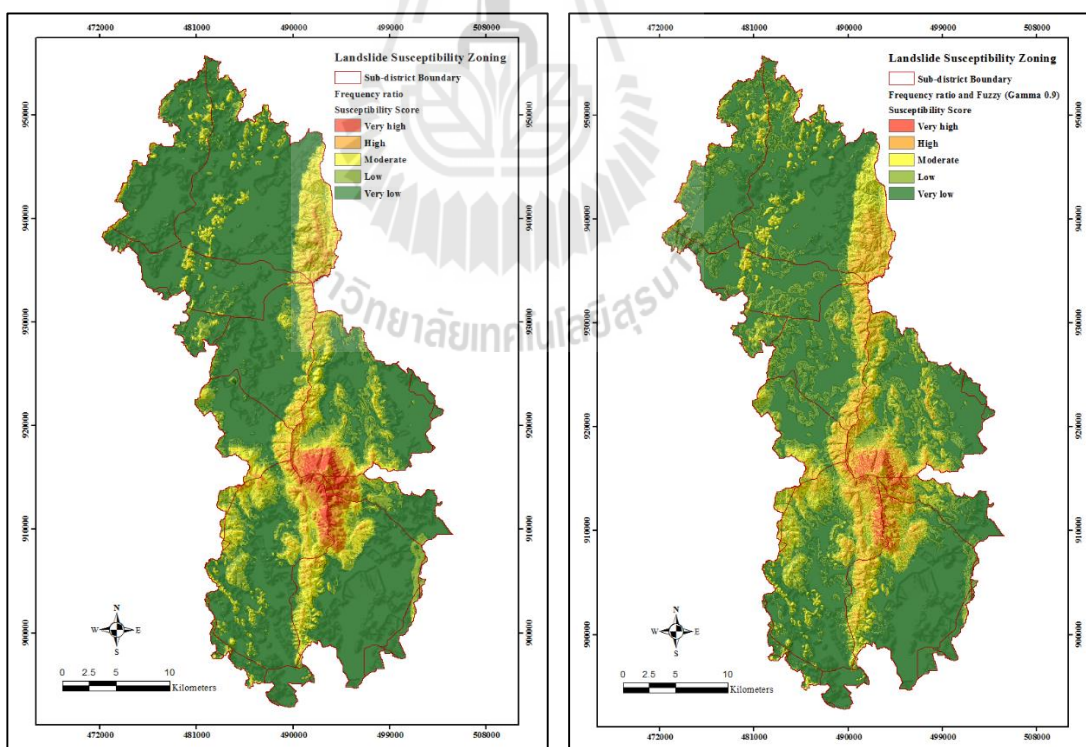
4.2.1 Map comparison and discussion

As described in Section 4.1, there were seven proposed methods to be examined for their capability in building credible landslide susceptibility map for the whole study area (Khao Phanom Bencha Watershed, Krabi Province), which are, the WLC, AHP, FR, FR-Fuzzy, MLR, ANN, and ANN-Fuzzy. Due to the conceptual differences in their working principles, their accomplished outputs in the form of landslide susceptibility map were intuitively expected to exhibit obvious distinctions in the predominant characteristics also as can be seen in Figures 4.8a-g, accompanied by the proportion of classified land data on the referred maps in Table 4.18 and Figure 4.10. The corresponding NSS histograms of these maps are also given in Figures 4.9a-g in which the equal-interval type of susceptibility classification was applied in all cases. Here, some methods tended to favor low to very-low susceptibility outcome, i.e., AHP, FR, FR-Fuzzy, MLR, ANN, ANN-Fuzzy, but some did bear the more moderate outcome one, i.e., WLC, AHP and some predicted noticeably high portion of land with high to very high landslide susceptibility scores over an area (e.g. > 10%), i.e., WLC (17.49%) and MLR (16.59%).



(a) WLC-based map

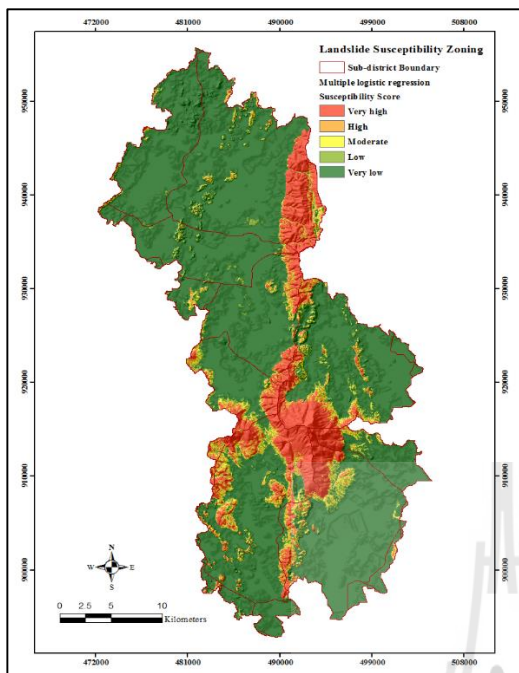
(b) AHP-based map



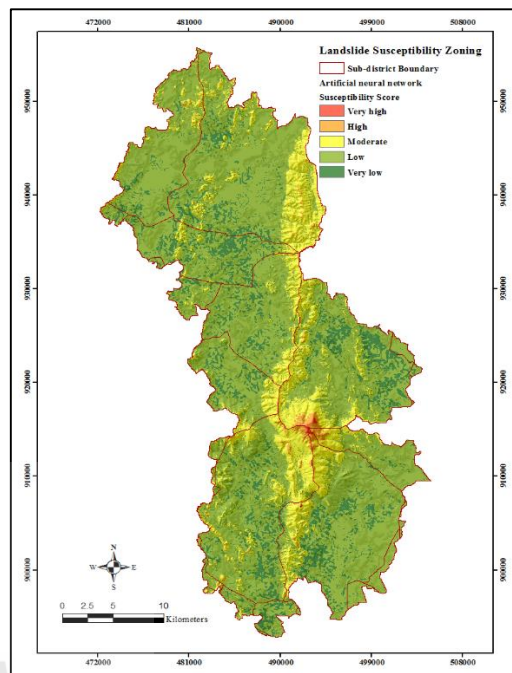
(c) FR-based map

(d) FR-Fuzzy based map

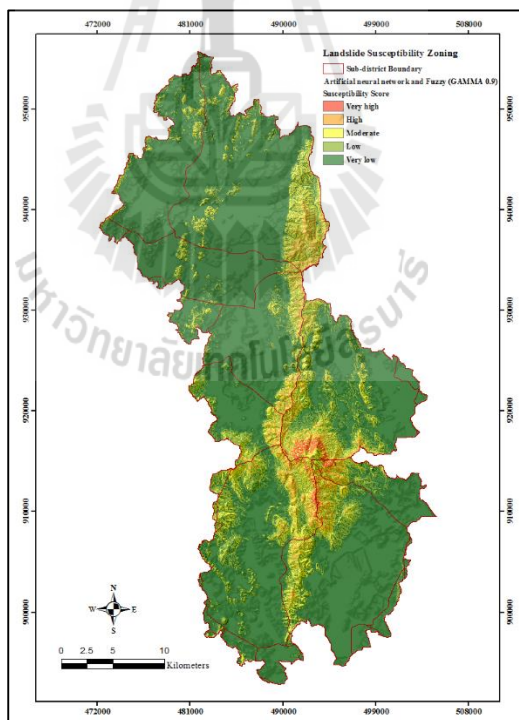
Figure 4.8 Classified landslide susceptibility maps based on all examined methods.



(e) MLR-based map



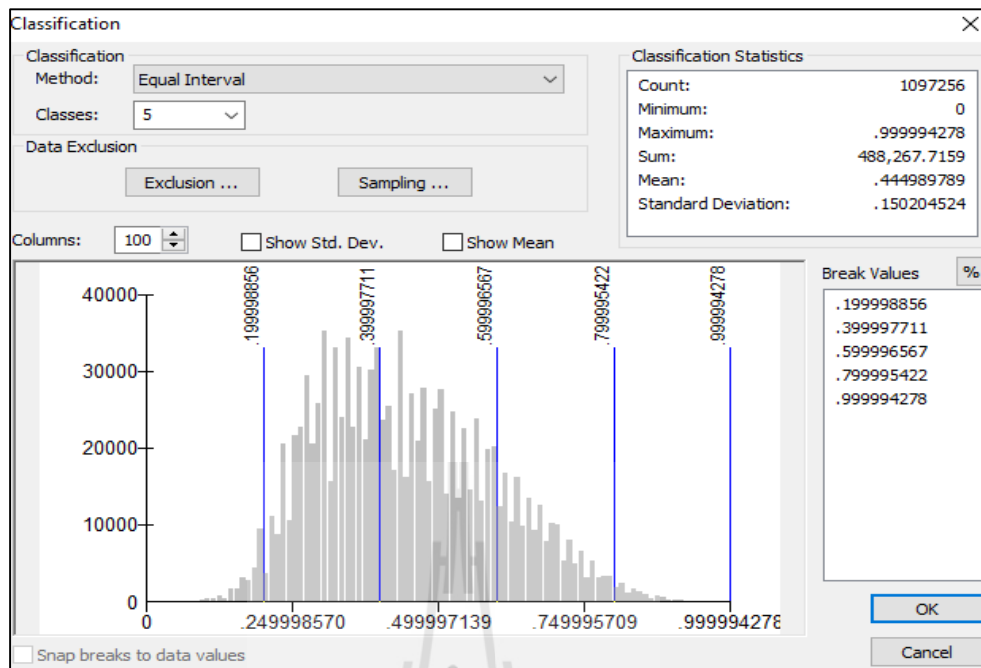
(f) ANN-based map



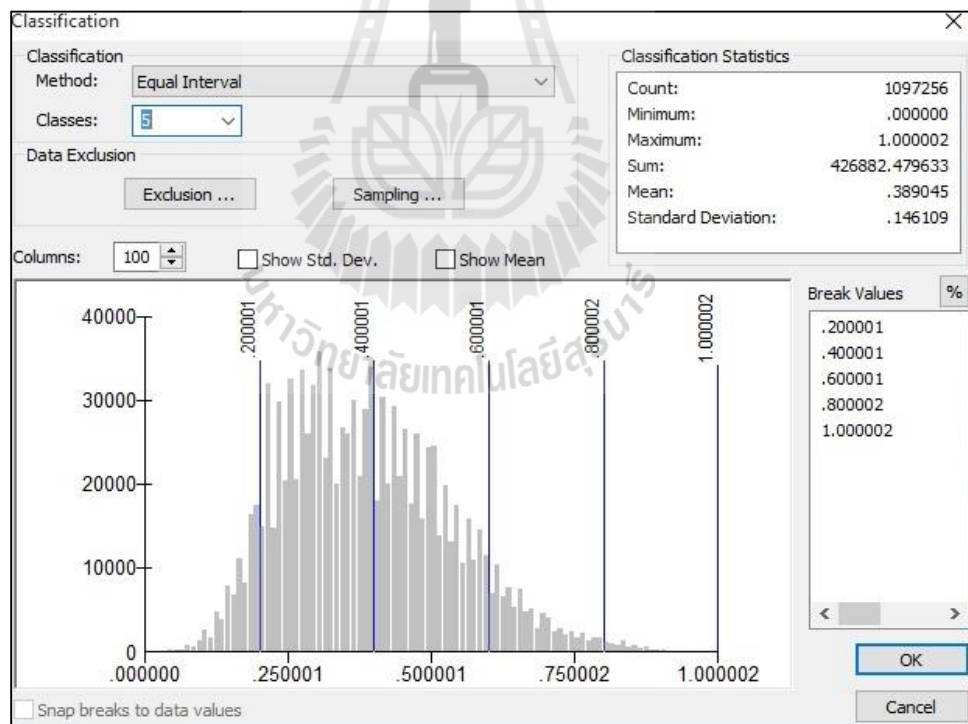
(g) ANN-Fuzzy based map

Figure 4.8 Classified landslide susceptibility maps based on all examined methods

(Continued).

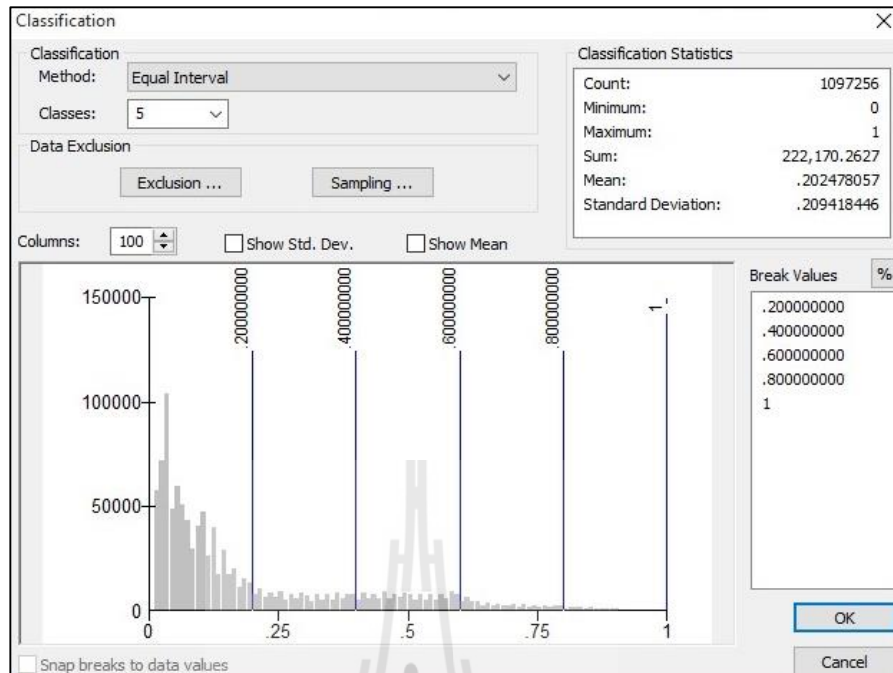


(a) WLC

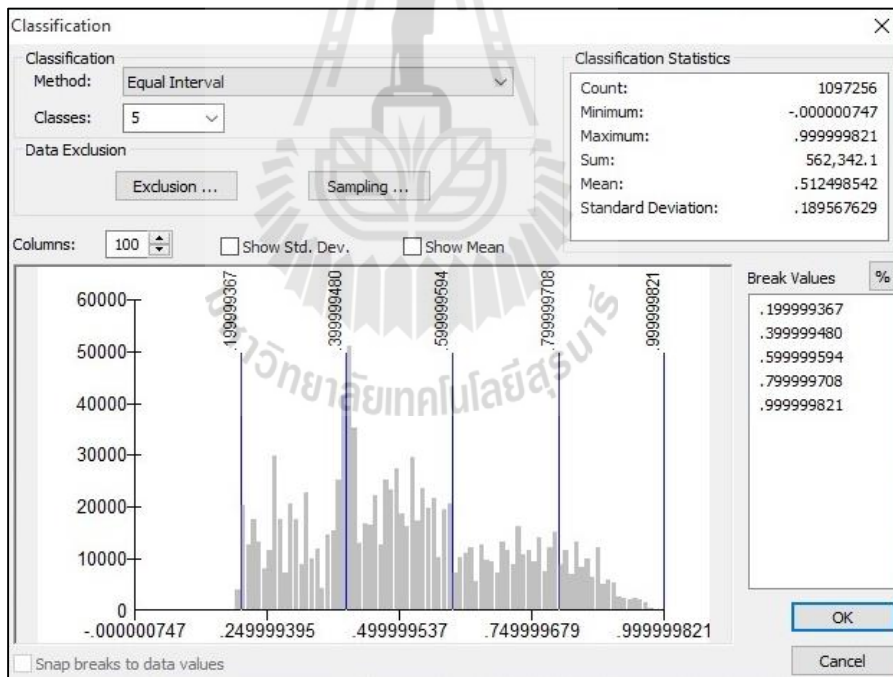


(b) AHP

Figure 4.9 NSS histograms of all derived susceptibility maps presented in Figure 4.8.



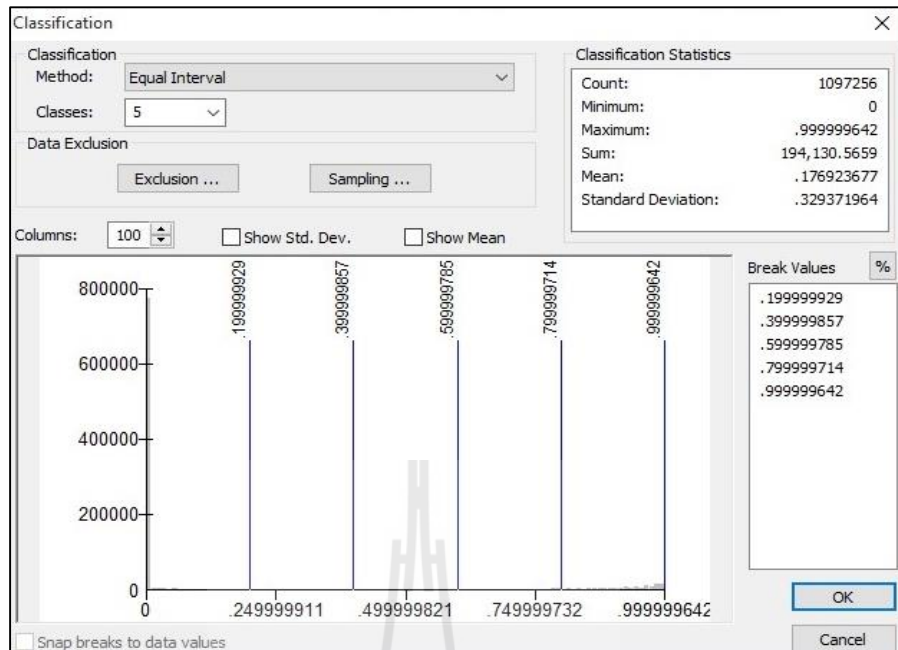
(a) FR



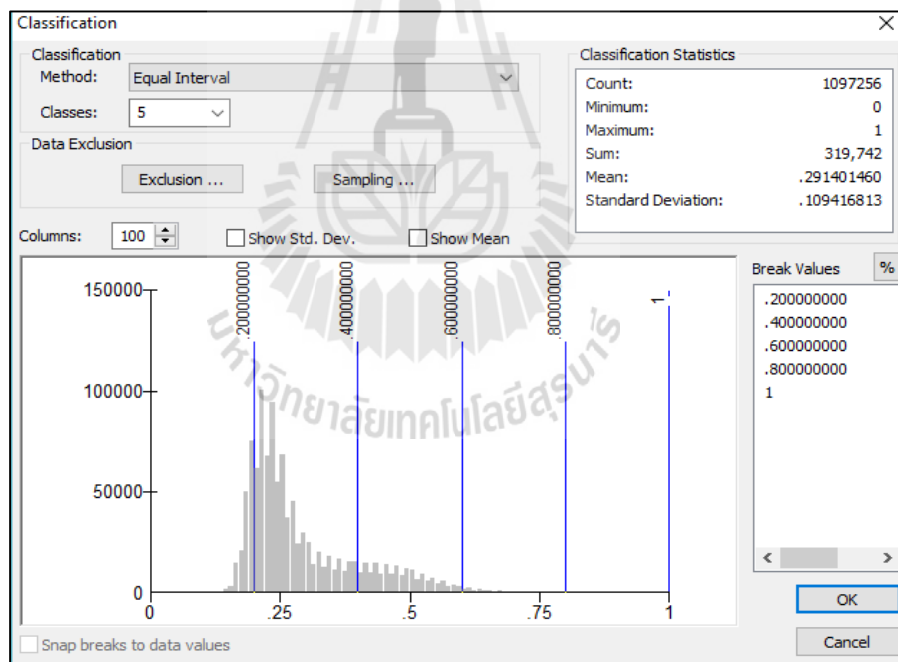
(b) FR-Fuzzy

Figure 4.9 NSS histograms of all derived susceptibility maps presented in Figure 4.8.

(Continued).



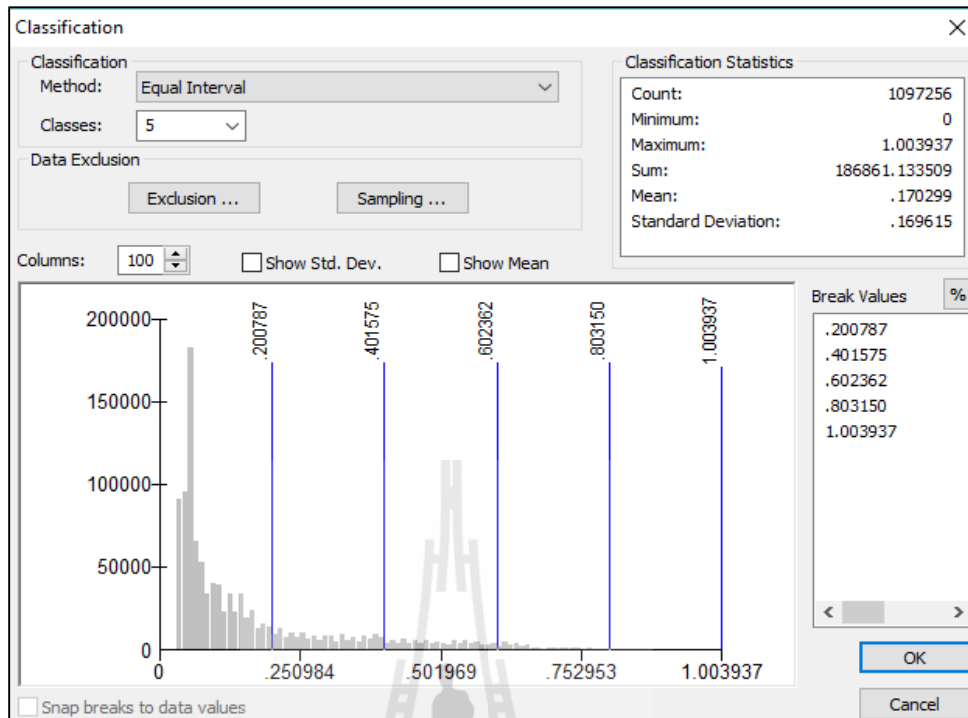
(a) MLR



(b) ANN

Figure 4.9 NSS histograms of all derived susceptibility maps presented in Figure 4.8.

(Continued).



(a) ANN-Fuzzy

Figure 4.9 NSS histograms of all derived susceptibility maps presented in Figure 4.8. (Continued).

From Figures 4.9a-g and Table 4.18, it is obvious that the two tested qualitative methods, WLC and AHP, exhibited an apparent preference towards the low to moderate level of susceptibility on their resulted maps while most evaluated quantitative methods (except the ANN) tended to create maps dominated by the very-low susceptibility land. The explanation for this difference might be about the way these maps were built as for the qualitative-type methods, the associated weights (both at factor and attribute levels) were judged from opinions of the surveyed experts, not from data of the past incidences as did in the quantitative-type methods, which made several factors (and their attributes) be somewhat overrated, or underrated, regarding to real situation observed in the area. For example in case of LULC, weights were distributed

to all classes under examination focusing on oil palm and para rubber (Tables 4.1 and 4.4), however, in reality just only about 5% of the reference landslide pixels were evidenced therein while another 94% were identified in the dense evergreen forest area, which was significantly less favored in both the WLC and AHP methods (but highly ranked by the FR and ANN methods).

Table 4.18 Landslide susceptibility classification of land for all examined methods.

Landslide susceptibility classes	NSS	Area (%)						
		WLC	AHP	FR	FR-Fuzzy	MLR	ANN	ANN-Fuzzy
Very low susceptibility (VLS)	0.0 – 0.2	2.11	7.37	67.31	59.13	76.30	12.60	72.99
Low susceptibility (LS)	0.2 – 0.4	40.75	48.48	13.09	20.62	3.76	69.71	15.07
Moderate susceptibility (MS)	0.4 – 0.6	39.66	35.37	12.70	12.36	3.35	16.29	8.24
High susceptibility (HS)	0.6 – 0.8	16.28	8.03	5.39	6.84	4.34	1.32	3.25
Very high susceptibility (VHS)	0.8 – 1.0	1.21	0.76	1.51	1.05	12.25	0.08	0.45

In addition, the correlation level (r) of the NSS data among tested methods was also determined as reported in Table 4.19. These data show prominently high correlation (of 0.93) between the two used qualitative-type methods (WLC and AHP), and also among the FR-based methods (FR, FR-Fuzzy, and ANN-Fuzzy). This high conformation among them led to resemble results on the derived maps as seen in Figures 4.8, 4.9 (map outlook and histogram pattern) and Table 4.18 (land classification outcome).

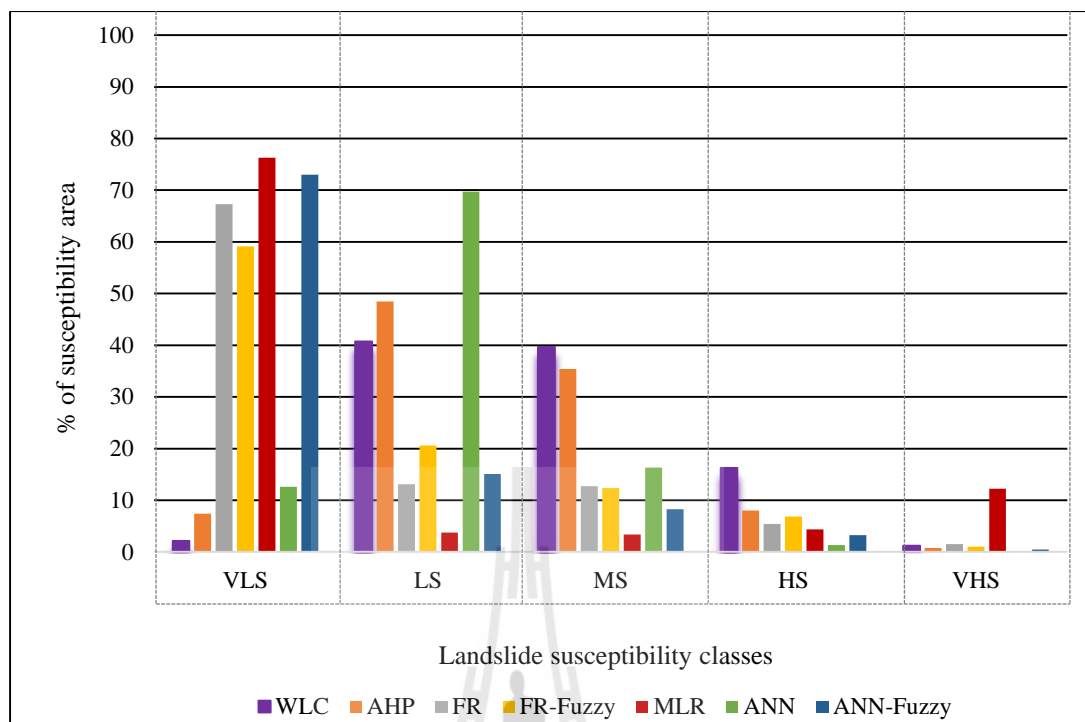


Figure 4.10 Proportion of land on classified susceptibility maps for all used methods.

Table 4.19 Correlation level (r) of the NSS data among all examined methods.

Methods	WLC	AHP	FR	FR-Fuzzy	MLR	ANN	ANN-Fuzzy
WLC	1.00						
AHP	0.93	1.00					
FR	0.71	0.68	1.00				
FR-Fuzzy	0.73	0.71	0.97	1.00			
MLR	0.61	0.54	0.88	0.85	1.00		
ANN	0.56	0.55	0.89	0.87	0.78	1.00	
ANN-Fuzzy	0.71	0.70	0.95	0.98	0.82	0.87	1.00

In terms of the hazard and risk management, maps with noticeably high portion of the land affixed with high to very high susceptibility level like those of the WLC (17.49%) and MLR (16.59%) might have less applicable value in practice as much effort than usual might be needed on the monitoring or examining of landslide condition in those areas for the prevention or mitigation purposes. Also, in principle,

this kind of result might lead to an overestimation of landslide proneness over an area as a high percentage of the observed landslides shall be more likely to be correctly identified on these obtained map with the drawback of producing many false alarms (or high sensitivity but low specificity).

Conversely, if the applied models emphasize too much on the very low to low outcome of the susceptibility prediction (i.e., FR, MLR, or ANN-Fuzzy), they might have less false alarm cases but number of landslides correctly predicted tend to be decreased also (low sensitivity and high specificity) (Segoni, Martelloni, and Catani, 2013).

However, at this stage, the applicable merit of each listed method mentioned earlier was still not yet conclusive as only the general outlook of the classified map was evaluated and compared so far. More definite judgment can be achieved through accuracy assessment of the formulated maps in which two popular methods, the AUC and ROC, shall be applied as detailed in following section. Noted that, in case of LULC, associated experts put high weights on para rubber and oil palm plantations but not on dense forest, however, the FR value for the dense forest was the highest one among others. This difference might arise from the fact that FR is the evidence-based analysis while WLC and AHP are knowledge-based ones, therefore in case of the 2011 incidence which was induced by the unusually high amount of rainfall, LULC might not be a key factor to determine chances of landslide occurrence compared to the topographic condition ones. As a consequence, the evidence-based methods, like FR, might be more effective to explain the real going-on circumstances over an area than the qualitative-type ones.

4.2.2 Map validation and optimal method identification

To assess for the applicable credibility of the gained susceptibility maps displayed in Figure 4.8, their respective accuracy in predicting reference landslide incidences was determined by two well-known methods: the Area-Under-Curve (AUC) and the Receiver Operating Characteristic (ROC) methods detailed in Chapter II. Here, in case of the AUC, two groups of reference dataset were applied: (1) data that were used to build the evaluated map before (490 points) and (2) data that were reserved for accuracy assessment only (210 points), but for the ROC, only the second dataset was incorporated. And for the AUC case, accuracy scores received from the first and second reference dataset are called “success rate” and “prediction rate”, respectively. Primary goal of the AUC method is to quantify the accurate prediction rate of the method in use while for the ROC curve analysis is to find a cutoff value that shall somehow minimize number of existing false predictions (positive/negative), or, maximizing sensitivity and specificity of the prediction. Figures 4.11 and 4.12 presents yielded outcome of accuracy assessment from all evaluated cases stated earlier (AUC-success/prediction rates, ROC).

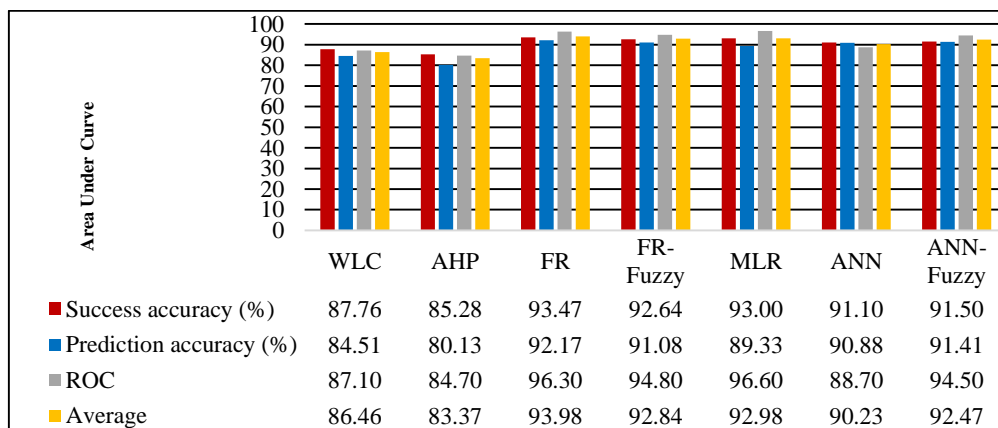
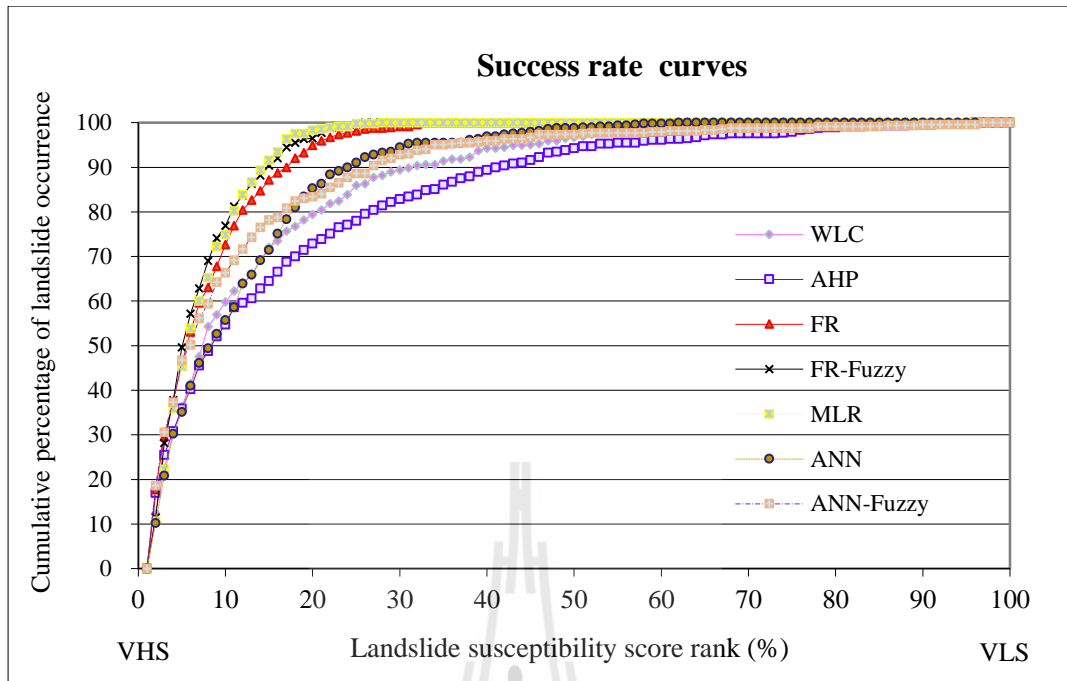
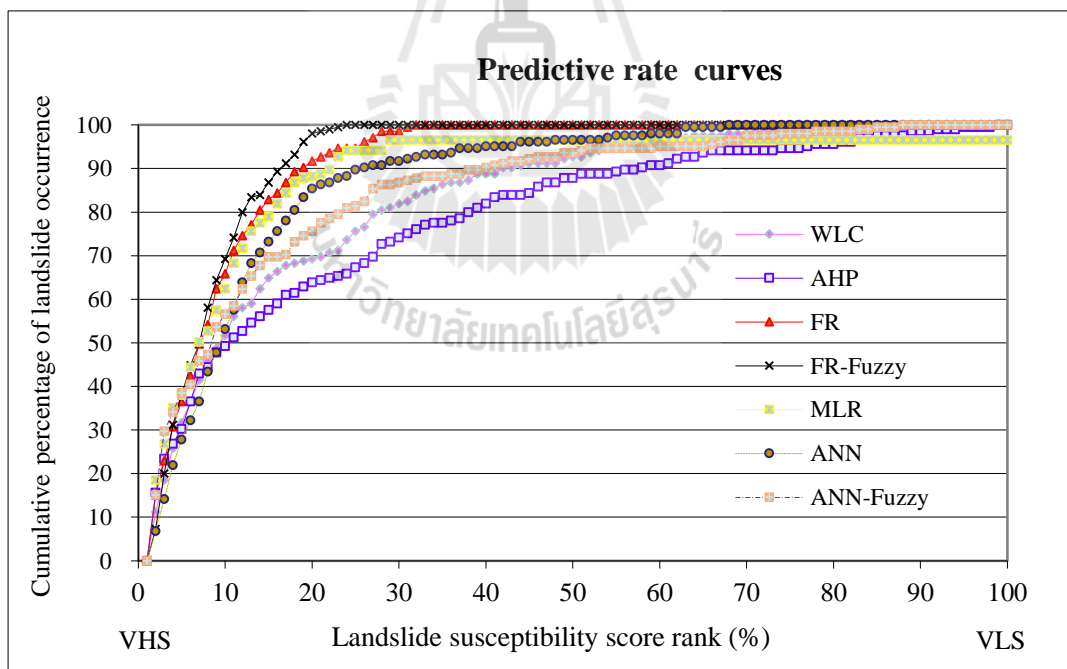


Figure 4.11 Comparative illustration of accuracies achieved by all examined methods.

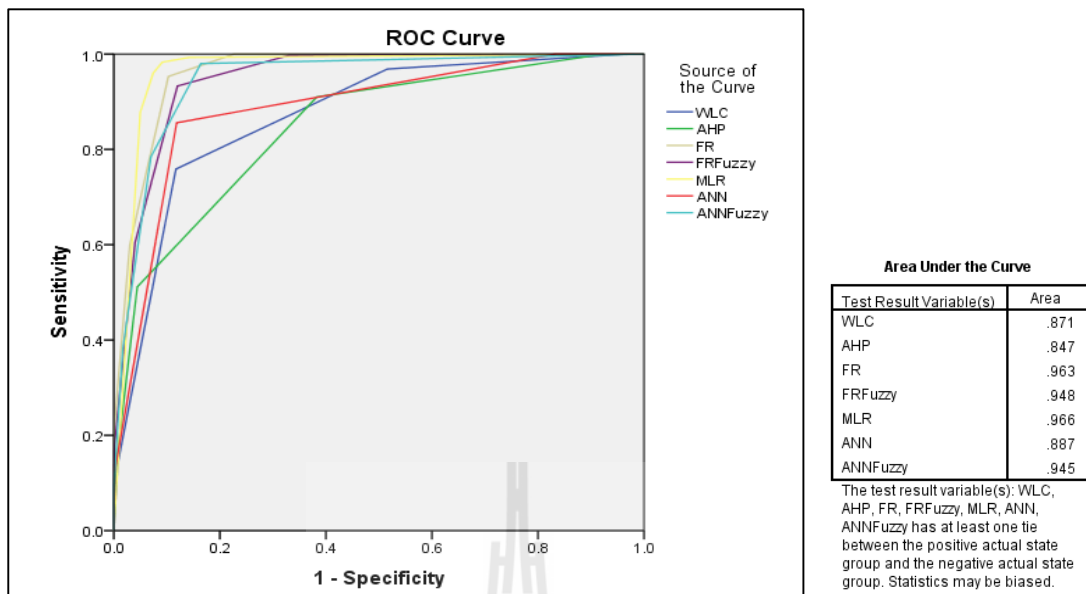


(a) AUC-Success rate



(b) AUC-Predictive rate

Figure 4.12 Graphic illustrations of the accuracy quantification by all three considered cases: (a) AUC-success rate, (b) AUC-predictive rate, and (c) ROC.



(c) ROC

Figure 4.12 Graphic illustrations of the accuracy quantification by all three considered cases: (a) AUC-success rate, (b) AUC-predictive rate, and (c) ROC (Continued).

In general, it was found that all utilized methods were well capable of producing susceptibility maps for the chosen area with remarkably high accuracy (mostly > 85%) in all cases though their generated map outlook and land classification results might be still somewhat different (as evidenced in Figures 4.8-4.9 and Table 4.18). However, if consider in terms of average accuracy, the FR method seemed to perform the best in all cases under consideration which led to average accuracy of 93.98%. This was closely followed by MLR (at 92.98%), FR-Fuzzy (at 92.84%), and ANN-Fuzzy (at 92.47%). The least successful ones evidenced here were those of both qualitative-type methods; the WLC (at 86.02%), and the AHP (at 83.94%). However, these apparent accuracy levels still look quite impressive under normal standard (of 80% up).

Through, the found top four methods (FR, FR-Fuzzy, MLR, and ANN-Fuzzy) are highly comparable in terms of attained average accuracy (93.98%, 92.84%, 92.98%, 92.47%), however, the FR was eventually considered to be an optimal candidate (to aid further construction of the associated landslide hazard and then risk maps for an area) due to its simplest structure and most comprehensible working concept if compared to the other two listed choices, as well as on the rather realistic outlook of its final output susceptibility map (Figure 4.3). These stated distinct abilities are of notable advantage in building in-depth understanding on complicated mechanism of landslide formation seen within the area, especially for the prevention, warning, and mitigation purposes. However, it should be noted that different works at different places and/or with different mapping, or classifying tools, might find different optimal method as an outcome, for examples, this was ANN model in work of Park, Choi, Kim, and Kim (2013), and Yilmaz (2013), or the support vector regression method in that of Kavzoglu, Sahin, and Colkesen (2015).

In addition, between the two studied qualitative methods, WLC and AHP, it seems WLC was the better one in terms of the yielded average accuracy (86.46% to 83.37%). This might be arisen from the weighting methodology at both factor and attribute levels as for the WLC, all opinions of all experts regarding to used factors and their associated attributes were included in the weighting analysis while for the AHP one, only opinions that passed the CR threshold of 0.1 were chosen for weight quantification at both levels.

However, high correlation between the yielded landslide susceptibility scores (of 0.93) suggest high similarity of their map products nevertheless. And for the used FR method, the reference landslide input data should be distributed well over the

area with sufficient amount needed to increase, or ensure, effectiveness of the mapping process.

4.2.3 Factor sensitivity analysis

As this study so far did not focus on finding most appropriate factors to be used in the mapping analysis but concentrated on finding the most effective mapping method for the study area based on ten chosen conventional causative factors as stated earlier. However, this kind of factor's sensitivity analysis shall conduct somehow in this part of the thesis to evaluate apparent effects of some prominent contributing factors in the building of landslide susceptibility maps for the area by the preferred FR model. These included the determination of relative importance of each used contributing factors and the factor-preferred formulation of the susceptibility map for the study area. In the first case, the importance of a particular factor of interest was judged by excluding it from the mapping process and compare the newly-achieved accuracy result with that of the original one (93.38%) and the finding outcome is as illustrated in the Table 4.20, in which low impact on original accuracy ($\leq 0.51\%$) were found in all cases. This means no factors came up as clear favorites as their perceived impact was equally negligible.

Through, all ten input factors were found to have rather comparable importance in the building of landslide susceptibility map by the FR method (as seen in Table 4.20), however, different combination of these factors in the map formulating procedure might lead to noticeable changes in map outlook and also accuracy outcome as demonstrated and reported in Figure 4.13 and Table 4.21 for four interesting cases. This combination list was guided by the perceived comparative importance of each individual input factor by the reviewed experts reported in Table 4.1. These results

indicated that the accuracy of 88.08% could be achieved using slope gradient alone and integration of more factors tended to gradually increase yielded accuracy to the reference value of 93.98%.

Table 4.20 Accuracy outcome in case of the sensitivity analysis for each used factor.

FR excluded	Accuracy (%)					Rank
	Success	Prediction	ROC	Average	Change	
None (reference case)	93.47	92.17	96.30	93.98	0.00	-
Elevation	92.96	91.95	95.50	93.47	-0.51	1
Slope gradient	93.01	91.60	95.90	93.50	-0.48	2
Slope aspect	93.26	91.95	96.30	93.84	-0.14	6
Slope curvature	93.49	92.22	96.20	93.97	-0.01	7
TWI	93.57	92.16	96.20	93.98	0.00	8
Distance from drainage	93.49	92.18	96.30	93.99	+0.01	9
Lithology	93.40	91.94	95.90	93.75	-0.23	4
Distance from lineament	93.41	92.21	96.50	94.04	+0.06	10
Soil texture	93.33	91.83	95.60	93.59	-0.39	3
LULC	93.44	92.17	95.80	93.80	-0.18	5

Table 4.21 Accuracy outcome in case of the factor-preferred map formulation.

Combination pattern	Accuracy (%)				
	Success	Prediction	ROC	Average	Change
Slope gradient	87.37	84.66	92.20	88.08	- 5.90
Slope gradient + Lithology	90.85	89.78	94.40	91.68	- 2.30
Slope gradient + Lithology + Soil texture	91.74	91.01	95.70	92.82	- 1.16
Slope gradient + Lithology + Soil texture + LULC + Distance from lineament	92.70	91.63	95.40	93.24	- 0.74
All factors included (reference case)	93.47	92.17	96.30	93.98	0.00

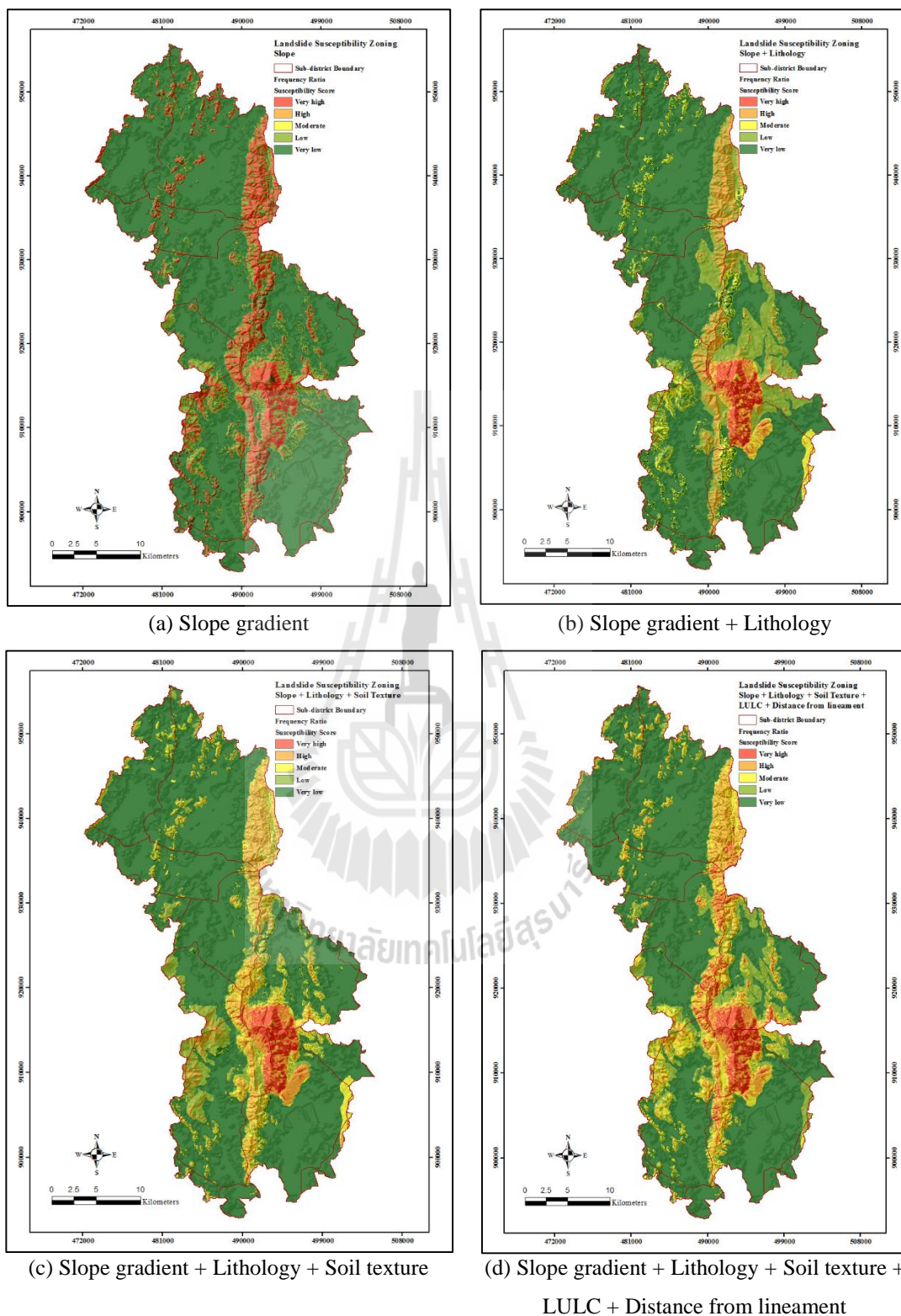


Figure 4.13 FR-based output maps form different combination of input factors.

4.3 Effects of rainfall integration on the susceptibility analysis

As mentioned in Chapter II, some reports on landslide susceptibility mapping had incorporated rainfall data as an individual input layer in their analysis also, e.g., in Lee and Pradhan (2006), Intarawichian and Dasananda (2011), and Thanh and de Smedt (2012). In theory, the inclusion of rainfall distribution data in the susceptibility analysis can lead to the formation of more dynamic output map (as the relevant rainfall scenarios can change rapidly with space and time). In this thesis, effects of rainfall integration in the FR-based formulation of landslide susceptibility map in two cases were examined, which are, (1) the long-term annual mean rainfall data between A.D. 1951- 2012, and (2) the event-based data receiving during 27th-29th March 2011 (as seen in Figure 3.11).

To accomplish this task, first, the appropriated FR values were assessed for each classified range of rainfall data in both cases and results are as expressed in Table 4.22. It was found that, in general, no outstanding classes of rainfall data in both cases (with noticeably high FR values) were evidenced wherein maximum FR stood at 2.12 only and higher FR values did not indicate higher chances for landslide activity in both cases. Due to the relatively low FR values of all considered rainfall classes over the entire area (around 1 in average), their combination to the original pixel-based NSS values existing on the original FR-based susceptibility map (Figure 4.3) to attain a new set of LSS data for the formulation of the new associated susceptibility map tended to have rather low impact on general outlook of the gained susceptibility maps as illustrated in Figure 4.14 and Tables 4.23 and 4.24. These results indicate that combination of the rainfall data in the FR-based landslide susceptibility mapping here may did not initiate tangible benefit per se compared to the original map without them included both in terms of map outlook and average accuracy of these maps (as detailed in Figure 4.15).

Table 4.22 FR values for the listed rainfall attributes in both cases.

Factors	Class	Total number of pixels		Landslide occurrence point		FR values
		Number	%	Number	%	
Rainfall (long-term annual mean)	< 1,750 mm	22147	2.0184	0	0.0000	0.0000
	1,750 mm – 1,942 mm	156684	14.2705	22	4.4898	0.3146
	1,941mm – 2,132 mm	697931	63.6069	387	78.9796	1.2417
	2,132 mm – 2,323 mm	196246	17.8852	77	15.7143	0.8786
	> 2,323 mm	24348	2.2190	4	0.8163	0.3679
Rainfall (event-based)	< 269 mm	59686	5.4396	18	3.6735	0.6753
	269 mm – 270 mm	243915	22.2295	15	3.0612	0.1377
	270 mm – 271 mm	575331	52.4336	353	72.0408	1.3739
	> 271 mm	218324	19.8973	104	21.2245	1.0667

Note: Total number of pixels in study area: 1,097,256. Number of landslide occurrence points: 490.

$$FR = \% \text{ Landslide occurrence points} / \% \text{ number of pixels}$$

Table 4.23a FR-based landslide susceptibility classification with the long-term annual mean rainfall data during 1951-2012 over the area integrated.

Landslide susceptibility classes	LSS values	NSS values	Area	
			%	km ²
Very low susceptibility (VLS)	1.25 – 10.33	0.00 – 0.20	66.21	653.80
Low susceptibility (LS)	10.33 – 19.41	0.20 – 0.40	13.83	136.62
Moderate susceptibility (MS)	19.41 – 28.49	0.40 – 0.60	12.72	125.62
High susceptibility (HS)	28.49 – 37.56	0.60 – 0.80	5.68	56.09
Very high susceptibility (VHS)	37.56 – 46.65	0.80 – 1.00	1.56	15.40

Table 4.23b FR-based landslide susceptibility classification with event-based rainfall data during 27th-29th March 2011 over the area integrated.

Landslide susceptibility classes	LSS values	NSS values	Area	
			%	km ²
Very low susceptibility (VLS)	1.03 – 10.18	0.00 – 0.20	65.70	648.84
Low susceptibility (LS)	10.18 – 19.33	0.20 – 0.40	14.27	140.88
Moderate susceptibility (MS)	19.33 – 28.48	0.40 – 0.60	13.14	129.76
High susceptibility (HS)	28.48 – 37.63	0.60 – 0.80	5.28	52.17
Very high susceptibility (VHS)	37.63 – 46.78	0.80 – 1.00	1.61	15.89

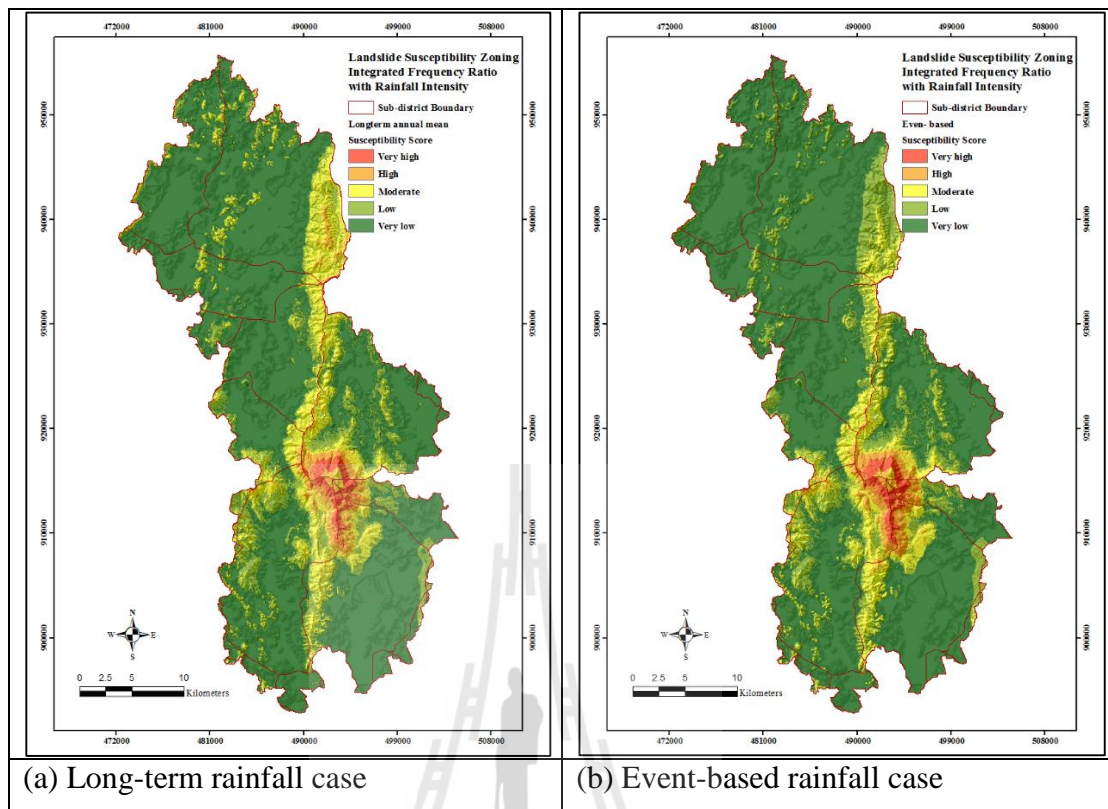


Figure 4.14 FR-based classified landslide susceptibility maps in two cases of rainfall data integration (long-term annual mean and event-based data).

Table 4.24 Comparison of area allocation on three FR-based susceptibility maps under consideration (original, with rainfall data integrated-long-term case, event-based case).

Landslide susceptibility classes	LSS values	% of Area		
		FR (original)	FR (long-term)	FR (event-based)
Very low susceptibility (VLS)	0.0 – 0.2	67.31	66.21	65.70
Low susceptibility (LS)	0.2 – 0.4	13.09	13.83	14.27
Moderate susceptibility (MS)	0.4 – 0.6	12.70	12.72	13.14
High susceptibility (HS)	0.6 – 0.8	5.39	5.68	5.28
Very high susceptibility (VHS)	0.8 – 1.0	1.51	1.56	1.61

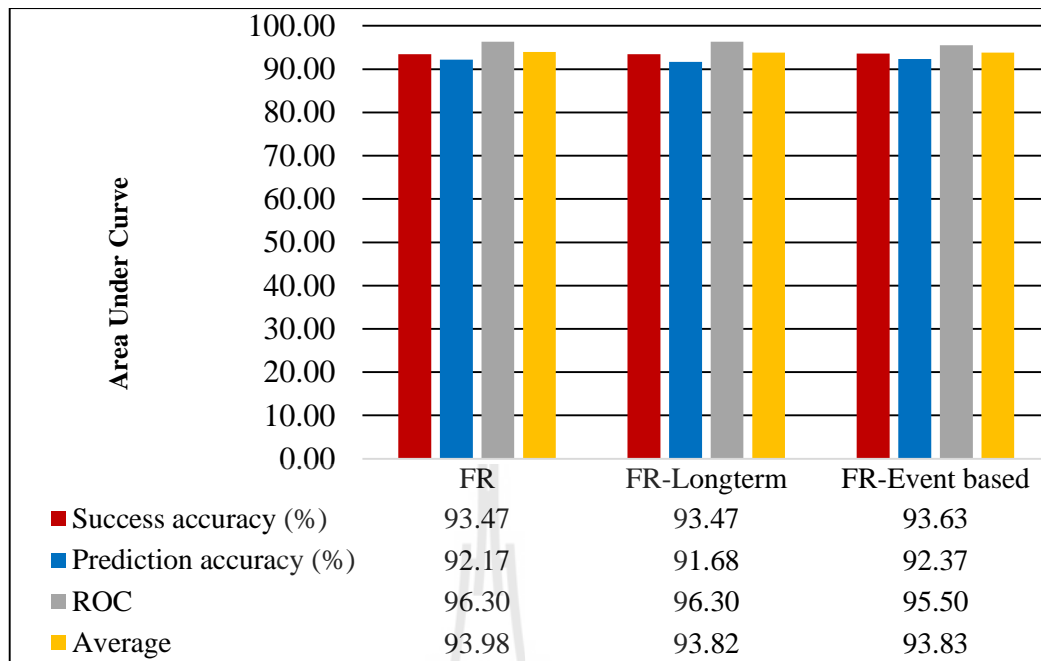


Figure 4.15 Comparison of accuracies achieved from the three FR-based susceptibility maps (original, with rainfall data integrated-long-term case, event-based case).

4.4 Establishment of landslide hazard and risk maps

As the ultimate goal of this present study (as stated in Objective 2 in Chapter I) was to build landslide hazard and risk maps for the study area based on the availability of landslide susceptibility map derived through the identified optimal method (i.e., FR), therefore this section shall be devoted to full report and discussion on accomplishments of this aforementioned issue in conclusive details.

4.4.1 Construction and evaluation of the landslide hazard maps

First, the time-dependent hazard maps for the area were constructed from a direct pixel-based product of the annual rainfall probability (ARP) data for the critical rainfall threshold of 100 mm/day and 300 mm/3-days (Figure 3.12) and the FR-based landslide susceptibility score (LSS). This relation can be written as:

$$\text{Hazard index (HI)} = \text{ARP} \times \text{LSS}. \quad (3.4)$$

The classified hazard maps (for each used rainfall criterion) were then established based on application of the equal-interval classifying method on the HI dataset and important outcomes are presented in Figures 4.16a and b and Table 4.25, respectively.

It was clear from these stated maps that, chances of having rainfall intensity of 100 mm/day in the area per year changed greatly from about 0.2 (in the southeastern part) to about 0.5 (in the southwestern part). Similarly, for a case of the rainfall intensity of 300 mm/3-days, chances of the success per year were found much lower than those of the 100 mm/day case, wherein peak values of about 0.054 were seen at the far south portion of the map and the lowest ones of about 0.022 were attained in the southeastern part. However, as critical rainfall data tended to happen over the low susceptibility part, both hazard maps seemed to highly resemble that of their susceptibility counterparts in terms of both the outlook (Figure 4.16) and distribution of occupied area (Table 4.25).

And according to very high correlation (of 0.99) between hazard scores from both cases, this suggests that their map products can be applied interchangeably. However, as chances of reaching the 100 mm/day threshold are typically much higher, therefore, attendance should be primarily given to map generated in this case first than that of the 300 mm/3-days case which should be more concerned about if that threshold is likely to be achieved during some unusual circumstances (like in the March 2011 incidence investigated in this thesis work).

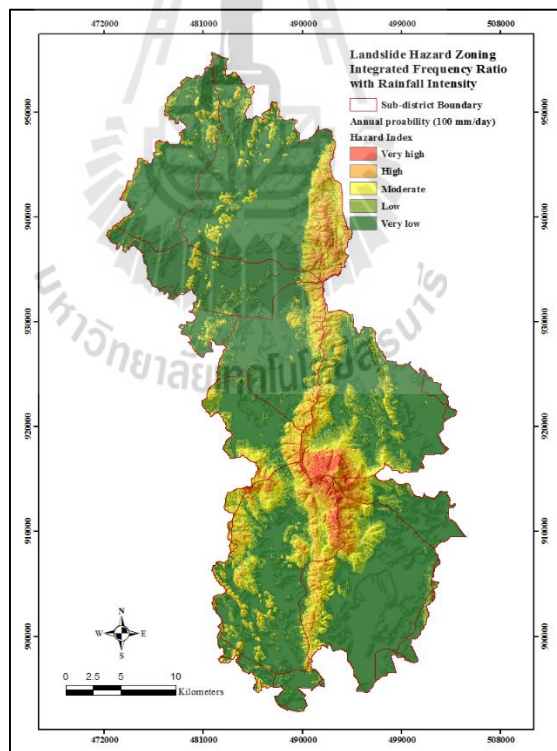
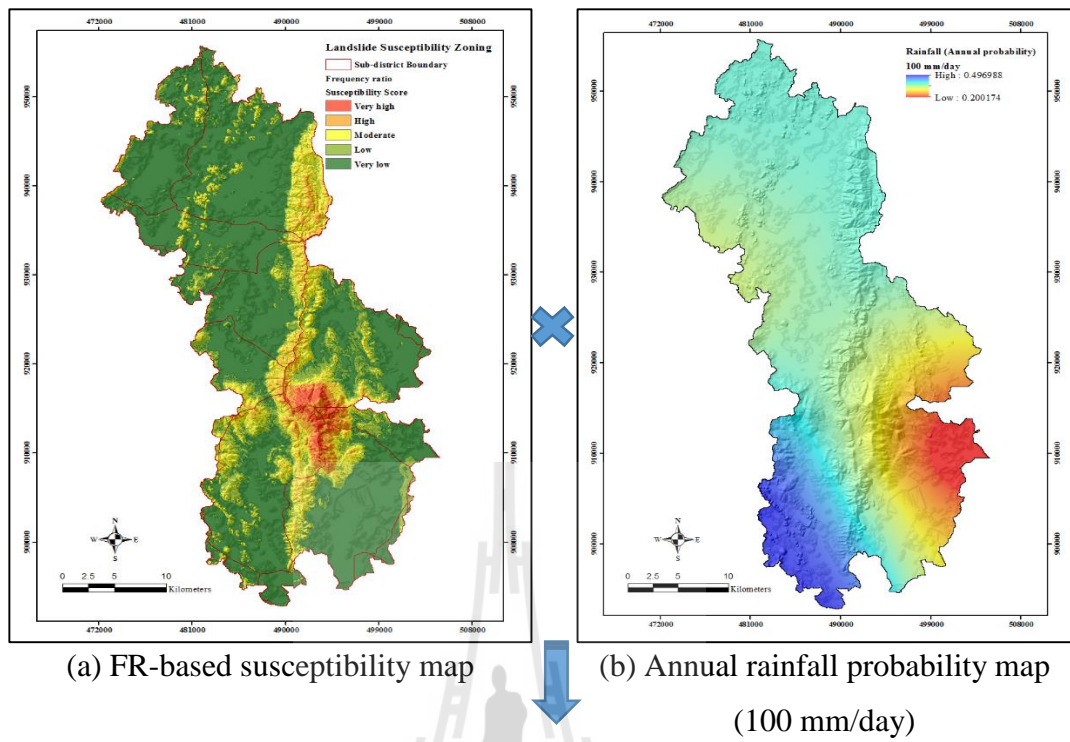


Figure 4.16a Landslide hazard map (case of critical rainfall threshold 100 mm/day).

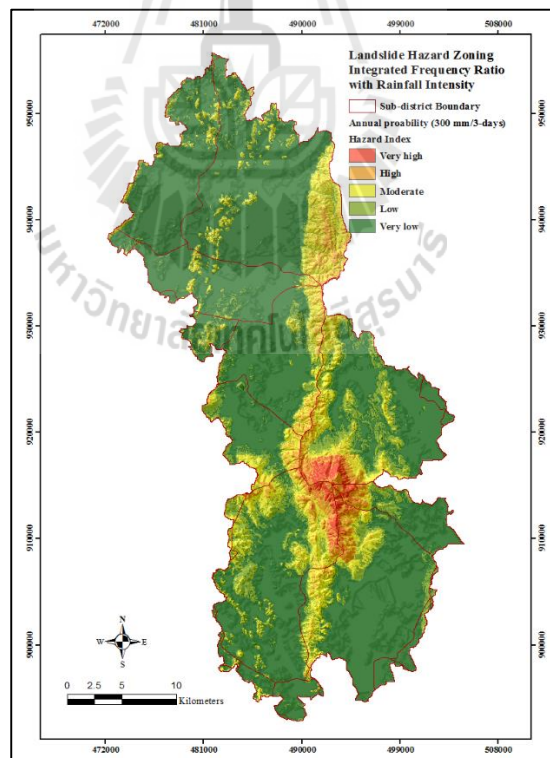
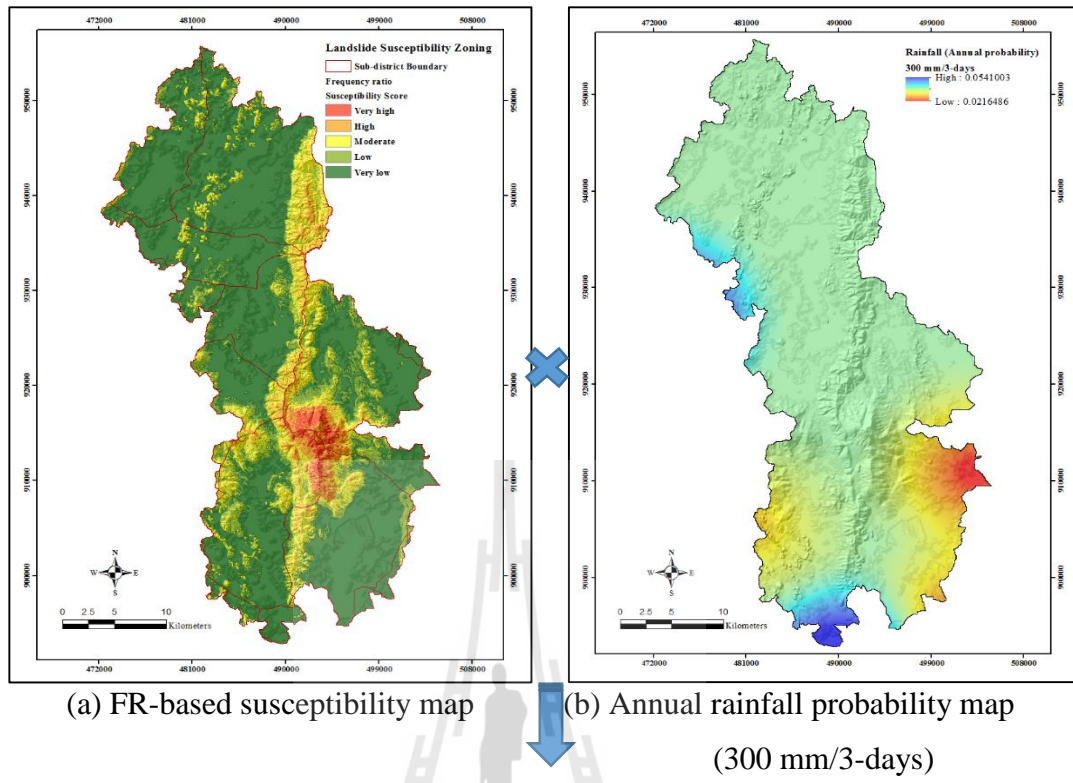


Figure 4.16b Landslide hazard map (case of critical rainfall threshold 300 mm/3-days).

Table 4.25 Landslide hazard classification for two cases of rainfall critical thresholds.

Landslide hazard classes	100 mm/day		300 mm/3-days	
	HI values	Area (%)	HI values	Area (%)
Very low hazard (VLH)			0.02 – 0.36	67.86
Low hazard (LH)	0.30 – 3.55	66.06	0.36 – 0.69	13.27
Moderate hazard (MH)	3.55 – 6.80	12.53	0.69 – 1.02	12.54
High hazard (HH)	6.80 – 10.05	11.80	1.02 – 1.34	5.05
Very high hazard (VHH)	10.05 – 13.30	8.29	1.34 – 1.67	1.28
	13.30 – 16.55	1.31		

4.4.2 Construction and evaluation of the landslide risk maps

Commonly, landslide hazard might put some valued components within the area at various degree of risk, depending on their natural vulnerability to the exposed hazard. In this work, the landslide risk maps for five crucial element-at-risk groups of the area (i.e., building, paddy field, field crops, horticulture, and para rubber) were established qualitatively for the two investigated cases of the rainfall thresholds reported earlier (in Figures 4.16a and b). The vulnerability degree of these elements was judged from their estimated economic value per given unit by the responsible government agency (mainly for compensation purpose) in the form of normalized vulnerability score (NVS) ranging from 0.1 to 0.9 as detailed in Table 4.26 and Figure 4.17. The utilized transformation formula was similar to that described in Eq. (3.2). Then, the corresponding risk map for each case was constructed from the following definition of the risk index (pixel-based):

$$\text{Risk index (RkI)} = \text{HI} \times \text{NVS}. \quad (3.5)$$

And, as usual, the equal-interval classifying method was used to categorize the obtained RkI data on the map into five different zones from very low to very high and results are as illustrated in Figure 4.18 and Table 4.27.

Table 4.26 Normalized vulnerability score (NVS) of each considered element at risk.

Element at risk	Subsidy rate	NVS
(1) Building	30,000 baht/unit	0.9000
(2) Para rubber	6,007 baht/rai	0.2355
(3) Horticulture	1,690 baht/rai	0.1160
(4) Field crop	1,148 baht/rai	0.1010
(5) Paddy field	1,113 baht/rai	0.1000

Source: Management's guide to disaster assistance in agriculture.

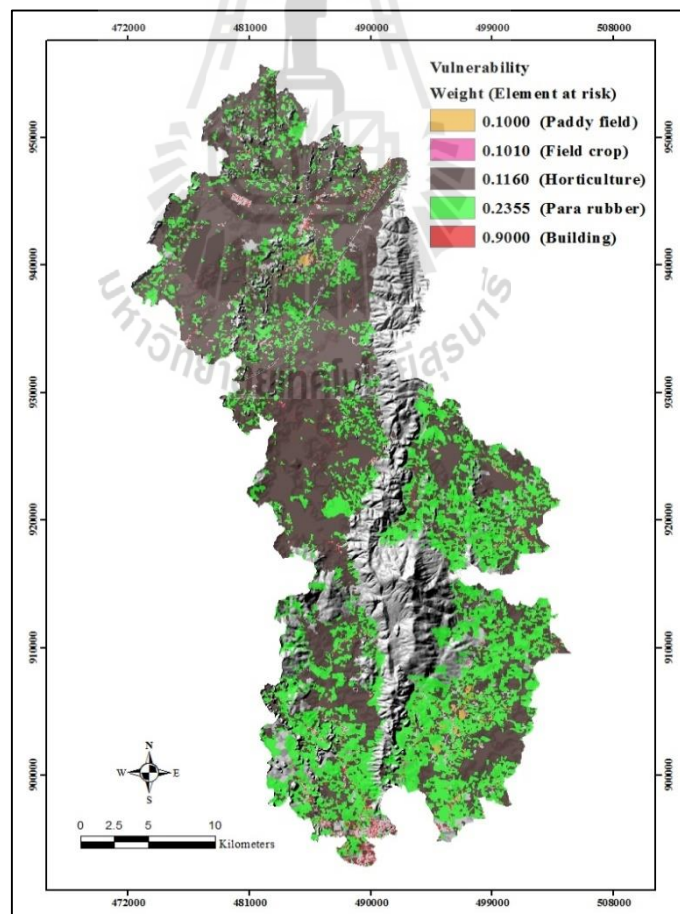


Figure 4.17 Normalized vulnerability score map of all examined element at risks.

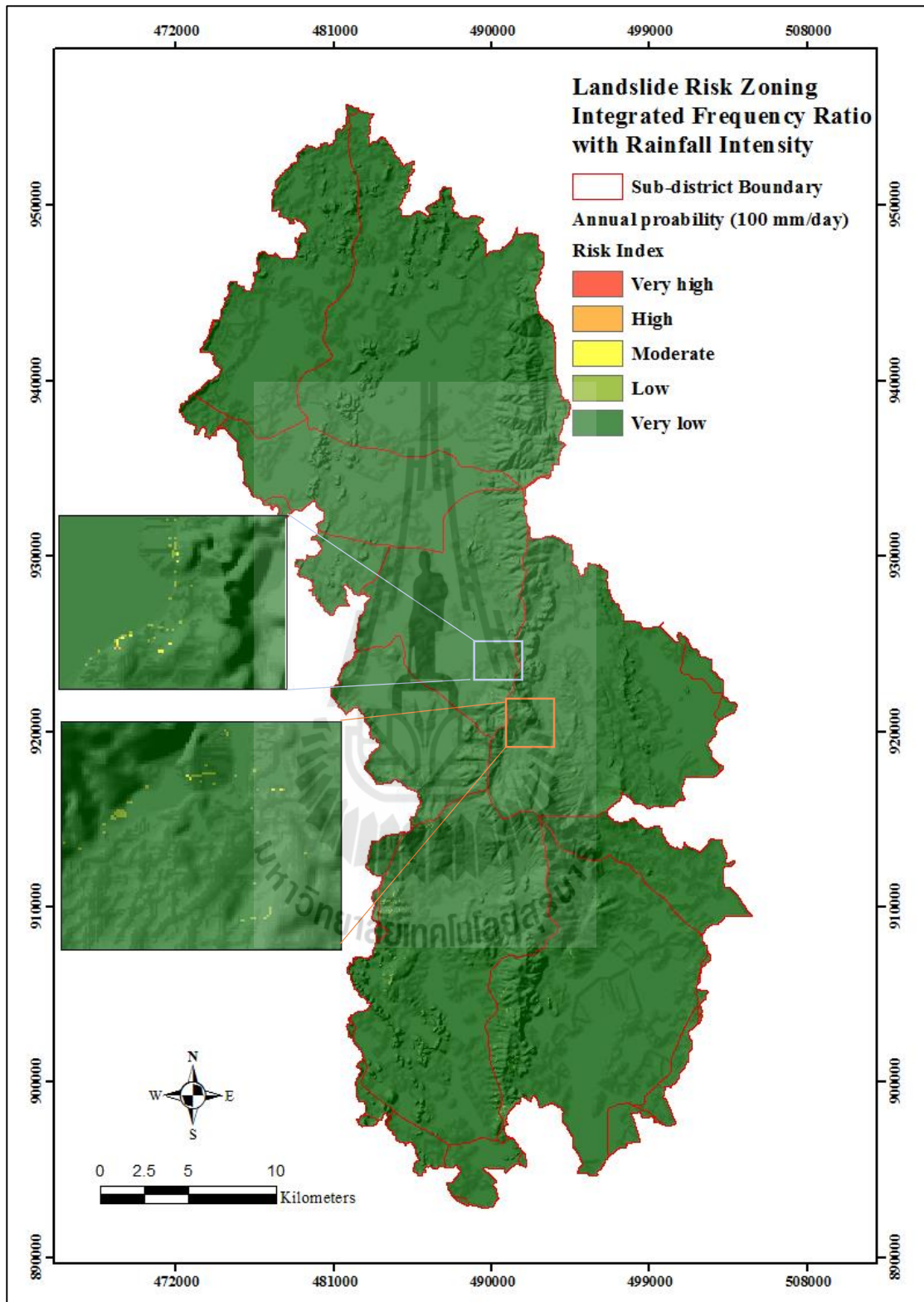


Figure 4.18a Landslide risk map (case of critical rainfall threshold 100 mm/day).

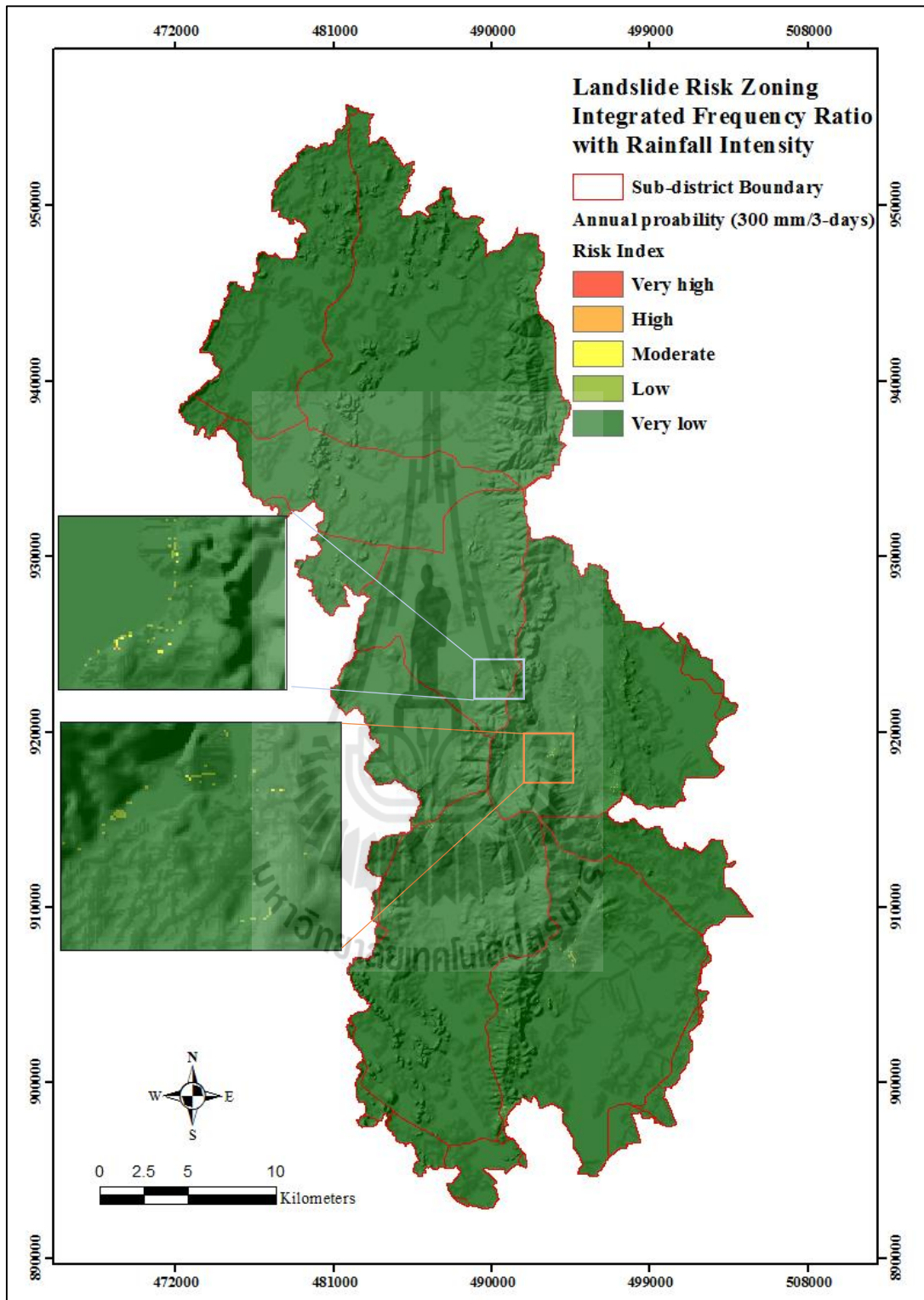


Figure 4.18b Landslide risk map (case of critical rainfall threshold 300 mm/3-days).

Table 4.27 Landslide risk classification for two cases of rainfall critical thresholds.

Landslide risk classes	100 mm/day			300 mm/3-days		
	RI values	Area (%)	Area (km ²)	RI values	Area (%)	Area (km ²)
Very low risk (VLR)			984.1392			983.3679
Low risk (LR)	0.00 – 2.29	99.6566	3.2184	0.00 – 0.20	99.5785	3.9348
Moderate risk (MR)	2.29 – 4.59	0.3259	0.1269	0.20 – 0.40	0.3984	0.1800
High risk (HR)	4.59 – 6.89	0.0129	0.0432	0.40 – 0.61	0.0182	0.0441
Very high risk (VHR)	6.89 – 9.19	0.0044	0.0027	0.61 – 0.81	0.0045	0.0036
	9.19 – 11.49	0.0003		0.81 – 1.02	0.0004	

Table 4.28 Distribution of classified element-at-risk land on the derived hazard map.

Element at risk	Area (%): 100 mm/day					Area (%): 300 mm/3-days				
	VLH	LH	MH	HH	VHH	VLH	LH	MH	HH	VHH
(1) Building	95.12	4.39	0.47	0.02	0.00	96.45	3.27	0.26	0.01	0.00
(2) Para rubber	78.53	17.34	3.89	0.24	0.00	80.66	16.74	2.57	0.03	0.00
(3) Horticulture	89.14	9.74	1.09	0.03	0.00	91.10	8.25	0.64	0.01	0.00
(4) Field crop	100.00	0.00	0.00	0.00	0.00	100.00	0.00	0.00	0.00	0.00
(5) Paddy field	100.00	0.00	0.00	0.00	0.00	100.00	0.00	0.00	0.00	0.00

In principle, landslide risk map at medium-scale is specifically preferred to aid the development planning and emergency response planning in respect to the incidence (Michael-Leiba, Baynes, Scott, and Granger, 2003). However, the eventual risk maps resulted in this work for both cases of the referred rainfall threshold were found to have only about 0.005% of the total area with high to very high risk while about 99.9% were located in the very low risk zone. This outcome of the map derivation is understandable as the most at-risk element in this case (building) covered only small portion of the total land (Table 3.8) while other considered at-risk elements (para rubber, horticulture, field crop, and paddy field) were having relatively low priority and distributing principally on the low to very low hazard areas (Table 4.28). In this circumstance, these yielded maps seem to have low practical benefit to accommodate

the aforementioned tasks as most at-risk elements were found situating in the low to very low hazard zones which finally led to the very low risk outcome as reported earlier.

Therefore, to make this thesis work more applicable in the effective preparation of landslide warning and mitigation programs in the area, associated landslide hazard due to the potential runout originating from landslide incidence upstream was evaluated using the FLOW-R model and results are to be reported in the following section.

4.5 Runout hazard analysis

As landslide-induced debris flow runout has frequently become a major source of huge losses evidenced worldwide, including within the chosen study area, therefore, prediction of its strength (especially, velocity and runout distance) to reduce such losses is very necessary. In this work, the runout hazard resulted from the landslide incidences upstream over the study area was evaluated and mapped numerically using the popular Flow-R model as detailed in Chapter II and III wherein the appropriated flow characters and deposition outcome were determined and presented as a runout hazard map for the area. This map was classified (using equal interval technique) to represent five groups of the runout-related hazard level, from the very low to very high as seen in Figure 4.19 (for the entire study area) and Figures 4.20a-f.

From these maps, it is rather clear that the highly-concerned areas with high to very high hazard level identified were usually located along the main drainage channels with peak hazard shown in mid-stream portion. And the hazard seemed to gradually drop with distance towards the downstream zone due to the reduced water speed from runout expansion over gentle terrain and the strong deposition of the carried debris material.

Eventually, as reported in Table 4.29, about 80% of the area was associated with very low to low hazard level while about 9% was possessing the high to very high level one. In terms of risk analysis, the highest priority in runout risk mitigation should be placed upon the safety of local residences living in the high-risk houses or building in the area. In this regards, the distribution of houses on the hazard-classified land was assessed and result is reported in Table 4.29 from which nine of them were found staying on the high to very high runout hazard zone.

Table 4.29 Distribution of land on classified runout-induced hazard map.

Runout hazard classes	Runout index values	Area		Number of houses	
		%	km ²	Number	%
Very low hazard (VLH)	0.00 – 758.80	54.44	5.48	23	37.70
Low hazard (LH)	758.80 – 1517.62	25.08	2.53	16	26.23
Moderate hazard (MH)	1517.62 – 2276.42	11.75	1.18	11	18.03
High hazard (HH)	2276.42 – 3035.22	5.37	0.54	9	14.75
Very high hazard (VHH)	3035.22 – 3794.04	3.36	0.34	2	3.28

To demonstrate applicability of this formulated runout hazard map on the study of actual runout incidences within the area, the close-up maps over some specific parts of the area at subdistrict level are presented in Figures 4.21a-f, which are, the Nakhao, Thapprik, Khlonghin, Khaophanom, and Krabinoi subdistricts. These stated places were reported to experience serious danger from the runout hazard during the 2011 landslide episode which resulted in 10 deaths and 58 houses destroyed (DMR, 2011). In this study, the high-resolution satellite images of the 2011 landslide and runout traces from THEOS and Google map resources are also presented as a background for further comparison with the derived runout hazard map.

In general, from the generated runout hazard maps, the top two subdistricts with the most severe impact from the runout hazard identified were found to be the Nakhao and Thapprik respectively, while the others did not find such serious hazard prediction much. And also, the used Flow- R model seemed to be able to produce the runout hazard map that conform rather well with the actual runout evidences (along the main drainage channels) and their apparent deposit downstream which were visually identified on the high-resolution satellite imagery (THEOS and Google map). As such, capability of this hazard map on runout warning purpose should be explored in more details in the future.



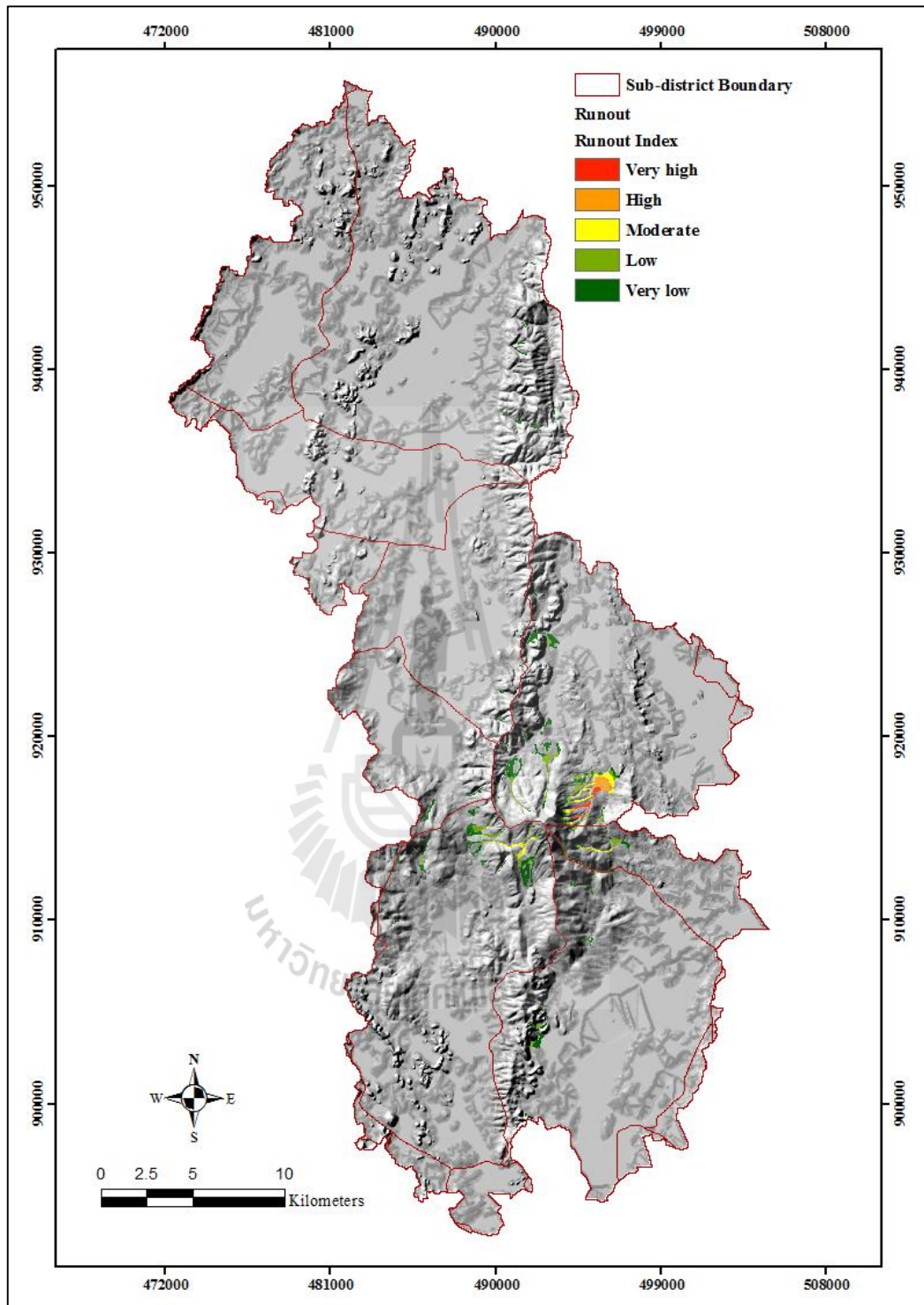


Figure 4.19 Runout hazard map based on hill-shad showing qualitative information on the runout spreading probabilities by the Flow-R model.

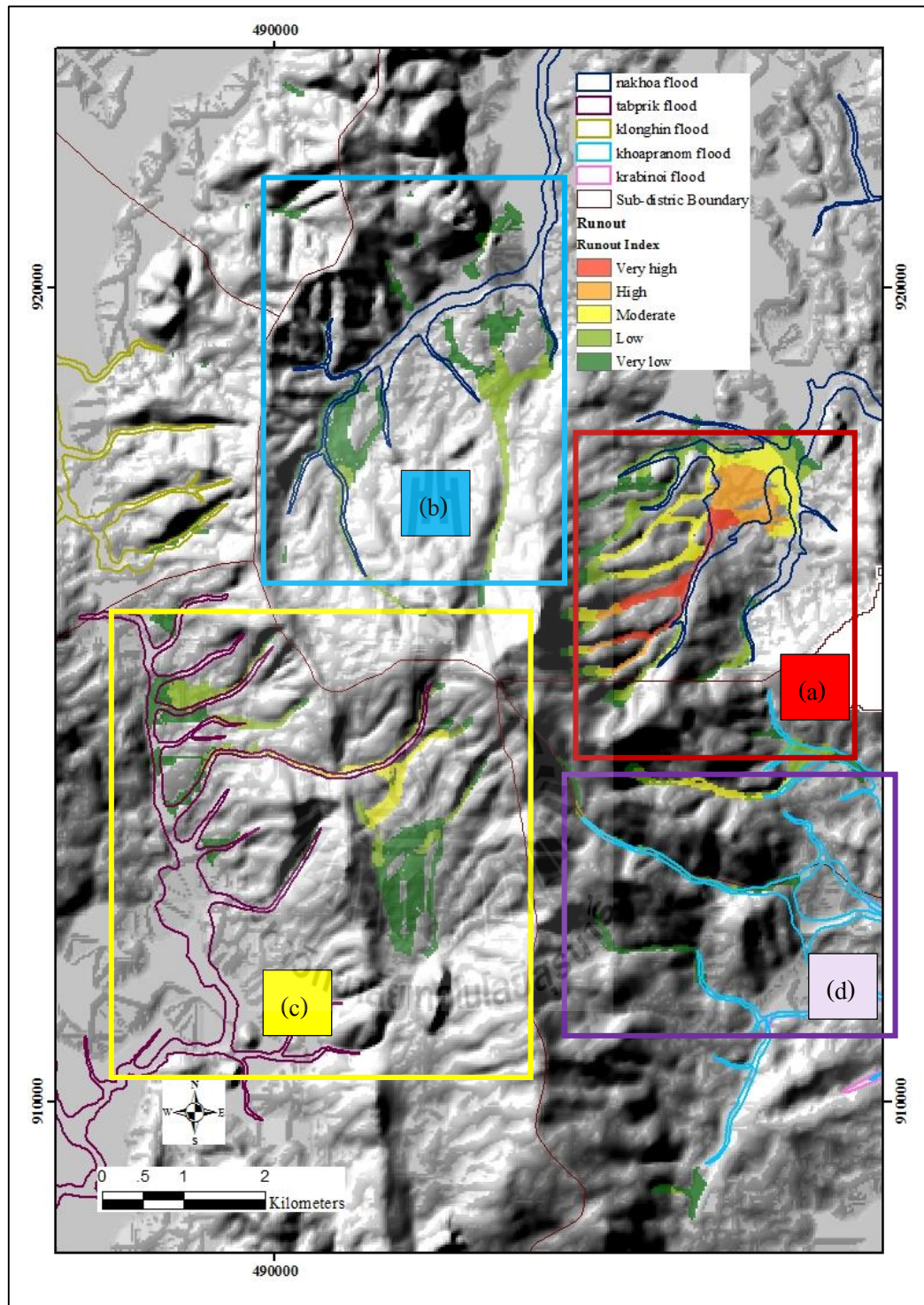


Figure 4.20a A closer look over some specific parts on the yielded runout hazard map of the area (subdistrict-level). The high-resolution satellite images of the 2011 landslide incidences from THEOS and Google map resources are also presented as background.

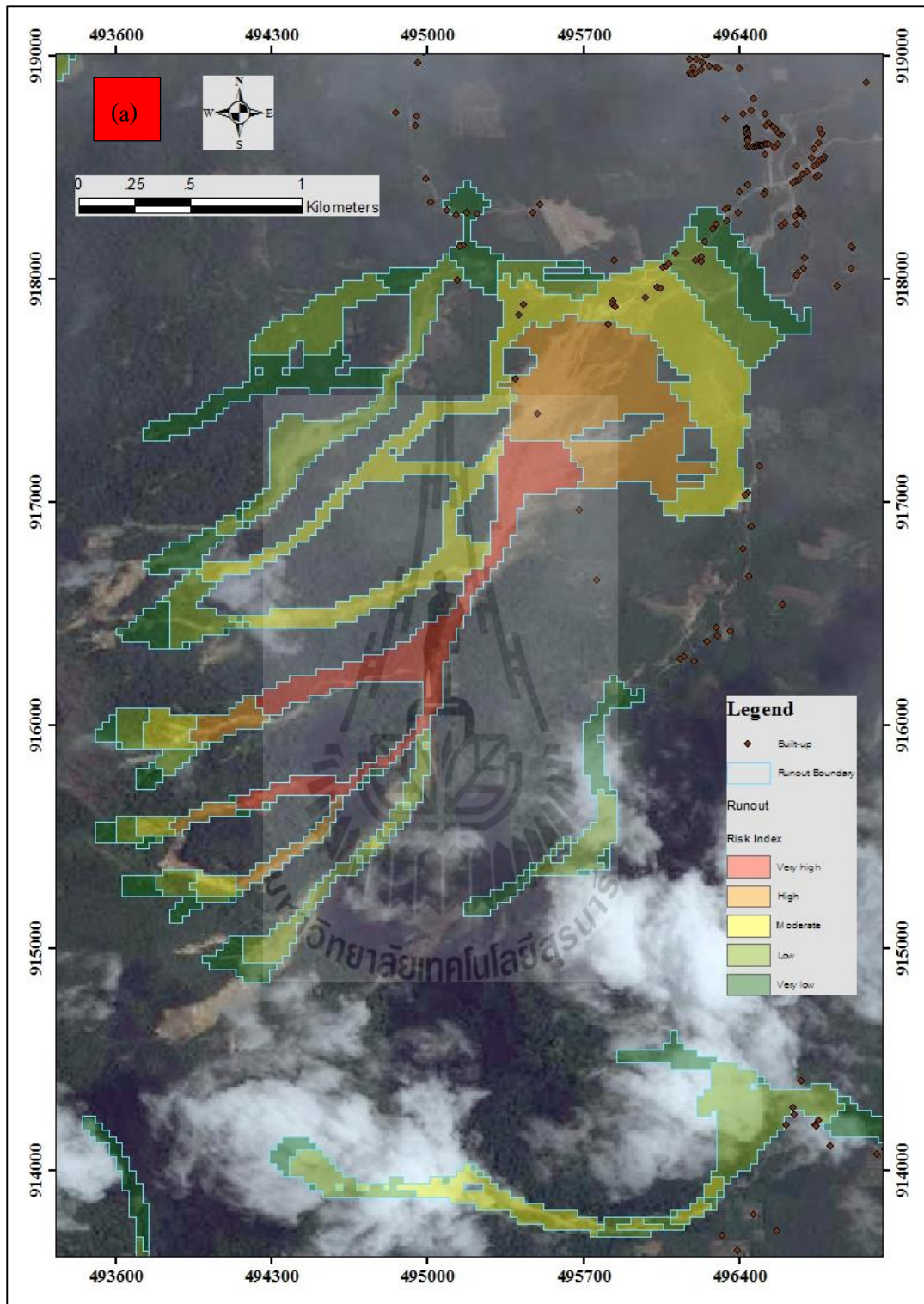


Figure 4.20b A case of Nakhao subdistrict.



Source: <http://www.bloggang.com>

Figure 4.20b Evidences at Ban Ton Han village (Continued).

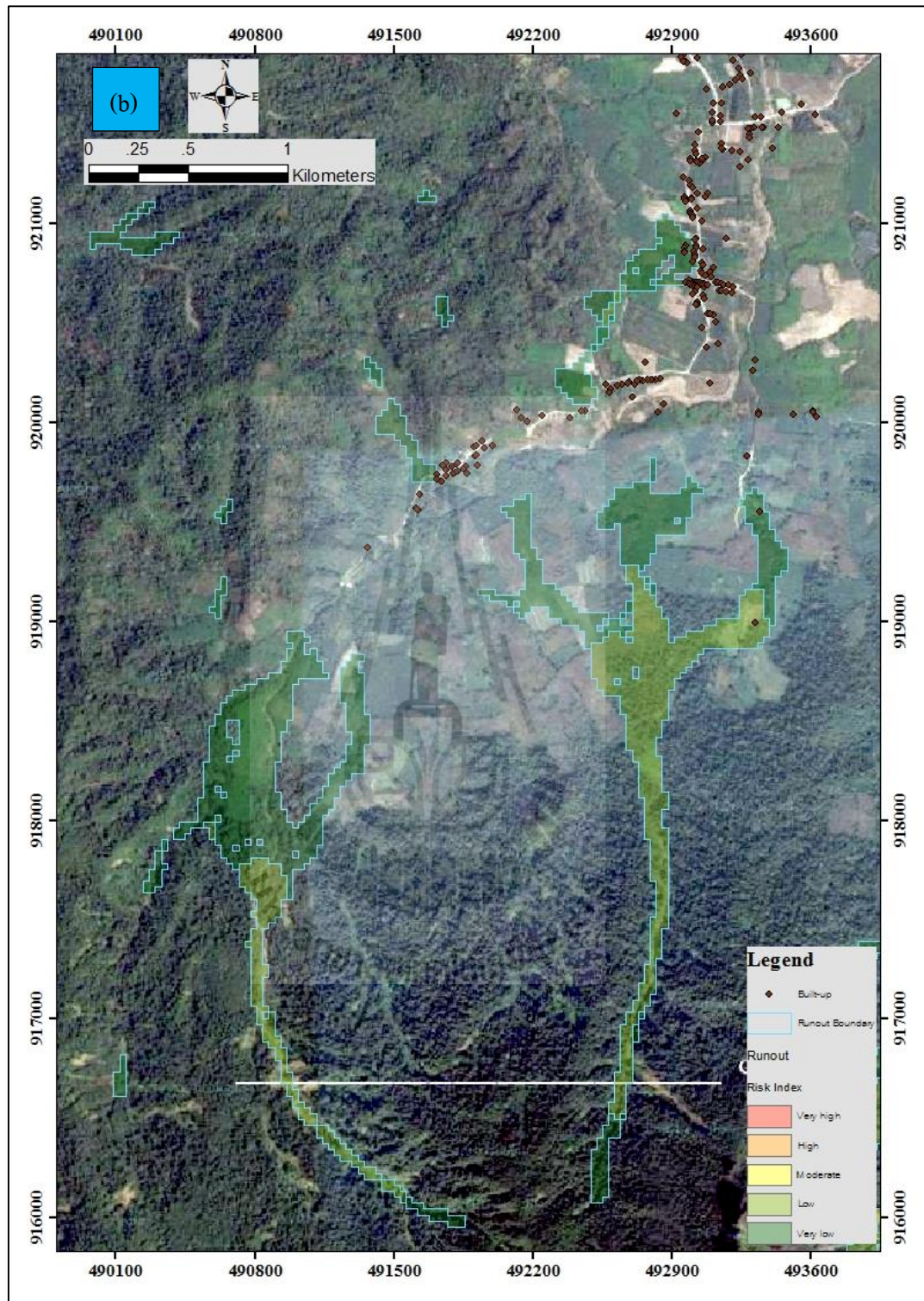


Figure 4.20c A case of Nakhao subdistrict.



Source: <https://pongphun.wordpress.com/2011/04/01>

Figure 4.20c Evidences at Ban Huay Nam Kaew village (Continued).

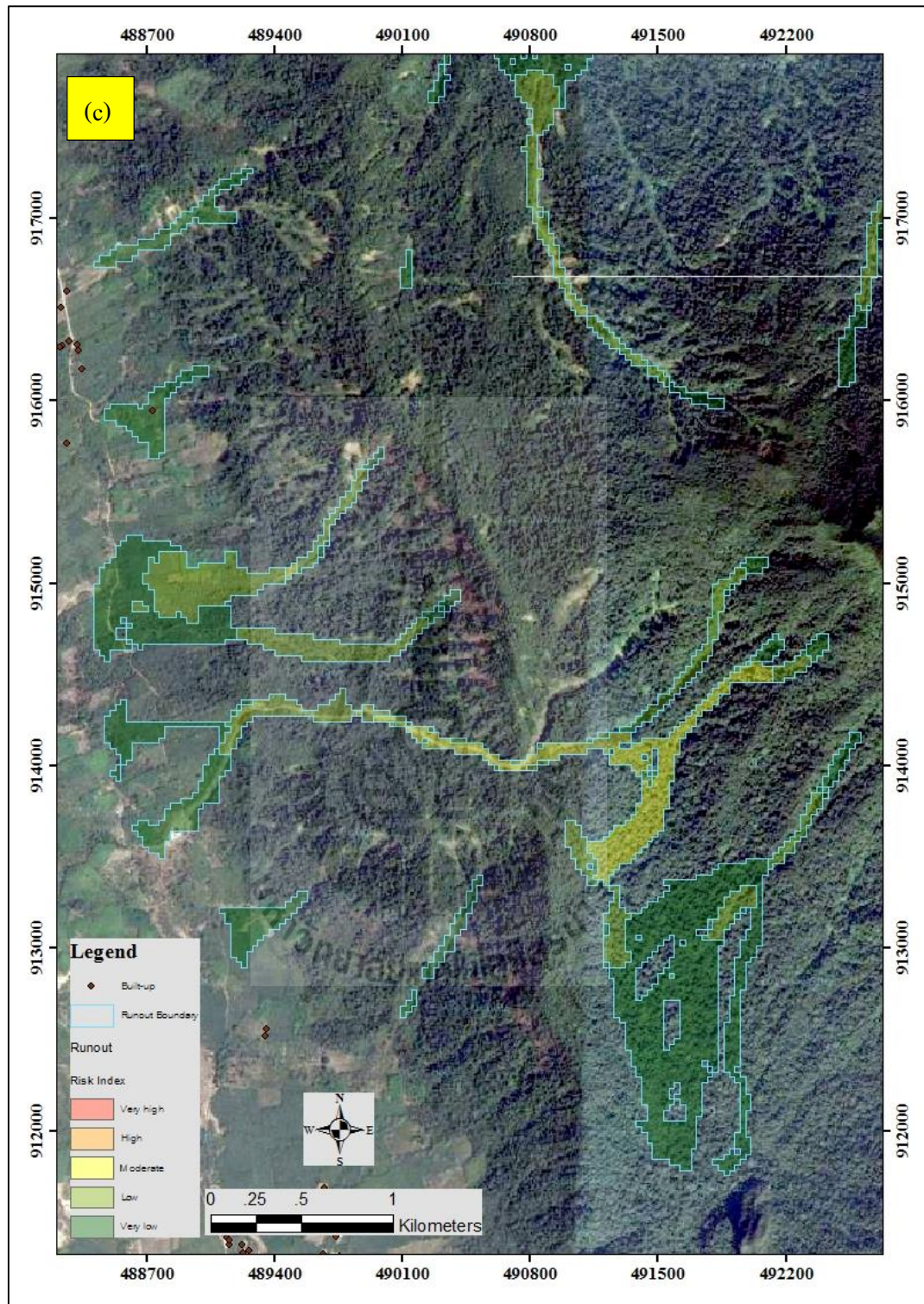


Figure 4.20d A case of Thapprik and Klonghin subdistrict.



Source: <http://www.krobkruakao.com>

Figure 4.20d Evidences at Ban Chong Mai Dam village (Continued).



Source: <http://www.numthang.org>

Figure 4.20d Evidences at Ban Huay Toh village (Continued).

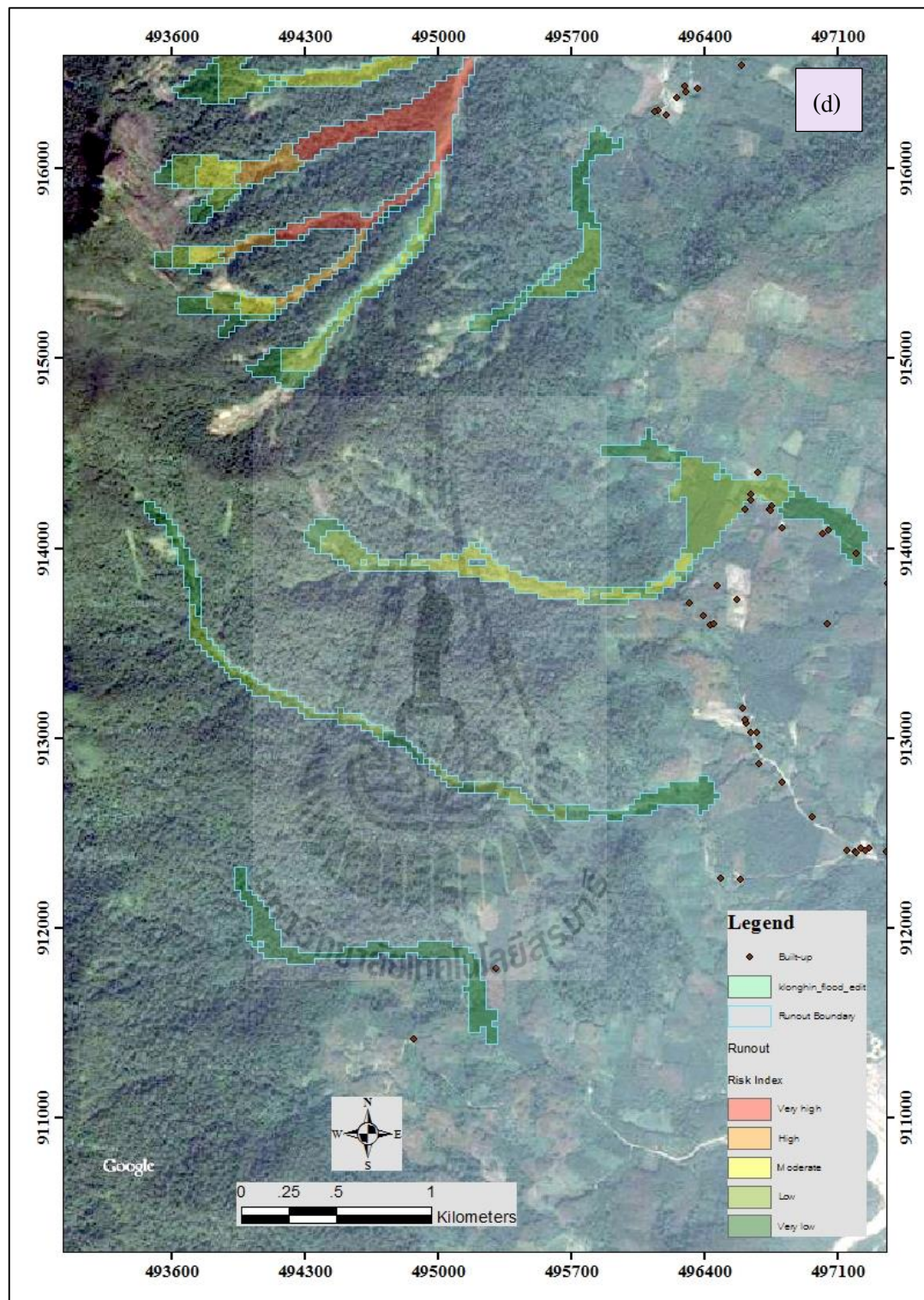


Figure 4.21e A case of Khaophanom subdistrict.



Source: <https://www.gotoknow.org/posts/440202>

Figure 4.21e Evidences at Ban Klong Hang village (Continued).

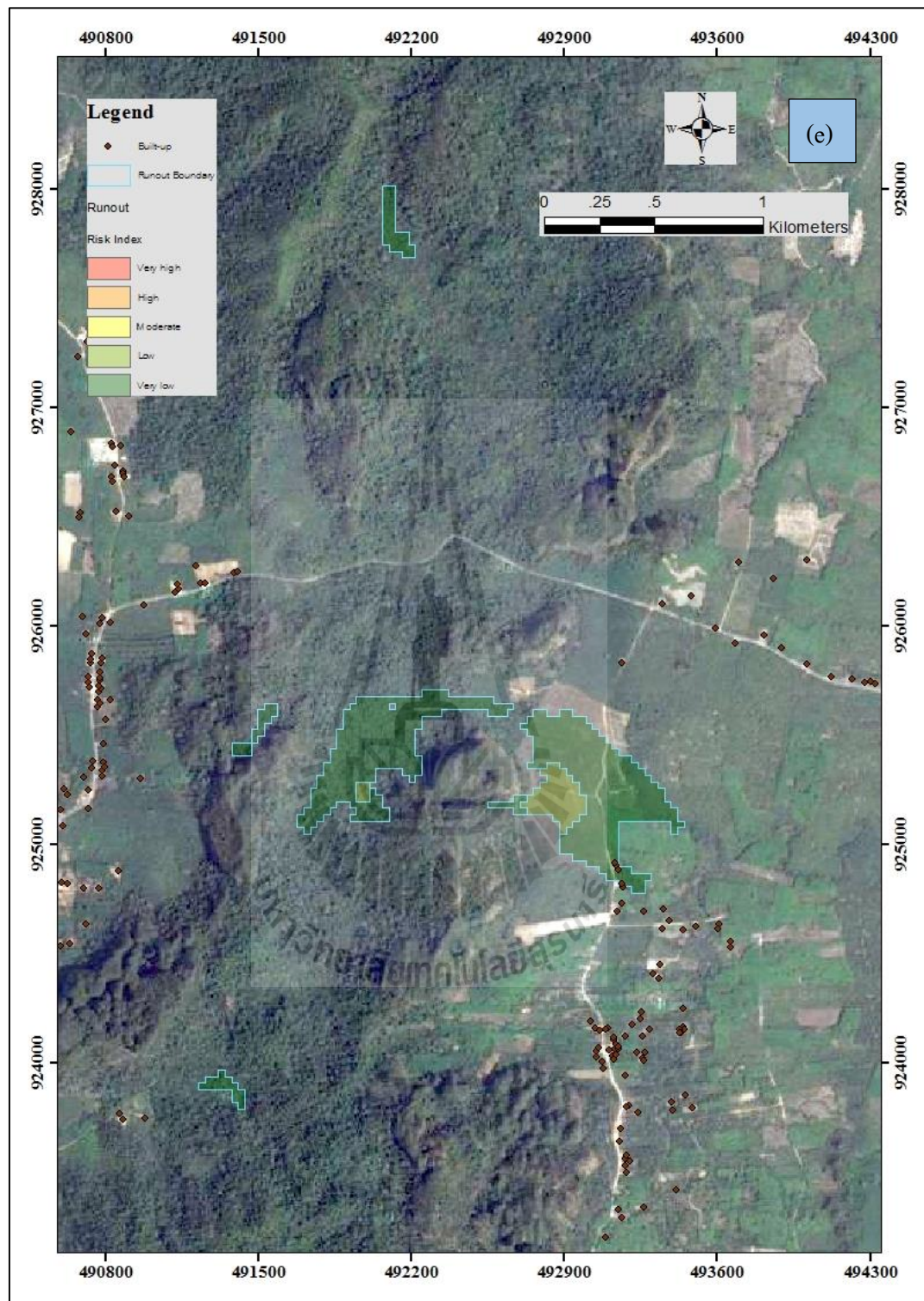


Figure 4.21f A case of Krabinoi subdistrict.

CHAPTER V

CONCLUSION AND RECOMMENDATION

This chapter summarizes the achievements of all works carried out in this thesis in accordance with the three objectives outlined in Chapter I, which are, (1) to identify optimal method to aid the formulation of landslide susceptibility map for the study area from a list of seven candidates, (2) to construct the associated landslide hazard and risk maps for the referred area through application of the optimal method identified earlier, and (3) to generate landslide-induced runout hazard zones for the examined area based on results obtained from the empirical Flow-R runout model. The overall achievements of each objective stated above are conclusively detailed as follows.

5.1 Landslide susceptibility maps formulation and evaluation

In this thesis work, the Khao Phanom Bencha Watershed in Krabi Province was chosen as a study area due to its frequent occurrences of devastated landslides and their severe debris flow consequences in recent decades. Seven well-acknowledged methods were included as candidates in the preparation of most accurate landslide susceptibility maps for the study area, including, (1) weighted linear combination (WLC), (2) analytical hierarchy process (AHP), (3) frequency ratio (FR), (4) integrated FR-fuzzy, (5) multiple logistic regression (MLR), (6) artificial neural network (ANN), and (7) integrated ANN-fuzzy. Ten contributing factors were incorporated as input dataset for

the determination of probability of landslide occurrences over entire area by each applied model whereas a total of 700 identified landslide locations were used as a reference for map production (490 samples) and validation (210 samples) purposes.

5.1.1 Factor priority analysis

It was found that, in terms of the factor preference, both qualitative-type methods (WLC and AHP) placed highest weights on the slope gradient, lithology, and soil texture while elevation and slope aspect were among the least favorite ones. And at attribute level, both stated methods considered high elevation, steep slope, close distance to lineament and drainage, high TWI, westward slope facing, and igneous-rock structure, as most effective landslide indicators in the area. For the LULC case, para rubber and oil palm plantations were judged as topmost landslide indicators in this category while dense evergreen forest attained relatively low priority one. In general, the appeared orders of preference at both factor and attribute levels (with respect to their affixed weights) did conform rather well to the prevalent beliefs on this issue found in most mainstream literature.

However, for the quantitative-type methods, which made a prediction of landslide occurring probability based on evidences of past landslide events observed within the area, the weight-based order of priority (both at factor and attribute levels) did vary from model to model, and sometimes not in a strong agreement with those of the qualitative-type ones, due crucially to the differences in main working concept of weight assessment process. For examples, for the FR method, some specific attributes were outstandingly valued with high FR score, e.g. (with $FR > 3.0$), elevation ≥ 400 meters, slope gradient at 20° - 40° range, TWI of 2.5-5.0, igneous-rock basis, and slope-complex area condition. However, for the LULC category, on the contrary to what

found in the WLC and AHP analysis, highest weight was seen at dense evergreen forest, with FR of 3.98, while those of the oil palm and para rubber were in much less favor, with FR of 0.04 and 1.13, respectively. This contradiction seemed to highlight the importance of method type in use as the FR based its analysis on number of actual landslide locations in which about 94.90% were found in this forest class.

For the MLR method, associated weights were quantified for 30 layers of the input data, including 7 layers at factor level for the numerical type and 23 layers at attribute level for the categorical type (i.e., lithology, soil texture, and LULC), and expressed in the form of coefficient for each used parameter. In principle, positive coefficients indicate positive correlation between that parameter and probability of landslide occurrence over an area while the negative ones signify the opposite outcome. Accomplished results from work in this case revealed strong positive impact of several well-known contributing factors and attributes referred to earlier, e.g. elevation, slope gradient, distance from lineament, igneous-rock basis, slope complex area condition, while the noble negative influencing ones were slope curvature, TWI, clay/clay-loam soil type, distance from drainage, quaternary sediments or saibon formation of bedrock. And for the LULC category, weak positive influences were expressed for dense evergreen forest, oil palm, and para-rubber plantations, which is rather contrary to that suggested by the FR model (in case of dense evergreen forest).

Similar to the MLR method, the ANN model in use tried to assess appropriate weights for all 30 layers of input data based on the found complex relationship of these parameters that could explain the occurrences of past landslide event within the area. Here, a three-layer ANN system consisting of one input layer (30 neurons), one hidden layer (16 neurons) and one output layer was adopted to

accomplish this task. Regarding to the apparent normalized weights (0 to 1) of these parameters, elevation and slope curvature were found having top priority with weights of 0.1856 and 0.1710. For lithology, saibon formation type was most valued with weight of 0.0543 while that of igneous rocks stood at just 0.0171 which was somewhat different from results discovered in most aforementioned methods. Strong role of slope gradient and the distance from drainage were also noticed with relatively high weights of 0.1407 and 0.0479.

5.1.2 Susceptibility map comparison and evaluation

The susceptibility maps were produced as an end product by each listed method wherein five levels of landslide susceptibility were mapped based on the equal-interval classifying technique (from very low to very high). In general, all yielded maps indicated that lands with high susceptibility were located along the Khao Phanom Bencha mountain network mostly where peak values appeared around the summit region of the mountain range in the upper southern portion of the area. However, associated data of the classified land on each map expressed obvious distinctions in the predominant characteristics of map product from which some methods tended to favor low to very-low susceptibility outcome, i.e., AHP, FR, FR-Fuzzy, MLR, ANN, ANN-Fuzzy, but some showed the more moderate outcome one, i.e., WLC, AHP, and some generated noticeably high portion of land with high to very high susceptibility level, e.g., WLC (17.49%), and MLR (16.59%). In addition, the correlation level (r) of the NSS data among all examined methods was also determined from which prominently high correlation (of 0.93) between the two used qualitative-type methods (WLC and AHP) were obtained, and also among the FR-based methods (FR, FR-Fuzzy, and ANN-

Fuzzy). This mutually high conformation among them led to highly resemble map outlook as well as distribution of classified land data outcome.

In principle, maps with relatively high proportion of high susceptibility lands might lead to an overestimation of landslide proneness within the area because high percentage of the reference landslides is likely to be correctly identified on these maps with drawback of producing many arisen false alarms (or high sensitivity but low specificity). Conversely, if the model's output map emphasizes too much on low susceptibility, they might have less false alarm occurrences but total number of the correctly-predicted landslides tend to be decreased also (or low sensitivity but high specificity).

5.1.3 Map accuracy assessment and optimal method identification

All yielded susceptibility maps were assessed for their respective accuracies in predicting the referred landslide incidences through the use of two well-known methods: the Area-Under-Curve (AUC) and the Receiver Operating Characteristic (ROC) analysis, in which, for the AUC case, accuracy product was differentiated into two distinct types called the "success rate" and "prediction rate" with respect to the difference in dataset of the reference landslides in use. In general, it was found that all applied methods were well capable of producing maps with remarkably high accuracy (mostly > 85%) in all cases regardless of the still differences in map outlook and land classification outcome. However, if consider in terms of average accuracy, the FR method seemed to perform the best in all cases under consideration which led to average accuracy of 93.98%. This was closely followed by the MLR (at 92.98%), FR-Fuzzy (at 92.84%), and ANN-Fuzzy (at 92.47%). The least successful ones evidenced here were those of both qualitative-type methods; the WLC (at 86.02%)

and the AHP (at 83.94%). However, these accomplished accuracy levels still look quite impressive under normal standard (of 80% up).

Through, the four most successful methods (FR, FR-Fuzzy, MLR, and ANN-Fuzzy) were highly comparable in terms of average accuracy, however, the FR one was eventually chosen as an optimal candidate due to its simplest structure and most comprehensible working concept, as well as on its rather realistic appearance of the achieved susceptibility map, with percentage of land for different level of susceptibility as follows: 67.31 (very low), 13.09 (low), 12.70 (moderate), 5.39 (high), and 1.51 (very high). In addition, addition of the rainfall data (long-term annual mean and short-term event-based) into the normal FR-based production of the susceptibility map yielded no appreciable merit in terms of accuracy improvement ($< 0.5\%$ change in average accuracy).

5.2 Landslide hazard and risk maps formulation and evaluation

To produce the landslide hazard map for the study area, temporal probability of landslide occurrence within the area, in terms of the annual rainfall probability (ARP) for the critical rainfall threshold (for slope failure) of 100 mm/day and 300 mm/3-days, was integrated with the FR-based susceptibility map formulated beforehand to generate the associated hazard map for the area based on the equal interval classification method and data of the computed hazard index. From the ARP maps, chances of having rainfall intensity of 100 mm/day per year over the entire area changed significantly from about 0.2 (in the southeastern part) to about 0.5 (in the southwestern part). Similarly, in case of the rainfall intensity of 300 mm/3-days, chances of the success per year were found much lower than that of the 100 mm/day case, wherein peak values of about 0.054 were

seen at the far south portion of the map and the lowest ones of about 0.022 were attained in the southeastern part. However, as most rainfall input layer possessed rather low FR values (of about 1 or lower) and the most intense ones tended to distribute over the low susceptibility part of the area, both obtained classified hazard maps were found highly resemble to that of their susceptibility counterpart in terms of both general map outlook and distribution of the classified land over the entire area.

The yielded hazard maps in both cases of the ARP mentioned earlier were then proceeded to establish the preferred landslide risk map for the area by integration with the vulnerability map derived for five groups of the element at risk (i.e., housing, paddy field, field crops, horticulture, and para rubber). Vulnerability degree for each element was judged from estimated economic value contributed by relevant government agency and expressed as normalized scores ranging from 0.1 to 0.9. Risk maps were produced from the classified risk index (RkI) over the area using equal interval method.

It was found that, on the contrary to what gained in the associated susceptibility and hazard maps, risk maps derived for both cases of the ARP contained extremely low percentage of land with high to very high risk level (about 0.005%), compared to about 6-10% in the susceptibility and hazard maps, while about 99.9% of land area belonged to the very low risk zone. This outcome stemmed from the fact that most at-risk element under consideration (housing) occupied very small portion of the total area while other at-risk elements (i.e. paddy field, field crops, horticulture, and para rubber) were having relatively low priority and distributing principally on the low to very low hazard areas. As such, the resulted hazard index tended to have extremely low values over the entire area except those locations that associated with housing utility.

5.3 Runout hazard zonation

Landslide-induced runout was also a case of interest in this study and its hazard map was produced for the study area through application of the popular Flow-R model. From this map, it was rather obvious that the highly-concerned areas with high to very high hazard level identified were usually located along the main drainage channels with peak hazard predicted at around mid-stream portion (with highest runout intensity). And the simulated hazard level (from its peak location) shall gradually decline with distance towards the downstream region due to the reduced water speed from runout expansion over gentle terrain and strong deposition of the transported debris material. Eventually, about 80% of the mapped area were identified with very low to low hazard level while about 9% were having the high to very high hazard level. In addition, the close-up maps over some specific parts of the area which experienced serious runout-induced damage during the referred 2011 landslide incidence showed rather good conformation between mapped hazard zone and the visible runout traces in the high resolution satellite images.

Figures 5.1-5.6 illustrate crucial maps to help preparing proper strategies for effective prevention or mitigation of potential landslide occurrences or their associated risk by responsible agencies and local authorities.

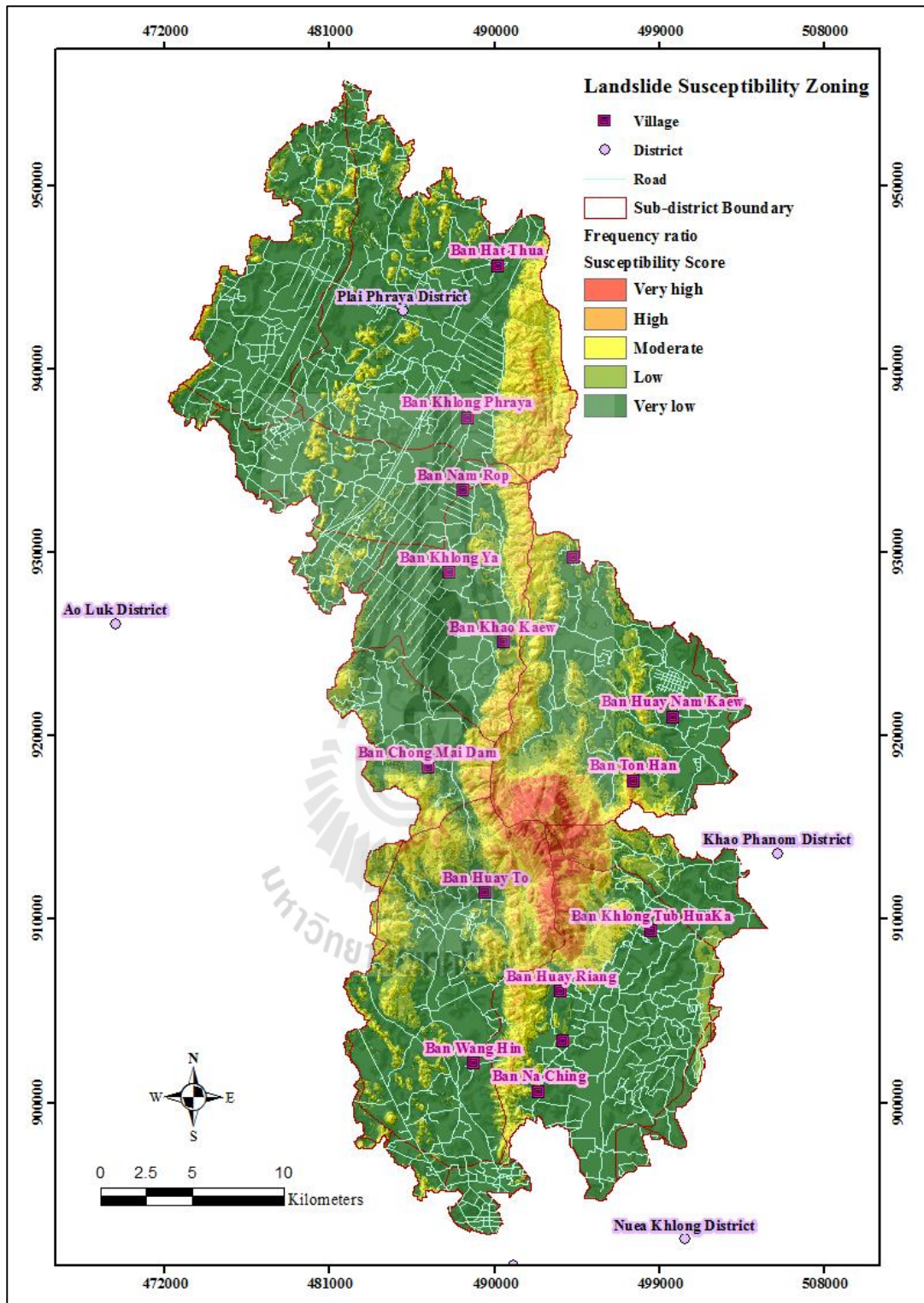


Figure 5.1 Landslide susceptibility map from the FR method.

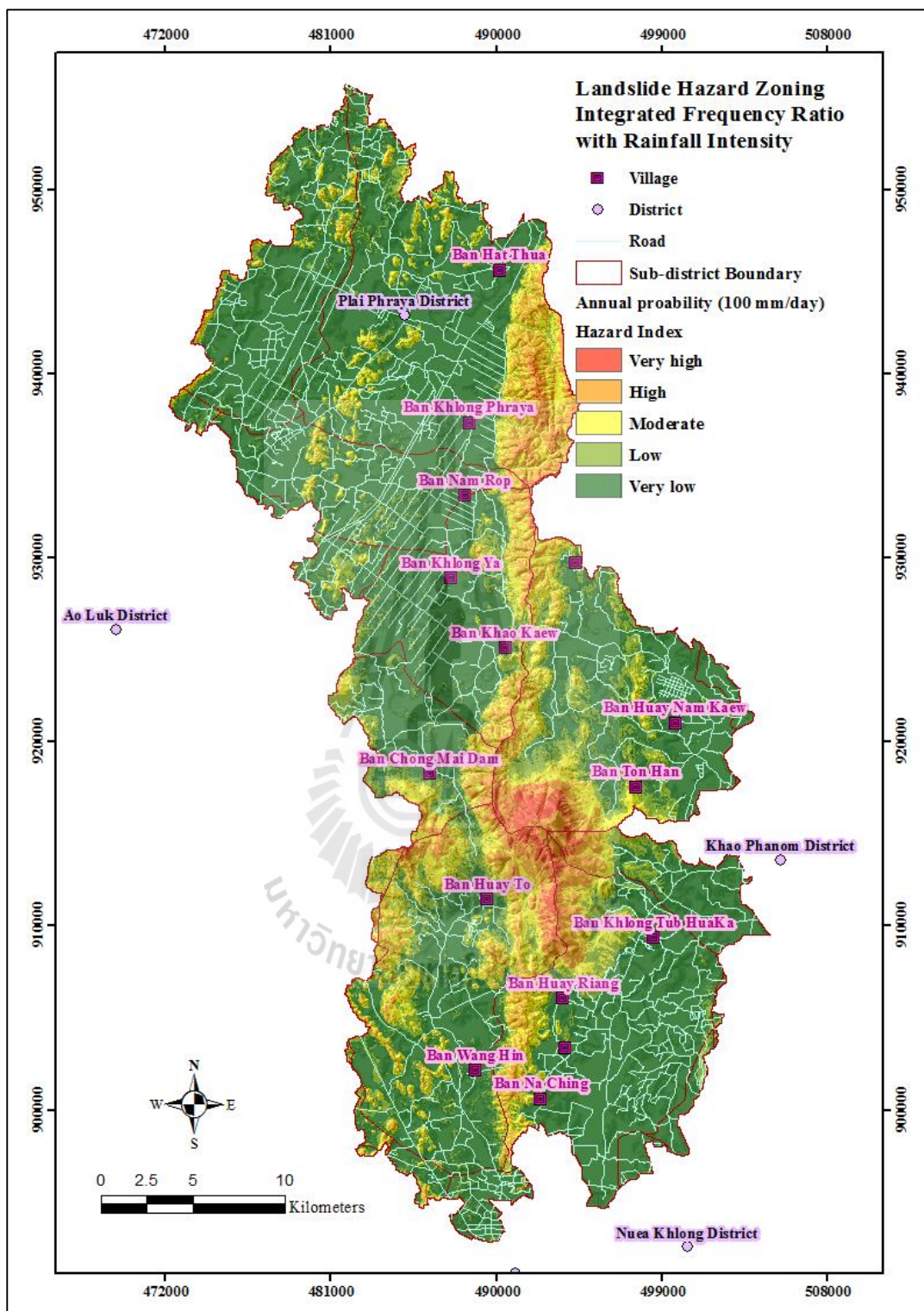


Figure 5.2 Landslide hazard map (case of critical rainfall threshold 100 mm/day).

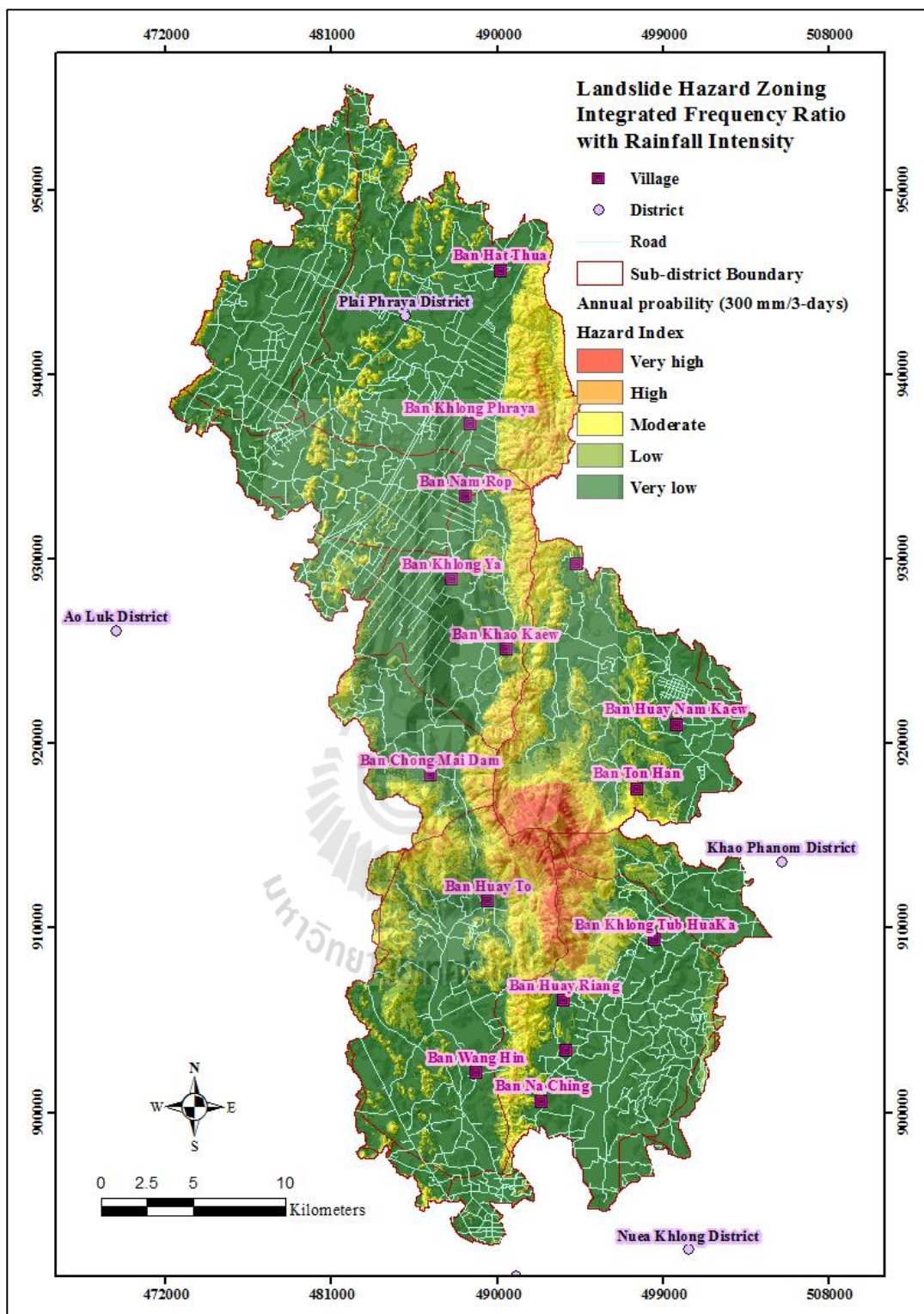


Figure 5.3 Landslide hazard map (case of critical rainfall threshold 300 mm/3-days).

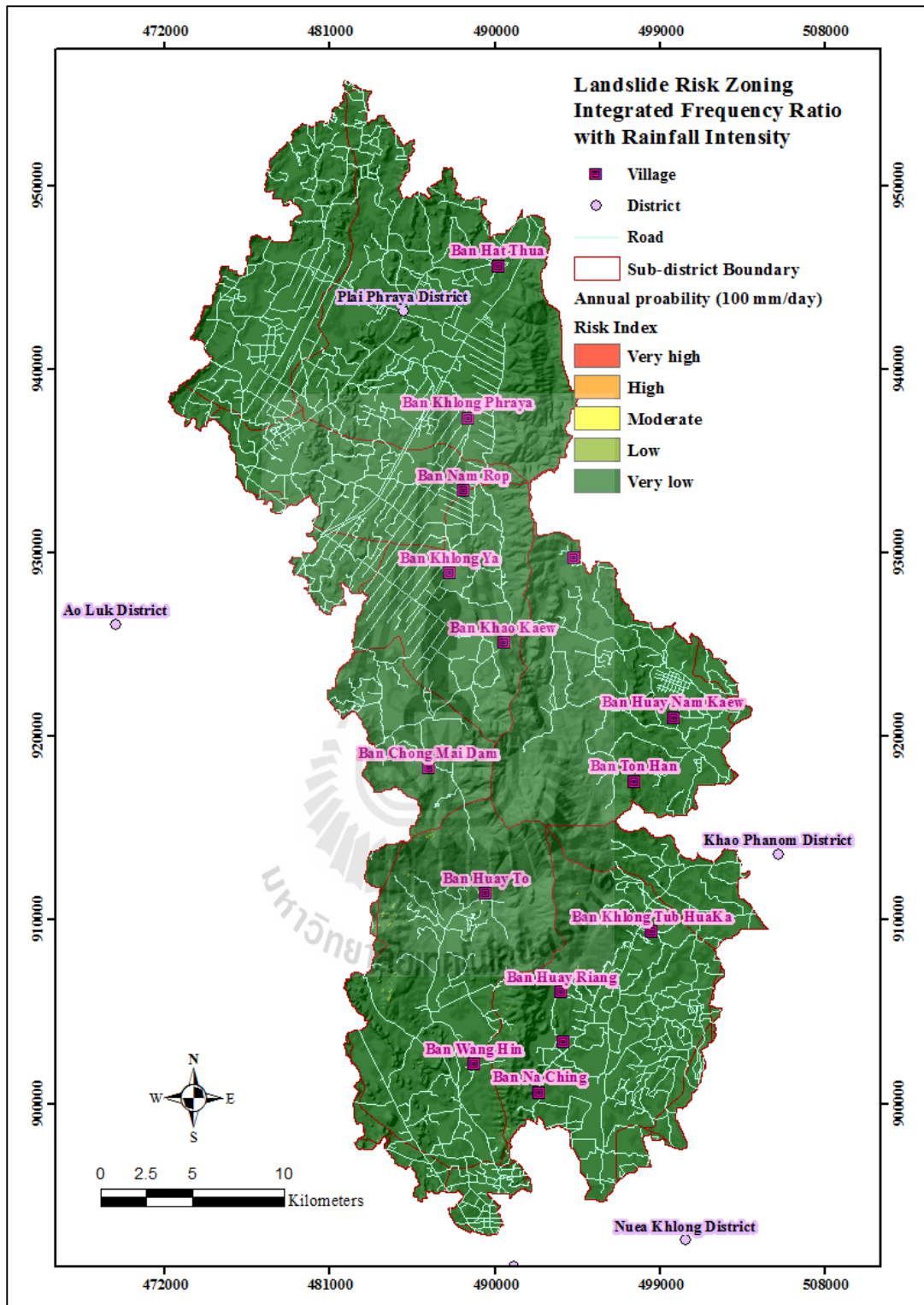


Figure 5.4 Landslide risk map (case of critical rainfall threshold 100 mm/day).

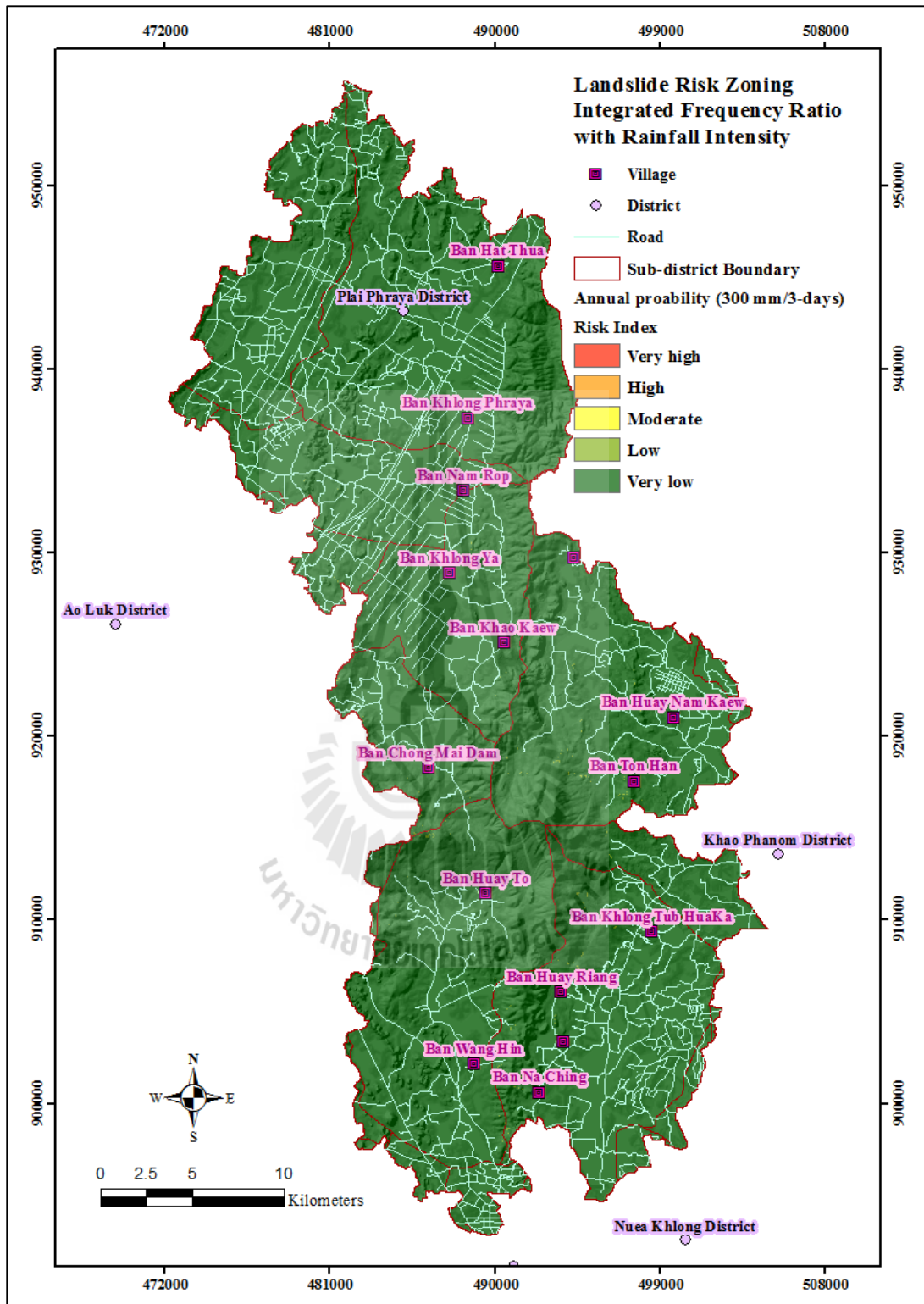


Figure 5.5 Landslide risk map (case of critical rainfall threshold 300 mm/3-days).

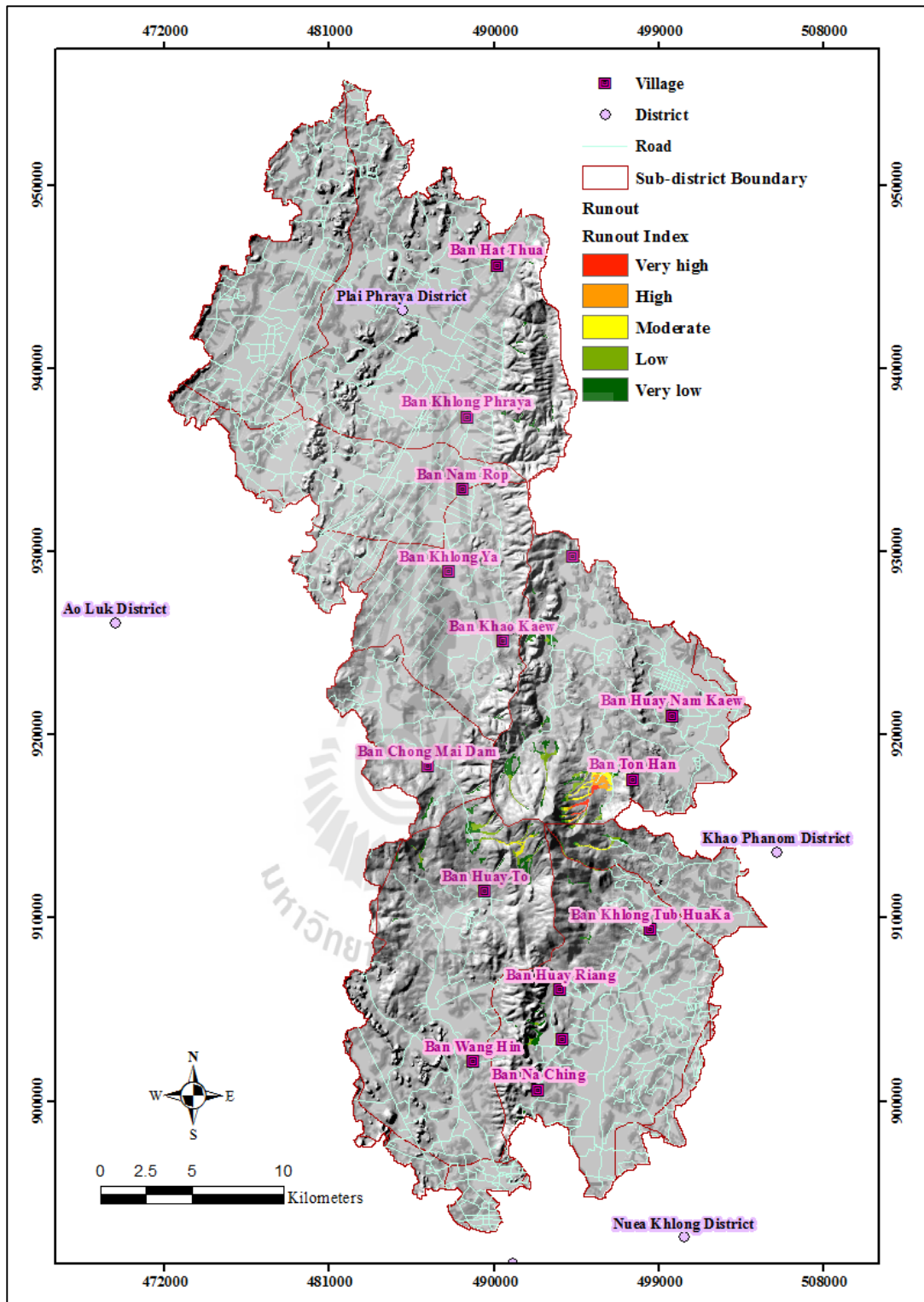


Figure 5.6 Runout hazard map based on hill-shad.

5.4 Recommendations

Though, the achievement of this study has satisfactorily fulfilled all needs stated in the prior objectives, however, several related interesting issues still worth exploring more in the future to support landslide activity assessment and associated risk reduction in Thailand and elsewhere as follows:

(1) Impact of LULC conversion on the probability of landslide occurrence under similar topological and environmental conditions (e.g. from fertile forest to crop field) which has still not been thoroughly investigated in this study.

(2) Effect of the inclusion or exclusion of initial contributing factors on accuracy of the yielded maps from other map producing method apart for the FR presented here (e.g. WLC, AHP, MLR, or ANN) to find potential best combination (if existing).

(3) Effect of classifying schemes (e.g. equal interval, equal area, natural break) on map outlook and accuracy determination.

(4) Application of the advanced runoff zonation modelling to some other hotspot landslide susceptible areas in different parts of the country.

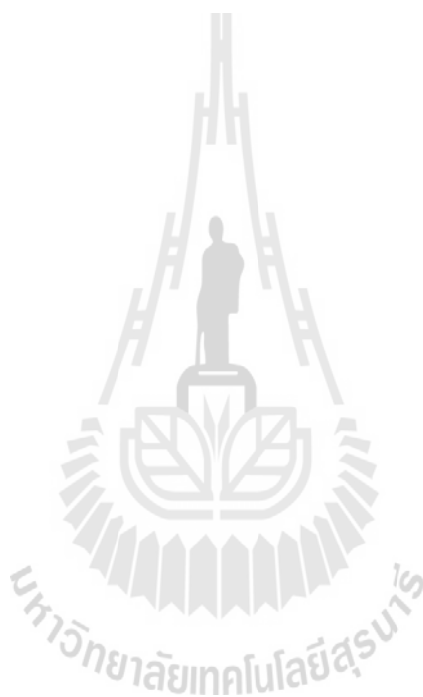
(5) Systematic and effective process to apply knowledge gained from this study in the prevention or reduction of landslide hazard and risk for local people in the area.

(6) Size and contained characteristics of the used study area should have direct effect on outcome of the mapping analysis, e.g. amount of flat terrain over an area, which needs more investigation to elucidate on this issue.

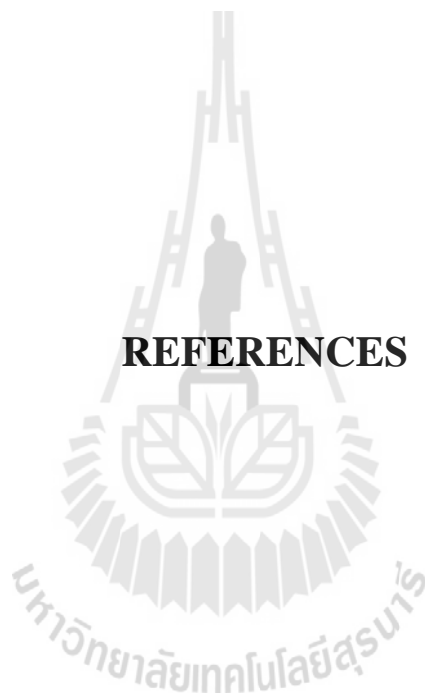
(7) Validity of the gained rainfall data should also be verified by a standard method like double mass curve analysis before putting in use.

(8) Instead of the distance from drainage system, or from the lineament, their density per unit area might be applied instead as seen in several reports to judge for

their efficiency in the mapping of landslide susceptibility over an interested area (compared to the distance-based one applied here).



REFERENCES



REFERENCES

- Abella, C.E.A. (2008). National landslide risk assessment. In: Castellanos Abella, E.A., Multi-scale landslide risk assessment in Cuba, Utrecht, Utrecht University, 2008. **ITC Dissertation**. 154: 11-42.
- Akgun, A. (2012). A comparison of landslide susceptibility maps produced by logistic regression, multi-criteria decision and likelihood ratio methods a case study at İzmir Turkey. **Landslides**. 9(1): 93-106.
- Akgun, A., Kincal, C. and Pradhan, B. (2011). Application of remote sensing data and GIS for landslide risk assessment as an environmental threat to Izmir city (west Turkey). **Environmental Monitoring and Assessment**. 184 (9): 5453-5470.
- Akkrawintawong, K., Chotikasathien, W., Daorerk, V. and Charusiri, P. (2008). GIS Application for Landslide Hazard Mapping in Phang Nga Region, Southern Thailand. In **Proceedings of the international symposium on geoscience resources and environments of Asian terranes (GREAT 2008)** Bangkok, Thailand: 4th IGCP 516, and 5th APSEG.
- Aksoy, B. and Ercanoglu, M. (2012). Landslide identification and classification by object-based image analysis and fuzzy logic: An example from the Azdavay region (Kastamonu, Turkey). **Computers & Geosciences**. 38(1): 87-98.
- Aleotti, P. and Chowdhury, R. (1999). Landslide hazard assessment: summary review and new perspectives. **Bulletin of Engineering Geology and the Environment**. 58(1): 21-44.

- Alexander, D.E. (2008). A brief survey of GIS in mass-movement studies, with reflections on theory and methods. **Geomorphology**. 94: 261-267.
- Alonso, J.A. and Lamata, M.T. (2006). Consistency in the analytic hierarchy process: a new approach. **International Journal of Uncertainty**. 14(4): 445-459.
- Asian Disaster Preparedness Center. (2006). **Rapid Assessment: Flashflood and Landslide disaster in the provinces of Uttaradit and Sukhothai, Northern Thailand, May 2006**.
- Australian Geomechanics Society (AGS). (2000). Landslide risk management concepts and guideline. **Australian Geomechanics Society**. 35(1): 49-92.
- Australian Geomechanics Society (AGS). (2007a). Guideline for Landslide Susceptibility, Hazard and Risk Zoning for Land Use Planning. **Australian Geomechanics**. 42(1): 1-36.
- Australian Geomechanics Society (AGS). (2007b). **Practice Note Guidelines for Landslide risk Management 2007** [On-line]. Available: <http://australiangeomechanics.org/admin/wp-content/uploads/2010/11/LRM2007-c.pdf>.
- Ayalew, L. and Yamagishi, H. (2005). The application of GIS-based logistic regression for landslide susceptibility mapping in the Kakuda-Yahiko Mountains, Central Japan. **Geomorphology**. 65: 15-31.
- Ayalew, L., Yamagishi, H., Marui, H. and Kanno, T. (2005). Landslides in Sado Island of Japan: Part II. GIS-based susceptibility mapping with comparisons of results from two methods and verifications. **Engineering Geology**. 81(4): 432-445.

- Bachri, S. and Shresta, R.P. (2010). Landslide hazard assessment using analytic hierarchy processing (AHP) and geographic information system in Kaligesing mountain area of Central Java Province Indonesia. In **5th Annual International Workshop & Expo on Sumatra Tsunami Disaster & Recovery 2010**.
- Bagherzadeh, A. and Daneshvar, M.R.M. (2012). Mapping of landslide hazard zonation using GIS at Golestan watershed, northeast of Iran. **Arabian Journal of Geosciences**. 6(9): 3377-3388.
- Bai, S., Lü, G., Wang, J., Zhou, P. and Ding, L. (2011). GIS-based rare events logistic regression for landslide-susceptibility mapping of Lianyungang, China. **Environmental Earth Sciences**. 62(1): 139-149.
- Bai, S.B., Wang, J., Lü, G.N., Zhou, P.G., Hou, S.S. and Xu, S.N. (2010). GIS-based logistic regression for landslide susceptibility mapping of the Zhongxian segment in the Three Gorges area, China. **Geomorphology**. 115: 23-31.
- Ballabio, C. and Sterlacchini, S. (2012). Support Vector Machines for Landslide Susceptibility Mapping: The Staffora River Basin Case Study, Italy. **Mathematical Geosciences**. 44(1): 47-70.
- Basheer, I.A. and Hajmeer, M. (2000). Artificial neural networks: fundamentals, computing, design, and application. **Journal of Microbiological Methods**. 43(1): 3-31.
- Biswajeet, P. and Saro, L. (2007). Utilization of Optical Remote Sensing Data and GIS Tools for Regional Landslide Hazard Analysis Using an Artificial Neural Network Model. **Earth Science Frontiers**. 14(6): 143-151.

- Bonham-Carter, G.F. (1994). **Geographic Information Systems for Geoscientists Modelling with GIS**. Oxford: Pergamon.
- Brenning, A. (2005). Spatial prediction models for landslide hazards: review, comparison and evaluation. **Natural Hazards and Earth System Sciences**. 5: 853–862.
- Bright, E.A., Coleman, P.R., Rose, A.N. and Urban, M.L. (2012). LandScan 2011 (2011 ed.). Oak Ridge, TN: Oak Ridge National Laboratory.
- Bui, D.T., Pradhan, B., Lofman, O. and Revhaug, I. (2012). Landslide Susceptibility Assessment in Vietnam Using Support Vector Machines, Decision Tree, and Naïve Bayes Models. **Mathematical Problems in Engineering**. 2012: 26.
- Bui, D.T., Pradhan, B., Lofman, O., Revhaug, I. and Dick, O.B. (2012). Spatial prediction of landslide hazards in Hoa Binh province (Vietnam): A comparative assessment of the efficacy of evidential belief functions and fuzzy logic models. **Catena**. 96: 28-40.
- Burrough, P.A. (1986). **Principles of Geographic Information Systems for Land Resource Assessment**. New York: Monographs on Soil and Resources Survey No. 12, Oxford Science Publications.
- Carrara, A., Guzzetti, F., Cardinali, M. and Reichenbach, P. (1999). Use of GIS Technology in the prediction and monitoring of landslide hazard. **Natural Hazards**. 20: 117-135.
- Carrara, A. and Guzzetti, F.E. (1995). **Geographical Information Systems in Assessing Natural Hazards**. Kluwer: Dordrecht.

- Cascini, L., Bonnard, c., Corominas, j., Jibson, r. and Montero-olarte, j. (2005). Landslide hazard and risk zoning for urban planning and development. 36.
- CGIAR-CSI. (2013). **SRTM 90m Digital Elevation Database v4.1** [On-line]. Available: <http://www.cgiar-csi.org/data/srtm-90m-digital-elevation-database-v4-1>.
- Chacon, J., Irigaray, C., Fernandez, T. and El Hamdouni, R. (2006). Engineering geology maps: landslides and geographical information systems. **Bulletin of Engineering Geology and the Environment**. 65(4): 341-411.
- Chen, C.Y. and Huang, W.L. (2013). Land use change and landslide characteristics analysis for community-based disaster mitigation. **Environmental monitoring and assessment**. 185(5): 4125-4139.
- Choi, J., Oh, H.J., Lee, H.J., Lee, C. and Lee, S. (2012). Combining landslide susceptibility maps obtained from frequency ratio, logistic regression, and artificial neural network models using ASTER images and GIS. **Engineering Geology**. 124: 12-23.
- Coe, J.A., Michael, J.A., Crovelli, R.A. and Savage, W.Z. (2000). **Preliminary map showing landslide densities, mean recurrence intervals, and exceedance probabilities as determined from historic records, Seattle, Washington**. Open-File Report 00-303, on-line edition. U.S. Geological Survey.
- Colesanti, C. and Wasowski, J. (2006). Investigating landslides with space-borne Synthetic Aperture Radar (SAR) interferometry. **Engineering Geology**. 88: 173-199.

- Corominas, J. and Moya, J. (2008). A review of assessing landslide frequency for hazard zoning purposes. **Engineering Geology**. 102: 193-213.
- Cortes, J.A.Z., Serna, M.D.A. and Martinez, S.P.M. (2012). Expertchoice© Decision support system implementation for vehicle selection in Colombian shipyard. **Dyna**. 79(173): 53-60.
- Coyle, G. (2004). **The analytic hierarchy process (AHP)**. Pearson Education Limited.
- Cruden, D.M. (1991). A simple definition of a landslide. **Bulletin International Association of Engineering Geology (IAEG)**. 43(1): 27-29.
- Czepiel, S.A. (2013). Maximum Likelihood Estimation of Logistic regression models: Theory and Implementation.
- Dahal, R.K., Hasegawa, S., Nonomura, A., Yamanaka, M., Masuda, T. and Nishino, K. (2007). GIS-based weights-of-evidence modelling of rainfall-induced landslides in small catchments for landslide susceptibility mapping. **Environmental Geology**. 54(2): 311-324.
- Dai, F.C., Lee, C.F. and Ngai, Y.Y. (2002). Landslide risk assessment and management: an overview. **Engineering Geology**. 64(1): 65-87.
- Dayton, C.M. (1992). **Logistic Regression Analysis** [On-line]. Available: [http://bus.utk.edu/stat/datamining/Logistic Regression Analysis \(Dayton\).pdf](http://bus.utk.edu/stat/datamining/Logistic%20Regression%20Analysis%20(Dayton).pdf).
- De Blasio, F.V. (2011). **Introduction to the Physics of Landslides: Lecture Notes on the Dynamics of Mass Wasting**. New York: Springer Dordrecht Heidelberg London.

- Deb, S.K. and El-Kadi, A.I. (2009). Susceptibility assessment of shallow landslides on Oahu, Hawaii, under extreme-rainfall events. **Geomorphology**. 108: 219-233.
- Department of Mineral Resources (DMR). (2010). **What is landslide? (in Thai)** [On-line]. Available: http://www.dmr.go.th/download/Landslide/what_landslide1.htm.
- Department of Mineral Resources (DMR). (2011). **Landslide hazard map at community level for Krabi Province (in Thai)** [On-line]. Available: http://www.dmr.go.th/ewtadmin/ewt/dmr_web/images/article/freetemp/article_20110801154204.pdf.
- Department of Mineral Resources (DMR). (2012). **Landslide records (1988-2012) (in Thai)** [On-line]. Available: http://www.dmr.go.th/download/Landslide/event_landslide1.htm.
- Department of Mineral Resources (DMR). (2013). **Landslide susceptibility map at community level** [On-line]. Available: http://www.dmr.go.th/main.php?filename=landslide_province.
- Department of Water Resources (DWR). (2013). **Early warning system (flood and landslide) (in Thai)** [On-line]. Available: http://ews.dwr.go.th/website/ews_all/index.php.
- Dilley, M., S. Chen, R., Deichmann, U., Lerner-Lam, A.L., Arnold, M., Agwe, J., Buys, P., Kjekstad, O., Lyon, B. and Yetman, G. (2005). **Natural Disaster Hotspots: A Global Risk Analysis**. Washington, D.C.: Hazard Management Unit, The world bank.

- Duman, T.Y., Can, T., Emre, O., Kecer, M., Doğan, A., Ates, S. and Durmaz, S. (2005). Landslide inventory of northwestern Anatolia, Turkey. **Engineering Geology**. 77: 99-114.
- Ercanoglu, M. and Gokceoglu, C. (2004). Use of fuzzy relations to produce landslide susceptibility map of a landslide prone area (West Black Sea Region, Turkey). **Engineering Geology**. 75: 229-250.
- Ercanoglu, M. and Temiz, F.A. (2011). Application of logistic regression and fuzzy operators to landslide susceptibility assessment in Azdavay (Kastamonu, Turkey). **Environmental Earth Sciences**. 64(4): 949-964.
- ERSDAC. (2013). **ASTER GDEM** [On-line]. Available: <http://www.jspacesystems.or.jp/ersdac/GDEM/E/4.html>.
- ESRI. (2009). **Classification methods** [On-line]. Available: http://webhelp.esri.com/arcgisdesktop/9.3/index.cfm?id=3888&pid=3886&topicname=Classification_methods.
- ESRI. (2010). **Understanding curvature rasters** [On-line]. Available: <http://blogs.esri.com/esri/arcgis/2010/10/27/understanding-curvature-rasters>.
- European Soil Portal. (2013). **Landslide** [On-line]. Available: <http://eusoils.jrc.ec.europa.eu/library/themes/landslides>.
- Fall, M., Azzam, R. and Noubactep, C. (2006). A multi-method approach to study the stability of natural slopes and landslide susceptibility mapping. **Engineering Geology**. 82(4): 241-263.

- Fell, R., Corominas, J., Bonnard, C., Cascini, L., Leroi, E. and Savage, W.Z. (2008). Guidelines for landslide susceptibility, hazard and risk zoning for land-use planning. **Engineering Geology**. 102: 99-111.
- Ferretti, A., Monti-Guarnieri, A., Prati, C. and Rocca, F. (2007). **InSAR Principles: Guidelines for SAR Interferometry Processing and Interpretation**. The Netherlands: ESA Publications.
- Francisco Javier Fano. [On-line]. Available: <http://www.mejoracompetitiva.es/2011/08/logica-difusa>.
- Gao, S., Zhang, Z. and Cao, C. (2009). New Methods of Estimating Weights in AHP. In **Proceedings of the 2009 International Symposium on Information Processing (ISIP'09)**. 21-23 August, 2009. Huangshan, P. R. China. 201-204.
- Garcia-Rodriguez, M.J. and Malpica, J.A. (2010). Assessment of earthquake-triggered landslide susceptibility in El Salvador based on an Artificial Neural Network model. **Natural Hazards and Earth System Science**. 10(6): 1307-1315.
- Garrett, J. (1994). Where and why artificial neural networks are applicable in civil engineering. **Journal of Computing in Civil Engineering**. 8: 129-130.
- Geotechnical Engineering Research and Development center (GERD). (2006). **Landslide data base of Thailand**.
- Ghuffar, S., Szekely, B., Roncat, A. and Pfeifer, N. (2013). Landslide Displacement Monitoring Using 3D Range Flow on Airborne and Terrestrial LiDAR Data. **Remote Sensing**. 5(6): 2720-2745.
- Glade, T. (2003). Landslide occurrence as a response to land use change: a review of evidence from New Zealand. **CATENA**. 51: 297-314.

- Glade, T. and Crozier, M. (2005). **A review of scale dependency in landslide hazard and risk analysis**. Quoted in Glade, T., Anderson M. and Crozier, M. J. (Eds.). **A review of scale dependency in landslide hazard and risk analysis**. John Wiley & Sons, Ltd, Chichester, West Sussex, England.
- Godt, J.W., Baum, R.L., Savage, W.Z., Salciarini, D., Schulz, W.H. and Harp, E.L. (2008). Transient deterministic shallow landslide modeling: Requirements for susceptibility and hazard assessments in a GIS framework. **Engineering Geology**. 102: 214-226.
- Gorsevski, P.V., Gessler, P.E., Boll, J., Elliot, W.J. and Foltz, R.B. (2006). Spatially and temporally distributed modeling of landslide susceptibility. **Geomorphology**. 80: 178-198.
- Gorsevski, P.V. and Jankowski, P. (2010). An optimized solution of multi-criteria evaluation analysis of landslide susceptibility using fuzzy sets and Kalman filter. **Computers & Geosciences**. 36(8): 1005-1020.
- Guettouche, M.S. (2012). Modeling and risk assessment of landslides using fuzzy logic. Application on the slopes of the Algerian Tell (Algeria). **Arabian Journal of Geosciences**. 6(9): 3163-3173.
- Guzzetti, F. (2002). Landslide hazard assessment and risk evaluation: limits and perspectives. In **Proceedings of the 4th EGS Plinius Conference held at Mallorca, Spain**. Universitat de les Illes Balears (Spain).
- Guzzetti, F., Cardinali, M., Reichenbach, P. and Carrara, A. (2000). Comparing Landslide Maps: A Case Study in the Upper Tiber River Basin, Central Italy. **Environmental Management**. 25(3): 247-263.

- Guzzetti, F., Carrara, A., Cardinali, M. and Reichenbach, P. (1999). Landslide hazard evaluation: a review of current techniques and their application in a multi-scale study, Central Italy. **Geomorphology**. 31(1): 181-216.
- Guzzetti, F., Mondini, A.C., Cardinali, M., Fiorucci, F., Santangelo, M. and Chang, K.-T. (2012). Landslide inventory maps: New tools for an old problem. **Earth-Science Reviews**. 112: 42-66.
- Guzzetti, F., Peruccacci, S., Rossi, M. and Stark, C.P. (2008). The rainfall intensity-duration control of shallow landslides and debris flows: an update. **Landslides**. 5(1): 3-17.
- Guzzetti, F., Peruccacci, S., Rossi, M. and Stark, C.P. (2007). Rainfall thresholds for the initiation of landslides in central and southern Europe. **Meteorology and Atmospheric Physics**. 98: 239-267.
- Hall, M., Frank, E., Holmes, G., Pfahringer, B., Reutemann, P. and Witten, I. H. (2009). The WEKA data mining software: An update. **SIGKDD Explorations**. 11(1): 10-18.
- Hansen, A. (1984). **Landslide hazard analysis**. In: **Brunsdon D. & Prior D.B. (eds.), Slope Instability**. New York: John Wiley and Sons.
- Hasekioğulları, G.D. and Ercanoglu, M. (2012). A new approach to use AHP in landslide susceptibility mapping: a case study at Yenice (Karabuk, NW Turkey). **Natural Hazards**. 63: 1157-1179.
- Highland, L.M. and Bobrowsky, P. (2008). **The landslide handbook-A guide to understanding landslides**. U.S. Geological Survey: Reston, Virginia.

- Ho, J.Y., Lee, K.T., Chang, T.C., Wang, Z.Y. and Liao, Y.H. (2012). Influences of spatial distribution of soil thickness on shallow landslide prediction. **Engineering Geology**. 124: 38-46.
- Ho, W. (2008). Integrated analytic hierarchy process and its applications – A literature review. **European Journal of Operational Research**. 186(1): 211-228.
- Hong Kong Geotechnical Engineering office. (2000). **Geotechnical manual for slopes (4th reprint)**. Hong Kong: Geotechnical Engineering Office.
- Hong, Y., Adler, R. and Huffman, G. (2007). Use of satellite remote sensing data in the mapping of global landslide susceptibility. **Natural Hazards**. 43(2): 245-256.
- Horton, P., Jaboyedoff, M., Rudaz, B. and Zimmermann M. (2013). Flow-R, a model for susceptibility mapping of debris flows and other gravitational hazards at a regional scale. **Natural Hazards Earth System Sciences**. 13: 869–885. doi:10.5194/nhess-13-869-2013.
- Huabin, W., Gangjun, L., Weiya, X. and Gonghui, W. (2005). GIS-based landslide hazard assessment: an overview. **Progress in Physical Geography December 2005**. 29(4): 548-567.
- Huberty, C. J. (1994). **Applied Discriminant Analysis**. New York: Wiley Interscience.
- Huggel, C., Käab, A., Haeberli, W. and Krummenacher, B. (2003). Regional-scale GIS-models for assessment of hazards from glacier lake outbursts: evaluation and application in the Swiss Alps, **Natural Hazards Earth System Sciences**. 3: 647-662. doi:10.5194/nhess-3-647-2003.
- Idaho Geological Survey. (2013). **Lanslides** [On-line]. Available: <http://www.idahogeology.org/DrawOnePage.asp?PageID=83>.

- Intarawichian, N. and Dasananda, S. (2010). Analytical hierachy process for landslide susceptibility mapping in lower mae chaem watershed, northern thailand. **Suranaree journal of science and technology**. 17(3): 277-292.
- Intarawichian, N. and Dasananda, S. (2011). Frequency ratio model based landslide susceptibility mapping in lower Mae Chaem watershed, Northern Thailand. **Environmental Earth Sciences**. 64(8): 2271-2285.
- Iverson, R.M. and Denlinger, R.P. (2001). Mechanics of debris flows and debris-laden flash floods, **7th Federal Interagency Sedimentation Conference**, Reno, Nevada, USA.
- Jadda, M.S., Helmi Z.M., Mansor, Shattri B., Sharifikia, Mohammad, Pirasteh, Saeid. (2009). Landslide Susceptibility Evaluation and Factor Effect Analysis Using Probabilistic-Frequency Ratio Model. **European Journal of Scientific Research**. 33(4): p654.
- Joyce, K., Belliss, S., Samsonov, S.V., McNeill, S.J. and Glassey, P. (2009). A review of the status of satellite remote sensing and image processing techniques for mapping natural hazards and disasters. **Progress in Physical Geography**. 33(2): 183-207.
- Kannan, M., Saranathan, E. and Anabalagan, R. (2012). Landslide vulnerability mapping using frequency ratio model: a geospatial approach in Bodi-Bodimettu Ghat section, Theni district, Tamil Nadu, India. **Arabian Journal of Geosciences**. 6(8): 2901-2913.

- Kanungo, D.P., Arora, M.K., Sarkar, S. and Gupta, R.P. (2006). A comparative study of conventional, ANN black box, fuzzy and combined neural and fuzzy weighting procedures for landslide susceptibility zonation in Darjeeling Himalayas. **Engineering Geology**. 85: 347-366.
- Kanungo, D.P., Arora, M.K., Sarkar, S. and Gupta, R.P. (2009). Landslide Susceptibility Zonation (LSZ) mapping Mapping-A Review. **Journal of South Asia Disaster Studies**. 2(1): 81-105.
- Karsli, F., Atasoy, M., Yalcin, A., Reis, S., Demir, O. and Gokceoglu, C. (2009). Effects of land-use changes on landslides in a landslide-prone area (Ardesen, Rize, NE Turkey). **Environmental Monitoring and Assessment**. 156: 241-255.
- Kavzoglu, T., Sahin, E.K., and Colkesen, I. (2015). An assessment of multivariate and bivariate approaches in landslide susceptibility mapping: a case study of Duzkoy district. **Natural Hazards**. 76: 471-496.
- Kayastha, P., Dhital, M.R. and De Smedt, F. (2013). Evaluation and comparison of GIS based landslide susceptibility mapping procedures in Kulekhani watershed, Nepal. **Journal of the Geological Society of India**. 81: 219-231.
- Kim S.K., Hong W.P. and Kim Y.M. (1992). Prediction of rainfall-triggered landslides in Korea. In: D.H. Bell (ed), **Proceedings of the 6th International Symposium on Landslides**. 10–14 February, 1992. Christchurch, New Zealand. (pp. 989-994).
- Kirschbaum, D.B., Adler, R., Hong, Y., Kumar, S., Peters-Lidard, C. and Lerner-Lam, A. (2011). Advances in landslide nowcasting: evaluation of a global and

- regional modeling approach. **Environmental Earth Sciences**. 66(6): 1683-1696.
- Klir, G.J. and Yuan, B. (1995). **Fuzzy Sets and Fuzzy Logic: Theory and Applications**. New Jersey: Prentice Hall.
- Komac, M. (2006). A landslide susceptibility model using the Analytical Hierarchy Process method and multivariate statistics in perialpine Slovenia. **Geomorphology**. 74: 17-28.
- Lee, M.J., Choi, J.W., Oh, H.J., Won, J.S., Park, I. and Lee, S. (2012). Ensemble-based landslide susceptibility maps in Jinbu area, Korea. **Environmental Earth Sciences**. 67(1): 23-37.
- Lee, S. (2005). Application of logistic regression model and its validation for landslide susceptibility mapping using GIS and remote sensing data. **International Journal of Remote Sensing**. 26(7): 1477-1491.
- Lee, S. (2007). Application and verification of fuzzy algebraic operators to landslide susceptibility mapping. **Environmental Geology**. 52(4): 615-623.
- Lee, S. and Evangelista, D.G. (2006). Earthquake-induced landslide-susceptibility mapping using an artificial neural network. **Natural Hazards Earth System Sciences**. 6(5): 687-695.
- Lee, S. and Lee, M.J. (2006). Detecting landslide location using KOMPSAT 1 and its application to landslide-susceptibility mapping at the Gangneung area, Korea. **Advances in Space Research**. 38(10): 2261-2271.
- Lee, S. and Pradhan, B. (2006). Probabilistic landslide hazards and risk mapping on Penang Island, Malaysia. **Journal of Earth System Science**. 115(6): 661-672.

- Lee, S. and Pradhan, B. (2007). Landslide hazard mapping at Selangor, Malaysia using frequency ratio and logistic regression models. **Landslides**. 4(1): 33-41.
- Lee, S., Ryu, J.H., Lee, M.J. and Won, J.S. (2006). The Application of Artificial Neural Networks to Landslide Susceptibility Mapping at Janghung, Korea. **Mathematical Geology**. 38(2): 199-220.
- Lee, S., Ryu, J.H., Won, J.S. and Park, H.J. (2004). Determination and application of the weights for landslide susceptibility mapping using an artificial neural network. **Engineering Geology**. 71: 289-302.
- Lee, S. and Sambath, T. (2006). Landslide susceptibility mapping in the Damrei Romel area, Cambodia using frequency ratio and logistic regression models. **Environmental Geology**. 50(6): 847-855.
- Lee, S. and Talib, J.A. (2005). Probabilistic landslide susceptibility and factor effect analysis. **Environmental Geology**. 47(7): 982-990.
- Lepore, C., Kamal, S.A., Shanahan, P. and Bras, R.L. (2011). Rainfall-induced landslide susceptibility zonation of Puerto Rico. **Environmental Earth Sciences**. 66(6): 1667-1681.
- LiDAR-UK. (2013). **Find out all you need to know about LiDAR, its history, its uses and the technologies behind it...** [On-line]. Available: <http://www.lidar-uk.com>.
- Mahidol University. (2003). **The study of landslide risk area (final report)**. Engineering Data and Research Center, Faculty of Engineering Mahidol University, Thailand.

- Malamud, B.D., Turcotte, D.L., Guzzetti, F. and Reichenbach, P. (2004). Landslide inventories and their statistical properties. **Earth Surface Processes and Landforms**. 29(6): 687-711.
- Malczewski, J. (1999). **GIS and Multicriteria Decision Analysis**. New York: John Wiley and Sons.
- Mancini, F., Ceppi, C. and Ritrovato, G. (2010). GIS and statistical analysis for landslide susceptibility mapping in the Daunia area, Italy. **Natural Hazards and Earth System Science**. 10(9): 1851-1864.
- Matori, A., Basith, A. and Harahap, I. (2011). Study of regional monsoonal effects on landslide hazard zonation in Cameron Highlands, Malaysia. **Arabian Journal of Geosciences**. 1–16.
- McKenna, J.P., Santi, P.M., Amblard, X. and Negri, J. (2011). Effects of soil-engineering properties on the failure mode of shallow landslides. **Landslides**. 9(2): 215-228.
- Metternicht, G., Hurni, L. and Gogu, R. (2005). Remote sensing of landslides: An analysis of the potential contribution to geo-spatial systems for hazard assessment in mountainous environments. **Remote Sensing of Environment**. 98: 284-303.
- Michael-Leiba, M., Baynes, F., Scott, G. and Granger, K. (2003). Regional Landslide Risk to the Cairns Community. **Natural Hazards**. 30: 233–249.
- Michie, R. (2013). **Shallow Landslide Approach** [On-line]. Available: <http://www.deq.state.or.us/wq/tmdls/docs/midcoast/advisory/032013ShallowLandslideApproach.pdf>.

- Ministry of Agriculture and Cooperatives (MOAC). (2013). **Management's guide to disaster assistance in agriculture** [On-line]. Available: <http://www.plan.doae.go.th/ndrc/work/05954.pdf>.
- Mondini, A.C., Chang, K.T. and Yin, H.Y. (2011). Combining multiple change detection indices for mapping landslides triggered by typhoons. **Geomorphology**. 134: 440-451.
- Moore, I.D., Grayson, R.B. and Ladson, A.R. (1991). Digital terrain modelling: a review of hydrological, geomorphological, and biological applications. **Hydrological Processes**. 5: 3-30.
- Nandi, A. and Shakoor, A. (2010). A GIS-based landslide susceptibility evaluation using bivariate and multivariate statistical analyses. **Engineering Geology**. 110: 11-20.
- NASA-TRMM. (2013). **The Tropical Rainfall Measuring Mission** [On-line]. Available: <http://pmm.nasa.gov/node/158>.
- National Marine Fisheries Service (NMFS). (2012, July 2002). **Landslide Terminology** [On-line]. Available: http://swr.nmfs.noaa.gov/simpson/Appendix_B.pdf.
- North Carolina Geological Survey (NCGS). (2012). Landslides in North Carolina [On-line]. Available: <http://portal.ncdenr.org/web/lr/landslides-information>.
- Nefeslioglu, H.A., Gokceoglu, C. and Sonmez, H. (2008). An assessment on the use of logistic regression and artificial neural networks with different sampling strategies for the preparation of landslide susceptibility maps. **Engineering Geology**. 97: 171-191.

- NOAA. (2013). **What is a GIS?** [On-line]. Available: <http://www.srh.noaa.gov/bmx/?n=gis>.
- Office of the National Economic and Social Development Board (NESDB). (2011). **The 11th national economic and social development plan (2012-2016)** [On-line]. Available: http://www.nesdb.go.th/Portals/0/news/plan/p11/Plan11_eng.pdf.
- Oh, H.-J. and Pradhan, B. (2011). Application of a neuro-fuzzy model to landslide-susceptibility mapping for shallow landslides in a tropical hilly area. **Computers & Geosciences**. 37(9): 1264-1276.
- Oh, H.J., Lee, S., Chotikasathien, W., Kim, C.H. and Kwon, J.H. (2009). Predictive landslide susceptibility mapping using spatial information in the Pechabun area of Thailand. **Environmental Geology**. 57(3): 641-651.
- Ono, K., Kazama, S. and Ekkawatpanit C. (2014). Assessment of rainfall-induced shallow landslides in Petchabun and Krabi provinces, Thailand. **Natural Hazards**. 74: 2089-2107.
- Paola, J.D. and Schowengerdt, R.A. (1995). A review and analysis of backpropagation neural networks for classification of remotely-sensed multi-spectral imagery. **International Journal of Remote Sensing**. 16(16): 3033-3058.
- Park, D., Lee, S., Nikhil, N.V., Kang, S. and Park, J. (2013). Debris flow hazard zonation by probabilistic analysis (MT. Woomyeon, Seoul, Korea). **International Journal of Innovative Research in Science, Engineering and Technology**. 2(6): (2381-2390).

- Park, S., Choi, C., Kim, B. and Kim, J. (2013). Landslide susceptibility mapping using frequency ratio, analytic hierarchy process, logistic regression, and artificial neural network methods at the Inje area, Korea. **Environmental Earth Sciences**. 68(5): 1443-1464.
- Pavel, M., Nelson, J.D. and Jonathan Fannin, R. (2011). An analysis of landslide susceptibility zonation using a subjective geomorphic mapping and existing landslides. **Computers & Geosciences**. 37(4): 554-566.
- Perla, R., Cheng, T.T. and McClung, D.M. (1980). A two-parameter model of snow-avalanche motion. **Journal of Glaciology**. 26: 197-207.
- Petley, D. (2012). Global patterns of loss of life from landslides. **Geology**. 40: 939-942.
- Pirulli, M. and Sorbino, G. (2008). Assessing potential debris flow runout: a comparison of two simulation models. **Natural Hazards Earth System Sciences**. 8: 961-971.
- Pontius, R.G. and Schneider, L.C. (2001). Land-use change model validation by an ROC method for the Ipswich watershed, Massachusetts, USA. **Agriculture, Ecosystems and Environment**. 85: 239-248.
- Pourghasemi, H.R., Pradhan, B. and Gokceoglu, C. (2012). Application of fuzzy logic and analytical hierarchy process (AHP) to landslide susceptibility mapping at Haraz watershed, Iran. **Natural Hazards**. 63(2): 965-996.
- Pradhan, B. (2010). Remote sensing and GIS-based landslide hazard analysis and cross-validation using multivariate logistic regression model on three test areas in Malaysia. **Advances in Space Research**. 45(10): 1244-1256.

- Pradhan, B. (2011). Use of GIS-based fuzzy logic relations and its cross application to produce landslide susceptibility maps in three test areas in Malaysia. **Environmental Earth Sciences**. 63(2): 329-349.
- Pradhan, B. and Lee, S. (2010). Delineation of landslide hazard areas on Penang Island, Malaysia, by using frequency ratio, logistic regression, and artificial neural network models. **Environmental Earth Sciences**. 60(5): 1037-1054.
- Pradhan, B., Lee, S. and Buchroithner, M.F. (2010). A GIS-based back-propagation neural network model and its cross-application and validation for landslide susceptibility analyses. **Computers, Environment and Urban Systems**. 34(3): 216-235.
- Radoš, D., Lozić, S. and Šiljeg, A. (2012). Morphometrical characteristics of the broader area of duvanjsko polje, bosnia and hercegovina. **Geoadria**. 17(2): 177-207.
- Rau, J.Y., Chang, K.T., Shao, Y.C. and Lau, C.C. (2012). Semi-automatic shallow landslide detection by the integration of airborne imagery and laser scanning data. **Natural Hazards**. 61(2): 469-480.
- Regmi, N.R., Giardino, J.R. and Vitek, J.D. (2010). Assessing susceptibility to landslides: Using models to understand observed changes in slopes. **Geomorphology**. 122: 25-38.
- Reliefweb. (2014). **Thailand: Floods and Landslides - March 2011** [On-line]. Available: <http://reliefweb.int/disaster/fl-2011-000032-tha>.

- Revellino, P., Hungr, O., Guadagno, F.M. and Evans, S.G. (2004). Velocity and runout simulation of destructive debris flows and debris avalanches in pyroclastic deposits, Campania region, Italy. **Environmental Geology**. 45(3): 295-311.
- Richards, M.A. (2007). A Beginner's Guide to Interferometric SAR Concepts and Signal Processing. **IEEE Aerospace & Electronic Systems Magazine**. 22(9).
- Ross, T.J. (1995). **Fuzzy logic with engineering applications** New York: McGraw-Hill.
- Saaty, T.L. (1977). A scaling method for priorities in hierarchical structures. **Journal of Mathematical Psychology**. 15(3): 234-281.
- Saaty, T.L. (1980). **The Analytic Hierarchy Process**. New York, NY, U.S.A.: McGraw Hill International.
- Saaty, T.L. (1990). How to make a decision: The analytic hierarchy process. **European Journal of Operational Research**. 48(1): 9-26.
- Saaty, T.L. (2008). Decision making with the analytic hierarchy process **International Journal Services Sciences**. 1(1): 83-98.
- Saaty, T.L. and Vargas, L.G. (2001). **Models, Methods, Concepts & Applications of the Analytic Hierarchy Process**. Boston: Kluwer Academic Publisher.
- Saboya Jr, F., da Glória Alves, M. and Dias Pinto, W. (2006). Assessment of failure susceptibility of soil slopes using fuzzy logic. **Engineering Geology**. 86(4): 211-224.
- Safeland-FP7. (2011). Recommended Procedures for validating landslide hazard and risk models and maps. Grant Agreement No. 226479. 2: 62-63.

- Sarapriome, S. and Tanang, S. (2012). Probability of landslide occurrence mapping using probability density function: a case study of the mae tha group in Nam Li watershed, Thailand. In **Proceeding of the 31st Asian Conference on Remote Sensing (ACRS)** Ambassador City Jomtien Hotel, Pattaya, Thailand.
- Sarkar, S. and Kanungo D.P. (2004). An integrated approach for landslide susceptibility mapping using remote sensing and GIS. **Photogrammetric Engineering and Remote Sensing**. 70: 617-625.
- Schmidt, J., Evans, I.S. and Brinkmann, J. (2003). Comparison of polynomial models for land surface curvature calculation. **International Journal of Geographical Information Science**. 17: 797-814.
- Schuurman. (2004). **GIS: A Short Introduction**. Oxford: Blackwell.
- Sezer, E.A., Pradhan, B. and Gokceoglu, C. (2011). Manifestation of an adaptive neuro-fuzzy model on landslide susceptibility mapping: Klang valley, Malaysia. **Expert Systems with Applications**. 38(7): 8208-8219.
- Sgzen, M.L. (2002). **Data Driven Landslide Hazard Assessment Using Geographical Information Systems and Remote Sensing**. Ph.D. Dissertation, Department of Geological Engineering: The graduate school of natural and applied sciences of the middle east technical university.
- Sidle, R.C. and Ochiai, H. (2006). **Landslides: processes, prediction, and land use**. Washington, DC: American Geophysical Union.
- Solaimani, K., Mousavi, S.Z. and Kavian, A. (2012). Landslide susceptibility mapping based on frequency ratio and logistic regression models. **Arabian Journal of Geosciences**. 6(7): 2557-2569.

- Soralump, S. (2010). Rainfall-Triggered Landslide: from research to mitigation practice in Thailand. **Geotechnical Engineering Journal of the SEAGS & AGSSEA**. 41(1): 39-44.
- Soralump, S., Pungsuwan, D., Chantasorn, M. and Inmala, N. (2010). Landslide risk management of Patong city, Phuket, Thailand.
- Soralump, S. (2007). Corporation of geotechnical engineering data for landslide hazard map in Thailand. In **EIT-JSCE Joint Seminar on Rock Engineering 2007**. Imperial Queen's Park Hotel.
- Soralump, S. and Kulsuwan, B. (2006). Landslide Risk Prioritization of Tsunami Affected Area in Thailand In **Symposium on Infrastructure Development and the Environment 2006**. Philippines: University of the Philippines, Diliman, Quezon City.
- Star, J. and Estes, J.E. (1990). **An Introduction to Geographic Information Systems**. Englewood Cliffs, NJ: Prentice Hall.
- Strozzi, T., Ambrosi, C. and Raetzo, H. (2013). Interpretation of Aerial Photographs and Satellite SAR Interferometry for the Inventory of Landslides. **Remote Sensing**. 5(5): 2554-2570.
- Sujatha, E.R., Rajamanickam, V., Kumaravel, P. and Saranathan, E. (2011). Landslide susceptibility analysis using probabilistic likelihood ratio model a geospatial-based study. **Arabian Journal of Geosciences**. 6(2): 429-440.
- Swets, J.A. (1988). Measuring the accuracy of diagnostic systems. **Science**. 240: 1285-1293.

- Tanang, S., Sarapirome, S. and Plaiklang, S. (2010). Landslide susceptibility map of Namli watershed, Uttaradit, Thailand. In **proceeding of: 31st Asian Conference on Remote Sensing**. Asian Association on Remote Sensing: Hanoi, Vietnam.
- Tanavud, C., Yongchalermchai, C., Bennui, A. and Navanugraha, C. (2000). Applications of GIS and Remote Sensing for landslide disaster management in southern Thailand. **Natural Disaster Science**. 22(2): 67-74.
- Teerarungsigul, S., Chonglakmani, C. and Kuehn, F. (2007). Landslide Prediction Model using Remote Sensing, GIS and Field Geology: a case study of Wang Chin District, Phrae Province, Northern Thailand. In **GEOTHAI'07 International Conference on Geology of Thailand: Towards Sustainable Development and Sufficiency Economy** (156-168).
- Thaiyuenwong, S. and Maireang, W. (2010). Triggered-rainfall landslide hazard prediction **Research and development journal**. 21(2): 43-50.
- Thanh, L.N. and De Smedt, F. (2012). Application of an analytical hierarchical process approach for landslide susceptibility mapping in A Luoi district, Thua Thien Hue Province, Vietnam. **Environmental Earth Sciences**. 66(7): 1739-1752.
- Tofani, V., Segoni, S., Agostini, A., Catani, F. and Casagli, N. (2013). Technical Note: Use of remote sensing for landslide studies in Europe. **Natural Hazards and Earth System Science**. 13(2): 299-309.
- Tourism Authority of Thailand. (2013). **Amazing Thailand-Krabi** [On-line]. Available: <http://www.tourismthailand.org/Where-to-Go/Krabi>.
- Transport Scotland. (2008). **Scottish road network landslides study: implementation**. Edinburgh.

- Triantaphyllou, E. and Mann, S.H. (1995). Using the analytic hierarchy process for decision making in engineering applications: some challenges. **Inter'l Journal of Industrial Engineering: Applications and Practice**. 2(1): 35-44.
- USGS. (2004). **Landslide Types and Processes** [On-line]. Available: <http://pubs.usgs.gov/fs/2004/3072/pdf/fs2004-3072.pdf>.
- Vaidya, O.S. and Kumar, S. (2006). Analytic hierarchy process: An overview of applications. **European Journal of Operational Research**. 169(1): 1-29.
- Van Beek, L.P.H. and Van Asch, T.W.J. (2004). Regional Assessment of the Effects of Land-Use Change on Landslide Hazard By Means of Physically Based Modelling. **Natural Hazards**. 31: 289-304.
- Van Weste, C. (2013). **Landslide types and causes** [On-line]. Available: http://www.adpc.net/casita/Course_Modules/Landslide_hazard_assessment/Landslides_types_and_causes.pdf.
- Van Westen, C.J. (2000). The modelling of landslide hazard using GIS. **Surveys in Geophysics**. 21: 241-255.
- Van Westen, C.J., Castellanos, E. and Kuriakose, S.L. (2008). Spatial data for landslide susceptibility, hazard, and vulnerability assessment: An overview. **Engineering Geology**. 102: 112-131.
- Van Westen, C.J., van Asch, T.W.J. and Soeters, R. (2006). Landslide hazard and risk zonation—why is it still so difficult? **Bulletin of Engineering Geology and the Environment**. 65(2): 167-184.

- Varnes, D.J. (1978). **Slope Movement Types and Processes**. Quoted in Schuster, R. L. Krizek, R. J. **Landslides: Analysis and Control**. Transportation and Road Research Board, National Academy of Science, Washington D. C.
- Varnes, D.J. (1984). **Landslide hazard zonation: a review of principles and practice**. UNESCO, Paris.
- Vijith, H. and Madhu, G. (2008). Estimating potential landslide sites of an upland sub-watershed in Western Ghat's of Kerala (India) through frequency ratio and GIS. **Environmental Geology**. 55(7): 1397-1405.
- Wachal, D.J. and Hudak, P.F. (2000). Mapping landslide susceptibility in Travis County, Texas, USA. **GeoJournal**. 51(3): 245-253.
- Wang, H.B. and Sassa, K. (2005). Comparative evaluation of landslide susceptibility in Minamata area, Japan. **Environmental Geology**. 47(7): 956-966.
- Wieczorek, G.F. (1983). Preparing a Detailed Landslide-inventory Map for Hazard Evaluation and Reduction. **Bulletin of the Association of Engineering Geologists**. 21: 337-342.
- Wiegand, C., Rutzinger, M., Heinrich, K. and Geitner, C. (2013). Automated Extraction of Shallow Erosion Areas Based on Multi-Temporal Ortho-Imagery. **Remote Sensing**. 5(5): 2292-2307.
- Williams C.J., Lee S.S., Fisher R.A. and Dickerman L.H. (1999). A comparison of statistical methods for prenatal screening for Down syndrome. **Applied Stochastic Models and Data Analysis**. 15: 89-101.

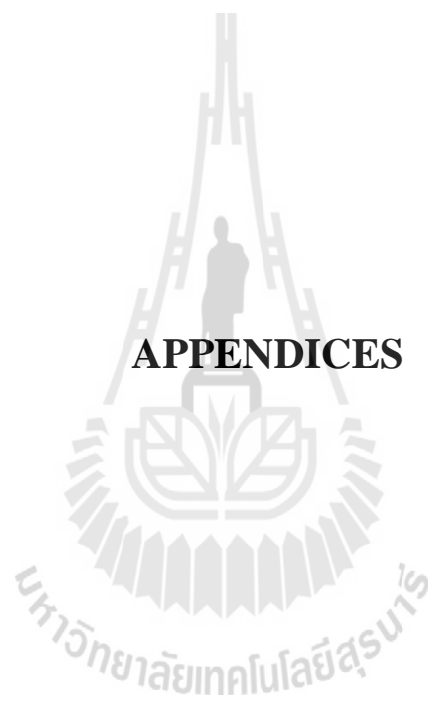
- Winter, M.G., Macgregor, F. and Shackman, L. (2008). **Scottish road network landslides study: implementation**. (No. 978-1-906006-38-9), Transport Scotland. Edinburgh.
- Witt, A.C. (2005). A Brief History of Debris Flow Occurrence in the French Broad River Watershed, Western North Carolina. **The North Carolina Geographer**. 59-82.
- Xu, C., Xu, X., Dai, F. and Saraf, A.K. (2012). Comparison of different models for susceptibility mapping of earthquake triggered landslides related with the 2008 Wenchuan earthquake in China. **Computers & Geosciences**. 46: 317-329.
- Yalcin, A. (2008). GIS-based landslide susceptibility mapping using analytical hierarchy process and bivariate statistics in Ardesen (Turkey): Comparisons of results and confirmations. **Catena**. 72(1): 1-12.
- Yalcin, A. and Bulut, F. (2007). Landslide susceptibility mapping using GIS and digital photogrammetric techniques: a case study from Ardesen (NE-Turkey). **Natural Hazards**. 41(1): 201-226.
- Yalcin, A., Reis, S., Aydinoglu, A.C. and Yomralioglu, T. (2011). A GIS-based comparative study of frequency ratio, analytical hierarchy process, bivariate statistics and logistics regression methods for landslide susceptibility mapping in Trabzon, NE Turkey. **Catena**. 85(3): 274-287.
- Yao, X., Tham, L.G. and Dai, F.C. (2008). Landslide susceptibility mapping based on Support Vector Machine: A case study on natural slopes of Hong Kong, China. **Geomorphology**. 101(4): 572-582.

- Yeon, Y.K., Han, J.G. and Ryu, K.H. (2010). Landslide susceptibility mapping in Injae, Korea, using a decision tree. **Engineering Geology**. 116: 274-283.
- Yesilnacar, E. and Topal, T. (2005). Landslide susceptibility mapping: A comparison of logistic regression and neural networks methods in a medium scale study, Hendek region (Turkey). **Engineering Geology**. 79: 251-266.
- Yilmaz, I. (2009). Landslide susceptibility mapping using frequency ratio, logistic regression, artificial neural networks and their comparison: A case study from Kat landslides (Tokat—Turkey). **Computers & Geosciences**. 35(6): 1125-1138.
- Yilmaz, I. (2010). Comparison of landslide susceptibility mapping methodologies for Koyulhisar, Turkey: conditional probability, logistic regression, artificial neural networks, and support vector machine. **Environmental Earth Sciences**. 61(4): 821-836.
- Yoshimatsu, H. and Abe, S. (2006). A review of landslide hazards in Japan and assessment of their susceptibility using an analytical hierarchic process (AHP) method. **Landslides**. 3(2): 149-158.
- Young, O.C., Jin, C.K. and Choi, C.U. (2003). **The Comparative Research of Landslide Susceptibility Mapping Using FR, AHP, LR, ANN** [On-line]. Available: http://proceedings.esri.com/library/userconf/educ10/educ/papers/pap_1476.pdf.
- Yumuang, S. (2006). 2001 debris flow and debris flood in Nam Ko area, Phetchabun province, central Thailand. **Environmental Geology**. 51(4): 545-564.
- Zadeh, L.A. (1965). Fuzzy sets. **Information and Control** 8: 338-353.

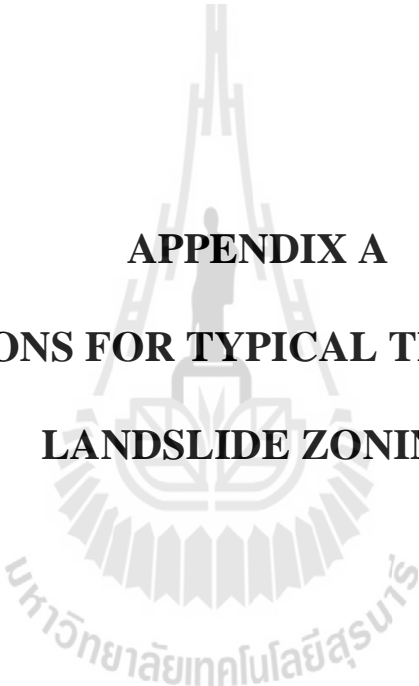
Zhang, Z., Gong, H., Zhao, W. and Zhang, Y. (2005). Application of Remote Sensing to Study of Landslide. **IEEE**: 1546-1549.

Zhong, C., Li, H., Xiang, W., Su, A. and Huang, X. (2012). Comprehensive study of landslides through the integration of multi remote sensing techniques: Framework and latest advances. **Journal of Earth Science**. 23(2): 243-252.





APPENDICES



APPENDIX A
DEFINITIONS FOR TYPICAL TERMS USED IN
LANDSLIDE ZONING

Definitions for common terms used in landslide zoning and risk management given here are followed those reported in AGS (2007a), which are:

Landslide. A movement of mass of rock, debris, or earth (soil) down a slope.

Landslide inventory. An inventory of location, classification, volume, activity and date of occurrence of individual landslides in an area.

Landslide susceptibility. A quantitative or qualitative assessment of the classification, volume (or area) and spatial distribution of the landslides which exist or may potentially arise in an area. Susceptibility may also include description of velocity and intensity of the existing or potential landsliding.

Hazard. A condition with potential for causing an undesirable consequence. Description of landslide hazard should have location, volume (or area), classification and velocity of potential landslides and any detached material and probability of their occurrence within a given period of time. Landslide hazard includes landslides which have their source in the area, or, may have their source outside the area but may travel on to or regress into the area.

Risk. A measure of the probability and severity of an adverse effect to health, property or the environment. Risk is often estimated by the product of probability and consequences. However, a more general interpretation of risk involves a comparison of the probability and consequences in a non-product form.

For these guidelines risk is further defined as:

(a) For life loss, the annual probability that the person most at risk will lose his/her life taking account of the landslide hazard and the temporal spatial probability and vulnerability of the person.

(b) For property loss, the annual probability of a consequence (or annualized loss) to elements at risk, their temporal spatial probability and vulnerability.

Elements at Risk. The population, buildings and engineering works, economic activities, public services utilities, infrastructure, environmental features in the area potentially affected by the landslide hazard.

Vulnerability. The degree of loss to a given element or set of elements within the area affected by the landslide hazard. It is expressed on a scale of 0 (no loss) to 1 (total loss). For property, the loss will be the value of the damage relative to the value of the property; for persons, it will be the probability that a particular life (the element at risk) will be lost, given the person(s) is (are) affected by the landslide.

Zoning. The division of land into homogeneous areas or domains and their ranking according to degrees of actual (or potential) landslide susceptibility, hazard or risk. The word 'landslide' implies both existing (or known landslides) and potential landslides which a practitioner might reasonably predict based on relevant geology, geometry and slope forming processes. Such potential landslides may be of varying likelihood of occurrence. The term landslip is sometimes used to describe landslides but is not the recommended term.

APPENDIX B
QUESTIONNAIRE AND LIST OF EXPERTS



QUESTIONNAIRE

The questionnaire is composed of 4 parts:

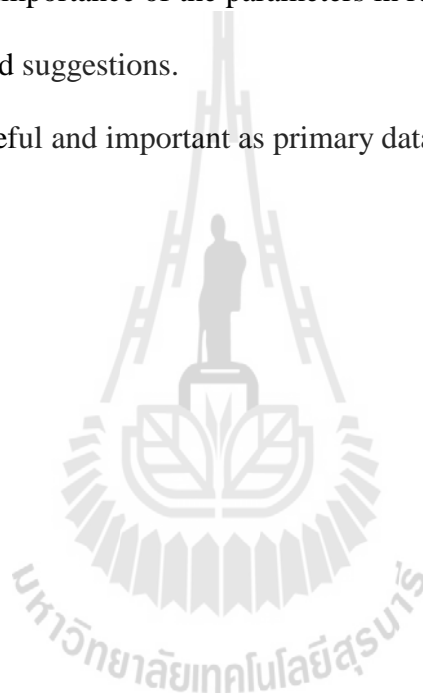
Part I: Briefly general expert information,

Part II: General information of the research,

Part III: Compare the importance of the parameters in relation, and

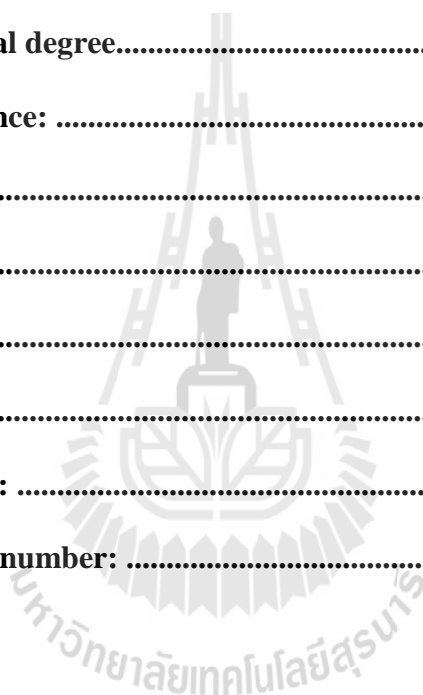
Part IV: Comments and suggestions.

This information is useful and important as primary data of the research. Your opinion will not be disclosed.



Part I: Briefly expert information

- 1.1 Name and surname:
- 1.2 Position:
- 1.3 Education background:
- 1.3.1 Bachelor degree.....
- 1.3.2 Master degree.....
- 1.3.3 Doctoral degree.....
- 1.4 Work experience:
-
-
-
-
-
- 1.5 Email address:
- 1.6 Mobile phone number:



Part II: General information of the research

2.1 Thesis title: Optimal landslide susceptibility and risk analyses at Kho Phanom Bencha, Krabi province, Thailand.

2.2 Objective

This part of the research used conventional weighted linear combination (WLC) and analytical hierarchy process (AHP).

WLC is one of the widely-used qualitative methods for landslide susceptibility analysis, especially at a regional scale. The comparative importance is normally represented by the assigned numerical values for the relevant factors and their affixed attributes like using ordinal scale from 1 (not important) to 5 (most important). These values are typically called factor weight (for factors) and class weight, or rating, (for attributes). Higher values of weight (or rating) indicate greater influence of the factors (or attributes) on landslide occurrence within the area.

AHP is a semi-qualitative method, which involves a matrix-based pair-wise comparison of the contribution of different factors for landslide. The analytical hierarchy process (AHP) is a Multi-Criteria Decision Making (MCDM) tool at the core of which lies a method for converting subjective assessments of relative importance to a set of overall scores or weights. Analytical hierarchy process (AHP) was developed by Saaty (1980). To get factor weights in AHP, one has to build a pair-wise comparison matrix with scores.

Table B1 Scale of preference between two parameters in AHP (Saaty, 2000).

Scales	Degree of preferences	Explanation
1	Equally	Two activities contribute equally to the objective.
3	Moderately	Experience and judgment slightly to moderately favor one activity over another.
5	Strongly	Experience and judgment strongly or essentially favor one activity over another.
7	Very strongly	An activity is strongly favored over another and its dominance is showed in practice.
9	Extremely	The evidence of favoring one activity over another is of the highest degree possible of an affirmation.
2, 4, 6, 8	Intermediate values	Used to represent compromises between the preferences in weights 1, 3, 5, 7 and 9.
Reciprocals	Opposites	Used for inverse comparison.

In this study, there are ten landslide inducing parameters which are considered for landslide susceptibility analysis. These parameters are elevation, slope gradient, slope aspect, slope curvature, topographic wetness index, distance from drainage, lithology, distance from lineament, soil texture, and land use and land cover.

Part III: Compare the importance of the parameters in relation

For example of the factor weight and class weight

Please input scale with values from 1 to 5 to rate the relative preferences. Assign as 1 = very low; 2 = low; 3 = moderate; 4 = high; and 5 = very high.

Factor	Factor weight					Class	Class weight				
	1	2	3	4	5		1	2	3	4	5
Elevation (meter)			✓			0-200	✓				
						200-400		✓			
						400-600			✓		
						600-800				✓	
						800-1,000					✓
						>1,000					✓

Explanation: Elevation is the factors affecting on the landslide occurrence show a moderate level number equal to 3. Hence divided by height range into individual classes that greater heights values became more vulnerable to landslides.

3.1 Fill ✓ for assign value of the factor weight and class weight in the blank according to the method of WLC.

Assign as 1 = very low; 2 = low; 3 = moderate; 4 = high; and 5 = very high.

Factor	Factor weight					Class	Class weights				
	1	2	3	4	5		1	2	3	4	5
Elevation (meter)						0-200					
						200-400					
						400-600					
						600-800					
						800-1,000					
						>1,000					
Slope aspect						Flat					
						North					
						Northeast					
						East					
						Southeast					
						South					
						Southwest					
						West					
						Northwest					

Factor	Factor weight					Class	Class weights				
	1	2	3	4	5		1	2	3	4	5
Slope gradient (degree)						0-10					
						ค.ก.-20					
						20-30					
						30-40					
						40-50					
						> 50					
Slope Curvature						Concave (-)					
						Flat (0)					
						Convex (+)					
Topographic wetness index (TWI)						0-2.5					
						2.5-5.0					
						5.0-7.5					
						7.5-10					
						10-12.5					
						>12.5					

Factor	Factor weight					Class	Class weights				
	1	2	3	4	5		1	2	3	4	5
Distance from drainage (meter)						0-50					
						50-100					
						100-150					
						150-200					
						200-250					
						>250					
Soil Texture						Clay					
						Silty clay					
						Loamy sand					
						Sandy loam					
						Silty clay loam					
						Sand					
						Sandy clay loam					
						Clay loam					
						Silt loam					
						Loam					
						Slope complex area					

Factor	Factor weight					Class	Class weights				
	1	2	3	4	5		1	2	3	4	5
Lithology						Thung Yai					
						Ratburi					
						Quaternary Sediments					
						Kaeng Krachan					
						Igneous rocks					
						Krabi					
						Saibon Formation					
Distance from Lineament (meter)						0-500					
						500 -1,000					
						1,000 -1,500					
						1,500 -2,000					
						2,000 -2,500					
						2,500 -3,000					
						> 3,000					
Land Use and Land Cover (LULC)						Disturbed evergreen forest					
						Dense evergreen forest					
						Para rubber					
						Oil palm					
						Miscellaneous					

For example of the class weight according to the method of AHP.

Factor	Class	No.	1	2	3
Slope Curvature	concave	1	1	5	1/3
	flat	2	1/5	1	
	convex	3	3		1

Explanation: 1. Concave class have a priority rather than flat class is numerically equal to 5, compared to the same flat class is to be 1/5 of the concave class.

2. Convex class have a priority rather than concave class is numerically equal to 3, compared to the same concave class is to be 1/3 of the convex class.

3.2 Please indicate the rating of the importance of factors according to the method of AHP.

Factor	elevation	slope	aspect	curvature	TWI	distance from drainage	lithology	distance from lineament	soil texture	LULC
elevation	1									
slope		1								
aspect			1							
curvature				1						
TWI					1					
distance from drainage						1				
lithology							1			
distance from lineament								1		
soil texture									1	
LULC										1

Remark: The evaluation scale must be 1, representing equally preferred criteria when comparing anything to itself.

Factor	Class	No.	1	2	3
Slope curvature	Concave (-)	1	1		
	Flat (0)	2		1	
	Convex (+)	3			1

Factor	Class	No.	1	2	3	4	5	6
Topographic Wetness Index (TWI)	0-2.5	1	1					
	2.5-5.0	2		1				
	5.0-7.5	3			1			
	7.5-10	4				1		
	10-12.5	5					1	
	>12.5	6						1

Factor	Class	No.	1	2	3	4	5	6
Distance from drainage (meter)	0-50	1	1					
	50-100	2		1				
	100-150	3			1			
	150-200	4				1		
	200-250	5					1	
	>250	6						1

Factor	Class	No.	1	2	3	4	5	6	7
Lithology	Thung Yai	1	1						
	Ratburi	2		1					
	Quaternary Sediments	3			1				
	Kaeng Krachan	4				1			
	Igneous rocks	5					1		
	Krabi	6						1	
	Saibon Formation	7							1

Part IV: Comments and suggestions

4.1 Do you agree with the above determining factors involved in the landslide occurrence?

Agree Not agree; because

.....

.....

.....

.....

.....

.....

.....

.....

4.2 Do you agree with class interval defined for each factor?

Agree Not agree; because

.....

.....

.....

.....

.....

.....

.....

Table B3 List of experts.

No.	Name	Position	Office
1	Assoc. Prof. Dr. Charlie Navanugraha	Lecturer	Faculty of Environment and Resource Studies, Mahidol University
2	Assist.Prof.Dr.Chao Yongchalemchai	Lecturer	Department of Earth, Faculty of Natural Resources, Prince of Songkla University
3	Mr.Sirisart Yangsanphu	Geologist	Geotechnical Engineering Research and Development center (GERD), Department of Civil Engineering, Faculty of Engineering, Kasetsart University
4	Mr.Worawat Thowiwat	Geotechnical	Department of Civil Engineering, Faculty of Engineering, Kasetsart University
5	Assist. Prof. Dr. Sodchol Wonprasaid	Lecturer	School of Plant Science, Institute of Agricultural Technology, Suranaree University of Technology
6	Dr.Rawee Rattanakom	Lecturer	Faculty of Technology and Environment, Prince of Songkla University Phuket Campus
7	Dr.Narumon Intarawichian	Lecturer	Faculty of Geoinformatics, Burapha University
8	Ms.Sirilak Tanang		School of Remote Sensing, Institute of Science, Suranaree University of Technology

APPENDIX C
CONVENTIONAL WEIGHTED LINEAR
COMBINATION METHOD: WLC'S FACTOR WEIGHTS
AND WLC'S CLASS WEIGHTS

มหาวิทยาลัยเทคโนโลยีสุรนารี

Table C1 Factor weights from questionnaires.

No.	Criteria	Expert								Weight
		1	2	3	4	5	6	7	8	
1	Elevation	3	3	3	2	2	1	4	1	2.38
2	Slope gradient	5	5	5	5	4	4	5	3	4.50
3	Slope aspect	4	1	3	2	3	1	3	2	2.38
4	Slope curvature	2	4	3	3	3	2	2	3	2.75
5	Topographic wetness index	4	2	3	3	2	3	2	4	2.88
6	Distance from drainage	4	1	4	1	3	4	4	2	2.88
7	Soil texture	5	3	4	4	4	4	5	2	3.88
8	Lithology	4	5	4	4	4	4	-	5	4.29
9	Distance from lineament	2	4	4	1	3	3	4	3	3.00
10	Land use and land cover	4	2	2	4	3	4	3	2	3.00

Table C2 Elevation's weights from questionnaires.

No.	Criteria	Expert								Weight
		1	2	3	4	5	6	7	8	
1	0 m - 200 m	1	1	3	1	1	1	1	1	1.25
2	200 m - 400 m	2	2	3	2	2	2	2	2	2.13
3	400 m - 600 m	3	3	3	3	3	2	3	3	2.88
4	600 m - 800 m	5	4	4	3	4	3	4	4	3.88
5	800 m - 1,000 m	5	5	4	4	5	4	5	5	4.63
6	>1,000 m	4	5	3	4	5	5	5	5	4.50

Table C3 Slope gradient's weights from questionnaires.

No.	Criteria 1	Expert								Weight
		1	2	3	4	5	6	7	8	
1	0° - 10°	1	1	1	1	1	1	1	1	1.00
2	10° - 20°	2	2	2	2	2	2	2	2	2.00
3	20° - 30°	3	3	4	3	3	3	3	2	3.00
4	30° - 40°	5	4	3	4	4	4	4	3	3.88
5	40° - 50°	4	5	1	4	5	5	5	4	4.13
6	> 50°	4	5	1	5	5	5	5	5	4.38

Table C7 Distance from drainage's weights from questionnaires.

No.	Criteria	Expert								Weight
		1	2	3	4	5	6	7	8	
1	0 m – 50 m	5	5	4	5	5	5	5	5	4.88
2	50m – 100 m	5	4	3	4	4	4	4	5	4.13
3	100 m – 150 m	4	3	2	3	3	4	3	4	3.25
4	150 m – 200 m	3	2	1	2	2	3	2	3	2.25
5	200 m – 250 m	2	1	1	1	1	2	1	2	1.38
6	>250 m	1	1	1	1	1	1	1	1	1.00

Table C8 Lithology's weights from questionnaires.

No.	Criteria	Expert								Weight
		1	2	3	4	5	6	7	8	
1	Thung Yai	3	3	2	3	4	3	-	4	3.14
2	Ratburi	1	1	1	2	2	2	-	2	1.57
3	Quaternary Sediment	3	1	1	1	1	1	-	3	1.57
4	Kaeng Krachan	4	3	4	4	4	4	-	3	3.71
5	Igneous rocks	5	5	5	5	5	5	-	5	5.00
6	Krabi	4	4	2	3	3	4	-	1	3.00
7	Saibon Formation	3	2	2	3	4	3	-	4	3.00

Table C9 Distance from lineament's weights from questionnaires.

No.	Criteria	Expert								Weight
		1	2	3	4	5	6	7	8	
1	0 m - 500 m	5	5	5	5	5	5	5	5	5.00
2	500 m - 1,000 m	4	5	3	4	4	4	4	5	4.13
3	1,000 m - 1,500 m	3	4	2	3	3	3	1	4	2.88
4	1,500 m - 2,000 m	2	3	2	2	2	2	1	3	2.13
5	2,000 m - 2,500 m	1	2	2	1	1	2	1	3	1.63
6	2,500 m - 3,000 m	1	1	2	1	1	1	1	2	1.25
7	> 3,000 m	1	1	2	1	1	1	1	1	1.13

Table C10 Soil texture weights from questionnaires.

No.	Criteria	Expert								Weight
		1	2	3	4	5	6	7	8	
1	Clay	1	1	1	4	2	4	1	1	1.88
2	Silty clay	2	1	3	3	2	3	1	2	2.13
3	Loamy sand	3	5	2	2	5	2	4	3	3.25
4	Sandy loam	3	5	2	2	5	2	3	3	3.13
5	Silty clay loam	3	3	3	4	3	4	2	2	3.00
6	Sand	5	5	1	1	4	1	5	4	3.25
7	Sandy clay loam	4	4	3	4	3	2	3	2	3.13
8	Clay loam	3	1	1	3	2	4	2	3	2.38
9	Silty loam	3	2	1	3	3	3	2	4	2.63
10	Loam	3	3	1	3	4	3	3	3	2.88
11	Slope complex area	2	5	4	1	4	5	5	3	3.63

Table C11 Distance from drainage's weights from questionnaires.

No.	Criteria	Expert								Weight
		1	2	3	4	5	6	7	8	
1	Disturbed evergreen forest	5	3	2	2	4	2	3	2	2.88
2	Dense evergreen forest	4	1	1	1	1	1	1	1	1.38
3	Para rubber	4	5	3	4	3	4	5	4	4.00
4	Oil palm	3	5	2	3	2	5	4	4	3.50
5	Miscellaneous	2	4	1	5	5	3	3	5	3.50



APPENDIX D

THE PAIR-WISE COMPARISON METHOD:

AHP'S FACTOR WEIGHTS

Example of calculation for the AHP method

The procedure consists of three major step for each factor

Step I: Generation of the pair-wise comparison matrix.

1. Suppose that **slope** is strongly preferred over the **elevation** attribute; that is the comparison results in a value of 5.
2. Suppose that **aspect** is moderately to strongly preferred to **elevation**; that is the comparison results in a value of 4.
3. **Slope** attribute compared to **aspect** and suppose that the former is moderately preferred to the latter, a score of 3

Criteria	elevation	slope	aspect
elevation	1	1/5	1/4
slope	5	1	3
aspect	4	1/3	1

Step II: Computation of the criterion weights.

1. Sum the values in each column of the pairwise comparison matrix
2. Divide each element in the matrix by its column total (the resulting matrix is referred to as the *normalized pairwise comparison matrix*)
3. Compute the average of the elements in each row of the normalized matrix, that is, divide the sum of normalized scores for each row by 3

Criteria	Step I			Step II			Step III
	e	s	a	e	s	a	Weight
Elevation (e)	1.00	1/5	1/4	0.10	0.13	0.60	$(0.10 + 0.13 + 0.60) / 3 = 0.10$
slope (s)	5.00	1.00	3.00	0.50	0.65	0.71	$(0.50 + 0.65 + 0.71) / 3 = 0.62$
aspect (a)	4.00	1/3	1.00	0.40	0.22	0.24	$(0.40 + 0.22 + 0.24) / 3 = 0.28$
Total	10.00	1.53	4.25	1.00	1.00	1.00	1.00

Step III: Estimation of the consistency ratio

1. Compute the weight sum vector
2. Compute the consistency vector

Criteria	Step I	Step II
elevation (e)	$(0.10)(1.00) + (0.62)(0.20) + (0.28)(0.25) = 0.29$	$0.29 / 0.10 = 2.90$
slope (s)	$(0.10)(5.00) + (0.62)(1.00) + (0.28)(3.00) = 1.95$	$1.95 / 0.62 = 3.15$
aspect (a)	$(0.10)(4.00) + (0.62)(0.33) + (0.28)(1.00) = 0.88$	$0.88 / 0.28 = 3.14$

Compute values for two more terms, *lambda* (λ) and the *consistency index* (CI)

$$\text{Lambda } (\lambda) = \frac{\sum CV}{n}; (\lambda) = \frac{2.90 + 3.15 + 3.14}{3} = 3.06$$

Number of criteria (n) = 3

Calculation of CI is based on the observation that λ is always greater than or equal to the number of criteria under consideration (n) for positive, reciprocal matrixes, and $\lambda = n$ if the pairwise comparison matrix is a consistent matrix. Accordingly, $\lambda - n$ can be considered as a measure of the degree of inconsistency.

$$\text{Consistency Index (CI)} = \frac{\lambda - n}{n - 1} = \frac{3.06 - 3}{3 - 1} = 0.03$$

The CI term, referred to as the consistency index, provides a measure of departure from consistency. Further, we can calculate the *consistency ratio* (CR), which is defined as follows:

$$\text{Consistency Ratio (CR)} = \frac{CI}{RI} = \frac{0.03}{0.58} = 0.05$$

RI = random index, depends on the number of elements being compared

Random Index (RI) for $n = 3$ is **0.58**

Table D1 Factor weights from questionnaires.

No.	Criteria 1	Criteria 2	Expert							
			1	2	3	4	5	6	7	8
1	EL	EL	1	1	1	1	1	1	1	1
2	EL	SL	1/5	1/5	1/4	1/3	1/5	1/7	1/3	1/5
3	EL	AS	1/4	5	2	1	1/5	1	3	1/6
4	EL	CT	1/3	1/3	2	1/3	1/3	1/2	3	1/5
5	EL	TWI	1/3	3	1/3	0	1/3	1/5	3	1/7
6	EL	DD	1/4	5	1/3	2	1/3	1/8	1	1/2
7	EL	LT	1/4	1/5	1/5	1/2	1/7	1/7		1/7
8	EL	DL	1/4	1/3	1/4	2	1/5	1/7	1	1/5
9	EL	ST	1/5	3	1	1/2	1/7	1/7	1/3	1/4
10	EL	LULC	1/3	3	2	1/5	1/5	1/7	1/3	1/3
11	SL	SL	1	1	1	1	1	1	1	1
12	SL	AS	5	9	5	1/2	5	7	5	2
13	SL	CT	5	3	5	1	3	6	5	1
14	SL	TWI	5	7	4	0	7	3	5	1/2
15	SL	DD	4	9	4	1/3	5	6	5	2
16	SL	LT	4	1	2	1/4	3	3		1/3
17	SL	DL	5	3	3	1/3	5	5	5	3
18	SL	ST	5	5	7	1/4	3	3	1	2
19	SL	LULC	5	7	8	1/4	5	6	1	3
20	AS	AS	1	1	1	1	1	1	1	1
21	AS	CT	4	1/7	1	3	3	1/3	1	1/2
22	AS	TWI	4	1/3	1/4	0	5	1/5	1	1/4
23	AS	DD	1/3	1	1/5	2	5	1/5	3	2
24	AS	LT	1/3	1/9	1/7	1/2	3	1/5		1/5
25	AS	DL	1/3	1/7	1/6	1/2	5	1/4	3	1/3
26	AS	ST	1/4	1/5	1/5	1/2	3	1/5	1/3	2
27	AS	LULC	1/3	1/5	2	1/2	5	1/8	1/3	2
28	CT	CT	1	1	1	1	1	1	1	1
29	CT	TWI	1/4	5	1/3	0	3	1/3	1/3	1/3
30	CT	DD	1/5	7	1/3	3	3	1/2	1	2
31	CT	LT	1/4	1/3	1/7	1/4	3	1/5		1/5
32	CT	DL	1/4	1/3	1/5	3	3	1/2	1	2
33	CT	ST	1/4	3	1/5	1/4	3	1/4	1/5	4
34	CT	LULC	1/3	5	2	1/4	5	1/4	1/5	5
35	TWI	TWI	1	1	1	1	1	1	1	1
36	TWI	DD	1/5	3	1/3	3	1/3	2	1	4

Table D1 (Continued).

No.	Criteria 1	Criteria 2	Expert							
			1	2	3	4	5	6	7	8
37	TWI	LT	1/3	1/7	1/7	1/4	1/5	1/2		1/2
38	TWI	DL	1/3	1/5	1/6	3	1/3	4	1	3
39	TWI	ST	1/4	1/3	1	1/4	1/5	1/2	1/5	3
40	TWI	LULC	1/4	1	5	1/4	1/3	1/2	1/5	3
41	DD	DD	1	1	1	1	1	1	1	1
42	DD	LT	4	1/9	1/2	1/2	1/5	1/2		1/5
43	DD	DL	3	1/7	1/3	2	3	1/3	1	1/4
44	DD	ST	3	1/5	1/2	1/2	1/5	1/2	1/5	2
45	DD	LULC	3	1/3	5	1/2	1/3	1/5	1/5	3
46	LT	LT	1	1	1	1	1	1	1	1
47	LT	DL	3	3	1/2	4	5	1/3		4
48	LT	ST	1/4	7	1/2	1	3	1/2		5
49	LT	LULC	4	7	7	1	5	1/4		5
50	DL	DL	1	1	1	1	1	1	1	1
51	DL	ST	1/5	5	3	1/4	1/5	1/6	1/5	2
52	DL	LULC	1/4	5	5	1/4	1/3	1/6	1/5	2
53	ST	ST	1	1	1	1	1	1	1	1
54	ST	LULC	5	3	3	1/5	3	2	1	3
55	LULC	LULC	1	1	1	1	1	1	1	1

Remark: EL = Elevation SL = Slope angle AS = Slope aspect

CT = Slope curvature TWI = Topographic wetness index

DD = Distance from Drainage LT = Lithology

DL = Distance from lineament ST = Soil texture

LULC = Land use/Land cover

THE PROCEDURE CONSISTS OF THREE MAJOR STEPS FOR EACH FACTOR

Expert 1

Table D2 Step I: Generation of the pair-wise comparison matrix for each factor.

Factor	elevation	slope	aspect	curvature	TWI	distance from drainage	lithology	distance from lineament	soil texture	LULC
elevation	1.00	0.20	0.25	0.33	0.33	0.25	0.25	0.25	0.20	0.33
slope	5.00	1.00	5.00	5.00	5.00	4.00	4.00	5.00	5.00	5.00
aspect	4.00	0.20	1.00	4.00	4.00	0.33	0.33	0.33	0.25	0.33
curvature	3.00	0.20	0.25	1.00	0.25	0.20	0.25	0.25	0.25	0.33
TWI	3.00	0.20	0.25	4.00	1.00	0.20	0.33	0.33	0.25	0.25
distance from drainage	4.00	0.25	3.00	5.00	5.00	1.00	4.00	3.00	3.00	3.00
lithology	4.00	0.25	3.00	4.00	3.00	0.25	1.00	3.00	0.25	4.00
distance from lineament	4.00	0.20	3.00	4.00	3.00	0.33	0.33	1.00	0.20	0.25
soil texture	5.00	0.20	4.00	4.00	4.00	0.33	4.00	5.00	1.00	5.00
LULC	3.00	0.20	3.00	3.00	4.00	0.33	0.25	4.00	0.20	1.00
Total	36.00	2.90	22.75	34.33	29.58	7.23	14.75	22.17	10.60	19.50

Table D3 Step II: Computation of the criterion weights for each factor.

Factor	elevation	slope	aspect	curvature	TWI	distance from drainage	lithology	distance from lineament	soil texture	LULC	Total	Weight	Weight (%)
elevation	0.03	0.07	0.01	0.01	0.01	0.03	0.02	0.01	0.02	0.02	0.2275	0.0227	2.2746
slope	0.14	0.34	0.22	0.15	0.17	0.55	0.27	0.23	0.47	0.26	2.7960	0.2796	27.9600
aspect	0.11	0.07	0.04	0.12	0.14	0.05	0.02	0.02	0.02	0.02	0.6001	0.0600	6.0015
curvature	0.08	0.07	0.01	0.03	0.01	0.03	0.02	0.01	0.02	0.02	0.2974	0.0297	2.9742
TWI	0.08	0.07	0.01	0.12	0.03	0.03	0.02	0.02	0.02	0.01	0.4153	0.0415	4.1529
distance from drainage	0.11	0.09	0.13	0.15	0.17	0.14	0.27	0.14	0.28	0.15	1.6255	0.1625	16.2547
lithology	0.11	0.09	0.13	0.12	0.10	0.03	0.07	0.14	0.02	0.21	1.0135	0.1014	10.1351
distance from lineament	0.11	0.07	0.13	0.12	0.10	0.05	0.02	0.05	0.02	0.01	0.6753	0.0675	6.7534
soil texture	0.14	0.07	0.18	0.12	0.14	0.05	0.27	0.23	0.09	0.26	1.5290	0.1529	15.2898
LULC	0.08	0.07	0.13	0.09	0.14	0.05	0.02	0.18	0.02	0.05	0.8204	0.0820	8.2039
Total	1.00	1.00	1.00	1.00	1.00	1.00	1.00	1.00	1.00	1.00			



Table D4 Step III: Estimation of the consistency ratio for each factor.

Factor	elevation	slope	aspect	curvature	TWI	distance from drainage	lithology	distance from lineament	soil texture	LULC	weight sum vector	Weight	Consistency Vector
elevation	0.03	0.07	0.01	0.01	0.01	0.03	0.02	0.01	0.02	0.02	0.2582	0.0227	11.3519
slope	0.14	0.34	0.22	0.15	0.17	0.55	0.27	0.23	0.47	0.26	3.6177	0.2796	12.9389
aspect	0.11	0.07	0.04	0.12	0.14	0.05	0.02	0.02	0.02	0.02	0.6681	0.0600	11.1314
curvature	0.08	0.07	0.01	0.03	0.01	0.03	0.02	0.01	0.02	0.02	0.3196	0.0297	10.7453
TWI	0.08	0.07	0.01	0.12	0.03	0.03	0.02	0.02	0.02	0.01	0.4472	0.0415	10.7684
distance from drainage	0.11	0.09	0.13	0.15	0.17	0.14	0.27	0.14	0.28	0.15	2.1726	0.1625	13.3663
lithology	0.11	0.09	0.13	0.12	0.10	0.03	0.07	0.14	0.02	0.21	1.2955	0.1014	12.7819
distance from lineament	0.11	0.07	0.13	0.12	0.10	0.05	0.02	0.05	0.02	0.01	0.7771	0.0675	11.5067
soil texture	0.14	0.07	0.18	0.12	0.14	0.05	0.27	0.23	0.09	0.26	2.0551	0.1529	13.4413
LULC	0.08	0.07	0.13	0.09	0.14	0.05	0.02	0.18	0.02	0.05	1.0218	0.0820	12.4553
Total													120.4872

Number of criteria (n) = 10 Lambda (λ) = $\frac{120.4872}{10} = 12.05$

Consistency Index (CI) = $\frac{\lambda - n}{n - 1} = \frac{12.05 - 10}{10 - 1} = 0.23$

Random Index (RI) for $n = 10$ is 1.49

Consistency Ratio (CR) = $\frac{CI}{RI} = \frac{0.23}{1.49} = 0.15$

Expert 2

Table D5 Step I: Generation of the pair-wise comparison matrix for each factor.

Factor	elevation	slope	aspect	curvature	TWI	distance from drainage	lithology	distance from lineament	soil texture	LULC
elevation	1.00	0.20	5.00	0.33	3.00	5.00	0.20	0.33	3.00	3.00
slope	5.00	1.00	9.00	3.00	7.00	9.00	1.00	3.00	5.00	7.00
aspect	0.20	0.11	1.00	0.14	0.33	1.00	0.11	0.20	0.20	0.14
curvature	3.00	0.33	7.00	1.00	5.00	7.00	0.33	0.33	3.00	5.00
TWI	0.33	0.14	3.00	0.20	1.00	3.00	0.14	0.20	0.33	1.00
distance from drainage	0.20	0.11	1.00	0.14	0.33	1.00	0.11	0.14	0.20	0.33
lithology	5.00	1.00	9.00	3.00	7.00	9.00	1.00	3.00	7.00	7.00
distance from lineament	3.00	0.33	7.00	3.00	5.00	7.00	0.33	1.00	5.00	5.00
soil texture	0.33	0.20	5.00	0.33	3.00	5.00	0.14	0.20	1.00	3.00
LULC	0.33	0.14	5.00	0.20	1.00	3.00	0.14	0.20	0.33	1.00
Total	18.40	3.57	52.00	11.35	32.67	50.00	3.52	8.61	25.07	32.48

Table D6 Step II: Computation of the criterion weights for each factor.

Factor	elevation	slope	aspect	curvature	TWI	distance from drainage	lithology	distance from lineament	soil texture	LULC	Total	Weight	Weight (%)
elevation	0.05	0.06	0.10	0.03	0.09	0.10	0.06	0.04	0.12	0.09	0.7353	0.0735	7.3528
slope	0.27	0.28	0.17	0.26	0.21	0.18	0.28	0.35	0.20	0.22	2.4309	0.2431	24.3087
aspect	0.01	0.03	0.02	0.01	0.01	0.02	0.03	0.02	0.01	0.00	0.1712	0.0171	1.7117
curvature	0.16	0.09	0.13	0.09	0.15	0.14	0.09	0.04	0.12	0.15	1.1792	0.1179	11.7918
TWI	0.02	0.04	0.06	0.02	0.03	0.06	0.04	0.02	0.01	0.03	0.3319	0.0332	3.3194
distance from drainage	0.01	0.03	0.02	0.01	0.01	0.02	0.03	0.02	0.01	0.01	0.1704	0.0170	1.7040
lithology	0.27	0.28	0.17	0.26	0.21	0.18	0.28	0.35	0.28	0.22	2.5107	0.2511	25.1066
distance from lineament	0.16	0.09	0.13	0.26	0.15	0.14	0.09	0.12	0.20	0.15	1.5126	0.1513	15.1258
soil texture	0.02	0.06	0.10	0.03	0.09	0.10	0.04	0.02	0.04	0.09	0.5875	0.0588	5.8753
LULC	0.02	0.04	0.10	0.02	0.03	0.06	0.04	0.02	0.01	0.03	0.3704	0.0370	3.7040
Total	1.00	1.00	1.00	1.00	1.00	1.00	1.00	1.00	1.00	1.00			



Table D7 Step III: Estimation of the consistency ratio for each factor.

Factor	elevation	slope	aspect	curvature	TWI	distance from drainage	lithology	distance from lineament	soil texture	LULC	weight sum vector	Weight	Consistency Vector
elevation	0.05	0.06	0.10	0.03	0.09	0.10	0.06	0.04	0.12	0.09	0.8198	0.0735	11.1498
slope	0.27	0.28	0.17	0.26	0.21	0.18	0.28	0.35	0.20	0.22	2.7621	0.2431	11.3627
aspect	0.01	0.03	0.02	0.01	0.01	0.02	0.03	0.02	0.01	0.00	0.1790	0.0171	10.4559
curvature	0.16	0.09	0.13	0.09	0.15	0.14	0.09	0.04	0.12	0.15	1.3202	0.1179	11.1956
TWI	0.02	0.04	0.06	0.02	0.03	0.06	0.04	0.02	0.01	0.03	0.3412	0.0332	10.2798
distance from drainage	0.01	0.03	0.02	0.01	0.01	0.02	0.03	0.02	0.01	0.01	0.1774	0.0170	10.4101
lithology	0.27	0.28	0.17	0.26	0.21	0.18	0.28	0.35	0.28	0.22	2.8796	0.2511	11.4696
distance from lineament	0.16	0.09	0.13	0.26	0.15	0.14	0.09	0.12	0.20	0.15	1.7743	0.1513	11.7306
soil texture	0.02	0.06	0.10	0.03	0.09	0.10	0.04	0.02	0.04	0.09	0.6188	0.0588	10.5320
LULC	0.02	0.04	0.10	0.02	0.03	0.06	0.04	0.02	0.01	0.03	0.3755	0.0370	10.1366
Total													108.7227

Number of criteria (n) = 10 Lambda (λ) = $\frac{108.7227}{10} = 10.87$

Consistency Index (CI) = $\frac{\lambda - n}{n - 1} = \frac{10.87 - 10}{10 - 1} = 0.10$

Random Index (RI) for $n = 10$ is 1.49

Consistency Ratio (CR) = $\frac{CI}{RI} = \frac{0.10}{1.49} = 0.07$

Expert 3

Table D8 Step I: Generation of the pair-wise comparison matrix for each factor.

Factor	elevation	slope	aspect	curvature	TWI	distance from drainage	lithology	distance from lineament	soil texture	LULC
elevation	1.00	0.20	0.17	0.20	0.14	0.50	0.14	0.20	0.25	0.33
slope	5.00	1.00	2.00	1.00	0.50	2.00	0.33	3.00	2.00	3.00
aspect	6.00	0.50	1.00	0.50	0.25	2.00	0.20	0.33	2.00	2.00
curvature	5.00	1.00	2.00	1.00	0.33	2.00	0.20	2.00	4.00	5.00
TWI	7.00	2.00	4.00	3.00	1.00	4.00	0.50	3.00	3.00	3.00
distance from drainage	2.00	0.50	0.50	0.50	0.25	1.00	0.20	0.25	2.00	3.00
lithology	7.00	3.00	5.00	5.00	2.00	5.00	1.00	4.00	5.00	5.00
distance from lineament	5.00	0.33	3.00	0.50	0.33	4.00	0.25	1.00	2.00	2.00
soil texture	4.00	0.50	0.50	0.25	0.33	0.50	0.20	0.50	1.00	3.00
LULC	3.00	0.33	0.50	0.20	0.33	0.33	0.20	0.50	0.33	1.00
Total	45.00	9.37	18.67	12.15	5.48	21.33	3.23	14.78	21.58	27.33

Table D9 Step II: Computation of the criterion weights for each factor.

Factor	elevation	slope	aspect	curvature	TWI	distance from drainage	lithology	distance from lineament	soil texture	LULC	Total	Weight	Weight (%)
elevation	0.04	0.08	0.05	0.06	0.01	0.02	0.02	0.04	0.07	0.05	0.46	0.0460	4.5967
slope	0.18	0.31	0.14	0.15	0.17	0.30	0.24	0.49	0.48	0.20	2.65	0.2652	26.5245
aspect	0.02	0.06	0.03	0.03	0.01	0.01	0.02	0.03	0.01	0.05	0.28	0.0276	2.7559
curvature	0.02	0.06	0.03	0.03	0.01	0.02	0.02	0.03	0.01	0.05	0.29	0.0295	2.9457
TWI	0.13	0.08	0.11	0.09	0.04	0.02	0.02	0.03	0.07	0.13	0.72	0.0718	7.1750
distance from drainage	0.13	0.08	0.14	0.09	0.13	0.07	0.06	0.05	0.03	0.13	0.92	0.0918	9.1751
lithology	0.22	0.15	0.19	0.22	0.30	0.15	0.12	0.08	0.03	0.18	1.65	0.1646	16.4638
distance from lineament	0.18	0.10	0.16	0.15	0.26	0.22	0.24	0.16	0.20	0.13	1.81	0.1815	18.1499
soil texture	0.04	0.04	0.14	0.15	0.04	0.15	0.24	0.05	0.07	0.08	1.01	0.1011	10.1060
LULC	0.02	0.04	0.01	0.02	0.01	0.01	0.02	0.03	0.02	0.03	0.21	0.0211	2.1075
Total	1.00	1.00	1.00	1.00	1.00	1.00	1.00	1.00	1.00	1.00			



Table D10 Step III: Estimation of the consistency ratio for each factor.

Factor	elevation	slope	aspect	curvature	TWI	distance from drainage	lithology	distance from lineament	soil texture	LULC	weight sum vector	Weight	Consistency Vector
elevation	0.04	0.08	0.05	0.06	0.01	0.02	0.02	0.04	0.07	0.05	0.50	0.0460	10.9279
slope	0.18	0.31	0.14	0.15	0.17	0.30	0.24	0.49	0.48	0.20	3.14	0.2652	11.8305
aspect	0.02	0.06	0.03	0.03	0.01	0.01	0.02	0.03	0.01	0.05	0.29	0.0276	10.3584
curvature	0.02	0.06	0.03	0.03	0.01	0.02	0.02	0.03	0.01	0.05	0.31	0.0295	10.5148
TWI	0.13	0.08	0.11	0.09	0.04	0.02	0.02	0.03	0.07	0.13	0.77	0.0718	10.6669
distance from drainage	0.13	0.08	0.14	0.09	0.13	0.07	0.06	0.05	0.03	0.13	1.04	0.0918	11.2925
lithology	0.22	0.15	0.19	0.22	0.30	0.15	0.12	0.08	0.03	0.18	1.90	0.1646	11.5451
distance from lineament	0.18	0.10	0.16	0.15	0.26	0.22	0.24	0.16	0.20	0.13	2.21	0.1815	12.1764
soil texture	0.04	0.04	0.14	0.15	0.04	0.15	0.24	0.05	0.07	0.08	1.18	0.1011	11.6589
LULC	0.02	0.04	0.01	0.02	0.01	0.01	0.02	0.03	0.02	0.03	0.23	0.0211	11.0051
Total													111.9765

Number of criteria (n) = 10 Lambda (λ) = $\frac{111.9765}{10} = 11.20$

Consistency Index (CI) = $\frac{\lambda - n}{n - 1} = \frac{11.20 - 10}{10 - 1} = 0.13$

Random Index (RI) for $n = 10$ is 1.49, Consistency Ratio (CR) = $\frac{CI}{RI} = \frac{0.13}{1.49} = 0.09$

Expert 4

Table D11 Step I: Generation of the pair-wise comparison matrix for each factor.

Factor	elevation	slope	aspect	curvature	TWI	distance from drainage	lithology	distance from lineament	soil texture	LULC
elevation	1.00	0.33	1.00	0.33	0.00	2.00	0.50	2.00	0.50	0.20
slope	3.00	1.00	0.50	1.00	0.00	0.33	0.25	0.33	0.25	0.25
aspect	1.00	2.00	1.00	3.00	0.00	2.00	0.50	0.50	0.50	0.50
curvature	3.00	1.00	1.50	1.00	0.00	3.00	0.25	3.00	0.25	0.25
TWI	0.67	1.00	1.50		1.00	3.00	0.25	3.00	0.25	0.25
distance from drainage	1.00	3.00	1.00	0.33	0.33	1.00	0.50	2.00	0.50	0.50
lithology	0.50	4.00	2.00	4.00	4.00	2.00	1.00	4.00	1.00	1.00
distance from lineament	2.00	3.00	0.50	0.33	0.33	0.50	0.25	1.00	0.25	0.25
soil texture	0.50	4.00	2.00	4.00	4.00	2.00	1.00	4.00	1.00	0.20
LULC	5.00	4.00	2.00	4.00	4.00	2.00	1.00	4.00	5.00	1.00
Total	17.67	23.33	13.00	18.00	13.67	17.83	5.50	23.83	9.50	4.40

Table D12 Step II: Computation of the criterion weights for each factor.

Factor	elevation	slope	aspect	curvature	TWI	distance from drainage	lithology	distance from lineament	soil texture	LULC	Total	Weight	Weight (%)
elevation	0.06	0.01	0.08	0.02	0.00	0.11	0.09	0.08	0.05	0.05	0.55	0.0551	5.5139
slope	0.17	0.04	0.04	0.06	0.00	0.02	0.05	0.01	0.03	0.06	0.47	0.0468	4.6795
aspect	0.06	0.09	0.08	0.17	0.00	0.11	0.09	0.02	0.05	0.11	0.78	0.0776	7.7621
curvature	0.17	0.04	0.12	0.06	0.00	0.17	0.05	0.13	0.03	0.06	0.81	0.0806	8.0630
TWI	0.04	0.04	0.12	0.00	0.07	0.17	0.05	0.13	0.03	0.06	0.69	0.0692	6.9184
distance from drainage	0.06	0.13	0.08	0.02	0.02	0.06	0.09	0.08	0.05	0.11	0.70	0.0702	7.0217
lithology	0.03	0.17	0.15	0.22	0.29	0.11	0.18	0.17	0.11	0.23	1.66	0.1663	16.6282
distance from lineament	0.11	0.13	0.04	0.02	0.02	0.03	0.05	0.04	0.03	0.06	0.52	0.0522	5.2173
soil texture	0.03	0.17	0.15	0.22	0.29	0.11	0.18	0.17	0.11	0.05	1.48	0.1481	14.8100
LULC	0.28	0.17	0.15	0.22	0.29	0.11	0.18	0.17	0.53	0.23	2.34	0.2339	23.3859
Total	1.00	1.00	1.00	1.00	1.00	1.00	1.00	1.00	1.00	1.00			



Table D13 Step III: Estimation of the consistency ratio for each factor.

Factor	elevation	slope	aspect	curvature	TWI	distance from drainage	lithology	distance from lineament	soil texture	LULC	weight sum vector	Weight	Consistency Vector
elevation	0.06	0.01	0.08	0.02	0.00	0.11	0.09	0.08	0.05	0.05	0.62	0.0551	11.3164
slope	0.17	0.04	0.04	0.06	0.00	0.02	0.05	0.01	0.03	0.06	0.51	0.0468	10.8881
aspect	0.06	0.09	0.08	0.17	0.00	0.11	0.09	0.02	0.05	0.11	0.91	0.0776	11.7092
curvature	0.17	0.04	0.12	0.06	0.00	0.17	0.05	0.13	0.03	0.06	0.91	0.0806	11.3297
TWI	0.04	0.04	0.12	0.00	0.07	0.17	0.05	0.13	0.03	0.06	0.77	0.0692	11.1790
distance from drainage	0.06	0.13	0.08	0.02	0.02	0.06	0.09	0.08	0.05	0.11	0.77	0.0702	10.9911
lithology	0.03	0.17	0.15	0.22	0.29	0.11	0.18	0.17	0.11	0.23	1.87	0.1663	11.2256
distance from lineament	0.11	0.13	0.04	0.02	0.02	0.03	0.05	0.04	0.03	0.06	0.56	0.0522	10.8054
soil texture	0.03	0.17	0.15	0.22	0.29	0.11	0.18	0.17	0.11	0.05	1.68	0.1481	11.3405
LULC	0.28	0.17	0.15	0.22	0.29	0.11	0.18	0.17	0.53	0.23	2.71	0.2339	11.5760
Total													112.3610

Number of criteria (n) = 10 Lambda (λ) = $\frac{112.3610}{10} = 11.24$

Consistency Index (CI) = $\frac{\lambda - n}{n - 1} = \frac{11.24 - 10}{10 - 1} = 0.14$

Random Index (RI) for $n = 10$ is 1.49

Consistency Ratio (CR) = $\frac{CI}{RI} = \frac{0.14}{1.49} = 0.09$

Expert 5

Table D14 Step I: Generation of the pair-wise comparison matrix for each factor.

Factor	elevation	slope	aspect	curvature	TWI	distance from drainage	lithology	distance from lineament	soil texture	LULC
elevation	1.00	0.20	0.20	0.33	0.33	0.33	0.14	0.20	0.14	0.20
slope	5.00	1.00	5.00	3.00	7.00	5.00	3.00	5.00	3.00	5.00
aspect	5.00	0.20	1.00	3.00	5.00	5.00	3.00	5.00	3.00	5.00
curvature	3.00	0.33	0.33	1.00	3.00	3.00	3.00	3.00	3.00	5.00
TWI	3.00	0.14	0.20	0.33	1.00	0.33	0.20	0.33	0.20	0.33
distance from drainage	3.00	0.20	0.20	0.33	3.00	1.00	0.20	3.00	0.20	0.33
lithology	7.00	0.33	0.33	0.33	5.00	5.00	1.00	5.00	3.00	5.00
distance from lineament	5.00	0.20	0.20	0.33	3.00	0.33	0.20	1.00	0.20	0.33
soil texture	7.00	0.33	0.33	0.33	5.00	5.00	0.33	5.00	1.00	3.00
LULC	5.00	0.20	0.20	0.20	3.00	3.00	0.20	3.00	0.33	1.00
Total	44.00	3.14	8.00	9.20	35.33	28.00	11.28	30.53	14.08	25.20

Table D15 Step II: Computation of the criterion weights for each factor.

Factor	elevation	slope	aspect	curvature	TWI	distance from drainage	lithology	distance from lineament	soil texture	LULC	Total	Weight	Weight (%)
elevation	0.02	0.06	0.03	0.04	0.01	0.01	0.01	0.01	0.01	0.01	0.21	0.0206	2.0624
slope	0.11	0.32	0.63	0.33	0.20	0.18	0.27	0.16	0.21	0.20	2.60	0.2601	26.0093
aspect	0.11	0.06	0.13	0.33	0.14	0.18	0.27	0.16	0.21	0.20	1.79	0.1790	17.8978
curvature	0.07	0.11	0.04	0.11	0.08	0.11	0.27	0.10	0.21	0.20	1.29	0.1292	12.9249
TWI	0.07	0.05	0.03	0.04	0.03	0.01	0.02	0.01	0.01	0.01	0.27	0.0271	2.7116
distance from drainage	0.07	0.06	0.03	0.04	0.08	0.04	0.02	0.10	0.01	0.01	0.46	0.0457	4.5710
lithology	0.16	0.11	0.04	0.04	0.14	0.18	0.09	0.16	0.21	0.20	1.33	0.1327	13.2711
distance from lineament	0.11	0.06	0.03	0.04	0.08	0.01	0.02	0.03	0.01	0.01	0.41	0.0413	4.1324
soil texture	0.16	0.11	0.04	0.04	0.14	0.18	0.03	0.16	0.07	0.12	1.05	0.1047	10.4654
LULC	0.11	0.06	0.03	0.02	0.08	0.11	0.02	0.10	0.02	0.04	0.60	0.0595	5.9541
Total	1.00	1.00	1.00	1.00	1.00	1.00	1.00	1.00	1.00	1.00			



Table D16 Step III: Estimation of the consistency ratio for each factor.

Factor	elevation	slope	aspect	curvature	TWI	distance from drainage	lithology	distance from lineament	soil texture	LULC	weight sum vector	Weight	Consistency Vector
elevation	0.02	0.06	0.03	0.04	0.01	0.01	0.01	0.01	0.01	0.01	0.23	0.0206	11.1462
slope	0.11	0.32	0.63	0.33	0.20	0.18	0.27	0.16	0.21	0.20	3.28	0.2601	12.6133
aspect	0.11	0.06	0.13	0.33	0.14	0.18	0.27	0.16	0.21	0.20	2.30	0.1790	12.8642
curvature	0.07	0.11	0.04	0.11	0.08	0.11	0.27	0.10	0.21	0.20	1.69	0.1292	13.0734
TWI	0.07	0.05	0.03	0.04	0.03	0.01	0.02	0.01	0.01	0.01	0.30	0.0271	11.1133
distance from drainage	0.07	0.06	0.03	0.04	0.08	0.04	0.02	0.10	0.01	0.01	0.51	0.0457	11.1819
lithology	0.16	0.11	0.04	0.04	0.14	0.18	0.09	0.16	0.21	0.20	1.65	0.1327	12.4250
distance from lineament	0.11	0.06	0.03	0.04	0.08	0.01	0.02	0.03	0.01	0.01	0.44	0.0413	10.6294
soil texture	0.16	0.11	0.04	0.04	0.14	0.18	0.03	0.16	0.07	0.12	1.23	0.1047	11.7728
LULC	0.11	0.06	0.03	0.02	0.08	0.11	0.02	0.10	0.02	0.04	0.68	0.0595	11.4240
Total													118.2436

Number of criteria (n) = 10 Lambda (λ) = $\frac{118.2436}{10} = 11.82$

Consistency Index (CI) = $\frac{\lambda - n}{n - 1} = \frac{11.82 - 10}{10 - 1} = 0.20$

Random Index (RI) for $n = 10$ is 1.49

Consistency Ratio (CR) = $\frac{CI}{RI} = \frac{0.20}{1.49} = 0.14$

Expert 6

Table D17 Step I: Generation of the pair-wise comparison matrix for each factor.

Factor	elevation	slope	aspect	curvature	TWI	distance from drainage	lithology	distance from lineament	soil texture	LULC
elevation	1.00	0.14	1.00	0.50	0.20	0.13	0.14	0.14	0.14	0.14
slope	7.00	1.00	7.00	6.00	3.00	6.00	3.00	5.00	3.00	6.00
aspect	1.00	0.14	1.00	0.33	0.20	0.20	0.20	0.25	0.20	0.13
curvature	2.00	0.17	3.00	1.00	0.33	0.50	0.20	0.50	0.25	0.25
TWI	5.00	0.33	5.00	3.00	1.00	2.00	0.50	4.00	0.50	0.50
distance from drainage	8.00	0.17	5.00	2.00	0.50	1.00	0.50	0.33	0.50	0.20
lithology	7.00	0.33	5.00	5.00	2.00	2.00	1.00	0.33	0.50	0.25
distance from lineament	7.00	0.20	4.00	2.00	0.25	3.00	3.00	1.00	0.17	0.17
soil texture	7.00	0.33	5.00	4.00	2.00	2.00	2.00	6.00	1.00	2.00
LULC	7.00	0.17	8.00	4.00	2.00	5.00	4.00	6.00	0.50	1.00
Total	52.00	2.99	44.00	27.83	11.48	21.83	14.54	23.56	6.76	10.63

Table D18 Step II: Computation of the criterion weights for each factor.

Factor	elevation	slope	aspect	curvature	TWI	distance from drainage	lithology	distance from lineament	soil texture	LULC	Total	Weight	Weight (%)
elevation	0.02	0.05	0.02	0.02	0.02	0.01	0.01	0.01	0.02	0.01	0.18	0.0181	1.8137
slope	0.13	0.33	0.16	0.22	0.26	0.27	0.21	0.21	0.44	0.56	2.81	0.2807	28.0690
aspect	0.02	0.05	0.02	0.01	0.02	0.01	0.01	0.01	0.03	0.01	0.19	0.0194	1.9407
curvature	0.04	0.06	0.07	0.04	0.03	0.02	0.01	0.02	0.04	0.02	0.35	0.0346	3.4580
TWI	0.10	0.11	0.11	0.11	0.09	0.09	0.03	0.17	0.07	0.05	0.93	0.0933	9.3309
distance from drainage	0.15	0.06	0.11	0.07	0.04	0.05	0.03	0.01	0.07	0.02	0.63	0.0626	6.2583
lithology	0.13	0.11	0.11	0.18	0.17	0.09	0.07	0.01	0.07	0.02	0.99	0.0986	9.8573
distance from lineament	0.13	0.07	0.09	0.07	0.02	0.14	0.21	0.04	0.02	0.02	0.81	0.0813	8.1266
soil texture	0.13	0.11	0.11	0.14	0.17	0.09	0.14	0.25	0.15	0.19	1.50	0.1498	14.9762
LULC	0.13	0.06	0.18	0.14	0.17	0.23	0.28	0.25	0.07	0.09	1.62	0.1617	16.1695
Total	1.00	1.00	1.00	1.00	1.00	1.00	1.00	1.00	1.00	1.00			



Table D19 Step III: Estimation of the consistency ratio for each factor.

Factor	elevation	slope	aspect	curvature	TWI	distance from drainage	lithology	distance from lineament	soil texture	LULC	weight sum vector	Weight	Consistency Vector
elevation	0.02	0.05	0.02	0.02	0.02	0.01	0.01	0.01	0.02	0.01	0.19	0.0181	10.5643
slope	0.13	0.33	0.16	0.22	0.26	0.27	0.21	0.21	0.44	0.56	3.53	0.2807	12.5687
aspect	0.02	0.05	0.02	0.01	0.02	0.01	0.01	0.01	0.03	0.01	0.21	0.0194	10.8489
curvature	0.04	0.06	0.07	0.04	0.03	0.02	0.01	0.02	0.04	0.02	0.38	0.0346	10.8867
TWI	0.10	0.11	0.11	0.11	0.09	0.09	0.03	0.17	0.07	0.05	1.13	0.0933	12.1486
distance from drainage	0.15	0.06	0.11	0.07	0.04	0.05	0.03	0.01	0.07	0.02	0.65	0.0626	10.4007
lithology	0.13	0.11	0.11	0.18	0.17	0.09	0.07	0.01	0.07	0.02	1.04	0.0986	10.5831
distance from lineament	0.13	0.07	0.09	0.07	0.02	0.14	0.21	0.04	0.02	0.02	0.97	0.0813	11.9343
soil texture	0.13	0.11	0.11	0.14	0.17	0.09	0.14	0.25	0.15	0.19	1.93	0.1498	12.8574
LULC	0.13	0.06	0.18	0.14	0.17	0.23	0.28	0.25	0.07	0.09	2.09	0.1617	12.8965
Total													115.6892

Number of criteria (n) = 10 Lambda (λ) = $\frac{115.6892}{10} = 11.57$

Consistency Index (CI) = $\frac{\lambda - n}{n - 1} = \frac{11.57 - 10}{10 - 1} = 0.17$

Random Index (RI) for $n = 10$ is 1.49

Consistency Ratio (CR) = $\frac{CI}{RI} = \frac{0.17}{1.49} = 0.12$

Expert 7

Table D20 Step I: Generation of the pair-wise comparison matrix for each factor.

Factor	elevation	slope	aspect	curvature	TWI	distance from drainage	lithology	distance from lineament	soil texture	LULC
elevation	1.00	0.33	3.00	3.00	3.00	1.00	-	1.00	0.33	0.33
slope	3.00	1.00	5.00	5.00	5.00	5.00	-	5.00	1.00	1.00
aspect	0.33	0.20	1.00	1.00	3.00	3.00	-	3.00	0.33	0.33
curvature	0.33	0.20	1.00	1.00	0.33	1.00	-	1.00	0.20	0.20
TWI	0.33	0.20	0.33	3.00	1.00	1.00	-	1.00	0.20	0.20
distance from drainage	1.00	0.20	0.33	1.00	1.00	1.00	-	1.00	0.20	0.20
lithology	-	-	-	-	-	-	1.00	1.00	0.20	0.20
distance from lineament	1.00	0.20	0.33	1.00	1.00	1.00	1.00	1.00	0.20	0.20
soil texture	3.00	1.00	3.00	5.00	5.00	5.00	5.00	5.00	1.00	1.00
LULC	3.00	1.00	3.00	5.00	5.00	5.00	5.00	5.00	1.00	1.00
Total	13.00	4.33	17.00	25.00	24.33	23.00	12.00	24.00	4.67	4.67

Table D21 Step II: Computation of the criterion weights for each factor.

Factor	elevation	slope	aspect	curvature	TWI	distance from drainage	lithology	distance from lineament	soil texture	LULC	Total	Weight	Weight (%)
elevation	0.08	0.08	0.18	0.12	0.12	0.04	0.00	0.04	0.07	0.07	0.80	0.0802	8.0161
slope	0.23	0.23	0.29	0.20	0.21	0.22	0.00	0.21	0.21	0.21	2.02	0.2015	20.1543
aspect	0.03	0.05	0.06	0.04	0.12	0.13	0.00	0.13	0.07	0.07	0.69	0.0692	6.9220
curvature	0.03	0.05	0.06	0.04	0.01	0.04	0.00	0.04	0.04	0.04	0.36	0.0355	3.5518
TWI	0.03	0.05	0.02	0.12	0.04	0.04	0.00	0.04	0.04	0.04	0.42	0.0423	4.2336
distance from drainage	0.08	0.05	0.02	0.04	0.04	0.04	0.00	0.04	0.04	0.04	0.39	0.0395	3.9464
lithology	0.00	0.00	0.00	0.00	0.00	0.00	0.08	0.04	0.04	0.04	0.21	0.0211	2.1071
distance from lineament	0.08	0.05	0.02	0.04	0.04	0.04	0.08	0.04	0.04	0.04	0.48	0.0478	4.7797
soil texture	0.23	0.23	0.18	0.20	0.21	0.22	0.42	0.21	0.21	0.21	2.31	0.2314	23.1445
LULC	0.23	0.23	0.18	0.20	0.21	0.22	0.42	0.21	0.21	0.21	2.31	0.2314	23.1445
Total	1.00	1.00	1.00	1.00	1.00	1.00	1.00	1.00	1.00	1.00			



Table D22 Step III: Estimation of the consistency ratio for each factor.

Factor	elevation	slope	aspect	curvature	TWI	distance from drainage	lithology	distance from lineament	soil texture	LULC	weight sum vector	Weight	Consistency Vector
elevation	0.08	0.08	0.18	0.12	0.12	0.04	0.00	0.04	0.07	0.07	0.83	0.0802	10.3557
slope	0.23	0.23	0.29	0.20	0.21	0.22	0.00	0.21	0.21	0.21	2.08	0.2015	10.3034
aspect	0.03	0.05	0.06	0.04	0.12	0.13	0.00	0.13	0.07	0.07	0.71	0.0692	10.3273
curvature	0.03	0.05	0.06	0.04	0.01	0.04	0.00	0.04	0.04	0.04	0.37	0.0355	10.2968
TWI	0.03	0.05	0.02	0.12	0.04	0.04	0.00	0.04	0.04	0.04	0.42	0.0423	9.8931
distance from drainage	0.08	0.05	0.02	0.04	0.04	0.04	0.00	0.04	0.04	0.04	0.40	0.0395	10.1671
lithology	0.00	0.00	0.00	0.00	0.00	0.00	0.08	0.04	0.04	0.04	0.16	0.0211	7.6619
distance from lineament	0.08	0.05	0.02	0.04	0.04	0.04	0.08	0.04	0.04	0.04	0.42	0.0478	8.8354
soil texture	0.23	0.23	0.18	0.20	0.21	0.22	0.42	0.21	0.21	0.21	2.04	0.2314	8.8293
LULC	0.23	0.23	0.18	0.20	0.21	0.22	0.42	0.21	0.21	0.21	2.04	0.2314	8.8293
Total													95.4993

Number of criteria (n) = 10 Lambda (λ) = $\frac{95.4993}{10} = 9.55$

Consistency Index (CI) = $\frac{\lambda - n}{n - 1} = \frac{9.55 - 10}{10 - 1} = -0.05$

Random Index (RI) for $n = 10$ is 1.49

Consistency Ratio (CR) = $\frac{CI}{RI} = \frac{-0.05}{1.49} = -0.03$

Expert 8

Table D20 Step I: Generation of the pair-wise comparison matrix for each factor.

Factor	elevation	slope	aspect	curvature	TWI	distance from drainage	lithology	distance from lineament	soil texture	LULC
elevation	1.00	0.20	0.17	0.20	0.14	0.50	0.14	0.20	0.25	0.33
slope	5.00	1.00	2.00	1.00	0.50	2.00	0.33	3.00	2.00	3.00
aspect	6.00	0.50	1.00	0.50	0.25	2.00	0.20	0.33	2.00	2.00
curvature	5.00	1.00	2.00	1.00	0.33	2.00	0.20	2.00	4.00	5.00
TWI	7.00	2.00	4.00	3.00	1.00	4.00	0.50	3.00	3.00	3.00
distance from drainage	2.00	0.50	0.50	0.50	0.25	1.00	0.20	0.25	2.00	3.00
lithology	7.00	3.00	5.00	5.00	2.00	5.00	1.00	4.00	5.00	5.00
distance from lineament	5.00	0.33	3.00	0.50	0.33	4.00	0.25	1.00	2.00	2.00
soil texture	4.00	0.50	0.50	0.25	0.33	0.50	0.20	0.50	1.00	3.00
LULC	3.00	0.33	0.50	0.20	0.33	0.33	0.20	0.50	0.33	1.00
Total	45.00	9.37	18.67	12.15	5.48	21.33	3.23	14.78	21.58	27.33

Table D21 Step II: Computation of the criterion weights for each factor.

Factor	elevation	slope	aspect	curvature	TWI	distance from drainage	lithology	distance from lineament	soil texture	LULC	Total	Weight	Weight (%)
elevation	0.02	0.02	0.01	0.02	0.03	0.02	0.04	0.01	0.01	0.01	0.20	0.0200	2.0008
slope	0.11	0.11	0.11	0.08	0.09	0.09	0.10	0.20	0.09	0.11	1.10	0.1101	11.0105
aspect	0.13	0.05	0.05	0.04	0.05	0.09	0.06	0.02	0.09	0.07	0.67	0.0671	6.7122
curvature	0.11	0.11	0.11	0.08	0.06	0.09	0.06	0.14	0.19	0.18	1.13	0.1127	11.2747
TWI	0.16	0.21	0.21	0.25	0.18	0.19	0.15	0.20	0.14	0.11	1.81	0.1807	18.0705
distance from drainage	0.04	0.05	0.03	0.04	0.05	0.05	0.06	0.02	0.09	0.11	0.54	0.0540	5.3961
lithology	0.16	0.32	0.27	0.41	0.37	0.23	0.31	0.27	0.23	0.18	2.75	0.2750	27.4994
distance from lineament	0.11	0.04	0.16	0.04	0.06	0.19	0.08	0.07	0.09	0.07	0.91	0.0908	9.0790
soil texture	0.09	0.05	0.03	0.02	0.06	0.02	0.06	0.03	0.05	0.11	0.53	0.0526	5.2584
LULC	0.07	0.04	0.03	0.02	0.06	0.02	0.06	0.03	0.02	0.04	0.37	0.0370	3.6984
Total	1.00	1.00	1.00	1.00	1.00	1.00	1.00	1.00	1.00	1.00			



Table D22 Step III: Estimation of the consistency ratio for each factor.

Factor	elevation	slope	aspect	curvature	TWI	distance from drainage	lithology	distance from lineament	soil texture	LULC	weight sum vector	Weight	Consistency Vector
elevation	0.02	0.02	0.01	0.02	0.03	0.02	0.04	0.01	0.01	0.01	0.2115	0.0200	10.5699
slope	0.11	0.11	0.11	0.08	0.09	0.09	0.10	0.20	0.09	0.11	1.2356	0.1101	11.2217
aspect	0.13	0.05	0.05	0.04	0.05	0.09	0.06	0.02	0.09	0.07	0.7161	0.0671	10.6686
curvature	0.11	0.11	0.11	0.08	0.06	0.09	0.06	0.14	0.19	0.18	1.2571	0.1127	11.1499
TWI	0.16	0.21	0.21	0.25	0.18	0.19	0.15	0.20	0.14	0.11	2.0421	0.1807	11.3008
distance from drainage	0.04	0.05	0.03	0.04	0.05	0.05	0.06	0.02	0.09	0.11	0.5780	0.0540	10.7105
lithology	0.16	0.32	0.27	0.41	0.37	0.23	0.31	0.27	0.23	0.18	3.0869	0.2750	11.2254
distance from lineament	0.11	0.04	0.16	0.04	0.06	0.19	0.08	0.07	0.09	0.07	1.0092	0.0908	11.1161
soil texture	0.09	0.05	0.03	0.02	0.06	0.02	0.06	0.03	0.05	0.11	0.5480	0.0526	10.4209
LULC	0.07	0.04	0.03	0.02	0.06	0.02	0.06	0.03	0.02	0.04	0.3860	0.0370	10.4360
Total													108.8199

Number of criteria (n) = 10 Lambda (λ) = $\frac{108.8199}{10} = 10.89$

Consistency Index (CI) = $\frac{\lambda - n}{n - 1} = \frac{10.89 - 10}{10 - 1} = 0.10$

Random Index (RI) for $n = 10$ is 1.49

Consistency Ratio (CR) = $\frac{CI}{RI} = \frac{0.10}{1.49} = 0.07$

Table D23 Mean weight from expert that CR < 0.1.

Expert								Mean weight
1	2	3	4	5	6	7	8	CR<0.1
0.0227	0.0735	0.0460	0.0551	0.0206	0.0181	0.0802	0.0200	0.0550
0.2796	0.2431	0.2652	0.0468	0.2601	0.2807	0.2015	0.1101	0.1733
0.0600	0.0171	0.0276	0.0776	0.1790	0.0194	0.0692	0.0671	0.0517
0.0297	0.1179	0.0295	0.0806	0.1292	0.0346	0.0355	0.1127	0.0752
0.0415	0.0332	0.0718	0.0692	0.0271	0.0933	0.0423	0.1807	0.0794
0.1625	0.0170	0.0918	0.0702	0.0457	0.0626	0.0395	0.0540	0.0545
0.1014	0.2511	0.1646	0.1663	0.1327	0.0986	0.0211	0.2750	0.1756
0.0675	0.1513	0.1815	0.0522	0.0413	0.0813	0.0478	0.0908	0.1047
0.1529	0.0588	0.1011	0.1481	0.1047	0.1498	0.2314	0.0526	0.1184
0.0820	0.0370	0.0211	0.2339	0.0595	0.1617	0.2314	0.0370	0.1121
0.1500	0.0700	0.0900	0.0900	0.1400	0.1200	-0.0300	0.0700	



CURRICULUM VITAE

Name Thidapath Anucharn

Date of Birth February 28, 1981

Place of Birth Songkhla

Education Background:

- 2004: Bachelor of Science (Computer Science),
Department of computer science, Faculty of Science,
Prince of Songkla University, Thailand.
- 2006: Master of Science (Management Information Technology),
Graduate School, Prince of Songkla University, Thailand.

Work Experiences:

- 2006-Present: Lecturer,
Faculty of Science and Technology, Hatyai University.
- 2004-2006: Plan and Policy Analyst,
Policy and Planning Section,
Faculty of Medicine, Prince of Songkla University.
- 2003-2004: Marketing Communication,
K.S.P. Interchem.